FROM MECHANISM TO THERAPEUTICS: DECIPHERING THE ROLES OF A NOVEL LIPID-BINDING PROTEIN IN WNT SIGNALING AND CANCER

A Dissertation

Presented to the Faculty of the Graduate School

of Cornell University

In Partial Fulfillment of the Requirements for the Degree of

Doctor of Philosophy

by

Adnan Shami Shah

May 2021

FROM MECHANISM TO THERAPEUTICS: DECIPHERING THE ROLES OF A NOVEL LIPID-BINDING PROTEIN IN WNT SIGNALING AND CANCER

Adnan Shami Shah, Ph.D.

Cornell University 2021

Phosphoinositides (PIPs) are essential lipids that localize in the cytoplasmic leaflet of the biological membranes. By providing a signature lipid interface on the eukaryotic cell membranes, PIPs act as the code of membrane identity. Despite their low cellular abundance, PIPs impart remarkable contributions to essentially all facets of the intra and intercellular signaling processes governing critical physiological outcomes. They do so by interacting with a large array of PIP-binding "reader" proteins (effectors) at membranes to organize and frame downstream signaling entities. Pleckstrin homology (PH) domain-containing proteins represent the 11th most expressed protein family spanning 1% of the entire proteome. Despite being the largest family of such PIP "reader" proteins, only a small number of PH domain-containing proteins are well characterized for their membrane recognition and downstream signaling.

This dissertation describes the biomolecular and pathophysiological characterization of a multidomain PH domain-containing protein, PLEKHA4 (Pleckstrin homology domain-containing family A, member 4). PLEKHA4 forms a phase separated signaling hub at PI(4,5)P_2-rich clusters of the plasma membrane and recruits the Cullin-3 (CUL3) E3 ubiquitin ligase substrate adaptor Kelch-like protein

12 (KLHL12) to these assemblies. This recruitment decreases CUL3–KLHL12-mediated polyubiquitination of Dishevelled (DVL), a central intermediate in both β-catenin-dependent and -independent Wnt signaling. I, therefore, establish a novel PLEKHA4 mediated nexus between phosphoinositide signaling at the plasma membrane with ubiquitination and Wnt signaling machineries.

Capitalizing on this new signaling axis, I further define the role of PLEKHA4 in melanoma, which despite promising advances in targeted and immunotherapies still accounts for the highest skin cancer mortality. PLEKHA4 knockdown in melanoma cells led to lower Dishevelled levels, attenuated Wnt/β-catenin signaling, and a block of progression through the G1/S cell cycle transition. In mouse allo/xenograft models, loss of PLEKHA4 attenuated tumor growth in BRAF- and NRAS-mutant melanomas and exhibited an additive effect with the clinically used inhibitor encorafenib in a BRAF-mutant model. This dissertation identifies PLEKHA4, an E3 ubiquitin ligase regulator with both lipid and protein interactors, as a promising drug target for melanoma and clarifies a controversial role for Wnt/β-catenin signaling in the control of melanoma proliferation.

BIOGRAPHICAL SKETCH

Adnan Shami Shah grew up in Nepal, a beautiful country known for its majestic Himalayan range, that houses eight of the ten highest peaks on earth. After being home schooled for a year mentored by his elder sister, Sajiya, Adnan was selected to attend Arniko Boarding School in Kathmandu where he was the highest academic achiever in the school for nine consecutive years earning himself a full ride scholarship every year through grade 10. He was then accepted to Delhi Public School in India with a residential education scholarship and finished his secondary education as the valedictorian of his graduating class.

Having been fortunate enough to complete all of his secondary education with scholarship, he felt the need to contribute to the education work force, so he taught science and math as a middle school teacher in Kathmandu while volunteering at United States Education Foundation in Nepal (USEF-N). While at USEF-N, Adnan learned the immense educational opportunities in the US for bright yet economically disadvantaged students. Fortunately, he was awarded a full ride scholarship to pursue his undergraduate degree in Chemistry as the only student from Nepal in his entering class at Bates College in Lewiston, Maine. Adnan is also the first from his family to pursue higher education.

While at Bates, he was introduced to laboratory research in protein biochemistry under the mentorship of Professor Rachel Austin in his freshman year. Pursuing his newly found passion for scientific research he further gained hands-on research experience through multiple highly selective summer research internships, a

Biomedicine research focused study abroad in Denmark and senior thesis research under the mentorship of Professor Rachel Austin.

Driven by the pursuit of a scientific career following his graduation in 2015, he pursued a PhD program in Chemistry and Chemical Biology at Cornell University, Ithaca. At Cornell, he decided to join the lab of Professor Jeremy Baskin. As one of the very first students to join the Baskin lab, Adnan repeatedly was at the forefront of driving the lab's research at the interface of chemistry and biology. In the Baskin lab, he continued his passion for protein biochemistry research by studying a novel class of lipid-binding protein family called PLEKHA. He primarily characterized the isoform PLEKHA4 and elucidated its biochemical roles in cell signaling and cancer progression discovering new therapeutic avenues for cancers such as melanoma. He also successfully established the first knock-out of PLEKHA4 in mouse and Drosophila melanogaster (fruit fly) model systems that will further aid in future research in the field and has fostered multiple collaborations at and outside of Cornell.

In the Baskin lab, he has developed as an independent researcher with a strong sense of mentorship that has led him to mentor both graduate and undergraduate students at different levels. Post-Cornell, he plans to apply his knowledge in the field of protein biochemistry and cell signaling to the area of protein diagnostics to discover novel biomarkers for cancers and other diseases in the lab of Professor David Walt at Harvard Medical School. His goals are to pursue a scientific career in the field of medical research and drug discovery. Most importantly, he plans to keep working to mentor and promote the next generation to pursue higher education despite all the odds.

To my family,

Thank you for your unwavering love and support…

And to my sister, Sajiya, my first mentor in life…

We did it together!

ACKNOWLEDGMENTS

I would like to express my immense gratitude to my advisor, Professor Jeremy Baskin for his endless guidance and support. Your dedication and determination to push the boundaries of science is awe inspiring. Few things are more critical to this world than the mentors whose passion in the value of their subject shape their students for the better. I will forever be grateful for your mentorship that has enabled me to strive to meet my best potential.

I thank my committee members, Professor Rick Cerione and Professor Chris Fromme, for their mentorship, support and letters of recommendations for my future endeavors. I want to thank my undergraduate advisors Professor Rachael Austin and Professor Loring Danforth for inspiring me to pursue a graduate degree to advance my research career. I also want to thank all my teachers and mentors throughout my secondary education for driving my curiosity toward science.

Financial support for this research was provided through NIH, Arnold and Mabel Beckman Foundation (Beckman Young Investigator Award) and the Alfred P. Sloan Foundation (Sloan Research Fellowship). Super-resolution structured illumination microscopy (SR-SIM) imaging was performed at the Cornell University Biotechnology Resource Center, with support from the National Science Foundation (NSF) (DBI-1428922). Scanning Electron Microscopy (SEM) imaging was performed at the Cornell Center for Materials Research Facilities, with support from the NSF (DMR-1719875).

Science is fun because of the people we do it with! I am fortunate to share this journey with an amazing group of friends, both in the lab and outside who have

always motivated and inspired me to strive for the best. I want to thank the first generation of Baskin lab members – Dr. Jessica Daughtry, Dr. Timothy Bumpus and Alex Batrouni for helping create an amazing start to graduate school. I will always remember our Friday evening Big Red Barn hangouts. I want to thank Xiaofu Cao, Amith Punyala and Wendy Cao, whom I had the opportunity to mentor. I have learned equally if not more from these invaluable mentoring experiences. I also want to acknowledge Dr. Hongyan Sun, Dr. Brittany White and all the Baskin lab members who have provided invaluable intellectual discussions and critiques on the progress of my research. Additionally, I want to thank all the Weill Institute for Cell and Molecular Biology members who I have gotten to know over the years. I will forever cherish the great friendship that has forged over the years, both at Cornell and Bates with whom I got to enjoy the richness of Ithaca in many ways.

I want to thank Mel for being my best friend and walking with me throughout this journey. I can never thank you enough for your love and support. Finally, I want to thank my family – mom, Sunita, dad, Shammi, diju (sister) Sajiya and sanu (brother) Pranik for always looking out for me.

As the first member of my family to go to college and eventually to graduate school, this dissertation is a testament to all the love, support and prayers of my family whose countless sacrifices have brought me to where I am today. Thank you all for supporting me to strive towards my purpose in life…

"He who has a why to live for can almost any how."

- Friedrich Nietzsche

TABLE OF CONTENTS

LIST OF FIGURES

LIST OF TABLES

LIST OF ABBREVIATIONS

APC	Adenomatous Polyposis Coli
APF	After Puparium Formation
AP2	Adaptor complex 2
BCA	Bicinchoninic Acid Assay
BRAFi	BRAF inhibitor
BSA	Bovine Serum Albumin
BTB	Broad-Complex, Tramtrack and Bric a brac domain
CARE	Center for Animal Resources and Education
Casp3	Caspase-3
Cav1	Caveolin-1
CC	Coiled coil domain
CDKN2A	Cyclin Dependent Kinase Inhibitor 2A
CLC	Clathrin Light Chain
CMV	Cytomegalovirus
CRISPR	Clustered Regularly Interspaced Short Palindromic Repeats
CRY2	Cryptochrome-2
CUL3	Cullin-3
Cyo	Curly O allele
DAPI	4′,6-diamidino-2-phenylindole
DMEM	Dulbecco's modified Eagle medium
DMSO	Dimethylsulfoxide
DOPC	Dioleoylphosphatidylcholine

DOPS	Dioleoylphosphatidylserine
Dox	Doxycycline
dsh	Dishevelled (Drosophila melanogaster)
dsh^{+}	Dishevelled wildtype allele
dsh^{1}	Dishevelled hypomorphic mutant allele
dsh^{3}	Dishevelled amorphic mutant allele
dsh^{75}	Dishevelled amorphic mutant allele
DTT	Dithiothreitol
DVL	Dishevelled
E. coli	Escherichia coli
EDTA	Ethylenediaminetetraacetic Acid
EEA1	Early Endosome Antigen 1
ER	Endoplasmic Reticulum
E-syt2/3	Extended synaptotagmin 2/3
FACS	Fluorescence-Activated Cell Sorting
FAPP1/1	Four-phosphate-adaptor protein 1/2
FBS	Fetal Bovine Serum
FPKM	Fragments Per Kilobase of transcript per Million mapped reads
FUCCI	Fluorescent Ubiquitination-based Cell Cycle Indicator
GAPDH	Glyceraldehyde phosphate dehydrogenase
GaAsP PMT	Gallium Arsenide Phosphide Photo Multiplier Tube
GFP	Green Fluorescent Protein
GST	Glutathione S–transferase

HA tag	Human influenza hemagglutinin tag
H-BP-PH	Amphipathic Helix-Basic Peptide-Pleckstrin Homology domain
HEK	Human Embryonic Kidney cells
HILIC	Hydrophilic Interaction Chromatography
Hu	Humeral
IDR	Intrinsically disordered region
IDT	Integrated DNA Technologies
IF	Immunofluorescence
IP	Immunoprecipitation
IPTG	Isopropyl β-D-1-thiogalactopyranoside
iRFP	Infrared Fluorescent Protein
IWP-4	Inhibitor of WNT Production-4
JNK	c-Jun N-terminal Kinase
KLHL12	Kelch-like protein 12
kmr	Kramer gene
kmr^{+}	Kramer wildtype allele
kmr^{1}	Kramer knock-out allele 1
kmr^{2}	Kramer knock-out allele 2
kmr^{-}	Kramer knock-out alleles
kmr^{df}	Kramer deletion fragment
KO	Knock-out
LAMP1	Lysosomal-Associated Membrane Protein 1
L3	Third instar larval stage

M1R	Muscarinic Receptor
mCh	mCherry tag
MEM	Minimum Essential Medium
MITF	Melanocyte Inducing Transcription Factor
mNG	monomeric Neon Green Fluorescent Protein
NC1	Negative Control 1
NSG	NOD *scid* gamma
OD_{600}	Optical Density at 600 nm
ORF	Open Reading Frame
ORP5	Oxysterol-binding Protein 5
Oxo-M	Oxotremorine M
PARP	Poly (ADP-ribose) polymerase
PAX2	Paired box gene 2
PBS	Phosphate Buffered Saline
PC	Phosphatidylcholine
PCP	Planar Cell Polarity
PCR	Polymerase Chain Reaction
PEPP1	Phosphoinositol 3-phosphate-binding protein 1
PH	Pleckstrin Homology domain
PHR	N-terminal Photolyase Homology Region
PIPs	Phosphoinositides
PI3P	Phosphatidylinositol 3-phosphate
$PI(4,5)P_2$	Phosphatidylinositol 4,5-bisphosphate

$PI(3,4,5)P_3$	Phosphatidylinositol 3,4,5-trisphosphate
p-JNK	phospho c-Jun N-terminal Kinase
PLC	Phospholipase C
PLEKHA4	Pleckstrin Homology domain containing family A member 4
PRD	Proline-Rich Domain
PROTAC	Proteolysis Targeting Chimera
PS	Phosphatidylserine
P/S	Penicillin/Streptomycin
RBX1	Ring Box 1
RFP	Red Fluorescent Protein
RNAi	RNA interference
Sb	Stubble
SDS-PAGE	Sodium Dodecyl Sulfate-Polyacrylamide Gel Electrophoresis
SEM	Scanning Electron Microscopy
sg/ sh/ siRNA	short guide/ short hairpin/ small interfering RNA
SILAC	Stable Isotope Labeling by Amino acids in Cell culture
Sp	Sternopleural
SR-SIM	Super-Resolution Structured Illumination Microscopy
TAPP1/2	Tandem Pleckstrin homology domain-containing Protein 1/2
Tb	Tubby
TB	Terrific Broth
TCF/LEF	T-Cell Factor/Lymphoid Enhancer Factor
TCGA	The Cancer Genome Atlas

Ub	Ubiquitin
VSVg	Vesicular Stomatitis Virus Glycoprotein
WB	Western Blot
Wg	Wingless
WIDs	Wing Imaginal Discs
WIF-1	Wnt Inhibitory Factor-1
WntRGreen	Wnt Reporter Green
WT	Wildtype
YUMM1.7	Yale University Mouse Melanoma 1.7

LIST OF SYMBOLS

β	Beta
δ	Delta
μ	Micro
Δ	Delta (Deletion)

PREFACE

This dissertation was largely adapted from the following articles co-written by the author:

Chapter 2 was adapted with permission from:

Shami Shah, A.; Batrouni, A. G.; Kim, D.; Punyala, A.; Cao, W.; Han, C.; Goldberg, M. L.; Smolka, M. B.; Baskin, J. M. PLEKHA4/Kramer Attenuates Dishevelled Ubiquitination to Modulate Wnt and Planar Cell Polarity Signaling. *Cell Rep.* **2019**, *27* (7), 2157-2170.e8. https://doi.org/10.1016/j.celrep.2019.04.060.

Chapter 3 was adapted with permission from:

Shami Shah, A.; Cao, X.; White, A. C.; Baskin, J. M. PLEKHA4 Promotes Wnt/Beta-Catenin Signaling-Mediated G1/S Transition and Proliferation in Melanoma. *Cancer Res.* **2021**, No. 607, canres.2584.2020. https://doi.org/10.1158/0008-5472.can-20-2584.

CHAPTER 1

LIPID-BINDING PROTEINS AT THE NEXUS OF UBIQUITINATION, WNT SIGNALING AND CANCER

Lipids are more than just the building blocks of cellular membranes. Beyond their conventional roles of acting as energy sources and providing structural integrity to the membranes serving as a semipermeable barrier, lipids are increasingly recognized as signaling molecules. As second messenger molecules, lipids have the capacity to trigger profound physiological responses[1]. There are many classes of lipids that harbor specific structural and functional roles within the cells[2,3]. Phospholipids are a class of lipids that comprise of a characteristic hydrophilic "head" group containing a phosphate molecule and two hydrophobic fatty acid "tails" linked together by a glycerol molecule[4,5]. The phosphate head group can be further derivatized with molecules such as choline, ethanolamine and serine forming abundant cellular phospholipids such as phosphatidylcholine, phosphatidylethanolamine and phosphatidylserine[4,5].

1.1 Phosphoinositides

Phosphoinositides, a class of phospholipids, are low abundance yet critical signaling lipids that encompass approximately 0.2-1% of the phospholipids of the biological membranes[4,5]. These lipids are derivatives of phosphatidylinositol that

consist of a *myo*-inositol headgroup and a phospho-glycerol linker followed by two acyl chains of varying length and saturation[4,5] (**Figure 1.1**).

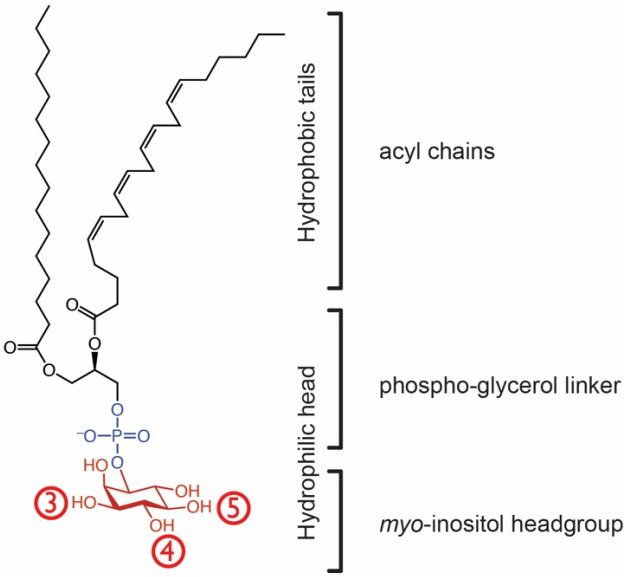

Figure 1.1 Phosphatidylinositol (PI) molecule comprised of a *myo*-inositol headgroup, a phospho-glycerol linker and two acyl chains of varying length and saturation.

Phosphoinositides are biosynthesized within the cells by the interplay of multiple "writer" proteins such as kinases and "eraser" proteins such as phosphatases that act upon their membrane-bound lipid substrates[4–6]. The hydroxyl group at positions -3, -4 and -5 of the *myo*-inositol headgroup can be phosphorylated and dephosphorylated in a combinatorial fashion by a number of such kinases and phosphatases (**Figure 1.2**). This interconversion phosphorylation dynamics yield a total of seven unique phosphoinositide species (PIPs) – PI(3)P, PI(4)P, PI(5)P, $PI(3,4)P_2$, $PI(3,5)P_2$, $PI(4,5)P_2$, and $PI(3,4,5)P_3$[4–6] (**Figure 1.2**).

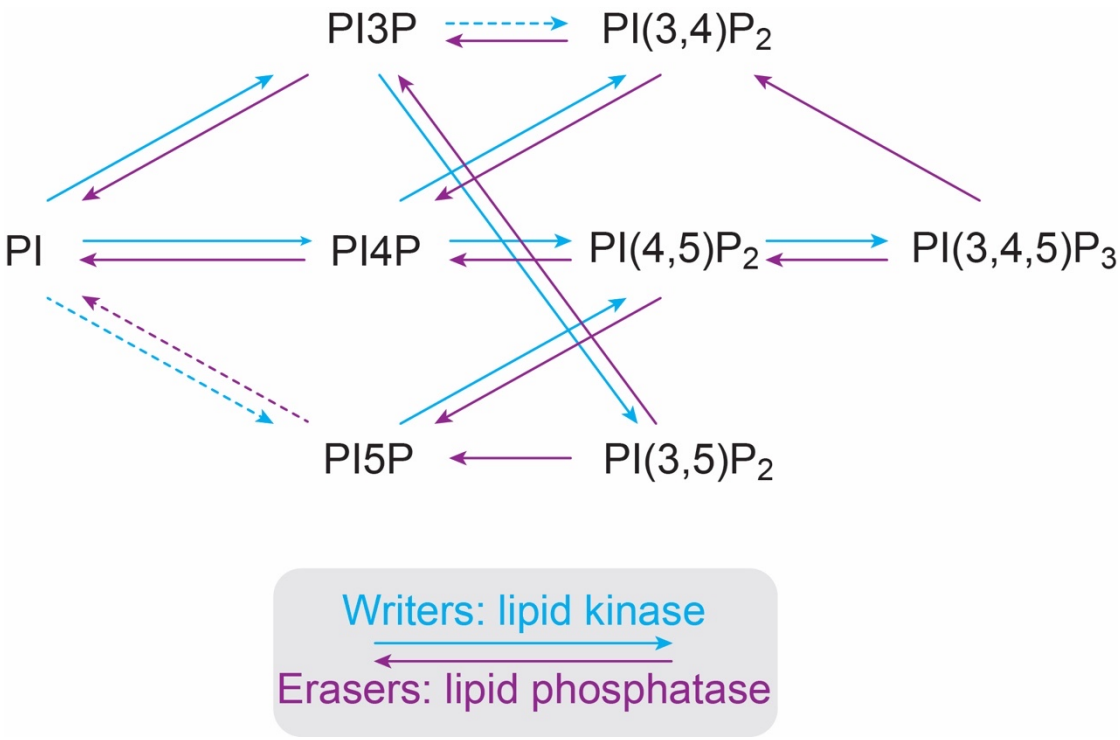

Figure 1.2 The interplay of "writer" proteins (lipid kinases) and "eraser" proteins (lipid phosphatases) in cells yield seven different phosphoinositide species.

Although minor components of the bulk of phospholipids of the cellular membranes, these anionic lipids are crucial as second messengers for a wide array of cellular functions[6]. PIPs are localized in the cytosolic leaflets of various organelle membranes and the plasma membrane within the cells and act as a "code" of the membrane identity[5,7,8]. For instance – majority of the cellular PI(3)P pools can be found on early endosomal autoantigen (EEA1)-positive vesicles, PI(4)P can be found significantly enriched at the trans-Golgi network and the plasma membrane, $PI(3,5)P_2$ is the highly enriched phosphoinositide of the late endosomal membrane and $PI(4,5)P_2$ is the most abundant signature phosphoinositide at the plasma membrane[5,7] (**Figure 1.3**).

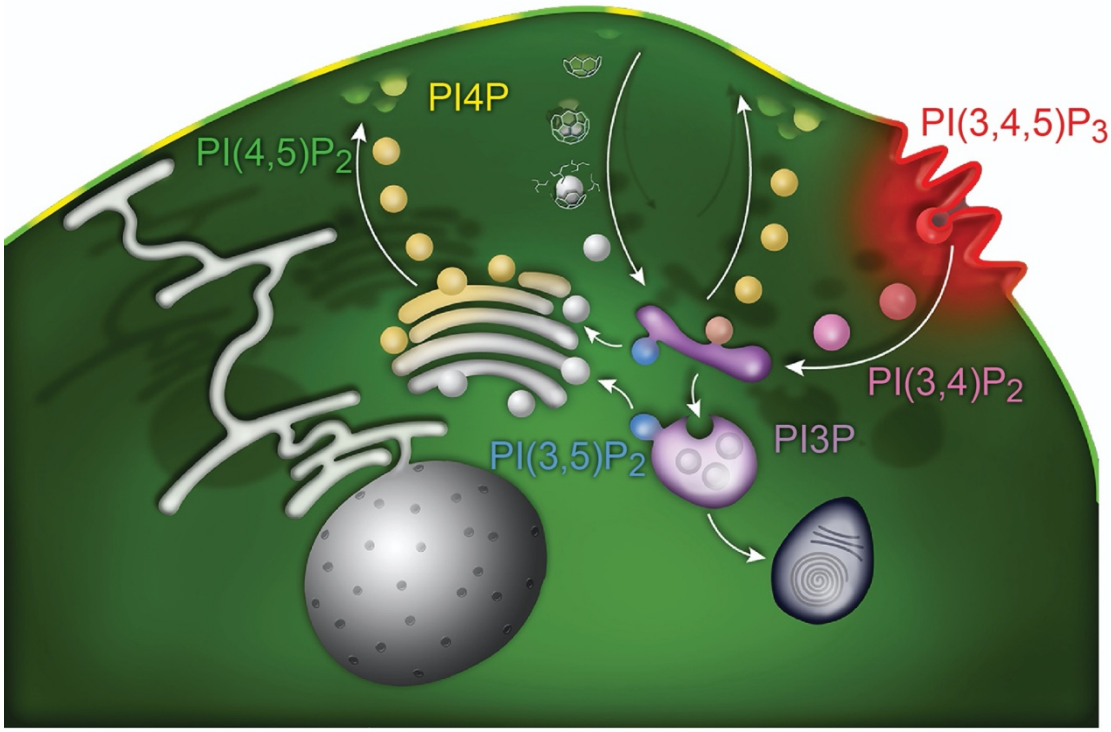

Figure 1.3 Phosphoinositides form a code of the membrane identity by enriching membranes in the cells. Figure adapted with permission from Idevall-Hagren and De Camilli. *BBA* **2015**[9].

1.2 Phosphoinositide "reader" proteins and their structural motifs

By providing a signature lipid interface on the membranes acting as the ZIP code of the cellular compartments, these phospholipids engage domains from several families of PIPs "reader" proteins (effectors) directing them where to bind and where to activate as necessary[5,7,8] (**Figure 1.4**).

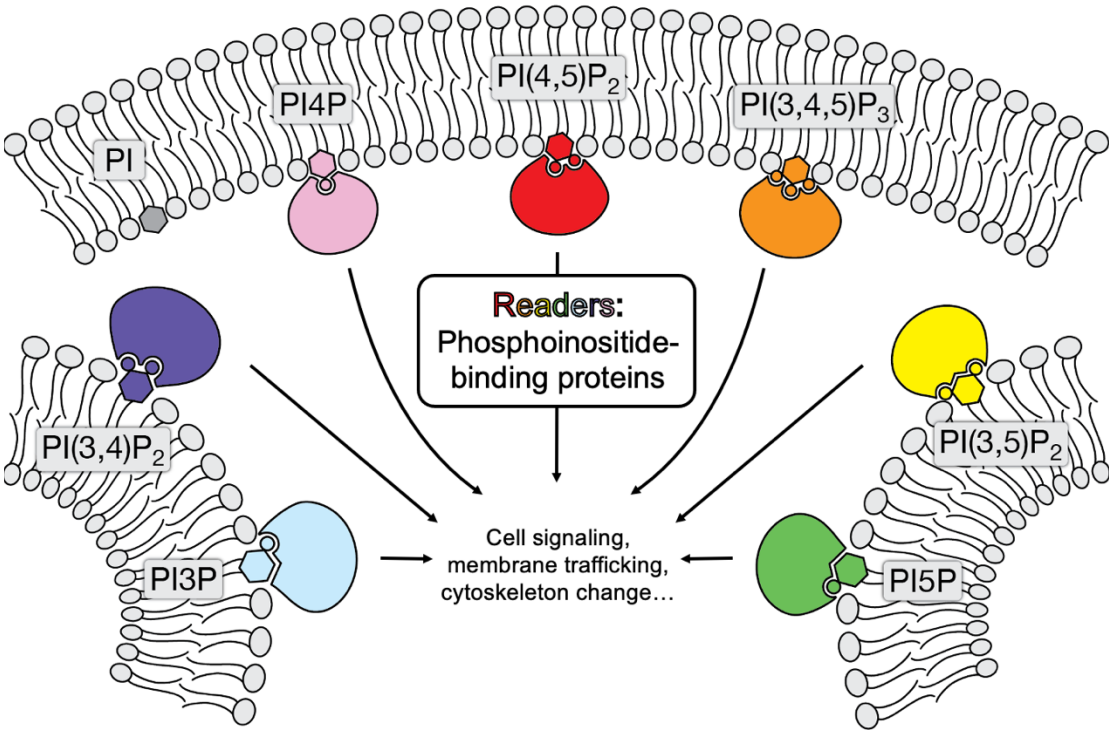

Figure 1.4 "Reader" proteins shown in different colors interact with various phosphoinositides in cellular membranes via their unique structural domains, eliciting an array of phenotypic responses.

The dynamic interactions between the reader proteins and the PIPs lead to changes in cytoskeleton dynamics, cell signaling and trafficking events resulting in key phenotypic outcomes[7,8,10]. A hallmark feature of these reader proteins is the signature structural motif/domain that they contain to facilitate the protein-lipid interaction. Domains such as PH (Pleckstrin Homology), PX (Phox Homology), FYVE (Fab1, YOTB, Vac1, and EEA1 – four cysteine-rich proteins in which this domain has been found), and C2 are some of the most prominently expressed structural motifs across the human proteome (**Figure 1.5**). These tertiary structural motifs span a wide range of physiological outcomes upon their interaction with their designated PIPs by propagating signaling from their precise membrane locations[5].

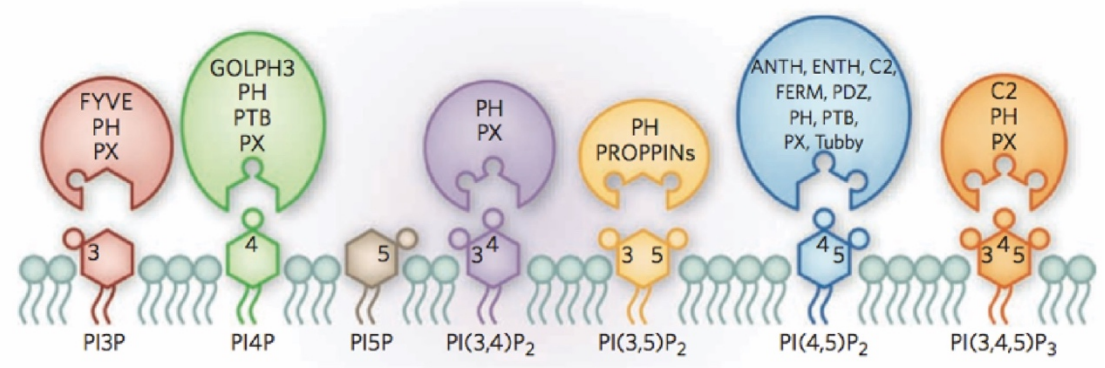

Figure 1.5 Phosphoinositide "reader" proteins shown in different colors exhibit a wide range of structural domains to facilitate their interactions with various PIPs. Of note, Pleckstrin Homology (PH) domain is the largest represented PIP-binding domain in the proteome. Figure adapted with permission from Kutateladze. *Nature Chemical Biology* **2010**[11].

1.3 Pleckstrin Homology (PH) domains

Among many such proteins with PIP-binding motifs (**Figure 1.5**), PH (Pleckstrin Homology) domain-containing protein family members have been of profound interest because of the ability of these proteins to couple phosphoinositide signaling to other complex intracellular networks within the cell. The PH domain was identified almost 30 years ago as regions spanning two approximately 120 amino acid regions in pleckstrin[12,13], a key substrate of protein kinase C (PKC)[14]. The first structure of PH domain was solved by Oschkinat[15] and Fesik[16] groups that identified the PH domain as a bent seven stranded antiparallel β-sheet closed on one end by a characteristic C-terminus α-helix (**Figure 1.6**). Since then, many groups have discovered the PH-domain and its promiscuity in cell signaling via the binding interactions of phosphoinositides with varying affinity and specificity. Canonically, these interactions are mostly electrostatic in nature between the negatively charged

head groups of the membrane phosphoinositides and the positively charged loops of lysine and arginine residues of the PH domain[17] (**Figure 1.6**).

Figure 1.6 Cartoon diagram of a prototypical pleckstrin homology domain representing a bent seven stranded antiparallel β-sheet closed on one end by a characteristic C-terminus a-helix. Structures obtained from PDB: 3VIA.

Research spanning almost three decades of work have shown growing number of proteins in the proteome that contain the PH motif. PH domains have been found in both enzymatic and non-enzymatic proteins. Some of the most well studied proteins such as Akt (Protein Kinase B) have been shown to interact with $PI(3,4,5)P_3$ via its PH-domain[18]. Akt is at the center of phosphoinositide 3-kinase (PI3K) pathway which has been a major pathway targeted for cancer diagnostics and therapeutics for over two decades[18]. Another well studied example of a PH domain protein family is phospholipase C (PLC), an enzyme that cleaves $PI(4,5)P_2$ to yield the secondary messengers diacylglycerol and inositol triphosphate (IP_3)[19].

PH domain-containing proteins represent the largest family of PIP-binding reader proteins in the proteome[10,20,11]. It is the 11th most common domain represented in almost 1% of the human proteome spanning >250 PH domain-containing proteins[10]. Of all the PH domain-containing proteins, only about 10% of them are known to bind phosphoinositides with high affinity and specificity, whereas 90% of them may bind to phosphoinositides often with low-affinity, but still high avidity, or perhaps do not bind to lipids at all[20]. In these low-affinity contexts, PH domains usually function as coincidence detectors where they utilize their structural affinity to phosphoinositides rich areas of the membranes and strengthen their interfaces with additional domains that facilitate protein-protein or protein-lipid interactions[10,7,20].

A major challenge in the field has been to deconvolute the low-affinity binding of phosphoinositides to functional relevance within the cells. This has led to a limited understanding of how all but only a small number of PH domain-containing proteins transduce membrane recognition to downstream signaling and critical physiological responses[10,20]. Elucidating these lipid-protein interactions and their biochemical outcomes are vital for understanding their roles within the cell and in many disease contexts, yielding tremendous opportunities to expand diagnostic and therapeutic windows.

1.4 Chapter 2 overview

This thesis describes the cellular, biochemical and mechanistic characterization of a previously uncharacterized PH domain-containing protein, PLEKHA4 (Pleckstrin homology domain-containing family A, member 4), with implications in diseases such

as melanoma. PLEKHA4, also known as PEPP1 (Phosphatidylinositol-three-phosphate-binding PH-domain protein-1) was initially discovered by Dowler and co-workers as member of the PLEKHA protein family that was proposed to interact with PI3P[21] (**Figure 1.7**). Further computational work showed predictions that PLEKHA4 might bind to $PI(3,4,5)P_3$ in the cells[22]. Whereas these studies paved a pathway towards understanding the lipid-protein interaction of PLEKHA4 and PIPs, they were significantly limited by lack of physiological evidence translating in vitro binding to in vivo cellular functions. Thus, **Chapter 2** of this dissertation describes a detailed molecular and biochemical characterization of PLEKHA4 in vitro in cell culture models and in vivo in *Drosophila melanogaster*.

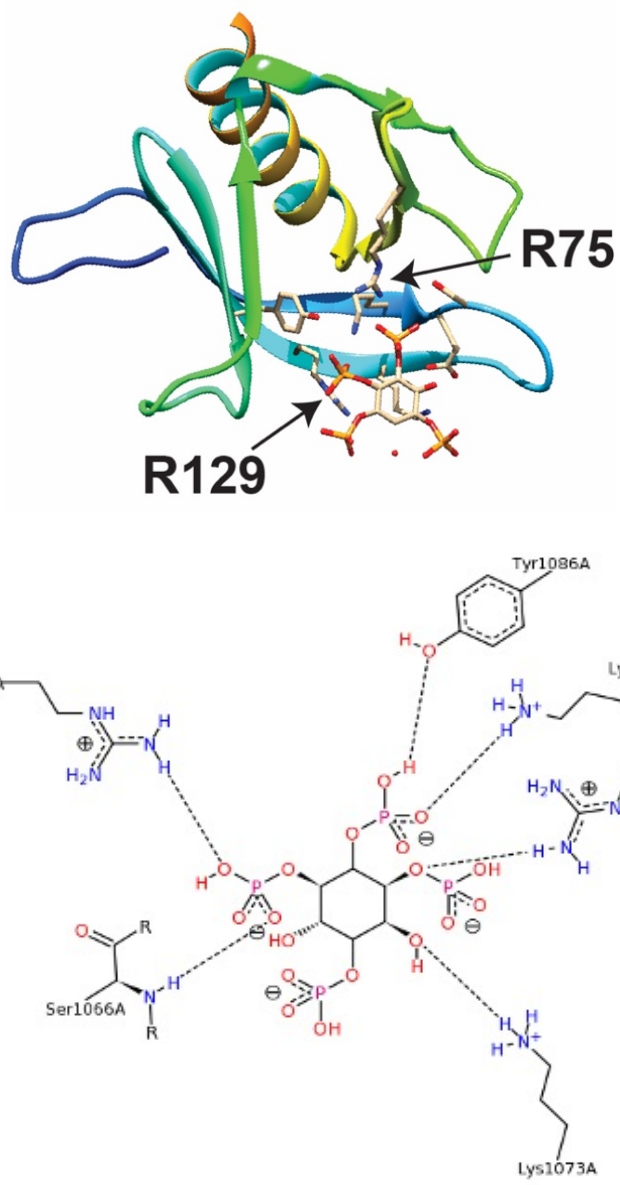

Figure 1.7 Structure of the PH domain of PLEKHA4 as shown on top interacting with inositol-(1,3,4,5)-tetrakisphosphate (IP_4). Two key arginine residues are highlighted. At the bottom, a two-dimensional image of key residues within the PH domain that are necessary for the interaction. IP_4 chemically mimics the PH domain binding to $PI(3,4,5)P_3$ headgroup in the cells. Structures obtained from PDB: 1UPR.

PLEKHA4 belongs to a larger family of PIP-binding proteins such as TAPP1/2 and FAPP1/2 that have been shown to bind $PI(3,4)P_2$ and PI4P respectively[21].

Chapter 2[23] describes a detailed domain map constructed after critical biochemical characterization of PLEKHA4 in vitro and in cell culture models (**Figure 1.8**) that shows an N-terminal amphipathic helix (H) and a stretch of basic amino acids (BP) preceding a pleckstrin homology (PH) domain together forming H-BP-PH motif (**Figure 1.9**). Lipid interaction studies performed with purified fragments of PLEKHA4 on a physiologically relevant liposome bilayer system showed PLEKHA4 interacts with $PI(4,5)P_2$ via this H-BP-PH motif and localizes at the plasma membrane of the cells (**Chapter 2**).

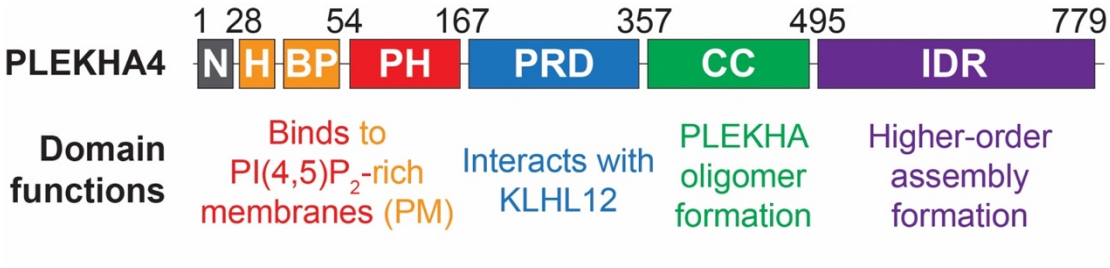

Figure 1.8 Domain map of PLEKHA4 constructed after characterizing the roles of each domain involved in PLEKHA4 functionality.

A proline-rich domain (PRD) in the middle of PLEKHA4 aids in interactions with other proteins. Finally, a coiled-coil domain (CC) and an intrinsically disordered region (IDR) is found at the C-terminus that mediate formation of PLEKHA4 oligomers and directs higher-order phase separated assembly formation (**Figure 1.8**). Through these domains, PLEKHA4 interacts with KLHL12 (Kelch-like protein 12) and forms a nexus between phosphoinositide binding, ubiquitination and Wnt signaling. We establish that PLEKHA4 modulates the activity of a key E3 ligase

complex (CUL3-KLHL12) that can polyubiquitinate Dishevelled (DVL) the so-called master regulator of Wnt signaling, targeting it for degradation.

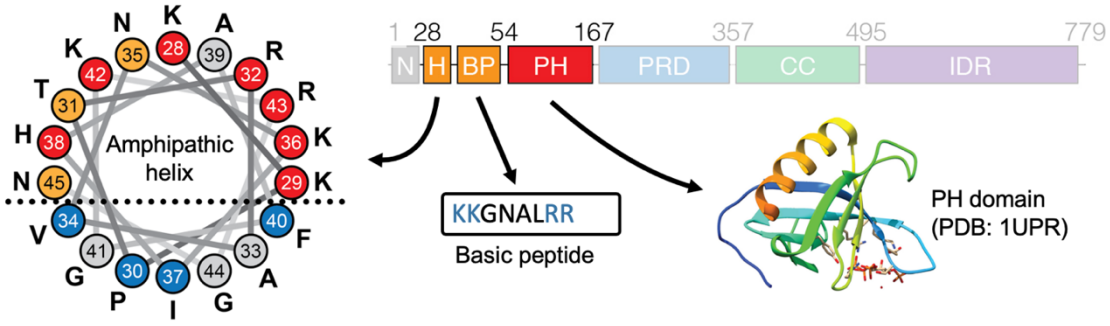

Figure 1.9 PLEKHA4 interacts with PI(4,5)P_2 at the plasma membrane of the cells via its lipid-binding motif, H-BP-PH where "H" represents the amphipathic helix, "BP" is the basic peptide region and PH is the pleckstrin homology domain.

1.5 PLEKHA4 and Wnt signaling

Wnt signaling (**Figure 1.10**) controls key cell fate decisions in the development of eukaryotes, and its dysregulation can cause many diseases[24,25,26]. Figure 1.11 shows simplified diagrams of Wnt pathways that are divide into two sub classes – canonical β-catenin dependent and non-canonical β-catenin independent pathways[27]. β-catenin independent Wnt pathway further consists of planar cell polarity (PCP) and Wnt-Ca^{2+} pathways[27] (**Figure 1.11**). Wnt pathways initiate at the plasma membrane by the recruitment of a key cytosolic protein Dishevelled (DVL) (**Figure 1.10**).

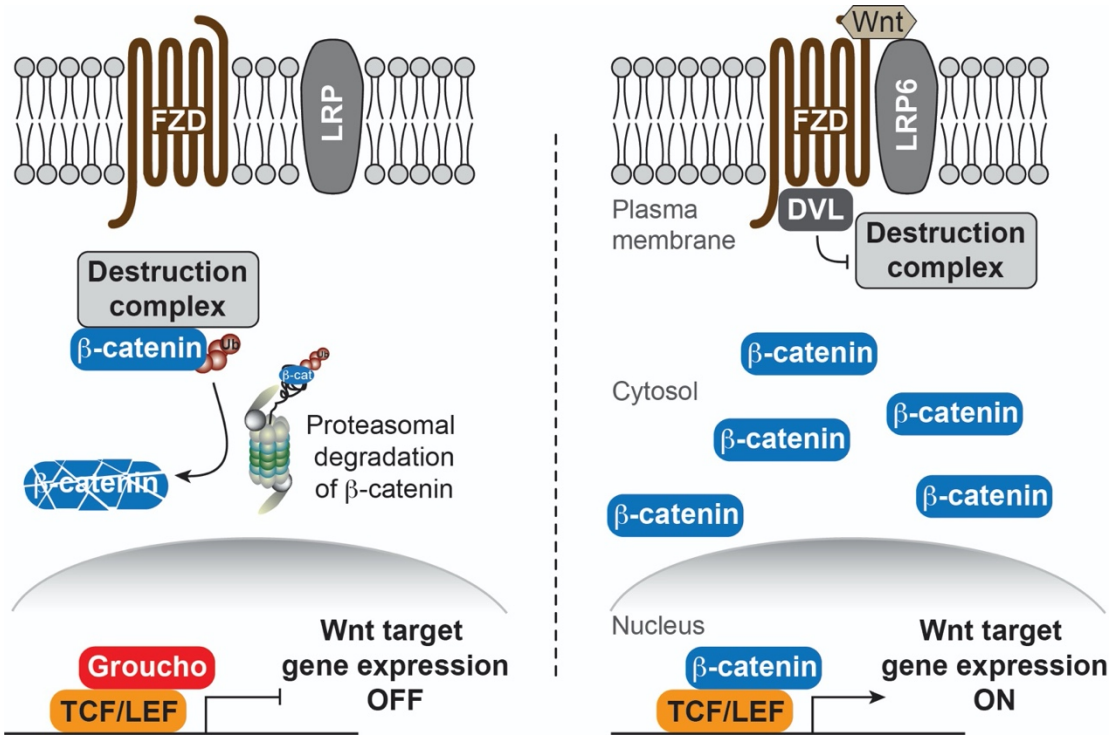

Figure 1.10 Wnt signaling pathway overview. In the absence of the Wnt ligand, b-catenin is ubiquitinated by the "destruction" complex and degraded via proteosome. In the presence of the Wnt ligand, cell surface receptors Frizzled (Fzd) and LRP5/6 together recruit Dishevelled (DVL) to the plasma membrane. DVL proteins further recruit and inhibit the β-catenin "destruction" complex leading to the cytosolic accumulation and eventual translocation of β-catenin to the nucleus leading to the expression of Wnt target genes. Figure adapted and modified with permission from Shami Shah et al. *Cell Chemical Biology* **2020**[25].

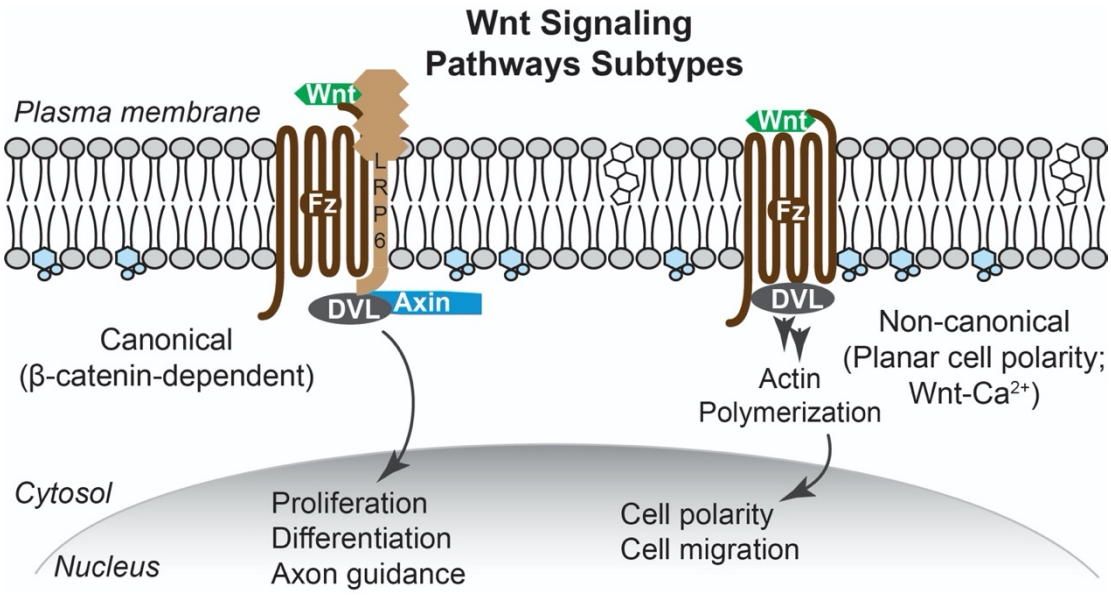

Figure 1.11 Wnt pathways can be divided into two major classes – canonical β-catenin-dependent and non-canonical β-catenin-independent pathways. Non-canonical pathway can be further subdivided into planar cell polarity (PCP) and Wnt-Ca^{2+} pathways. These pathways govern key phenotypes within the cells.

DVL proteins are key mediators of the Wnt signal so their levels are tightly regulated. The E3 ubiquitin ligase Cullin-3 (CUL3), in complex with one of its substrate adaptors, KLHL12, negatively modulates the levels of DVL via ubiquitination[28] (**Figure 1.12**). A major unanswered question is how this activity of CUL3-KLHL12 toward DVL is regulated at the plasma membrane, the site of DVL action in Wnt signaling[29].

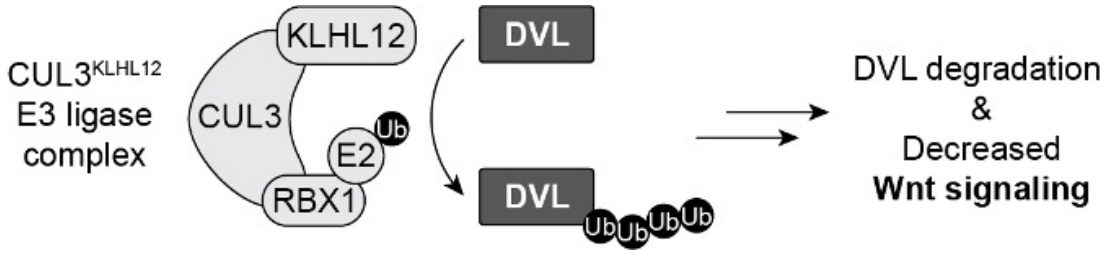

Figure 1.12 The homeostatic levels of DVL proteins are tightly regulated in the cells by the interplay of KLHL12, a substrate specific ubiquitination adaptor, with the CUL3 E3 ligase machinery. CUL3-KLHL12 complex leads to the ubiquitination mediated proteasomal degradation of DVL proteins resulting in the down regulation of Wnt signaling pathway.

Chapter 2[23] thus, provides a mechanistic basis for PLEKHA4 as a key modulator of the strength of Wnt signaling through its function as a novel adaptor that modulates CUL3-KLHL12 activity at the plasma membrane. In an *in vivo* context, I discovered that knockout of the *Drosophila melanogaster* PLEKHA4 homolog, *kramer*, selectively affects planar cell polarity (PCP), equivalent to non-canonical Wnt signaling in this organism. With this work, I provide mechanistic evidence that PLEKHA4 is a novel lipid-binding protein acting as a bona-fide regulator of the Wnt signaling pathways by coupling phosphoinositides, critical lipids at the plasma membrane of the cells, to the control of the proximal events of Wnt signaling machinery.

1.6 PLEKHA4 as a disease-related gene

Many studies have implicated the roles of PLEKHA4 in disease contexts[21,30,31]. Dowler and co-workers previously reported that the levels of PLEKHA4 were significantly elevated in melanoma although they did not identify any molecular or

functional consequences[21]. Huang et al. identified in a transcriptomic analysis of CNS myelin regeneration post injury in a rat model, PLEKHA4 was one of the highly upregulated genes during the myelin repair stage in this phenomenon[30]. Furthermore, a whole exome sequencing and neurite outgrowth analysis in autism spectrum disorder identified PLEKHA4 as a vulnerable gene in this complex and poorly understood disease[31]. Although the physiological implications of these observations remain completely unexplored nonetheless, they provide a clear picture of PLEKHA4 as a vulnerable gene in several different diseases.

I made a phenotypic observation during an experiment in HeLa cells that showed proliferation defects in PLEKHA4 knockdown cells compared to the control. This phenotype was mild yet general, occurring in several cell lines that I tested. Proliferation is one of the hallmark phenotypes in the context of cancer progression[32] so analyzing PLEKHA4 expression patterns in various cancers led me to hypothesize the role of PLEKHA4 in this context. TCGA real patient cancer database analysis revealed that PLEKHA4 mRNA is ubiquitously expressed in many types of cancers[33] (**Chapter 3, Figure 3.1A**). Further bioinformatic analysis using the Genevestigator database revealed that the expression pattern of PLEKHA4 was highest in melanoma cancer cells compared to healthy melanocytes[34].

1.7 Melanoma

Melanoma, the most aggressive form of skin cancer accounts only for 1% of all the skin cancers diagnosed in the US but has the highest skin cancer related mortality rate[35]. Almost 65% of melanoma show somatic mutations in BRAF-

V600D/E and around 10% show mutations in NRAS Q61K/R[33]. These genetic alterations cause phenotypic changes that lead to cell proliferation, differentiation and apoptosis ultimately leading to malignancy and tumorigenesis[36].

Whereas targeted therapies toward mutant BRAF via immunotherapy or small molecule or both have been incredible breakthroughs in treating melanoma, many challenges still linger after decades of research in this field[37,38]. Immunotherapy can lead to lack of tumor cell specificity further causing skin and/or gastrointestinal toxicity[39]. BRAF targeted therapy can lead to resistance, thus a reduced drug efficiency and disease relapse over time[40]. By contrast no known therapies for N-RAS mutant melanoma have been discovered yet[40].

1.8 Wnt signaling in melanoma

Besides BRAF or NRAS mutations, aberrations in the Wnt signaling pathway have also been extensively reported in melanoma[41]. Many cancers including melanoma can exhibit pathologically high levels of Wnt signaling causing direct transcriptional changes throughout cancer progression such as during the stages of cell cycle[41]. *Cyclin D1* and *c-Myc*, key genes for G1-S progression have been reported as direct targets of this pathway and any alterations in these genes can lead to tumorigenesis and malignancy[41].

The Wnt/β-catenin pathway has been a subject of controversy in the field of melanoma and extensive efforts have been made to clarify the roles of Wnt in melanoma[41,42,43,44]. It has been proposed that the Wnt pathway follows a phenotype switching model in melanoma pathogenesis[41,45] (**Figure 1.13**). The canonical pathway

has been implicated in stages such as proliferation and tumorigenicity whereas the non-canonical pathway has been associated with invasiveness and metastasis[46,47]. Melanomas exhibit differential expression of Wnt/β-catenin pathway and many studies have associated elevated levels of β-catenin with poor survival and prognosis[41]. In contrast, many others have underlined Wnt pathway activation to have varying degree of prognosis for melanoma patients[43,48,49,50,51]. Despite extensive research, it has still been an open question as to whether Wnt is a major driver of proliferation in melanoma. Numerous efforts have been made to drug Wnt signaling in cancer[24,51]. A major challenge is targeting pathological Wnt signaling without perturbing Wnt signaling necessary for homeostasis in non-diseased tissues[52]. Given the tight regulation of this pathway throughout development and that many core Wnt signaling proteins are essential, the modulators or tuners of Wnt such as PLEKHA4 are ideal targets for therapy[24,26,53].

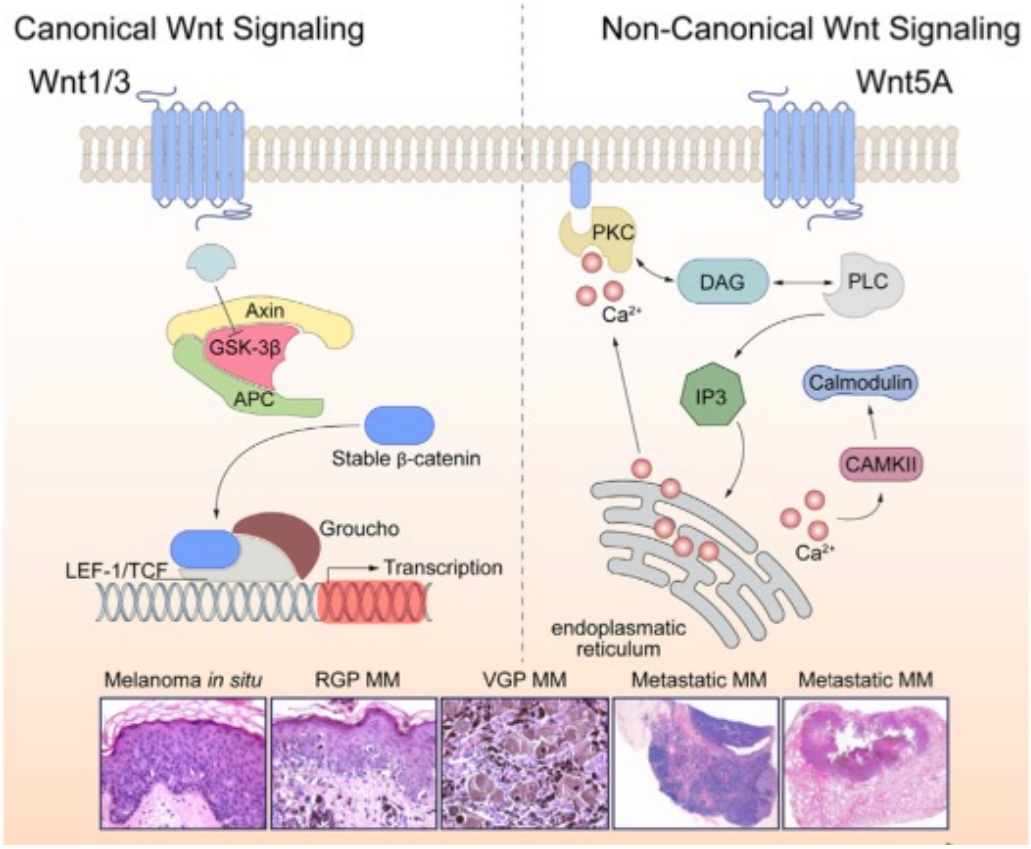

Figure 1.13 Wnt signaling pathways regulate phenotype switching in melanoma. The canonical pathway has been shown to majorly regulate the phenotypes at the earlier stages of melanoma transformation (e.g., proliferation). The non-canonical pathway has been shown to govern the phenotypes in the later stages of melanoma (ex: metastatic invasion and migration). Figure adapted with permission from Xue et al. *Cancer Treatment Reviews* **2016**[51].

1.9 Chapter 3 overview

In **Chapter 3**[54] of this dissertation, I report that melanoma cells require PLEKHA4 for survival and proliferation in vitro and in vivo in tumor xenografts. Attenuation of Wnt signaling using inhibitors or siRNA knockdown of core components block melanoma cell proliferation, establishing a key role for Wnt signaling in melanoma progression. Excitingly, such inhibition of Wnt signaling through knockdown of PLEKHA4 was effective both in BRAF and NRAS mutant

melanoma in vitro and in vivo. Further manipulation of PLEKHA4 in presence of Encorafenib (BRAF V600E/D inhibitor) in vivo displayed a striking additive effect revealing the therapeutic potential of PLEKHA4. **Chapter 3**[54] provides a molecular mechanism for PLEKHA4 as a key modulator of the strength of Wnt/β-catenin signaling in melanoma and sheds light to understanding the controversial role of Wnt in this disease. PLEKHA4 promotes Wnt/β-catenin mediated G1-S cell cycle transition and thus maintains cell proliferation in melanoma. **Chapter 3**[54] thus provides a basis for pharmacological inhibition of PLEKHA4 could represent a promising new targeted therapy avenue in melanoma. Overall, this dissertation provides a molecular basis for the biochemical characterization of PLEKHA4 in vitro and in vivo. This dissertation also establishes the modulatory role of PLEKHA4 in Wnt signaling and sheds light on the pathological role of PLEKHA4 and thus Wnt signaling in melanoma progression.

1.10 REFERENCES

(1) Wymann, M. P.; Schneiter, R. Lipid Signalling in Disease. *Nat. Rev. Mol. Cell Biol.* **2008**, *9* (2), 162–176. https://doi.org/10.1038/nrm2335.

(2) Fahy, E.; Cotter, D.; Sud, M.; Subramaniam, S. Lipid Classification, Structures and Tools. *Biochim. Biophys. Acta - Mol. Cell Biol. Lipids* **2011**, *1811* (11), 637–647.

(3) Gyamfi, D.; Awuah, E. O.; Owusu, S. *Classes, Nomenclature, and Functions of Lipids and Lipid-Related Molecules and the Dietary Lipids*; Elsevier Inc., 2018. https://doi.org/10.1016/B978-0-12-811297-7.00001-9.

(4) Balla, T. Phosphoinositides: Tiny Lipids with Giant Impact on Cell Regulation. *Physiol. Rev.* **2013**, *93* (3), 1019–1137. https://doi.org/10.1152/physrev.00028.2012.

(5) Dickson, E. J.; Hille, B. Understanding Phosphoinositides: Rare, Dynamic, and Essential Membrane Phospholipids. *Biochem J* **2019**, *476* (1), 1–23. https://doi.org/10.1042/BCJ20180022.

(6) Prestwich, G. D. Phosphoinositide Signaling: From Affinity Probes to Pharmaceutical Targets. *Chem. Biol.* **2004**, *11*, 619–637. https://doi.org/10.1016/j.chembiol .2004.03.025.

(7) Di Paolo, G.; De Camilli, P. Phosphoinositides in Cell Regulation and Membrane Dynamics. *Nature* **2006**, *443* (7112), 651–657. https://doi.org/10.1038/nature05185.

(8) Jean, S.; Kiger, A. A. Coordination between RAB GTPase Functions. *Nat. Rev. Mol. Cell Biol.* **2012**, *13*, 463.

(9) Idevall-Hagren, O.; De Camilli, P. Detection and Manipulation of Phosphoinositides. *Biochim. Biophys. Acta - Mol. Cell Biol. Lipids* **2015**, *1851* (6). https://doi.org/10.1016/j.bbalip.2014.12.008.

(10) Lemmon, M. A. Membrane Recognition by Phospholipid-Binding Domains. *Nat. Rev. Mol. Cell Biol.* **2008**, *9* (2), 99–111. https://doi.org/10.1038/nrm2328.

(11) Kutateladze, T. G. Translation of the Phosphoinositide Code by PI Effectors. *Nat. Chem. Biol.* **2010**, *6* (7), 507–513. https://doi.org/10.1038/nchembio.390.

(12) Haslam, R. J.; Koide, H. B.; Hemmings, B. A. Pleckstrin Domain Homology. *Nature* **1993**, *363*, 309–310.

(13) Mayer, B. J.; Ren, R.; Clark, K. L.; Baltimore, D. A Putative Modular Domain Present in Diverse Signaling Proteins. *Cell* **1993**, *73* (4), 629–630. https://doi.org/10.1016/0092-8674(93)90244-K.

(14) Tyers, M.; Haslam, R. J.; Rachubinski, R. A.; Harley, C. B. Molecular Analysis of Pleckstrin: The Major Protein Kinase C Substrate of Platelets. *J. Cell. Biochem.* **1989**, *40* (2), 133–145. https://doi.org/10.1002/jcb.240400202.

(15) Macias, M. J.; Musacchio, A.; Ponstlngl, H.; Nilges, M.; Saraste Be Hartmut Oschkinat, M. Structure of the Pleckstrin Homology Domain from P-Spectrin. *Huber, R. a/. J. molec. Bioi* **1988**, *333* (8), 103–106.

(16) Yoon, H. S.; Hajduk, P. J.; Petros, A. M.; Olejniczak, E. T.; Meadows, R. P.; Fesik, S. W.; Division, P. D.; Laboratories, A.; Park, A. Solution Structure of a Pleckstrin-Homology Domain. **1994**, *369* (June), 672–675.

(17) Lemmon, M. A.; Ferguson, K. M. Signal-Dependent Membrane Targeting by Pleckstrin Homology (PH) Domains. *Biochem. J.* **2000**, *350* (1), 1–18. https://doi.org/10.1042/0264-6021:3500001.

(18) Manna, P.; Jain, S. K. Phosphatidylinositol-3,4,5-Triphosphate and Cellular Signaling: Implications for Obesity and Diabetes Prasenjit. *Cell Physiol Biochem.* **2015**, *35* (4), 1253–1275. https://doi.org/10.1159/000373949.Phosphatidylinositol-3.

(19) Sekiya, F. Phospholipase C. In *Encyclopedia of Biological Chemistry (Second Edition)*; Lennarz, W. J., Lane, M. D., Eds.; Academic Press: Waltham, 2013; pp 467–471. https://doi.org/https://doi.org/10.1016/B978-0-12-378630-2.00346-7.

(20) Lemmon, M. A. Pleckstrin Homology (PH) Domains and Phosphoinositides. *Biochem. Soc. Symp.* **2007**, *74* (74), 81–93. https://doi.org/10.1042/BSS0740081.

(21) Dowler, S.; Currie, R. A.; Campbell, D. G.; Deak, M.; Kular, G.; Downes, C. P.; Alessi, D. R. Identification of Pleckstrin-Homology-Domain-Containing Proteins with Novel Phosphoinositide-Binding Specificities. *Biochem J* **2000**, *351* (Pt 1), 19–31. https://doi.org/10.1042/0264-6021:3510019.

(22) Jungmichel, S.; Sylvestersen, K. B.; Choudhary, C.; Nguyen, S.; Mann, M.; Nielsen, M. L. Specificity and Commonality of the Phosphoinositide-Binding Proteome Analyzed by Quantitative Mass Spectrometry. *Cell Rep.* **2014**, *6* (3), 578–591. https://doi.org/10.1016/j.celrep.2013.12.038.

(23) Shami Shah, A.; Batrouni, A. G.; Kim, D.; Punyala, A.; Cao, W.; Han, C.; Goldberg, M. L.; Smolka, M. B.; Baskin, J. M. PLEKHA4/Kramer Attenuates Dishevelled Ubiquitination to Modulate Wnt and Planar Cell Polarity Signaling. *Cell Rep.* **2019**, *27* (7), 2157-2170.e8. https://doi.org/10.1016/j.celrep.2019.04.060.

(24) Nusse, R.; Clevers, H. Wnt/β-Catenin Signaling, Disease, and Emerging Therapeutic Modalities. *Cell* **2017**, *169* (6), 985–999. https://doi.org/10.1016/j.cell.2017.05.016.

(25) Shami Shah, A.; Sun, H.; Baskin, J. M. For Wnt Signaling, Fucosylation of LRP6 Is a Bitter Pill. *Cell Chem. Biol.* **2020**, *27* (9), 1114–1116. https://doi.org/10.1016/j.chembiol.2020.08.003.

(26) MacDonald, B. T.; Tamai, K.; He, X. Wnt/β-Catenin Signaling: Components, Mechanisms, and Diseases. *Dev. Cell* **2009**, *17* (1), 9–26. https://doi.org/10.1016/j.devcel.2009.06.016.

(27) Komiya, Y.; Habas, R. Wnt Secretion and Extra-Cellular Regulators. *Biochem. Pharmacol.* **2008**, *4* (2), 68–75.

(28) Angers, S.; Thorpe, C. J.; Biechele, T. L.; Goldenberg, S. J.; Zheng, N.; MacCoss, M. J.; Moon, R. T. The KLHL12–Cullin-3 Ubiquitin Ligase Negatively Regulates the Wnt–β-Catenin Pathway by Targeting Dishevelled for Degradation. *Nat. Cell Biol.* **2006**, *8* (4), 348–357. https://doi.org/10.1038/ncb1381.

(29) Angers, S.; Moon, R. T. Proximal Events in Wnt Signal Transduction. *Nat. Rev. Mol. Cell Biol.* **2009**, *10* (juLY), 1–10. https://doi.org/10.1038/nrm2717.

(30) Huang, J. K.; Jarjour, A. A.; Oumesmar, B. N.; Kerninon, C.; Williams, A.; Krezel, W.; Kagechika, H.; Bauer, J.; Zhao, C.; Evercooren, A. B. Van; Chambon, P.; Ffrench-Constant, C.; Franklin, R. J. M. Retinoid X Receptor Gamma Signaling Accelerates CNS Remyelination. *Nat. Neurosci.* **2011**, *14* (1), 45–55. https://doi.org/10.1038/nn.2702.

(31) Hashimoto, R.; Nakazawa, T.; Tsurusaki, Y.; Yasuda, Y.; Nagayasu, K.; Matsumura, K.; Kawashima, H.; Yamamori, H.; Fujimoto, M.; Ohi, K.; Umeda-Yano, S.; Fukunaga, M.; Fujino, H.; Kasai, A.; Hayata-Takano, A.; Shintani, N.; Takeda, M.; Matsumoto, N.; Hashimoto, H. Whole-Exome Sequencing and Neurite Outgrowth Analysis in Autism Spectrum Disorder. *J.Hum.Genet.* **2015**, *61* (1435-232X (Electronic)), 1–8. https://doi.org/10.1038/jhg.2015.141.

(32) Hanahan, D.; Weinberg, R. A. Hallmarks of Cancer: The next Generation. *Cell* **2011**, *144* (5), 646–674. https://doi.org/10.1016/j.cell.2011.02.013.

(33) Akbani, R.; Akdemir, K. C.; Aksoy, B. A.; Albert, M.; Ally, A.; Amin, S. B.; Arachchi, H.; Arora, A.; Auman, J. T.; Ayala, B.; Baboud, J.; Balasundaram, M.; Balu, S.; Barnabas, N.; Bartlett, J.; Bartlett, P.; Bastian, B. C.; Baylin, S. B.; Behera, M.; Belyaev, D.; Benz, C.; Bernard, B.; Beroukhim, R.; Bir, N.; Black, A. D.; Bodenheimer, T.; Boice, L.; Boland, G. M.; Bono, R.; Bootwalla, M. S.; Bosenberg, M.; Bowen, J.; Bowlby, R.; Bristow, C. A.; Brockway-Lunardi, L.; Brooks, D.; Brzezinski, J.; Bshara, W.; Buda, E.; Burns, W. R.; Butterfield, Y. S. N.; Button, M.; Calderone, T.; Cappellini, G. A.; Carter, C.; Carter, S. L.; Cherney, L.; Cherniack, A. D.; Chevalier, A.; Chin, L.; Cho, J.; Cho, R. J.; Choi, Y. La; Chu, A.; Chudamani, S.; Cibulskis, K.; Ciriello, G.; Clarke, A.; Coons, S.; Cope, L.; Crain, D.; Curley, E.; Danilova, L.; D'Atri, S.; Davidsen, T.; Davies, M. A.; Delman, K. A.; Demchok, J. A.; Deng, Q. A.; Deribe, Y. L.; Dhalla, N.; Dhir, R.; Dicara, D.; Dinikin, M.; Dubina, M.; Ebrom, J. S.; Egea, S.; Eley, G.; Engel, J.; Eschbacher, J. M.; Fedosenko, K. V.; Felau, I.; Fennell, T.; Ferguson, M. L.; Fisher, S.; Flaherty, K. T.; Frazer, S.; Frick, J.; Fulidou, V.; Gabriel, S. B.; Gao, J.; Gardner, J.; Garraway, L. A.; Gastier-Foster, J. M.; Gaudioso, C.; Gehlenborg, N.; Genovese, G.; Gerken, M.; Gershenwald, J. E.; Getz, G.; Gomez-Fernandez, C.; Gribbin, T.; Grimsby, J.; Gross, B.; Guin, R.; Gutschner, T.; Hadjipanayis, A.; Halaban, R.; Hanf, B.; Haussler, D.; Haydu, L. E.; Hayes, D. N.; Hayward, N. K.; Heiman, D. I.; Herbert, L.; Herman, J. G.; Hersey, P.; Hoadley, K. A.; Hodis, E.; Holt, R. A.; Hoon, D. S.; Hoppough, S.; Hoyle, A. P.; Huang, F. W.; Huang, M.; Huang, S.; Hutter, C. M.; Ibbs, M.; Iype, L.; Jacobsen, A.; Jakrot, V.; Janning, A.; Jeck, W. R.; Jefferys, S. R.; Jensen, M. A.; Jones, C. D.; Jones, S. J. M.; Ju, Z.; Kakavand, H.; Kang, H.; Kefford, R. F.; Khuri, F. R.; Kim, J.; Kirkwood, J. M.; Klode, J.; Korkut, A.; Korski, K.; Krauthammer, M.; Kucherlapati, R.; Kwong, L. N.; Kycler, W.; Ladanyi, M.; Lai, P. H.; Laird, P. W.; Lander, E.; Lawrence, M. S.; Lazar, A. J.; Łaźniak, R.; Lee, D.; Lee, J. E.; Lee, J.; Lee, K.; Lee, S.; Lee, W.; Leporowska, E.; Leraas, K. M.; Li, H. I.; Lichtenberg, T. M.; Lichtenstein, L.; Lin, P.; Ling, S.; Liu, J.; Liu, O.; Liu, W.; Long, G. V.; Lu, Y.; Ma, S.; Ma, Y.; Mackiewicz, A.; Mahadeshwar, H. S.; Malke, J.; Mallery, D.; Manikhas, G. M.; Mann, G. J.; Marra, M. A.; Matejka, B.; Mayo, M.; Mehrabi, S.; Meng, S.; Meyerson, M.; Mieczkowski, P. A.; Miller, J. P.; Miller, M. L.; Mills, G. B.; Moiseenko, F.; Moore, R. A.; Morris, S.; Morrison, C.; Morton, D.; Moschos, S.; Mose, L. E.; Muller, F. L.; Mungall, A. J.; Murawa, D.; Murawa, P.; Murray, B. A.; Nezi, L.; Ng, S.; Nicholson, D.; Noble, M. S.; Osunkoya, A.; Owonikoko, T. K.; Ozenberger, B. A.; Pagani, E.; Paklina, O. V.; Pantazi, A.; Parfenov, M.; Parfitt, J.; Park, P. J.; Park, W. Y.; Parker, J. S.; Passarelli, F.; Penny, R.; Perou, C. M.; Pihl, T. D.; Potapova, O.; Prieto, V. G.; Protopopov, A.; Quinn, M. J.; Radenbaugh, A.; Rai, K.; Ramalingam, S. S.; Raman, A. T.; Ramirez, N. C.; Ramirez, R.; Rao, U.; Rathmell, W. K.; Ren, X.; Reynolds, S. M.; Roach, J.; Robertson, A. G.; Ross, M. I.; Roszik, J.; Russo, G.; Saksena, G.; Saller, C.; Samuels, Y.; Sander, C.; Sander, C.; Sandusky, G.; Santoso, N.; Saul, M.; Saw, R. P.; Schadendorf, D.; Schein, J. E.; Schultz, N.;

Schumacher, S. E.; Schwallier, C.; Scolyer, R. A.; Seidman, J.; Sekhar, P. C.; Sekhon, H. S.; Senbabaoglu, Y.; Seth, S.; Shannon, K. F.; Sharpe, S.; Sharpless, N. E.; Shaw, K. R. M.; Shelton, C.; Shelton, T.; Shen, R.; Sheth, M.; Shi, Y.; Shiau, C. J.; Shmulevich, I.; Sica, G. L.; Simons, J. V.; Sinha, R.; Sipahimalani, P.; Sofia, H. J.; Soloway, M. G.; Song, X.; Sougnez, C.; Spillane, A. J.; Spychała, A.; Stretch, J. R.; Stuart, J.; Suchorska, W. M.; Sucker, A.; Sumer, S. O.; Sun, Y.; Synott, M.; Tabak, B.; Tabler, T. R.; Tam, A.; Tan, D.; Tang, J.; Tarnuzzer, R.; Tarvin, K.; Tatka, H.; Taylor, B. S.; Teresiak, M.; Thiessen, N.; Thompson, J. F.; Thorne, L.; Thorsson, V.; Trent, J. M.; Triche, T. J.; Tsai, K. Y.; Tsou, P.; Van Den Berg, D. J.; Van Allen, E. M.; Veluvolu, U.; Verhaak, R. G.; Voet, D.; Voronina, O.; Walter, V.; Walton, J. S.; Wan, Y.; Wang, Y.; Wang, Z.; Waring, S.; Watson, I. R.; Weinhold, N.; Weinstein, J. N.; Weisenberger, D. J.; White, P.; Wilkerson, M. D.; Wilmott, J. S.; Wise, L.; Wiznerowicz, M.; Woodman, S. E.; Wu, C. J.; Wu, C. C.; Wu, J.; Wu, Y.; Xi, R.; Xu, A. W.; Yang, D.; Yang, L.; Yang, L.; Zack, T. I.; Zenklusen, J. C.; Zhang, H.; Zhang, J.; Zhang, W.; Zhao, X.; Zhu, J.; Zhu, K.; Zimmer, L.; Zmuda, E.; Zou, L. Genomic Classification of Cutaneous Melanoma. *Cell* **2015**, *161* (7), 1681–1696. https://doi.org/10.1016/j.cell.2015.05.044.

(34) Hruz, T.; Laule, O.; Szabo, G.; Wessendorp, F.; Bleuler, S.; Oertle, L.; Widmayer, P.; Gruissem, W.; Zimmermann, P. Genevestigator V3: A Reference Expression Database for the Meta-Analysis of Transcriptomes. *Adv. Bioinformatics* **2008**, *2008*, 1–5. https://doi.org/10.1155/2008/420747.

(35) Domingues, B.; Lopes, J.; Soares, P.; Populo, H. Melanoma Treatment in Review. *ImmunoTargets Ther.* **2018**, *Volume 7*, 35–49. https://doi.org/10.2147/itt.s134842.

(36) Hayward, N. K.; Wilmott, J. S.; Waddell, N.; Johansson, P. A.; Field, M. A.; Nones, K.; Patch, A.-M.; Kakavand, H.; Alexandrov, L. B.; Burke, H.; Jakrot, V.; Kazakoff, S.; Holmes, O.; Leonard, C.; Sabarinathan, R.; Mularoni, L.; Wood, S.; Xu, Q.; Waddell, N.; Tembe, V.; Pupo, G. M.; De Paoli-Iseppi, R.; Vilain, R. E.; Shang, P.; Lau, L. M. S.; Dagg, R. A.; Schramm, S.-J.; Pritchard, A.; Dutton-Regester, K.; Newell, F.; Fitzgerald, A.; Shang, C. A.; Grimmond, S. M.; Pickett, H. A.; Yang, J. Y.; Stretch, J. R.; Behren, A.; Kefford, R. F.; Hersey, P.; Long, G. V; Cebon, J.; Shackleton, M.; Spillane, A. J.; Saw, R. P. M.; López-Bigas, N.; Pearson, J. V; Thompson, J. F.; Scolyer, R. A.; Mann, G. J. Whole-Genome Landscapes of Major Melanoma Subtypes. *Nature* **2017**, *545* (7653), 175–180. https://doi.org/10.1038/nature22071.

(37) Long, G. V; Stroyakovskiy, D.; Gogas, H.; Levchenko, E.; de Braud, F.; Larkin, J.; Garbe, C.; Jouary, T.; Hauschild, A.; Grob, J. J.; Chiarion Sileni, V.; Lebbe, C.; Mandalà, M.; Millward, M.; Arance, A.; Bondarenko, I.; Haanen, J. B. A. G.; Hansson, J.; Utikal, J.; Ferraresi, V.; Kovalenko, N.; Mohr, P.; Probachai, V.; Schadendorf, D.; Nathan, P.; Robert, C.; Ribas, A.; DeMarini, D.

J.; Irani, J. G.; Casey, M.; Ouellet, D.; Martin, A.-M.; Le, N.; Patel, K.; Flaherty, K. Combined BRAF and MEK Inhibition versus BRAF Inhibition Alone in Melanoma. *N. Engl. J. Med.* **2014**, *371* (20), 1877–1888. https://doi.org/10.1056/NEJMoa1406037.

(38) Larkin, J.; Ascierto, P. A.; Dréno, B.; Atkinson, V.; Liszkay, G.; Maio, M.; Mandalà, M.; Demidov, L.; Stroyakovskiy, D.; Thomas, L.; de la Cruz-Merino, L.; Dutriaux, C.; Garbe, C.; Sovak, M. A.; Chang, I.; Choong, N.; Hack, S. P.; McArthur, G. A.; Ribas, A. Combined Vemurafenib and Cobimetinib in BRAF-Mutated Melanoma. *N. Engl. J. Med.* **2014**, *371* (20), 1867–1876. https://doi.org/10.1056/NEJMoa1408868.

(39) Hamid, O.; Robert, C.; Daud, A.; Hodi, F. S.; Hwu, W.-J.; Kefford, R.; Wolchok, J. D.; Hersey, P.; Joseph, R. W.; Weber, J. S.; Dronca, R.; Gangadhar, T. C.; Patnaik, A.; Zarour, H.; Joshua, A. M.; Gergich, K.; Elassaiss-Schaap, J.; Algazi, A.; Mateus, C.; Boasberg, P.; Tumeh, P. C.; Chmielowski, B.; Ebbinghaus, S. W.; Li, X. N.; Kang, S. P.; Ribas, A. Safety and Tumor Responses with Lambrolizumab (Anti–PD-1) in Melanoma. *N. Engl. J. Med.* **2013**, *369* (2), 134–144. https://doi.org/10.1056/NEJMoa1305133.

(40) Lito, P.; Rosen, N.; Solit, D. B. Tumor Adaptation and Resistance to RAF Inhibitors. *Nat. Med.* **2013**, *19* (11), 1401–1409. https://doi.org/10.1038/nm.3392.

(41) Zhan, T.; Rindtorff, N.; Boutros, M. Wnt Signaling in Cancer. *Oncogene* **2017**, *36* (11), 1461–1473. https://doi.org/10.1038/onc.2016.304.

(42) Webster, M. R.; Weeraratna, A. T. A Wnt-Er Migration: The Confusing Role of β-Catenin in Melanoma Metastasis. *Sci. Signal.* **2013**, *6* (268), pe11. https://doi.org/10.1126/scisignal.2004114.

(43) Jackstadt, R.; Hodder, M. C.; Sansom, O. J. WNT and β-Catenin in Cancer: Genes and Therapy. *Annu. Rev. Cancer Biol.* **2020**, *4* (1), 177–196. https://doi.org/10.1146/annurev-cancerbio-030419-033628.

(44) Gajos-Michniewicz, A.; Czyz, M. Wnt Signaling in Melanoma. *Int J Mol Sci* **2020**, *21*, 4852.

(45) Webster, M. R.; Kugel, C. H.; Weeraratna, A. T. The Wnts of Change: How Wnts Regulate Phenotype Switching in Melanoma. *Biochim. Biophys. Acta - Rev. Cancer* **2015**, *1856* (2), 244–251. https://doi.org/10.1016/j.bbcan.2015.10.002.

(46) Webster, M. R.; Xu, M.; Kinzler, K. A.; Kaur, A.; Appleton, J.; O'Connell, M.

P.; Marchbank, K.; Valiga, A.; Dang, V. M.; Perego, M.; Zhang, G.; Slipicevic, A.; Keeney, F.; Lehrmann, E.; Wood III, W.; Becker, K. G.; Kossenkov, A. V; Frederick, D. T.; Flaherty, K. T.; Xu, X.; Herlyn, M.; Murphy, M. E.; Weeraratna, A. T. Wnt5A Promotes an Adaptive, Senescent-like Stress Response, While Continuing to Drive Invasion in Melanoma Cells. *Pigment Cell Melanoma Res.* **2015**, *28* (2), 184–195. https://doi.org/10.1111/pcmr.12330.

(47) Anastas, J. N.; Kulikauskas, R. M.; Tamir, T.; Rizos, H.; Long, G. V; von Euw, E. M.; Yang, P.-T.; Chen, H.-W.; Haydu, L.; Toroni, R. A.; Lucero, O. M.; Chien, A. J.; Moon, R. T. WNT5A Enhances Resistance of Melanoma Cells to Targeted BRAF Inhibitors. *J. Clin. Invest.* **2014**, *124* (7), 2877–2890. https://doi.org/10.1172/JCI70156.

(48) Kageshita, T.; Hamby, C. V; Ishihara, T.; Matsumoto, K.; Saida, T.; Ono, T. Loss of β-Catenin Expression Associated with Disease Progression in Malignant Melanoma. *Br. J. Dermatol.* **2001**, *145* (2), 210–216. https://doi.org/10.1046/j.1365-2133.2001.04336.x.

(49) Bachmann, I. M.; Straume, O.; Puntervoll, H. E.; Kalvenes, M. B.; Akslen, L. A. Importance of P-Cadherin, β-Catenin, and Wnt5a/Frizzled for Progression of Melanocytic Tumors and Prognosis in Cutaneous Melanoma. *Clin. Cancer Res.* **2005**, *11* (24), 8606 LP – 8614. https://doi.org/10.1158/1078-0432.CCR-05-0011.

(50) Chien, A. J.; Moore, E. C.; Lonsdorf, A. S.; Kulikauskas, R. M.; Rothberg, B. G.; Berger, A. J.; Major, M. B.; Hwang, S. T.; Rimm, D. L.; Moon, R. T. Activated Wnt/ß-Catenin Signaling in Melanoma Is Associated with Decreased Proliferation in Patient Tumors and a Murine Melanoma Model. *Proc. Natl. Acad. Sci.* **2009**, *106* (4), 1193–1198. https://doi.org/10.1073/pnas.0811902106.

(51) Xue, G.; Romano, E.; Massi, D.; Mandalà, M. Wnt/β-Catenin Signaling in Melanoma: Preclinical Rationale and Novel Therapeutic Insights. *Cancer Treat. Rev.* **2016**, *49*, 1–12. https://doi.org/10.1016/j.ctrv.2016.06.009.

(52) Kahn, M. Can We Safely Target the WNT Pathway? *Nat. Rev. Drug Discov.* **2014**, *13* (7), 513–532. https://doi.org/10.1038/nrd4233.

(53) Clevers, H.; Nusse, R. Wnt/β-Catenin Signaling and Disease. *Cell* **2012**, *149* (6), 1192–1205. https://doi.org/10.1016/j.cell.2012.05.012.

(54) Shami Shah, A.; Cao, X.; White, A. C.; Baskin, J. M. PLEKHA4 Promotes Wnt/Beta-Catenin Signaling-Mediated G1/S Transition and Proliferation in Melanoma. *Cancer Res.* **2021**, No. 607, canres.2584.2020. https://doi.org/10.1158/0008-5472.can-20-2584.

CHAPTER 2

PLEKHA4/*KRAMER* ATTENUATES DISHEVELLED UBIQUITINATION TO MODULATE WNT AND PLANAR CELL POLARITY SIGNALING

2.1 ABSTRACT

Wnt signaling pathways direct key physiological decisions in development. Here, we establish a role for a pleckstrin homology domain-containing protein, PLEKHA4, as a modulator of signaling strength in Wnt-receiving cells. PLEKHA4 oligomerizes into clusters at PI(4,5)P_2-rich regions of the plasma membrane and recruits the Cullin-3 (CUL3) E3 ubiquitin ligase substrate adaptor Kelch-like protein 12 (KLHL12) to these assemblies. This recruitment decreases CUL3–KLHL12-mediated polyubiquitination of Dishevelled, a central intermediate in canonical and non-canonical Wnt signaling. Knockdown of PLEKHA4 in mammalian cells demonstrates that PLEKHA4 positively regulates canonical and non-canonical Wnt signaling via these effects on the Dishevelled polyubiquitination machinery. In vivo knockout of the *Drosophila melanogaster* PLEKHA4 homolog, *kramer*, selectively affects the non-canonical, planar cell polarity (PCP) signaling pathway. We propose that PLEKHA4 tunes the sensitivities of cells toward stimulation of Wnt or PCP signaling by sequestering a key E3 ligase adaptor controlling Dishevelled polyubiquitination within PI(4,5)P_2-rich plasma membrane clusters.

2.2 INTRODUCTION

Wnt signaling controls key cell fate decisions in the development of multicellular eukaryotes, and its dysregulation can cause many human diseases[1]. As such, Wnt signaling is subject to many points and types of regulation, both in cells that produce and in those that receive the secreted Wnt signals. In the Wnt-receiving cell, engagement of Wnt proteins by the Frizzled family of cell-surface receptors[2] can activate different intracellular signaling pathways, including the canonical, β-catenin-dependent pathway and the non-canonical planar cell polarity (PCP) and Wnt–Ca^{2+} routes[3–7].

A feature common to all Wnt signaling pathways is the involvement of the cytoplasmic protein Dishevelled (DVL), whose recruitment to the plasma membrane upon Wnt binding to Frizzled initiates the intracellular signal transduction pathways. Because of this dynamic behavior, the DVL proteins represent key factors that Wnt-receiving cells can use to tune the strength of the Wnt signal[8–10]. DVL levels are modulated by ubiquitination[11–16]. In particular, the E3 ubiquitin ligase Cullin-3 (CUL3), in complex with one of its substrate adaptors, Kelch-like protein 12 (KLHL12), catalyzes the polyubiquitination of DVL3, leading to the latter's proteasomal degradation[11]. By lowering DVL3 levels, the CUL3–KLHL12 E3 ligase diminishes the strength of Wnt signaling. Given that cells must dynamically tune their Wnt ligand sensitivities to different physiological settings, a major unanswered question is how this activity of CUL3–KLHL12 toward DVL3 is regulated.

CUL3 interacts physiologically with adaptors other than KLHL12[17] and, in complex with KLHL12, functions at intracellular locations distinct from the plasma

membrane[18,19]. For example, at the endoplasmic reticulum, CUL3–KLHL12 mediates monoubiquitination of the COPII vesicle component SEC31 to facilitate the formation of enlarged COPII vesicles that transport large cargoes such as collagen to the Golgi complex; local bursts of calcium regulate this action of CUL3–KLHL12 via the calcium-binding adaptor proteins PEF1 and ALG2[18,20]. It remains unknown how these distinct activities of CUL3–KLHL12 are regulated. What factors modulate the interaction of CUL3–KLHL12 with DVL3? Do such putative factors act analogously to how PEF1 and ALG2 regulate CUL3–KLHL12 activity at the ER? One possibility is that plasma membrane-localized factors control CUL3–KLHL12 activity toward DVL3 in this membrane, the site of DVL3 action in Wnt signaling.

Key signaling molecules at the plasma membrane are the phosphoinositides (PIPs) PI4P and PI(4,5)P_2, which function in part by recruiting soluble proteins to the plasma membrane and allosterically regulating their function[21,22]. The largest family of PIP-binding proteins in humans consists of the ~250 proteins containing a pleckstrin homology (PH) domain[23]. Although a small minority of PH domain-containing proteins are known to bind a specific PIP species and to elicit defined signaling outcomes (e.g., PH domains from AKT and BTK), the molecular properties and physiological functions of the vast majority of PH domain-containing proteins remain unknown[24].

Here, we report that the uncharacterized protein PLEKHA4 (Pleckstrin homology domain-containing family A, member 4) is a plasma membrane-localized signaling adaptor that regulates CUL3–KLHL12-mediated ubiquitination of DVL3 and thus tunes the strength of Wnt signaling. We find that PLEKHA4 molecules

assemble at PI(4,5)P_2-rich regions of the plasma membrane, via a unique combination of its lipid-binding, oligomerization, and intrinsically disordered domains. PLEKHA4 physically interacts with CUL3–KLHL12 to recruit the E3 ligase to these plasma membrane assemblies. Surprisingly, this recruitment is accompanied by a decrease in CUL3–KLHL12 E3 ligase activity toward DVL, its substrate whose site of action in both the canonical Wnt and PCP signaling pathways is the plasma membrane. Consequently, PLEKHA4 causes DVL to accumulate, upregulating Wnt signaling in cultured mammalian cells. A knockout of the *Drosophila* PLEKHA4 homolog, *kramer*, exhibits defects in PCP signaling, speaking to the physiological relevance of our in vitro findings. We thus propose PLEKHA4 as a key modulator of Wnt and PCP signaling pathways through its function as an adaptor that tunes CUL3–KLHL12 activity at the plasma membrane.

2.3 RESULTS

2.3.1 *PLEKHA4 localizes to the plasma membrane via interactions with PI(4,5)P_2*

Our interest in PLEKHA4 emerged from a motivation to understand roles for phosphoinositides in directing signaling via engagement of their head group by effector proteins bearing both PH domains and additional domains for mediating signaling. PH domain-containing proteins number approximately 250 in humans, and the majority have not been extensively characterized[25]. In particular, the PH domain-containing protein PLEKHA4, also known as PEPP1, is part of a family that includes several mediators of intracellular signaling (e.g., FAPP1/2[26,27], TAPP1/2[28], and PLEKHA7/Hadp1[29]). Other than a single report suggesting that its PH domain binds

to phosphatidylinositol 3-phosphate (PI3P)[30] and a computational study predicting that its PH domain binds to phosphatidylinositol 3,4,5-trisphosphate ($PI(3,4,5)P_3$)[31], PLEKHA4 is an unstudied protein with no known cellular functions. We thus set out to elucidate its molecular properties, subcellular localization, protein interaction partners, and cellular and physiological roles.

We began our studies of PLEKHA4 by examining the properties of the PH domain and how it influences the protein's subcellular localization. We found that a fluorescent protein fusion to PLEKHA4 localized to the plasma membrane (**Figure 2.1A**). This result was surprising, because protein-lipid overlay assays had previously suggested to other investigators that the PH domain of PLEKHA4 binds to PI3P, which localizes to endosomes and not to the plasma membrane[30,32].

We revisited the PIP binding of the PLEKHA4 PH domain (residues 45–167), using liposome sedimentation assays that assess protein-lipid interactions in the context of intact lipid bilayers, which represent a more physiologically relevant environment[33]. Intriguingly, the PLEKHA4 PH domain partially co-sedimented with liposomes containing any one of the three bis-phosphorylated PIPs ($PI(3,4)P_2$, $PI(3,5)P_2$, and $PI(4,5)P_2$) and exhibited little affinity for PI3P or the other PIP species (**Figure 2.1B**). Though moderate, the observed binding was specific, as it was abolished by mutation of either of two key Arg residues in the PH domain predicted by a crystal structure to contact the PIP head group[34] (**Figure 2.1C** and **Figure S2.1A**).

A GFP-tagged PH domain adopted a diffuse cytosolic localization, suggesting that a monomeric PH domain was not sufficient to confer membrane targeting of

PLEKHA4 (**Figure 2.1D**). We noticed that just upstream of the PH domain were two other motifs that could potentially mediate membrane binding: a putative amphipathic helix (H, residues 28–41) and a basic peptide (BP, residues 42–50) (**Figure S2.1A**). The fusion of these motifs to the PH domain afforded a minimal construct (PLEKHA4$^{H\text{-}BP\text{-}PH}$, residues 28–167) that mediated both strong and specific co-sedimentation with PI(4,5)P_2-containing liposomes and localization to the plasma membrane within cells (**Figure 2.1E–F**). Importantly, either a single F40E mutation in the helix motif or a quadruple mutation of Arg/Lys residues within the basic peptide to Ala (4A) abolished binding to PI(4,5)P_2-containing liposomes and the plasma membrane localization of a GFP fusion to this minimal construct (**Figure 2.1G–H** and **Figure S2.1A**).

To further establish the requirement of PI(4,5)P_2 for the plasma membrane localization of the PLEKHA4$^{H\text{-}BP\text{-}PH}$ construct, we transiently depleted this lipid by stimulation of cells expressing the M1 muscarinic receptor (M1R) with its ligand, oxotremorine M, to induce phospholipase C-mediated PI(4,5)P_2 hydrolysis[35,36]. Activation of M1R in HeLa cells expressing H-BP-PH caused shifts in localization of both a PI(4,5)P_2 reporter (PH domain of PLCδ1) and GFP-tagged PLEKHA4$^{H\text{-}BP\text{-}PH}$ from the plasma membrane to the cytosol (**Figure S2.1B**).

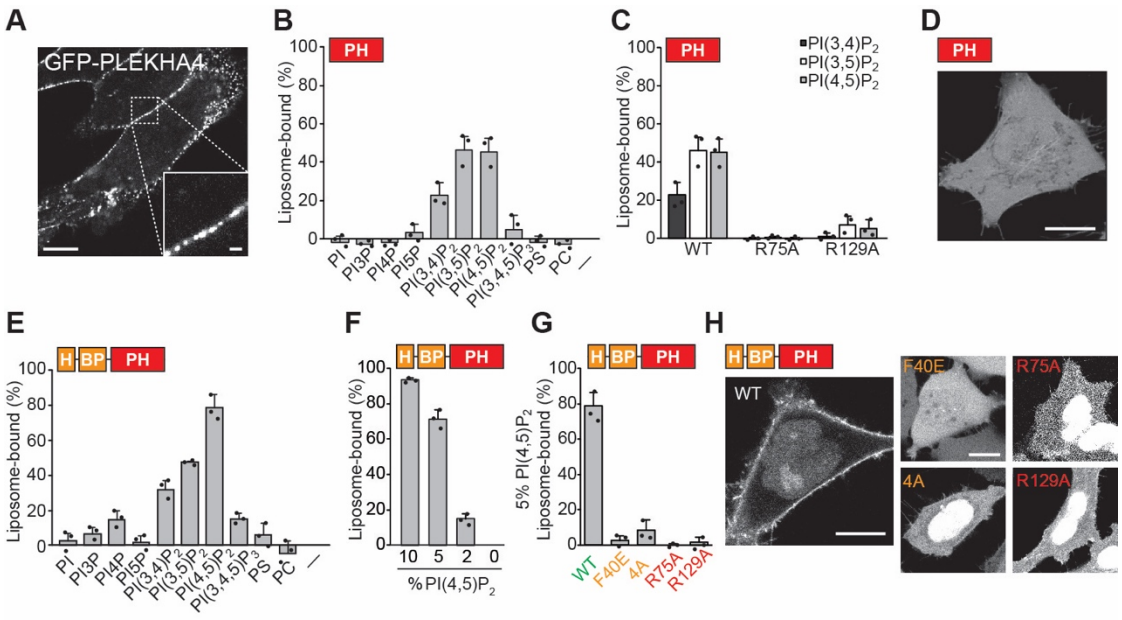

Figure 2.1 PLEKHA4 localizes to the plasma membrane via recognition of PI(4,5)P_2.

(A) Confocal microscopy of HeLa cells transfected with GFP-PLEKHA4. (B–G) Lipid-binding assays via co-sedimentation of PLEKHA4 domains with liposomes. Graphs show percentage of protein construct that co-sediments with an excess of liposome of defined composition. (B–C) Co-sedimentation of the wildtype (B) or indicated point mutants (C) of the PLEKHA4 PH domain (amino acids 54–167) with liposomes with 5% of the indicated PIP (or 20% of dioleoylphosphatidylserine, PS) and the remainder as dioleoylphosphatidylcholine (PC) (n = 3). The (–) sign indicates no liposomes. (D) Confocal microscopy of HeLa cells transfected with a GFP-tagged PLEKHA4 PH domain (GFP-PLEKHA4PH). (E–G) Co-sedimentation of wild-type (E–F) or indicated point mutants (G) of a fusion of amphipathic helix, basic peptide, and PH domain (PLEKHA4H-BP-PH, amino acids 28–167) with liposomes containing 5% of the indicated PIP (or 20% PS) and the remainder as PC (E), the indicated concentration of PI(4,5)P2 (F), or 5% PI(4,5)P2 (G) (n = 3). (H) Confocal microscopy of wild-type or the indicated mutant of GFP-PLEKHA4H-BP-PH. 4A refers to the quadruple mutant K42A/R43A/R48A/R49A. Scale bars: 10 μm (A (full-size), D, H); 1 μm (A (inset)). See also **Figure S2.1**.

2.3.2 *PLEKHA4 assembles into higher-order structures at the plasma membrane*

The above data establish a sequence of three N-terminal motifs responsible for PLEKHA4 plasma membrane localization. However, full-length PLEKHA4 is not uniformly distributed at the plasma membrane but is instead strikingly localized to

puncta visible by conventional confocal microscopy (**Figure 2.1A**) and super-resolution structured illumination microscopy (**Figure 2.2A**). Thus, additional factors beyond the N-terminal PI(4,5)P_2-binding domains might control the localization and/or assembly of the full-length protein.

The PLEKHA4 puncta did not colocalize with markers of established assemblies at the plasma membrane, including clathrin-coated pits, caveolae, or endoplasmic reticulum–plasma membrane contact sites (**Figure S2.2A–C**). We also observed no colocalization with endosomal and lysosomal markers, consistent with our finding that the PH domain does not bind to PI3P (**Figure S2.2D**). We thus hypothesized that the puncta were the result of PLEKHA4 self-association. PLEKHA4 has two adjacent domains at the C terminus that potentially could be responsible for oligomerization into higher-order structures: a coiled coil domain (CC) and an intrinsically disordered region (IDR).

Biochemical and imaging experiments support a role for both of these domains in the formation of the PLEKHA4 clusters. First, the isolated CC domain was cytoplasmically localized but could be recruited to the plasma membrane by co-overexpression with full-length PLEKHA4, suggesting a role in dimerization or higher-order oligomerization (**Figure 2.2B**). Second, a version of PLEKHA4 lacking the IDR remained at the plasma membrane but no longer assembled into puncta (**Figure 2.2A**). Third, a fusion of the CC and IDR domains formed large puncta in the cytoplasm that could, like the isolated CC domain, be recruited to the plasma membrane by full-length PLEKHA4 (**Figure 2.2B**). To complement these imaging data, we found via co-immunoprecipitation (co-IP) assays that both the isolated CC

domain and a CC–IDR fusion could physically interact with full-length PLEKHA4 (**Figure 2.2C**).

The requirement of the IDR for puncta formation and the failure of full-length PLEKHA4 to colocalize with known organelle markers led us to hypothesize that the PLEKHA4 puncta may represent liquid-liquid phase-separated domains. Also referred to as membrane-less organelles, these structures form via controlled aggregation of proteins and other biological molecules and can lead to their sequestration from the bulk cytosol[37–40]. A recently recognized mechanism of phase separation in biological systems is via non-covalent interactions between highly unstructured, intrinsically disordered protein domains[41–43].

To test whether the IDR of PLEKHA4 can mediate assembly into higher-order structures within cells, we deployed an optogenetic method that capitalizes on the propensity of the protein Cryptochrome-2 (CRY2) to homo-oligomerize upon exposure to blue light. By fusing a putative IDR to mCherry-tagged CRY2, light can be used to trigger the formation of highly fluorescent, spherical cytoplasmic aggregates termed optoDroplets whose presence indicates that the IDR can mediate cluster formation[44,45].

We generated mCherry-CRY2 fusion constructs to either the PLEKHA4 IDR or the CC–IDR domains. Exposure of cells expressing these domains to blue light led to rapid formation of intensely fluorescent cytoplasmic aggregates (**Figure 2.2D**). Removal of blue light stimulation led to a partial disaggregation, indicating that cluster formation was reversible. As a negative control, irradiation of cells expressing

mCherry-CRY2 under identical conditions did not lead to aggregate formation (**Figure 2.2D**).

These results indicate that the C-terminal domains of PLEKHA4 are capable of assembly into higher-order structures in a cellular context. To further bolster the notion that avidity and cluster formation is a strong driving force for PLEKHA4 assembly at the plasma membrane, we note that transient $PI(4,5)P_2$ depletion did not cause a substantial shift in the localization of full-length GFP-PLEKHA4 (**Figure S2.1C**). Attempts to purify the isolated C-terminal domains or full-length protein for in vitro analysis were not successful, and a comprehensive in vitro characterization would be necessary to fully understand the nature of the plasma membrane PLEKHA4 puncta. Nevertheless, it is interesting to speculate that the PLEKHA4-positive puncta at the plasma membrane may represent oligomeric, liquid-liquid phase-separated clusters.

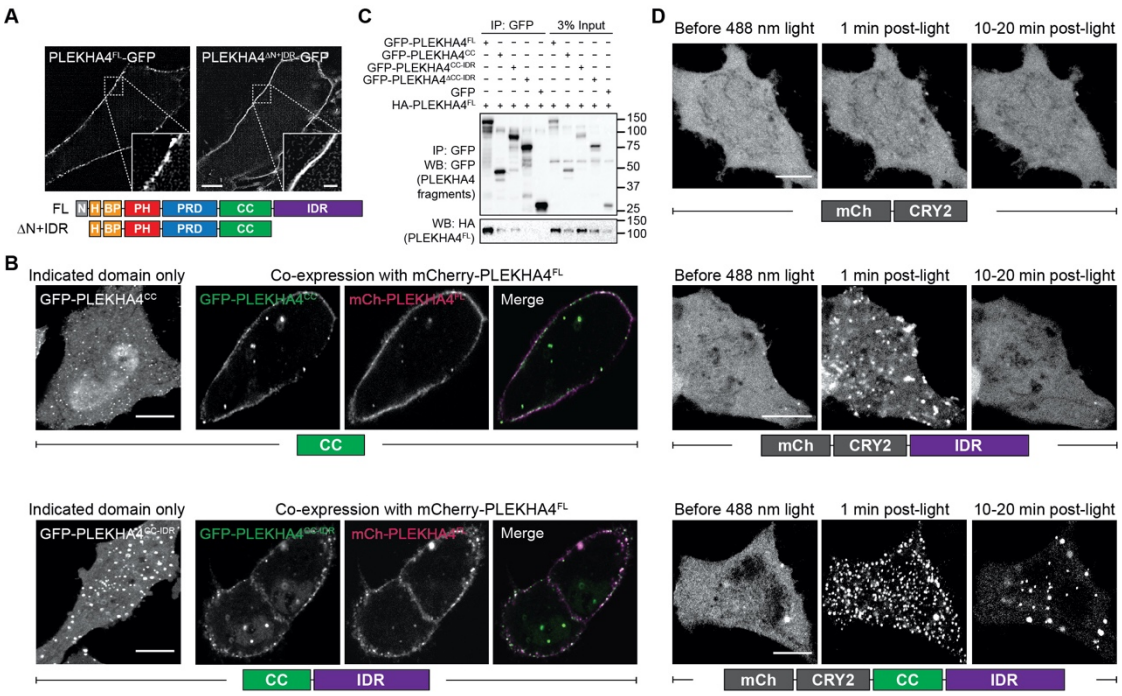

Figure 2.2 PLEKHA4 oligomerizes into clusters via its coiled coil and intrinsically disordered regions.

(A) Super-resolution structured illumination microscopy (SR-SIM) of HeLa cells transfected with PLEKHA4^{FL}-GFP or PLEKHA4$^{\Delta IDR}$-GFP (amino acids 28–495). (B) Confocal microscopy of HeLa cells transfected with a GFP-tagged PLEKHA4 coiled-coil domain construct (GFP-PLEKHA4^{CC}, amino acids 357–495) either alone or in combination with mCherry (mCh)-PLEKHA4^{FL} (top) or a GFP-tagged PLEKHA4 coiled-coil and intrinsically disordered region construct (GFP-PLEKHA4$^{CC\text{-}IDR}$, amino acids 357–779) alone or in combination with mCh-PLEKHA4^{FL} (bottom). (C) Western blot analysis of anti-GFP immunoprecipitates of HeLa cells co-transfected with HA-PLEKHA4^{FL} and either the indicated GFP-PLEKHA4 fragment or GFP as a control. (D) Relevant frames from time series of HeLa cells transfected with mCherry-CRY2, mCherry-CRY2-PLEKHA4^{IDR}, or mCherry-CRY2-PLEKHA4$^{CC\text{-}IDR}$ subjected to brief photo-activation with 488 nm pulse and monitored for the formation of reversible clusters, or aggregates. Scale bars: 5 µm (A); 10 µm (B, D); and 1 µm (B, inset). See also **Figure S2.2**.

2.3.3 *PLEKHA4 associates with KLHL12, an adaptor of the E3 ubiquitin ligase CUL3*

To explore possible additional components of the PLEKHA4 puncta and to ascertain a function for these assemblies, we searched for protein-protein interaction partners of PLEKHA4. We generated stable HEK 293 cell lines expressing GFP-PLEKHA4 or, as a negative control, GFP, and performed SILAC-enabled quantitative proteomics[46] of anti-GFP immunoprecipitates from each of these cell lines (**Figure 2.3A** and **Table S2.1**). The strongest hit from these experiments was KLHL12.

We validated the interaction of both PLEKHA4-GFP and GFP-PLEKHA4 with endogenous KLHL12 by co-IP followed by Western blot (**Figure 2.3B**). To map the interacting regions, we performed co-IP of KLHL12 with several PLEKHA4 truncations and isolated domains (**Figure 2.3C**). The minimal region that interacted with KLHL12 is the Pro-rich domain (PRD) of PLEKHA4. A construct including both the PRD and the CC domains (PLEKHA4$^{PRD–CC}$) exhibited a much stronger interaction with KLHL12, which we attribute to the capacity of PLEKHA4$^{PRD–CC}$ to oligomerize.

We found that PLEKHA4 can control KLHL12 localization in cells. Whereas fluorescently tagged KLHL12 localizes to cytoplasmic puncta consistent with previous studies[47] (**Figure 2.3D**, lower cell), co-overexpression of PLEKHA4 with KLHL12 recruited KLHL12 to the plasma membrane (**Figure 2.3D**, upper cell). Loss-of-function studies provide further evidence of a PLEKHA4–KLHL12 interaction. Knockdown of either protein by siRNA resulted in a decrease in the level of the other,

consistent with the idea that they mutually stabilize one another within a complex (**Figure 2.3E**).

The interaction of PLEKHA4 with KLHL12 provides a window into potential roles of PLEKHA4 in the cell. KLHL12 is a member of the family of BTB proteins, which function as adaptors that direct the E3 ubiquitin ligase Cullin-3 (CUL3) to specific substrates[48,49]. To explore whether the PLEKHA4–KLHL12 interaction influences KLHL12's ability to regulate CUL3, we ascertained the ability of all three proteins to colocalize. Indeed, immunofluorescence analysis of cells co-transfected with tagged PLEKHA4, KLHL12, and CUL3 revealed that PLEKHA4 could recruit the CUL3–KLHL12 complex to the plasma membrane (**Figure 2.3F**).

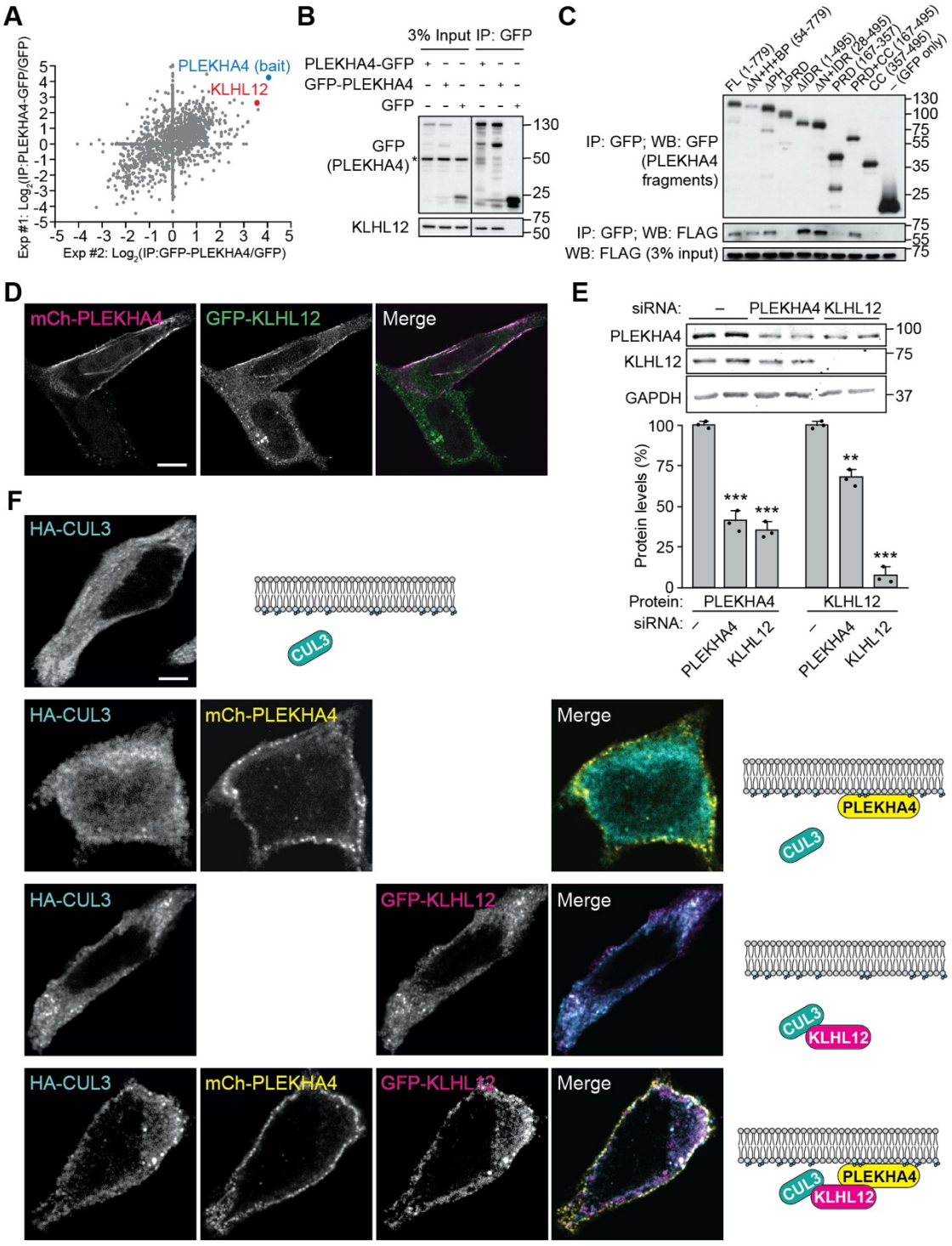

Figure 2.3 PLEKHA4 associates with KLHL12, an adaptor of the E3 ubiquitin ligase CUL3.

(A) KLHL12 is an interactor of PLEKHA4. Scatterplot showing the enrichment of proteins present in anti-GFP immunoprecipitates from SILAC-labeled cells expressing

GFP-PLEKHA4 or PLEKHA4-GFP compared to those expressing GFP only. Plot shows correlation between two different experiments, one using PLEKHA4-GFP as the experimental bait (y-axis) and one using GFP-PLEKHA4 as the bait (x-axis). Proteins were identified by shotgun proteomics (see **Table S2.1** for full list of identified proteins). (B–C) Western blot analysis of anti-GFP immunoprecipitates of HeLa cell lines that were transfected with GFP, GFP-PLEKHA4 or PLEKHA-GFP for immunoprecipitation of endogenous KLHL12 (B) or transfected with HA-PLEKHA4^{FL} and the indicated GFP-PLEKHA4 fragment (C). Asterisk indicates non-specific background immunoreactivity. (D) Live-cell confocal microscopy of HeLa cells co-transfected with mCh-PLEKHA4 and GFP-KLHL12. Note that top cell expresses both proteins whereas bottom cell expresses only GFP-KLHL12. (E) Western blot analysis and quantification of lysates from HeLa cells treated with siRNA against PLEKHA4 or KLHL12 or a control siRNA (–). **, $p < 0.01$; ***, $p < 0.001$ ($n = 3$). (F) Immunofluorescence analysis of HeLa cells transfected with the indicated combination of HA-CUL3 (cyan), mCh-PLEKHA4 (yellow) and GFP-KLHL12 (magenta), with cartoon representation of the subcellular localizations at right. Scale bars: 10 μm.

2.3.4 *PLEKHA4 negatively regulates the E3 ligase activity of CUL3–KLHL12*

We first tested whether PLEKHA4 is simply a ubiquitination substrate of the CUL3–KLHL12 E3 ubiquitin ligase. We found that GFP-PLEKHA4 was minimally, if at all, ubiquitinated, and, importantly, that its marginal levels of ubiquitination were not affected by overexpression of KLHL12 (**Figure S2.3**).

If PLEKHA4 is not a ubiquitination substrate of CUL3–KLHL12, it instead might function as an adaptor to recruit CUL3–KLHL12 to a site of action at the plasma membrane. Among the established ubiquitination substrates of CUL3–KLHL12, the protein Dishevelled-3 (DVL3) can localize to the plasma membrane. We thus interrogated the levels of total amount of DVL3 and the extent of DVL3 ubiquitination after modulating PLEKHA4 and/or KLHL12 levels.

First, we co-expressed FLAG-DVL3 with KLHL12, PLEKHA4, or both KLHL12 and PLEKHA4 (**Figure 2.4A**). As expected, overexpression of KLHL12

decreased FLAG-DVL3 levels[11]. Surprisingly, overexpression of PLEKHA4 along with KLHL12 led to higher levels of FLAG-DVL3 than overexpression of KLHL12 alone, suggesting that PLEKHA4 attenuates the effect of KLHL12 on DVL3 levels. Expression of PLEKHA4 alone had no significant effect relative to control, consistent with the idea that PLEKHA4 acts through CUL3–KLHL12.

Using a similar approach, we investigated how PLEKHA4 influences the ubiquitination of FLAG-DVL3 (**Figure 2.4B**). Here, we found that overexpression of full-length PLEKHA4 along with KLHL12 attenuates the massive increase of FLAG-DVL3 ubiquitination caused by overexpression of KLHL12 alone. As negative controls, we used versions of PLEKHA4 and KLHL12 that are non-functional (i.e., PLEKHA4$^{\Delta PRD}$, which does not interact with KLHL12, and KLHL12^{Q405X}, which does not engage CUL3[11]). Thus, we conclude that the effect of overexpressed PLEKHA4 on FLAG-DVL3 ubiquitination requires its interaction with an active CUL3–KLHL12 E3 ligase.

Loss-of-function studies using siRNA and examining endogenous DVL proteins led to the same conclusions. Knockdown of PLEKHA4 decreased the levels of all three DVL isoforms (DVL1, DVL2, and DVL3), whereas, as expected[11], knockdown of KLHL12 led increases in the levels of the three DVL proteins (**Figure 2.4C**). Further, knockdown of PLEKHA4 led to increased ubiquitination of endogenous DVL3, whereas knockdown of KLHL12 led to decreased ubiquitination of DVL3 (**Figure 2.4D**). Importantly, the effect of PLEKHA4 knockdown could be rescued by transfection with an siRNA-resistant GFP-PLEKHA4 construct, confirming the specificity of the PLEKHA4 siRNA and the GFP-PLEKHA4

construct's functionality (**Figure 2.4E**). Collectively, these overexpression and knockdown studies support the hypothesis that PLEKHA4 negatively regulates CUL3–KLHL12-mediated ubiquitination of the DVL proteins.

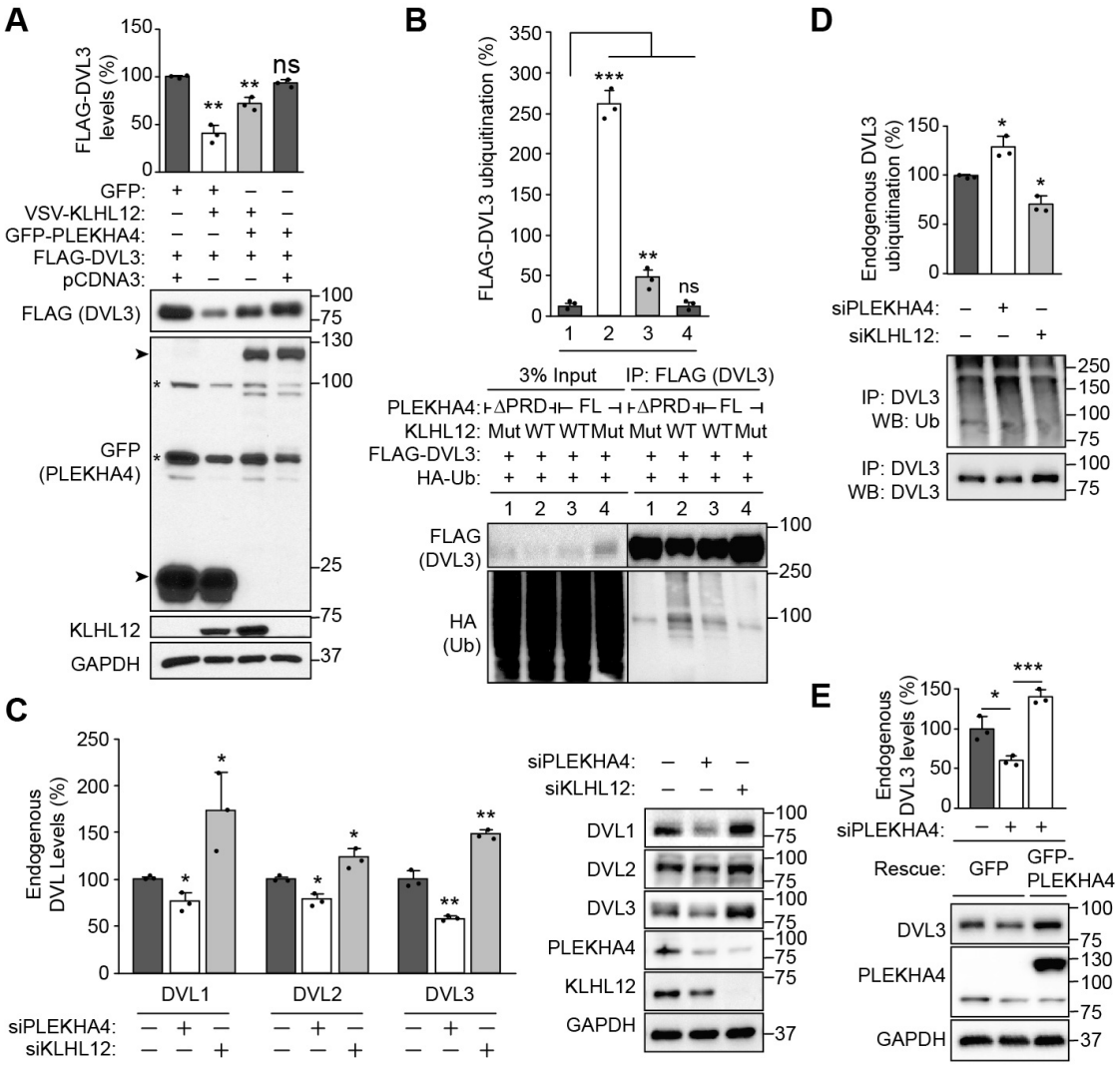

Figure 2.4 PLEKHA4 negatively regulates the CUL3–KLHL12-mediated ubiquitination and degradation of DVL3.

(A–E) Western blot analysis and quantification of HeLa cells transfected with the indicated plasmids and/or siRNA duplexes. (A) Overexpression of PLEKHA4 attenuates KLHL12-dependent decrease in FLAG-DVL3 levels. On the anti-GFP Western blot, arrowheads indicate GFP-PLEKHA4^{FL} (which migrates at

approximately 120 kD) and GFP (which migrates at approximately 25 kD), and asterisks on blots indicate non-specific background immunoreactivity. **, $p < 0.01$; ns, not significant (n = 3). (B) Overexpression of PLEKHA4^{FL}, which is capable of interaction with KLHL12, but not PLEKHA4$^{\Delta PRD}$, which cannot, attenuates the ubiquitination of FLAG-DVL3 by a functional VSV-tagged KLHL12 (WT) but not an inactive KLHL12 mutant that does not engage CUL3 (Q405X, Mut). One day after transfection with appropriate plasmids, cells were subjected to anti-FLAG immunoprecipitation and Western blot analysis. Note increased levels of DVL3 and decreased ubiquitination of DVL3 in lane 3 compared to lane 2. ***, $p < 0.001$; **, $p<0.01$; ns, not significant (n = 3). (C) PLEKHA4 modulates the levels of endogenous DVL1, DVL2 and DVL3. Western blot analysis of lysates from HeLa cells treated with siRNA duplexes against PLEKHA4 (siPLEKHA4), KLHL12 (siKLHL12), or a negative control siRNA (–). *, $p < 0.05$; **, $p < 0.01$ (n = 3). (D) PLEKHA4 modulates the ubiquitination of endogenous DVL3. Western blot analysis of anti-DVL3 immunoprecipitates from HeLa cells treated with the indicated siRNA duplexes. *, $p < 0.05$ (n = 3). (E) Full-length GFP-PLEKHA4 can functionally rescue changes of DVL3 levels induced by siPLEKHA4. Western blot analysis of lysates from HeLa cells subjected to siPLEKHA4 and/or transfection with an siRNA-resistant GFP-PLEKHA4^{FL} construct (which migrates at approximately 120 kD). *, $p < 0.05$ (n = 3); ***, $p < 0.001$. All quantifications were normalized to the loading control (GAPDH). See also **Figure S2.3**.

2.3.5 *PLEKHA4 is a positive regulator of canonical and non-canonical Wnt signaling in mammalian cells*

DVL3 and its paralogs DVL1 and DVL2 are central intermediates in the canonical and non-canonical branches of Wnt signaling, which collectively can control many developmental processes[1,8]. We thus asked whether modulation of PLEKHA4 levels would affect Wnt signaling strength. For these assays, we used a mouse fibroblast cell line (C57MG) responsive to Wnt stimulation that contained a Wnt-inducible GFP transcriptional reporter termed WntRGreen[50,51], as well as human cell lines such as HeLa cells.

PLEKHA4 knockdown decreased WntRGreen fluorescence, as visualized by microscopy (**Figure 2.5A**) and as quantified by flow cytometry (**Figure 2.5B**). As

expected, KLHL12 knockdown increased WntRGreen fluorescence, consistent with a role for KLHL12 in mediating DVL3 ubiquitination (**Figure 2.5B**). We observed similar effects on DVL3 levels in these C57MG cells (**Figure 2.5C**) as we had previously seen in HeLa cells (**Figure 2.4C**). From these data, we conclude that PLEKHA4 functions in cells as a positive modulator of Wnt signaling via its effects on DVL3 levels.

To complement the β-catenin-dependent reporter, we also examined the effect of PLEKHA4 knockdown on endogenous levels of the Wnt3a target gene Axin2, whose levels are induced by canonical Wnt signaling. We found that knockdown of PLEKHA4 attenuated the Wnt3a-stimulated increase in endogenous Axin2 (**Figure 2.5D**) and that this effect could be rescued by transfection with GFP-PLEKHA4 (**Figure 2.5E**).

Finally, we assessed the effect of PLEKHA4 knockdown on a non-canonical Wnt signaling pathway. We found that knockdown of PLEKHA4 attenuated the Wnt5a-stimulated increase in phosphorylation of c-Jun N-terminal kinase (JNK), which becomes activated upon exposure of cells to Wnt5a, a stimulus of β-catenin-independent, non-canonical Wnt signaling[52] (**Figure 2.5F**).

Collectively, these data indicate that, in mammalian cells, PLEKHA4 is a positive regulator of both canonical, β-catenin-dependent, and non-canonical, β-catenin-independent, Wnt signaling.

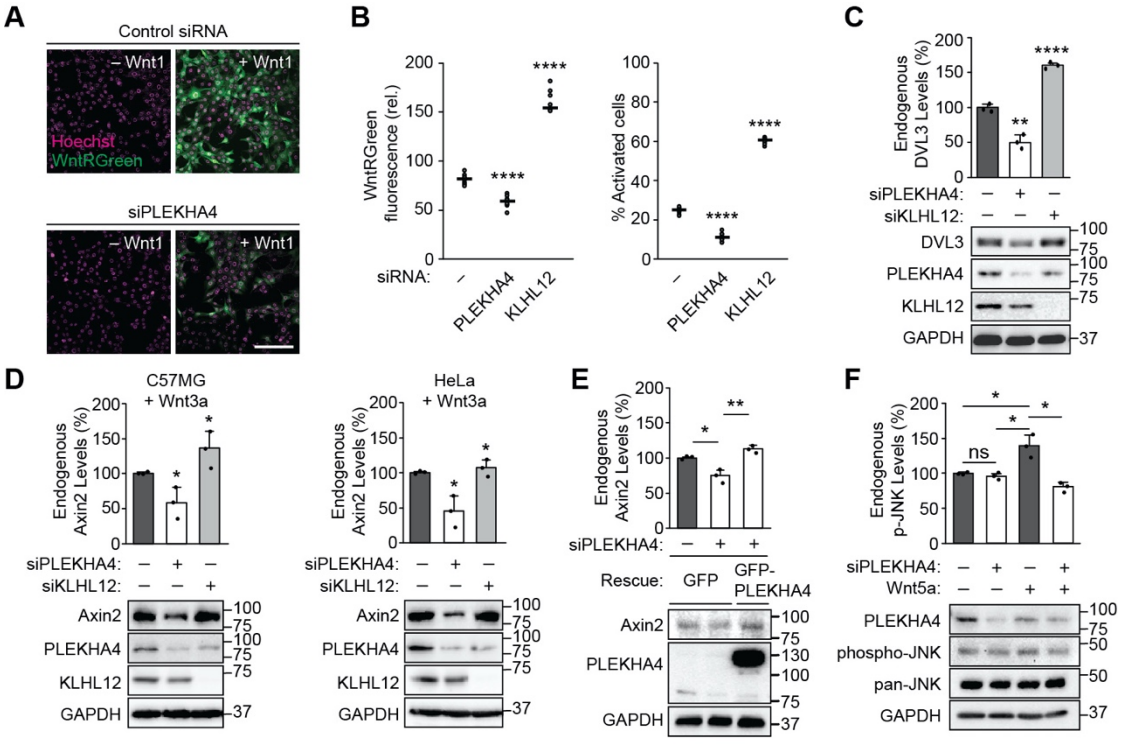

Figure 2.5 PLEKHA4 is a positive regulator of canonical and non-canonical Wnt signaling in mammalian cells.

(A) Knockdown of PLEKHA4 decreases Wnt1-induced expression of GFP in C57MG cells stably expressing the WntRGreen reporter. Control siRNA or PLEKHA4 knockdown (siPLEKHA4) was performed in C57MG-WntRGreen cells, which were co-cultured with Wnt1-expressing MV7-Rat2a-Wnt1 cells (+ Wnt1) or control MV7-Rat2a cells (– Wnt1), followed by imaging of WntRGreen-derived GFP fluorescence (green) and nuclei (Hoechst 33342, magenta) by confocal microscopy. (B) Quantification of changes in WntRGreen fluorescence induced by knockdown of PLEKHA4 or KLHL12. Cells were treated with siRNA against PLEKHA4, KLHL12, or negative control siRNA (–), followed by quantification of GFP fluorescence by flow cytometry. Each dot on the plot represents a separate biological replicate. **, $p < 0.01$; ***, $p < 0.001$; ****, $p < 0.0001$ (n = 9). (C) PLEKHA4 and KLHL12 regulate levels of endogenous DVL3 in C57MG-WntRGreen cells. Western blot analysis of cells treated with an siRNA duplex against PLEKHA4 (siPLEKHA4), KLHL12 (siKLHL12), or negative control siRNA (–). **, $p < 0.01$; ****, $p < 0.0001$ (n = 3). (D) PLEKHA4 and KLHL12 regulate Wnt3a-stimulated changes in the levels of endogenous Axin2. C57MG or HeLa cells were treated with the indicated siRNA duplex and stimulated with Wnt3a-containing conditioned media. *, $p < 0.05$ (n = 3). (E) Full-length GFP-PLEKHA4 can functionally rescue the attenuation of Wnt3a-stimulated increase in levels of endogenous Axin2 induced by knockdown of PLEKHA4 (siPLEKHA4). Western blot analysis of lysates from HeLa cells subjected to siPLEKHA4 or negative control siRNA (–), stimulation with Wnt3a-containing

conditioned media, and transfection with either GFP only or an siRNA-resistant GFP-PLEKHA4^{FL} construct. *, $p < 0.05$; **, $p < 0.01$ (n = 3). (F) PLEKHA4 regulates the phosphorylation of JNK, a marker associated with non-canonical Wnt (planar cell polarity) signaling pathway. Western blot analysis of C57MG cells subjected to siPLEKHA4 or negative control siRNA (–) and stimulation with control or Wnt5a-containing conditioned media. *, $p < 0.05$; ns, not significant (n = 3). In graphs showing quantification, all levels were normalized to the loading control (GAPDH) except (F), in which levels were normalized to pan-JNK. Scale bar: 200 μm.

2.3.6 *The fly PLEKHA4 homolog, kramer, is a specific modulator of planar cell polarity signaling*

To establish the physiological relevance of our in vitro findings linking PLEKHA4 to Wnt signaling, we investigated the loss of PLEKHA4 function in vivo in *Drosophila melanogaster*. Both canonical Wnt (Wingless) signaling and planar cell polarity (PCP) pathway are well established in this organism[53–55]. Though PCP signaling is not known to respond to Wnt ligands, it shares key intracellular signaling molecules and outputs with vertebrate non-canonical Wnt signaling and is considered the *Drosophila* counterpart of this pathway[56,57]. Importantly, to simplify the analysis, the fly genome has only a single PLEKHA4 homolog, *CG34383*, which shares the overall domain architecture and 31% sequence identity with PLEKHA4 (including 53% identity between the PH domains).

We generated two *CG34383* knockout alleles using CRISPR/Cas9-mediated mutagenesis, both carrying frameshift mutations early in the coding sequence and thus predicted to be null (**Figure S2.4**). We first assessed the physiological effects of loss of *CG34383* in vivo by viewing hair patterning in the adult wing. The uniform wing hair orientation (proximal to distal) is controlled by the PCP pathway, which depends on *dishevelled (dsh)*, a core PCP signaling component[5,57]. Disruption of PCP signaling

leads to mis-oriented hair patterns, for example as seen in a strain homozygous for *dsh*^{1} (**Figure 2.6A** and **Figure S2.5A**), a hypomorphic allele defective in PCP[52]. Strikingly, we found that knockout of *CG34383* causes aberrant wing hair patterns similar to those in the *dsh*^{1} flies (**Figure 2.6A** and **Figure S2.5A**). Due to the defects in adult hair patterning in the *CG34383* mutants, we named this locus *kramer (kmr)* and denoted our two knockout mutant alleles *kmr*^{1} and *kmr*^{2}. In all of our experiments, both *kmr* alleles exhibited identical phenotypes and may be referred to interchangeably as *kmr*$^{-}$.

We performed two experiments to demonstrate the specificity of these effects. First, we confirmed that loss of function in *kmr* was responsible for the wing hair phenotype by generating flies hemizygous for the *kmr*$^{-}$ alleles with a deletion covering *kmr* and 22 additional genes (*Df(3R)Exel6170,* termed *df*). The *kmr*$^{df/}$*kmr*^{1} and *kmr*^{df}/*kmr*^{2} hemizygotes exhibited wing hair polarity defects identical to those seen in the *kmr*^{1} and *kmr*^{2} strains (**Figure 2.6B** and **Figure S2.5B**).

Second, we tested the genetic interaction of *kmr* with *dsh* by examining hair patterning in transheterozygotic strains containing one allele each of either *kmr*^{1} or *kmr*^{2} and one of three different *dsh* alleles, the hypomorphic *dsh*^{1} and the amorphic *dsh*^{3} and *dsh*^{75} alleles. Whereas heterozygotes carrying only one copy of these alleles (*kmr*$^{+}$/*kmr*^{1}, *kmr*$^{+}$/*kmr*^{2}, *dsh*$^{+}$/*dsh*^{1}, *dsh*$^{+}$/*dsh*^{3}, and *dsh*$^{+}$/*dsh*^{75}) exhibited wild-type wing hair patterning (**Figure 2.6C** and **Figure S2.5C**), transheterozygotes containing one copy of mutant alleles each of *kmr* and *dsh* exhibited modest but consistent defects in wing hair patterning (**Figure 2.6D** and **Figure S2.5D**). This kind of genetic interaction indicates that partial loss of the function of both proteins causes synthetic

defects in PCP signaling, strongly suggesting that *kmr* and *dsh* function in the same pathway.

We analyzed defects in hair patterning in two additional adult tissues, the eye and the thorax, using scanning electron microscopy (SEM) imaging. Again, we found that homozygous kmr^{1} and kmr^{2} flies exhibited loss of polarized hair patterning in these tissues, similar to the dsh^{1} homozygote (**Figures 2.6E, H, S2.6A,** and **S2.7A**). Transheterozygote analysis revealed synthetic defects between the two *kmr* alleles and three *dsh* alleles in the PCP phenotypes in these tissues as well (**Figures 2.6F, G, I, J, S2.6B, S2.6C, S2.7B,** and **S2.7C**).

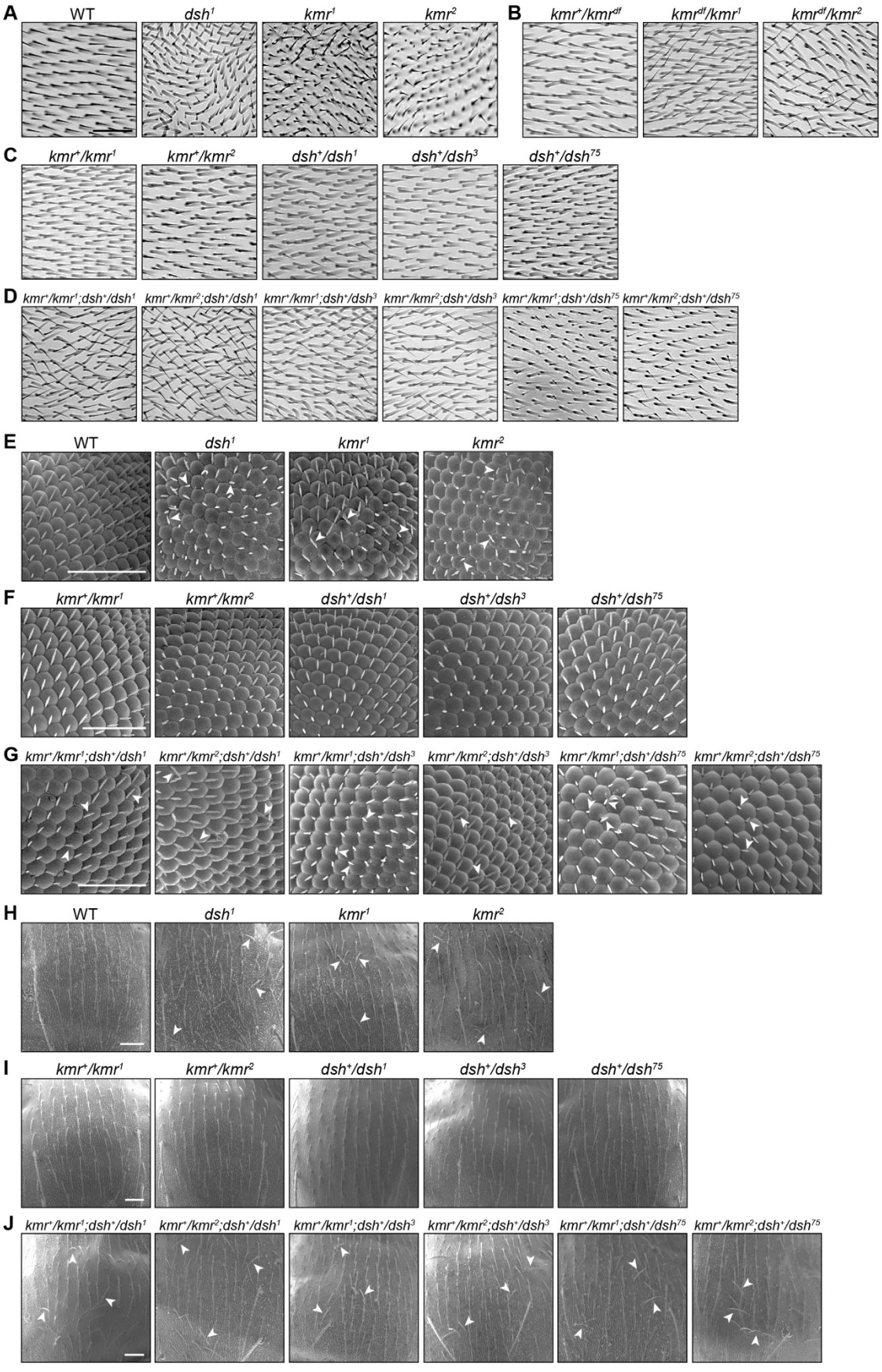
A
WT
dsh1
kmr1
kmr2
B
kmr+/kmrdf
kmrdf/kmr1
kmrdf/kmr2
C
kmr+/kmr1
kmr+/kmr2
dsh+/dsh1
dsh+/dsh3
dsh+/dsh75
D
kmr+/kmr1;dsh+/dsh1
kmr+/kmr2;dsh+/dsh1
kmr+/kmr1;dsh+/dsh3
kmr+/kmr2;dsh+/dsh3
kmr+/kmr1;dsh+/dsh75
kmr+/kmr2;dsh+/dsh75
E
WT
dsh1
kmr1
kmr2
F
kmr+/kmr1
kmr+/kmr2
dsh+/dsh1
dsh+/dsh3
dsh+/dsh75
G
kmr+/kmr1;dsh+/dsh1
kmr+/kmr2;dsh+/dsh1
kmr+/kmr1;dsh+/dsh3
kmr+/kmr2;dsh+/dsh3
kmr+/kmr1;dsh+/dsh75
kmr+/kmr2;dsh+/dsh75
H
WT
dsh1
kmr1
kmr2
I
kmr+/kmr1
kmr+/kmr2
dsh+/dsh1
dsh+/dsh3
dsh+/dsh75
J
kmr+/kmr1;dsh+/dsh1
kmr+/kmr2;dsh+/dsh1
kmr+/kmr1;dsh+/dsh3
kmr+/kmr2;dsh+/dsh3
kmr+/kmr1;dsh+/dsh75
kmr+/kmr2;dsh+/dsh75

Figure 2.6 Knockout of the fly PLEKHA4 homolog, *kramer (kmr)*, results in defects in planar cell polarity (PCP) signaling.

(A–D) Brightfield imaging analysis of *Drosophila melanogaster* adult wing, oriented proximal to distal (left to right), to evaluate effects of various gene disruptions on PCP signaling. (A) Two knockout strains of *kramer* (*kmr*^{1} and *kmr*^{2}, referred to interchangeably as *kmr*$^{-}$) exhibit aberrant wing bristles similar to that exhibited in a homozygous, hypomorphic mutant of Dishevelled (*dsh*^{1}). See **Figure S2.4** for details on generation of *kmr* KO alleles by CRISPR/Cas9-mediated mutagenesis. (B) Validation of specificity of phenotype in *kmr*$^{-}$ via complementation with a chromosomal deletion strain, *Df(3R)Exel6170 (Δ 87F10–87F14)*, denoted here as *df*. Note that *kmr*^{df}*/kmr*$^{-}$, which bears one CRISPR/Cas9-deleted allele and one chromosomal deletion allele, phenocopies either homozygous *kmr*$^{-}$ strain. (C–D) Genetic interaction between *kmr* and *dsh.* Analysis of five simple heterozygote strains (*kmr*$^{+}$*/kmr*^{1}, *kmr*$^{+}$*/kmr*^{2}, *dsh*$^{+}$*/dsh*^{1}, *dsh*$^{+}$*/dsh*^{3}, and *dsh*$^{+}$*/dsh*^{75}) (C) and six transheterozygote strains (*kmr*$^{+}$*/kmr*$^{-}$;*dsh*$^{+}$*/dsh*^{1}, *kmr*$^{+}$*/kmr*$^{-}$;*dsh*$^{+}$*/dsh*^{3}, *or kmr*$^{+}$*/kmr*$^{-}$;*dsh*$^{+}$*/dsh*^{75} for both the *kmr*^{1} and *kmr*^{2} alleles) (D), demonstrating that dysfunction of a single allele of both genes within the same organism leads to a modest PCP phenotype (D), compared to simple heterozygotic strains (C), whose patterning resembles wild-type. (E–J) Scanning electron microscopy (SEM) imaging reveals aberrant hair patterning resulting from defects in PCP signaling in eyes (E–G) and thorax (H–J) of *kmr* mutant and *kmr/dsh* transheterozygote adult flies. For these experiments, the same genotypes as in (A), (C), and (D) were used for analysis. Arrowheads indicate examples of hairs with altered orientations due to defective PCP signaling. This figure shows one representative image per genotype, and **Figures S2.5–S2.7** show three additional images per genotype for wing, eye, and thorax imaging, respectively. Scale bars: 50 μm.

2.3.7 *kramer modulates PCP signaling by affecting Dishevelled levels and polarized localization in the developing wing*

Finally, to evaluate the mechanism by which *kmr* affects PCP signaling, we examined the levels of the Dsh protein in the homozygous *kmr*^{1} and *kmr*^{2} flies. Due to the unavailability of suitable antibodies for immunofluorescence, we used a strain expressing a functional, fluorescently tagged Dsh under the control of the endogenous *dsh* promoter (*dsh::Clover*)[58].

We first examined Dsh-Clover expression in the wing imaginal wing disc, a larval tissue that gives rise to the adult wing. Dsh is moderately enriched at the apical

membrane of wing disc epithelial cells[58,59], which are best visualized at the folds because these locations are where apical membranes of opposing epithelial cells meet (**Figure 2.7A**, arrows). Compared to the wildtype, homozygous *kmr*^{1} and *kmr*^{2} flies exhibited reduced Dsh-Clover levels or enrichment within the epithelial folds (**Figure 2.7B**). These data suggest that loss of *kmr* leads to a downregulation of Dsh levels in this tissue and at this developmental timepoint.

Second, we evaluated the subcellular localization of Dsh-Clover at 30 h after puparium formation. At this stage, Dsh and other core PCP proteins adopt an asymmetric, polarized localization within the epithelium, in advance of the formation of actin bundles where the trichome (hair) will emerge. In the wild-type background, we observed Dsh-Clover enrichment in the proximal/distal membranes within the hexagonal array of epithelial cells, as expected[5,57,58,60] (**Figure 2.7C**). Homozygous *kmr*^{1} or *kmr*^{2} flies exhibit a loss of this asymmetry, with Dsh-Clover adopting an apparent stochastic, or less polarized, distribution within the plasma membrane. These results indicate that *kmr* modulates PCP signaling via effects on Dsh levels and polarized localization, speaking to the physiological relevance of our findings.

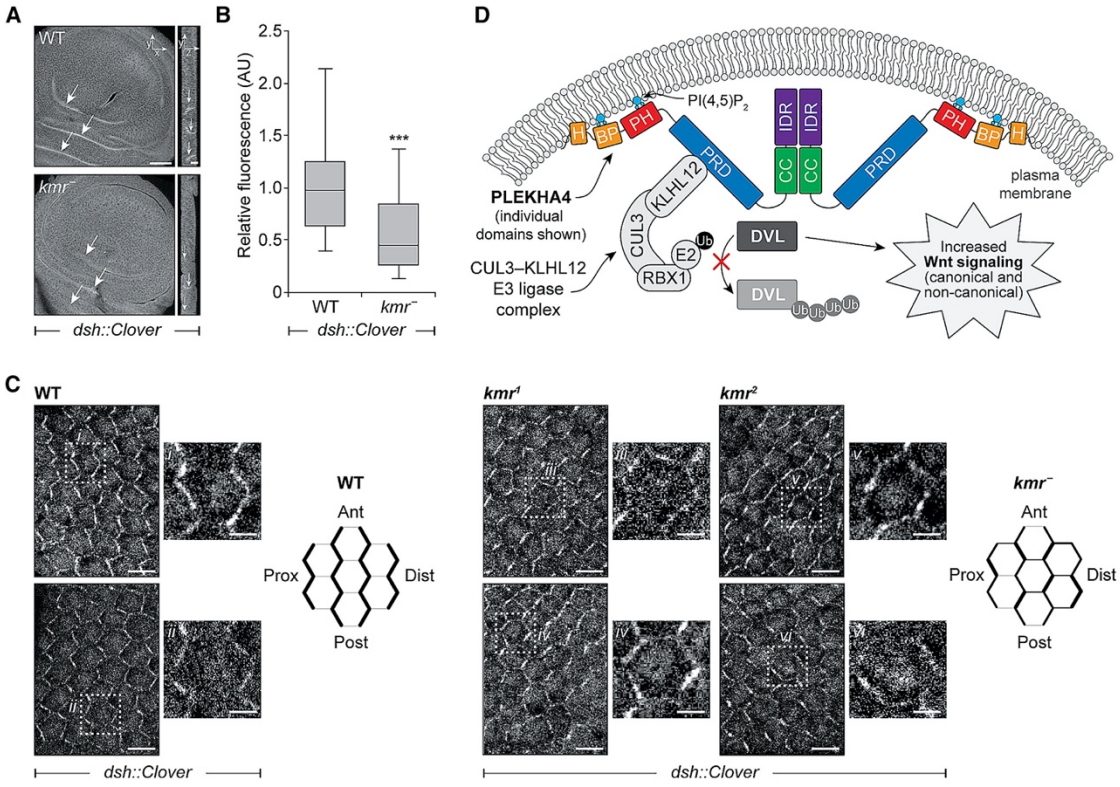

Figure 2.7 Knockout of *kmr* causes defects in Dishevelled levels and polarized localization during *Drosophila* development.

(A–B) Knockout of *kmr* leads to lower levels of Dsh-Clover in imaginal wing discs. Confocal microscopy analysis (A) and quantification (B) of Dsh-Clover fluorescence in L3 larval imaginal wing discs expressing Dsh-Clover (top, wild-type (*dsh::Clover*); bottom, *kmr* knockout (*dsh::Clover;kmr*$^{-}$)). Shown are xy and orthogonal (yz) projections. Arrows indicate the epithelial folds of the wing discs. In the box plot representing quantification of the Dsh-Clover fluorescence at epithelial folds, boxes represent the second and third quartiles, with the line in the middle representing the median, and the whiskers denote the maximum and minimum values. ***, $p < 0.001$ ($n = 12$). (C) Knockout of *kmr* leads to a loss of asymmetric, polarized subcellular localization of Dsh-Clover within the pupal wing epithelium. (C) Confocal microscopy of Dsh-Clover fluorescence of 30 h after puparium formation wings of the same genotypes as in (A). Note that Dsh is asymmetrically enriched at proximal-distal boundaries in wild-type background. This asymmetry is partially lost, causing gain of symmetry, in both *kmr*$^{-}$ strains. Two representative images are shown for each genotype and zoomed-in images showing a single cell (i–vi) are indicated by the dotted line. Cartoon diagrams represent Dsh subcellular localization pattern in wild-type and in the *kmr*$^{-}$ mutant. Ant, anterior; Dist, distal; Post, posterior; Prox, proximal. Scale bars: 50 µm (A, z-projection); 10 µm (A, orthogonal projection); 5 µm (C, full-size image); 2.5 µm (C, zoomed-in images (i–vi)). (D) Working model for

PLEKHA4/Kmr function wherein it attenuates DVL ubiquitination by sequestering the CUL3–KLHL12 E3 ubiquitin ligase in clusters at the plasma membrane to, depending on the context, enhance canonical Wnt signaling and/or non-canonical Wnt/PCP signaling pathways.

2.4 DISCUSSION

Phosphoinositides are present in low abundance but act as important constituents of eukaryotic membranes[21,61,62]. A major function of these lipids is to act as membrane identity markers by presenting their head groups as ligands to facilitate recruitment of cytosolic proteins to the correct target membrane. The most prevalent PIP-binding module is the PH domain, which is the 11th-most abundant domain in the human proteome, and the physiological functions of the vast majority of PH domain-containing proteins remain unknown[23]. Our studies reveal a link between PIPs and the control of ubiquitination and Wnt signaling pathways that is mediated by the PH domain-containing protein PLEKHA4.

We found that PLEKHA4 interacts specifically with $PI(4,5)P_2$ at the plasma membrane within cells. Three motifs at the N-terminus of PLEKHA4 — an amphipathic helix, a basic peptide, and the PH domain — collectively confer the specificity of this recognition. The full-length PLEKHA4 protein assembles into higher-order structures at the plasma membrane that are, strikingly, visible by confocal microscopy as puncta. This assembly is mediated by two C-terminal domains of PLEKHA4: a coiled coil and an intrinsically disordered region (IDR). Intriguingly, these C-terminal domains can self-associate in cells, as ascertained by colocalization, co-immunoprecipitation, and optoDroplet assays[44,45]. While the nature of the PLEKHA4 clusters remains unknown, the puncta fail to colocalize with markers of

known plasma membrane assemblies, organelles, or membrane contact sites, and it is interesting to speculate they may represent liquid-liquid phase separated domains (i.e., membrane-less organelles) containing PLEKHA4 and other interaction partners[37–40,63].

We characterized a protein-protein interaction between PLEKHA4 and the CUL3 E3 ubiquitin ligase adaptor KLHL12, to which PLEKHA4 binds via its central, proline-rich domain. Mechanistic studies in mammalian cells using both overexpression and RNAi-mediated knockdown of PLEKHA4 indicate a role for this protein as a positive regulator of DVL levels by preventing its polyubiquitination by the CUL3–KLHL12 E3 ligase. These in vitro studies also indicated that PLEKHA4 is a positive modulator of both canonical, β-catenin-dependent, and non-canonical, β-catenin-independent, Wnt signaling pathways. These in vitro studies support a model wherein PLEKHA4 recruits the CUL3–KLHL12 E3 ligase complex to the plasma membrane and downregulates its ubiquitination of the DVL proteins, permitting DVL levels to rise and increasing the strength of DVL-dependent canonical and non-canonical Wnt signaling pathways (**Figure 2.7D**).

A fascinating aspect of this model is that PLEKHA4 can bring CUL3–KLHL12 to the very membrane where its substrate, DVL3, is activated in Wnt signaling, and yet this recruitment results in less DVL3 polyubiquitination. We propose that PLEKHA4 sequesters CUL3–KLHL12 in an inactive state in plasma membrane regions where CUL3–KLHL12 cannot physically access its substrate DVL3, in effect creating an "exclusion zone" devoid of CUL3–KLHL12 E3 ligase activity. Interestingly, DVL proteins form cytoplasmic phase-separated clusters[64], and

it is possible that sequestration of CUL3–KLHL12 at the plasma membrane by PLEKHA4 serves to spatially segregate the E3 ligase from these cytoplasmic clusters.

The knockout studies of the PLEKHA4 homolog in *Drosophila melanogaster*, *kramer (kmr)*, provided both a validation of our in vitro model in a physiologically relevant setting and also revealed layers of regulation of Dishevelled-dependent signaling in this organism. We found that knockout of *kmr* led to selective defects in PCP signaling, which corresponds to non-canonical Wnt signaling in *Drosophila*[55–57]. *Kmr* knockout flies exhibited defects in hair patterning in the adult wing, eye, and thorax. Mechanistically, we established that *kmr* and *dsh* act in the same genetic pathway, as we observed synthetic defects in PCP signaling in transheterozygotic strains. Finally, we assessed the effect of *kmr* knockout on Dsh levels and localization in the developing wing. We found lower levels of Dsh enriched at the apical epithelium in the larval imaginal wing disc and a loss of asymmetric, polarized Dsh distribution at the plasma membrane in the pupal wing epithelium.

In contrast to these PCP phenotypes, we did not observe any phenotypes associated with Wingless signaling, which corresponds to canonical, β-catenin-dependent pathway in flies, in kmr^{1} and kmr^{2} flies[54]. Given the substantial remaining levels of Dsh in the kmr^{-} larval imaginal wing disc and pupal wing, it is possible that the partial, modulatory effect of *kmr* knockout on Dsh levels and localization is not sufficient to cause defects in Wingless signaling in *Drosophila*. As well, *kmr* specifically regulates the localization of Dsh and thus affects PCP signaling in flies. Nonetheless, our results in cultured mammalian cell lines demonstrating effect of PLEKHA4 knockdown on both the β-catenin-dependent and -independent signaling

pathways suggest that the regulatory role of PLEKHA4 in vivo may go beyond the non-canonical Wnt signaling pathway in other organisms.

Interestingly, a study by Strutt and colleagues of the *Drosophila* homologs of KLHL12 (*diablo* and *kelch*) established roles for the Cullin-3–Diablo/Kelch E3 ligase complex in modulating PCP signaling in vivo in this organism[60]. Notably, they found that subtle changes to the levels of core PCP proteins such as Dsh leads to a breakdown of their asymmetric localization in the pupal wing, leading to PCP phenotypes. As well, they found that Cul3–Diablo/Kelch-mediated modulation of Dsh levels in *Drosophila* led to selective effects on PCP signaling, with no observed effects on Wingless signaling. By contrast, Moon and colleagues found that, in vertebrate systems (mammalian cells and zebrafish embryos), the homologous CUL3–KLHL12 E3 ligase complex modulates DVL levels and the strength of canonical, β-catenin-dependent Wnt signaling[11].

Our data suggest that PLEKHA4/*kmr* acts as a tuner to attenuate polyubiquitination of DVL proteins by sequestration of their E3 ligase, CUL3–KLHL12. By creating different DVL setpoints, we propose that PLEKHA4/*kmr* can modulate the sensitivity of cells to stimulation by appropriate ligands that propagate canonical Wnt and/or non-canonical Wnt/PCP signaling pathways. In this model, the pathway most affected by PLEKHA4/*kmr* is determined by the relative dependence of that pathway on changes to DVL levels in that tissue context. Further, PLEKHA4/*kmr* may affect DVL levels to different extents in different contexts. Given the critical importance of Wnt signaling pathways in mammalian development and disease, PLEKHA4 may function as a regulator of these pathways in vivo in mammals as well.

Finally, the production and maintenance of $PI(4,5)P_2$ at the plasma membrane is important for both canonical and non-canonical Wnt signaling pathways. $PI(4,5)P_2$ enhances the strength of canonical Wnt signaling via effects on the Wnt co-receptor LRP6, and Wnt3a stimulation increases $PI(4,5)P_2$ synthesis via the direct action of DVL on lipid kinases that synthesize $PI(4,5)P_2$, effectively amplifying this lipid-based signal[65,66]. $PI(4,5)P_2$ is also a key determinant of cell polarity, aiding in both establishing the asymmetric spatial arrangement of polarity proteins and in activating actin-nucleating factors[67–70]. Given the central role of DVL in PCP signaling[8,9], its ability to stimulate $PI(4,5)P_2$ synthesis[66,71], and the critical role of actin dynamics in PCP signaling[55,72], changes to $PI(4,5)P_2$ synthesis may directly affect this pathway as well. As a factor that binds to plasma membrane $PI(4,5)P_2$ and impacts DVL levels, PLEKHA4 adds a further layer of regulation to DVL-dependent pathways, including Wnt and PCP signaling.

2.5 EXPERIMENTAL MODEL AND SUBJECT DETAILS

2.5.1 *Cell culture*

FIp-In T-REx HeLa (Thermo Fisher), Flp-In HEK 293 (Thermo Fisher), C57MG WntRGreen (Anthony Brown), L, L Wnt-3a, and L Wnt-5a cells (ATCC) and HEK 293TN cells (Anthony Bretscher) were cultured in Dulbecco's modified Eagle medium (DMEM, Corning) supplemented with 10% fetal bovine serum (FBS, Corning) and 1% penicillin/streptomycin (P/S, Corning) at 37 ºC in a 5% CO_2 atmosphere. HEK 293 cell lines were also supplemented with 1% sodium pyruvate (Corning) in the media. MV7-Rat2a-Wnt1 (Wnt1-secreting) and MV7-Rat2a (control)

were cultured in above-mentioned conditions but in low glucose (1 g/L) DMEM. Stable expression of GFP, GFP-PLEKHA4 or PLEKHA4-GFP was achieved by transfecting FIp-In T-REx HeLa or Flp-In HEK 293 cells (Thermo Fisher) with flippase (pOG44, Thermo Fisher) and above-mentioned plasmids cloned in pCDNA5-FRT vector following the manufacturer's protocol (Thermo Fisher). Twenty-four h post transfection, cells were selected with 100 µg/mL hygromycin B (Sigma). Conditioned media (CM) from L, L Wnt-3a, and L Wnt-5a cells was harvested by collection of supernatant from cells grown for at least 48 h and that had achieved at least 80% confluence, followed by passage through a 0.2 µm filter and storage at 4 ºC until use. Cell lines were obtained and used without further authentication.

2.5.2 *Drosophila melanogaster husbandry*

Information on individual fly strains is provided in the **Table S2.3**. Flies were reared at room temperature in density-controlled vials (60-100 embryos/vial) on standard yeast-glucose medium, for experiments at L3 larval or adult stages. For experiments at 30 h after puparium stage, flies were reared in an incubate at 25 ºC and collected at the appropriate stage. Where possible, experiments were performed on both male and female flies to avoid sex-specific effects. Due to lethality of alleles on the x chromosome, involving flies with FM7a-balanced chromosomes, only female flies from such crosses were used for further analysis.

2.6 METHOD DETAILS

2.6.1 *Plasmids and cloning*

A PLEKHA4 cDNA (obtained from DNASU, corresponding to BC024157) was cloned into the pEGFP-C1 and -N1 vectors (Clontech) using EcoRI and SalI to generate GFP-PLEKHA4 and PLEKHA4-GFP, respectively. The full-length proteins were subcloned into mCherry-C1 and -N1 vectors using EcoRI and SalI. Fragments and deletions of PLEKHA4 were subsequently generated by subcloning into these vectors using standard or overlap PCR-based methods, again with EcoRI and SalI. The amino acid sequences of the deletions/fragments are the following: PLEKHA4^{PH} (45–167), PLEKHA4^{PRD} (167–357), PLEKHA4$^{PRD\text{-}CC}$ (167–495), PLEKHA4$^{PRD\text{-}CC\text{-}IDR}$ (167–779), PLEKHA4^{CC} (357–495), PLEKHA4$^{CC\text{-}IDR}$ (357–779), PLEKHA4^{IDR} (495–779), PLEKHA4$^{H\text{-}BP\text{-}PH}$ (28–167), PLEKHA4$^{\Delta N+IDR}$ (28–495), PLEKHA4$^{\Delta CC+IDR}$ (1–357), PLEKHA4$^{\Delta N+H+BP}$ (54–779), PLEKHA4$^{\Delta PH}$ (1–45, 167–779), PLEKHA4$^{\Delta H+BP+PH}$ (1–27, 168–779), PLEKHA4$^{\Delta PRD}$ (1–167, 357–779), PLEKHA4$^{\Delta IDR}$ (1–495). For bacterial expression, N-terminal fusions to GST of PLEKHA4^{PH} and PLEKHA4$^{H\text{-}BP\text{-}PH}$ were generated by subcloning into the pGEX-6P-1 vector (GE Healthcare) using EcoRI and SalI.

For generation of stable HeLa or HEK 293 cells, GFP-PLEKHA4, PLEKHA4-GFP, and GFP were subcloned into the pCDNA5-FRT vector (Thermo Fisher) using NheI and KpnI (GFP-PLEKHA4), NheI and NotI (PLEKHA4-GFP and GFP). mCherry-KLHL12, GFP-KLHL12 and 3xFLAG-KLHL12 were generated by subcloning pcDNA3.1+zeo-VSV-KLHL12 (Addgene #16761) into mCherry-C1, pEGFP-C1 vector using KpnI and ApaI, and into pCMV10-3xFLAG (Sigma) using

HindIII and NotI. HA-CUL3 was cloned into pCMV-HA-N vector using XhoI and NotI by amplifying the CUL3 ORF from the ORFeome8.1 library (corresponding to Genbank BC039598.1, a gift from Haiyuan Yu, Cornell University). HA-Ub, M1R-mCherry, and iRFP-PLCδ1-PH was a gift from the De Camilli lab (Yale University). For optoDroplet experiments, mCherry-CRY2-PLEKHA4^{IDR} and mCherry-CRY2-PLEKHA4$^{CC\text{-}IDR}$ were generated by cloning of the relevant PLEKHA4 fragment into mCherry-CRY2(PHR)[73] (a gift from Pietro De Camilli) using PvuI and KpnI.

The following mutations were introduced by Quikchange site-directed mutagenesis (Agilent) followed by DpnI digestion of the parental DNA strand. GFP-PLEKHA4^{PH}, GST-PLEKHA4^{PH}, PLEKHA4$^{H\text{-}BP\text{-}PH}$-GFP, GST-PLEKHA4$^{H\text{-}BP\text{-}PH}$: F40E, 4A (K42A/R43A/R48A/R49A), R75A, R129A; pcDNA3.1+zeo-VSV-KLHL12: Q405X. For rescue experiments, siRNA-resistant GFP-PLEKHA4 or PLEKHA4-GFP were generated by performing silent mutations at the following codons S103, I106, R107, D109, and G110, which is within the siRNA target region. All constructs were verified by Sanger sequencing (Cornell University Biotechnology Resource Center Genomics Facility).

2.6.2 *Transfection of plasmids and siRNAs*

Plasmid transfections were performed using Lipofectamine 2000 (Thermo Fisher) according to the manufacturer's protocol but using Transfectagro (Corning) instead of Opti-MEM. Cells were incubated with transfection mix in Transfectagro supplemented with 10% FBS for 6–8 h, following by a change of media to regular growth media and analysis after 18–20 h.

DsiRNA duplexes were obtained from Integrated DNA Technologies. Transfections with siRNA were performed with the appropriate duplexes (see **Table S2.3**) using Lipofectamine RNAiMAX (Thermo Fisher) following the manufacturer's protocol except using Transfectagro in place of Opti-MEM. Cells were incubated wit transfection mix in Transfectagro supplemented with 10% FBS for 12–16 h, followed by exchange with fresh media. NC1 (negative control 1, IDT) was used as the control siRNA duplex for all experiments. Forty-eight h post transfection, cells were subjected to analysis via Western blot, microscopy or flow cytometry.

2.6.3 *Confocal microscopy*

Prior to transfections (24 h), cells were seeded on 35 mm glass-bottom MatTek (#1.5 thickness, MatTek Corporation) imaging dishes for live cell imaging or on 12 mm cover glass (#1.5 thickness, Fisherbrand) for fixed cell imaging by immunofluorescence. Live cells were imaged 24–30 h post transfection. For immunofluorescence, cells were fixed in 4% paraformaldehyde in 100 mM sodium phosphate buffer (81 mM Na_2HPO_4-$7H_2O$, 21 mM NaH_2PO_4 pH 7.4) for 20 min, rinsed three times with PBS, blocked and permeabilized with blocking buffer (5% BSA and 0.1% Triton-X in 1X PBS) for 30 min. Cells were treated with primary antibody in blocking buffer for 1 h, rinsed with wash buffer (0.1% Triton-X, 1X PBS), incubated with secondary antibody in blocking buffer for 1 h at room temperature, rinsed with wash buffer and then PBS, mounted on slides in ProLong Diamond Antifade with DAPI (Thermo Fisher), and incubated overnight at room temperature in dark before imaging. For long-term storage, slides were stored at 4 ºC.

Images were acquired on a Zeiss LSM 800 confocal laser scanning microscope equipped with Plan Apochromat objectives (20x 0.8 NA or 40x 1.4 NA), and two GaAsP PMT detectors. Solid-state lasers (405, 488, 561, and 640 nm) were used to excite blue, green, red and far-red fluorescence respectively. Live-cell time-series movies were acquired using definite focus. For optoDroplet experiments, a brief 488 nm pulse was used for photoactivation at the indicated frame in the time series. For colocalization-based analysis, multicolor images were acquired using line-scanning mode. Super-resolution structured illumination microscopy (SR-SIM) was performed on a Zeiss Elyra Super Resolution Inverted Axio Observe.Z1 microscope equipped with 405, 488, 561 and 640 nm lasers, definite focus and a Piezo-Z stage insert for fast focusing. Images were acquired using Zeiss Zen Blue 2.3 (confocal), Zeiss Zen Black (SR-SIM) and analyzed using FIJI[74].

2.6.4 *Immunoprecipitation and Western blots*

Cells were harvested (500 x g, 3 min), lysed in lysis buffer (150 mM NaCl, 1% NP-40, 0.25% sodium deoxycholate, 5 mM EDTA, 50 mM Tris pH 7.5), sonicated for 3-5 pulses at 10% intensity, and centrifuged for 10 min at 13000 x g. A fraction of the supernatant was saved, quantified using the BCA assay (Thermo Fisher), and normalized as input, and the remainder was immunoprecipitated by rotation at 4 ºC overnight using either anti-GFP-nanobody sepharose (Chromotek), EZview anti-FLAG-M2, or EZview anti-HA resins (Sigma). For immunoprecipitation using the soluble DVL3 antibody, the sample was incubated with primary antibody for 1 h at 4 ºC with rotation, followed by rotation overnight at 4 ºC with Protein G sepharose

(BioVision). The resin was then centrifuged for 10 min at 1000 x g, washed three times with lysis buffer and analyzed by SDS-PAGE and Western blot, with detection by chemiluminescence (using SuperSignal West Pico (Thermo) or Clarity (Bio-Rad)) or, as described below in detail, mass spectrometry-based proteomics.

2.6.5 *SILAC labeling and mass spectrometry-based proteomics analysis*

For quantitative proteomics analysis, Flp-In HEK 293 cells stably expressing GFP, GFP-PLEKHA4, or PLEKHA4-GFP were cultured in SILAC DMEM media (Thermo 89985) supplemented with 10% dialyzed FBS (JR Scientific) and 1% P/S for at least 5 passages (approximately 2 weeks) to allow full labeling of cells before analysis. "Light" SILAC media contained arginine $^{12}C_6$, $^{14}N_2$ and lysine $^{12}C_6$, $^{14}N_4$, while "heavy" SILAC media contained "heavy" lysine $^{13}C_6$, $^{15}N_2$ and "heavy" arginine $^{13}C_6$, $^{15}N_4$.

Cells were lysed and immunoprecipiated with anti-GFP-nanobody sepharose as described above and processed for mass spectrometry as described[75,76] Briefly, the resin was washed three times with lysis buffer before treatment with elution buffer (100 mM Tris pH 8.0, 1% SDS) by incubation at 65 ºC for 15 min with intermittent tapping. The samples were reduced (10 mM DTT for 15 min), alkylated (10 mM iodoacetamide, 50 mM Tris pH 8.0), and then the "heavy" and "light" solutions were mixed in a 1:1 ratio. The protein was then incubated on ice for 30 min, centrifuged (4700 x g, 10 min) and washed with a solution of 50% acetone, 49.9% methanol, 0.1% acetic acid. The pellet was air-dried and resuspended in urea/Tris solution (8 M urea, 50 mM Tris pH 8.0) and NaCl/Tris solution (150 mM NaCl, 50 mM Tris pH 8.0) in a

ratio of 1:3 respectively. Proteins were digested at 37 ºC overnight on a nutator with Gold trypsin (1 mg/mL, Promega) and then acidified with 10% trifluoroacetic acid and 10% formic acid. Samples were stored at –80 ºC if not analyzed immediately.

The samples were then desalted using a C18 column (WAT0549-55) and dried on a speedvac. The samples were then resuspended in 80% acetonitrile and 1% formic acid followed by fractionation using Hydrophilic Interaction Chromatography (HILIC). HILIC fractions were dried and reconstituted in 0.1% trifluoroacetic acid and analyzed using a Q-Exactive Orbitrap. Database search and quantitation of heavy/light peptide isotope ratios were performed using Sorcerer as previously described[75,76]. A complete list of hits from these proteomics studies is provided in **Table S2.1** and describes two different experiments. Experiment #1: PLEKHA4-GFP (Light), GFP (Heavy); Experiment #2: GFP-PLEKHA4 (Heavy), GFP (Light).

2.6.6 *Protein expression and purification in E. coli*

A single colony of *E. coli* BL21-pRosetta2 transformed with wild-type or mutant GST-PLEKHA4^{PH} or GST-PLEKHA4$^{H\text{-}BP\text{-}PH}$ was grown in terrific broth (TB) supplemented with potassium phosphate buffer (0.17 M monobasic potassium phosphate, 0.17 M dibasic potassium phosphate), ampicillin and chloramphenicol for 6–8 h at 37 ºC, 250 rpm until OD_{600} was between 2 and 3. The temperature was then shifted to 18 ºC for 1 h, expression was induced with 0.25 mM isopropylthio-β-galactosidase (IPTG), and cells were grown overnight for at least 18–20 h at 18 ºC, 250 rpm. Cells were harvested (2100 x g, 15 min, 4 ºC) and stored at –80 ºC until use.

Frozen cell pellets were thawed in bacterial lysis buffer (20 mM Tris pH 8, 500 mM NaCl, 5% glycerol, 10 mM β-mercaptoethanol and 0.1 mM phenylmethylsulfonyl fluoride), sonicated, and centrifuged at 16,500 x g for 30 min to clear the lysate. The supernatant was incubated with washed Glutathione Sepharose 4B resin (GE Healthcare) for 1–2 h under nutation at 4 ºC. Bound complex was washed 15–20 times with lysis buffer and incubated overnight with PreScission protease to cleave off the GST tags. Supernatant was concentrated in 3K Amicon concentrators (Millipore), quantified using a Bradford assay, and flash frozen for storage at –80 ºC until use.

2.6.7 *Liposome co-sedimentation assays*

Liposomes were prepared by mixing 5:94:1 mol% ratio of phosphoinositide species:dioleoylphosphatidylcholine (DOPC):DiR (to aid in visualization of liposomes following SDS-PAGE) in 18:1 chloroform:methanol. Control liposome were DOPC:DiR (99:1 ratio) and dioleoylphosphatidylserine (DOPS):DOPC:DiR (20:79:1 ratio). After mixing, lipids were vacuum-dried, rehydrated in 25 mM HEPES pH 7.4 and 125 mM potassium acetate and incubated overnight at 37 ºC. Liposomes were generated by extruding lipids through 400 nm membranes (Whatman) and stored at 4 ºC protecting from light. The final phosphoinositide concentration was 20–100 μM (2–10 mol%), and the total lipid concentration was 1 mM. Catalog numbers of the exact lipid species used are reported in the **Table 2.3**.

Liposome pelleting assay was performed to assess the binding of purified PLEKHA4 constructs to varying concentrations of phosphoinositide species *in vitro*. To avoid using any aggregates, each aliquot of purified protein was centrifuged at

163,000 x g for 10 min at 4 ºC following thawing and then re-quantified prior to use. This protein (2 μg) was incubated with liposomes (500 μM), giving a total lipid:protein ratio of 150:1 (phosphoinositide species:protein of 15:1 for 10% phosphoinositide-containing liposomes) for 10 min at room temperature in the dark. The reaction mixture was centrifuged at 163,000 x g for 30 min at 4 ºC. Supernatant and pellet were separated, denatured in SDS sample buffer and analyzed via SDS-PAGE gel. Images were acquired and quantified using a ChemiDoc MP system (Bio-Rad).

2.6.8 *PI(4,5)P_2 depletion assay*

HeLa cells were co-transfected with plasmids encoding M1R-mCherry, iRFP-PLCδ1^{PH}, and either GFP-PLEKHA4^{FL} or GFP-PLEKHA4$^{H\text{-}BP\text{-}PH}$ as described in **Figure S2.1B–C**. Twenty-four h after transfection, live-cell time-series with 5 s intervals between each frame, using definite focus as described above. During the time series, oxotremorine-M (10 μM) was added to induce PI(4,5)P_2 depletion.

2.6.9 *Western blot analysis of DVL levels*

Overexpression: HeLa cells were co-transfected with 500 ng each of FLAG-hDVL3 and the combination of GFP, GFP-PLEKHA4 or pCDNA3-VSV-KLHL12 plasmids as described in **Figure 2.4A**. The total DNA amount was normalized to 2.5 μg using pCDNA3 empty vector. After 36 h of cell growth post-transfection, the cells were lysed, quantified, normalized and analyzed by Western blot. Experiments were

performed in biological replicates, and chemiluminescence measured and quantified using a ChemiDoc MP system.

Endogenous levels: SiRNA duplexes (50 nM) against PLEKHA4 or KLHL12 was performed on either HeLa (human) or C57MG WntRGreen (mouse) cells on a 6-well plate. Forty-eight h post RNAi, cells were harvested, analyzed by Western blot and levels of DVL1, DVL2 and DVL3 were quantified. Reported quantifications are from at least three biological replicates.

2.6.10 *Analysis of DVL3 ubiquitination*

Over-expression: HeLa cells were co-transfected with the combination of plasmids as described in **Figure 2.4A–B**. After 36 h of cell growth post-transfection, the cells were lysed, quantified, immunoprecipitated using EZview α-FLAG resin and analyzed by Western blot.

Endogenous: SiRNA-mediated knockdown was performed against PLEKHA4 or KLHL12 on 60 mm dishes. After 48 h of cell growth post-transfection, cells were lysed and immunoprecipitated using 1 µg DVL3 primary antibody per 800 µg of lysate following the immunoprecipitation protocol as described above. Samples were analyzed in biological replicates via Western blot and quantified as described above.

2.6.11 *Rescue of DVL3 levels by PLEKHA4 transfection*

RNAi was performed as described in HeLa cells but with cells seeded on 35-mm MatTek imaging dishes. Thirty-six h after the RNAi transfection, NC1-treated cells were transfected with 2 μg of GFP plasmid, siPLEKHA4 treated cells were transfected, using Lipofectamine 2000, with 2 μg of a plasmid encoding either GFP or PLEKHA4-GFP bearing silent mutations to render it resistant to siRNA (**Figure 2.4E**). After 24 h of cell growth after the plasmid transfection, cells were treated with Hoechst 33342 (Thermo Fisher) and imaged via confocal microscopy to assess the transfection efficiency (which, for these experiments, was determined to be 50–70%). After imaging, cells were harvested and analyzed via Western blot.

2.6.12 *Western blot analysis of β-catenin dependent Axin2 levels*

Endogenous levels: Appropriate siRNA duplexes (50 nM) against PLEKHA4 or KLHL12 were transfected into HeLa (human) or C57MG WntRGreen (mouse) cells on a 6-well plate. Cells were stimulated with Wnt3a conditioned media 24 h post transfection. Forty-eight h post RNAi, cells were harvested, analyzed by Western blot and quantified for Axin2 levels. Reported quantifications are from at least three biological replicates.

2.6.13 *Rescue of Axin2 levels by PLEKHA4 transfection*

RNAi was performed as described in HeLa cells. Thirty-six h after the RNAi transfection, NC1-treated cells were transfected with 2 μg of GFP plasmid, siPLEKHA4 treated cells were transfected with 2 μg of a plasmid encoding either

GFP or PLEKHA4-GFP bearing silent mutations to render it resistant to siRNA (**Figure 2.5E**). Eight h after the plasmid transfection, cells were stimulated with Wnt3a conditioned media for 24 h, and analyzed by Western blot. Reported quantifications are from at least three biological replicates

2.6.14 *Western blot analysis of β-catenin independent p-JNK levels*

SiRNA duplexes (50 nM) against PLEKHA4 was transfected into C57MG WntRGreen cells on a 6-well plate. Cells were stimulated with conditioned media from L cells (control) or L Wnt-5a cells 24 h post transfection. Forty-eight h post RNAi, cells were harvested, analyzed by Western blot and p-JNK levels were quantified. Reported quantifications are from at least three biological replicates.

2.6.15 *Fluorescent Wnt reporter assay*

RNAi (50 nM) was performed on C57MG WntRGreen as described above. After Thirty-six h after the siRNA treatment, MV7-Rat2a-Wnt1 (Wnt1-secreting) or MV7-Rat2a (control) cells were co-cultured with knockdown sample dishes in a 10:1 ratio of C57MG WntRGreen cells to MV7-Rat2a cells) and incubated at 37 ºC, 5% CO_2 atmosphere for an additional 26–30 h. Cells were then analyzed in biological replicates via flow cytometry (BD Accuri C6) or treated with Hoechst 33342 and analyzed by confocal microscopy. Separate dishes treated in exactly the same way were harvested for Western blot analysis.

2.6.16 *Generation of kramer (kmr) knockout flies*

Sequences encoding an sgRNA targeting a region near the beginning of *kramer* (FlyBase: *CG34383*) open reading frame were cloned into the vector pCFD3 (Addgene # 49410). The construct was integrated into an *attP* docking site on the *Drosophila* chromosome 2 by injection into the strain y^1 v^1 $P\{y^{+t7.7}$ *nos-phiC31\int.NLS}; P{CaryP}attP40* (Bloomington stock center line 25709). Injected animals were mated to *y v* flies, and progeny with wildtype eyes were selected.

To make *kmr* knockout flies, males with the integrated sgRNA construct were mated with females of genotype y^1 $M\{w^{+mC}$ *Act5C-Cas9.P}ZH-2A w** (Bloomington stock center line 54590). Male progeny expressing Cas9 and the sgRNA were crossed with *y v; TM3, Sb / TM6B, Tb Hu* females. Single male progeny with the *TM3* balancer were then crossed to the same double balancer stock. Male and female progeny of this latter cross with the *TM6B, Tb Hu* balancer were intercrossed, and generating animals homozygous for putative mutations in *kmr.* These lines were genotyped by sequencing of appropriate PCR products to verify the homozygous knockout of *kmr* gene. We isolated and sequenced two *kmr* alleles with frameshift mutations early in the coding sequence predicted to result in loss of function, kmr^1 and kmr^2. In kmr^1, a 1 bp deletion created a frameshift mutation starting at the 89th codon. In kmr^2, a 2 bp deletion created a frameshift mutation starting at the 88th codon. See **Figure S2.4** for relevant genomic sequences around the deletions that were determined by Sanger sequencing. Both stocks behaved identically in all subsequent experiments, and the either of the kmr^1 and kmr^2 alleles may be referred to simply as kmr^-.

2.6.17 *Generation of flies containing kmr⁻ and other alleles*

To examine possible phenotypes associated with heterozygosity, five simple heterozygote strains (*kmr*$^{+}$*/kmr*^{1}, *kmr*$^{+}$*/kmr*^{2}, *dsh*$^{+}$*/dsh*^{1}, *dsh*$^{+}$*/dsh*^{3}, and *dsh*$^{+}$*/dsh*^{75}) were generated by crossing either homozygous (*kmr*^{1}, *kmr*^{2}, and *dsh*^{1}) or balanced (*dsh*^{3}*/FM7a* or *dsh*^{75}*/FM7a*) strains each separately with *w*^{1118}. The six transheterozygote strains (*kmr*$^{+}$*/kmr*$^{-}$;*dsh*$^{+}$*/dsh*^{1}, *kmr*$^{+}$*/kmr*$^{-}$;*dsh*$^{+}$*/dsh*^{3}, and *kmr*$^{+}$*/kmr*$^{-}$;*dsh*$^{+}$*/dsh*^{75} for both the *kmr*^{1} and *kmr*^{2} alleles) were generated by crossing the appropriate homozygous *kmr* strain with either *dsh*^{1}, *dsh*^{3}*/FM7a*, or *dsh*^{75}*/FM7a*. To control for possible maternal effects, each cross involving *kmr*^{1}, *kmr*^{2}, or *dsh*^{1} was carried out in two ways by switching the males and females and collecting the appropriate F1-generation flies for analysis; the results were identical. For crosses involving *dsh*^{3}*/FM7a* and *dsh*^{75}*/FM7a*, only virgin female flies were used and non-*FM7a* F1-generation female flies were selected for further analysis.

To determine whether wing hair polarity effects are due to knockout of *kmr* as opposed to off-target effects, complementation testing was performed between *kmr*$^{-}$ and the deletion fragment *Df(3R)6170* (abbreviated as *df*), a chromosomal deletion encompassing 23 genes including *kmr*. *kmr*$^{-}$ flies were crossed with *Df(3R)Exel6170* / *TM6B, Tb*^{1} (Bloomington stock 7649), and non-Tb flies (*kmr*^{df}*/kmr*$^{-}$) were selected for analysis.

For assessing Dsh protein levels in wing imaginal discs and loss of proximal-distal asymmetry in pupal wings 30 h after puparium formation, we utilized *dsh::Clover* flies (a gift from Jeffrey Axelrod, Stanford University), which were generated by replacing the EGFP in pCasper4-Dsh-EGFP[58] with the fluorescent

protein Clover2 followed by creation of transgenic lines with insertions on the second and third chromosomes (BestGene Inc.). First, *dsh::Clover/dsh::Clover* virgins (with *dsh::Clover* on chromosome 2 because *kmr* is on chromosome 3) were crossed with *sp/CyoW (II); TM2/TM6B, Tb (III) males*. In the F1 generation *dsh::Clover/CyoW; +/ TM6B, Tb* flies were collected and then crossed with kmr^{-} flies. Finally, the *Tb* progeny of the previous cross (*dsh::Clover/+;* kmr^{-}*/TM6B*) were collected and mated with kmr^{-} flies, generating kmr^{-} flies with a single *dsh::Clover* allele (*dsh::Clover;* kmr^{-}). Control flies that were wild-type at the *kmr* locus and bearing a single *dsh::Clover* allele (*dsh::Clover*), were also generated.

2.6.18 *Dissection and imaging of wing imaginal discs, pupal wings, and adult wings*

Wing imaginal discs: Wing imaginal discs (WIDs) were dissected from individual L3 larvae as described[77], and WIDs were fixed in 4% paraformaldehyde for 30 min, washed three times with wash buffer (5% BSA, 0.1% Triton-X, 1X PBS) and twice with 1X PBS. Genomic DNA was extracted from the remaining unfixed tissues from each individual larva for genotyping. From each animal, one pair of fixed and washed WIDs were mounted with ProLong Diamond Antifade without DAPI (Thermo Fisher) on glass slides under 12 mm coverglass (Fisher Scientific), and the slides were incubated overnight at room temperature in the dark before imaging. For long term storage, slides were stored at 4 ºC. For quantification of fluorescence from the Dsh-Clover protein fusion in WIDs, orthogonal view images were generated from the images of larvae that showed Clover signals post-genotyping. Dsh-Clover localizes in the epithelial folds of the WIDs (shown in **Figure 2.7A** with arrow). Three integrated

density values (independent of the area) were generated from each image, and background was subtracted to obtain corrected integrated densities. Image analysis was performed in a manner blinded with respect to the animals' genotypes.

Pupal wings: Pupal wings were dissected from individual 30 h post puparium formation (APF) pupa as described[78]. From each animal, one pair of fixed and washed pupal wings was mounted with ProLong Diamond Antifade without DAPI (Thermo Fisher) on glass slides under 12 mm coverglass (Fisher Scientific), and the slides were incubated overnight at room temperature in the dark before imaging. For long term storage, slides were stored at 4 ºC. Wings were imaged by confocal fluorescence microscopy, and maximum intensity z-projection images were generated and assessed for extent of proximal-distal symmetry.

Adult wings: Wings of appropriate genotypes were dissected and mounted on glass slides with mounting media (3:1 ratio of DPX:xylenes), and the slides were dried overnight at 50 ºC. Mounted wings were imaged by widefield brightfield microscopy.

2.6.19 *Scanning electron microscopy (SEM)*

Adult flies of correct genotype were collected and fixed in 2% glutaraldehyde in 0.05 M cacodylate buffer pH 7.4 for 2 h at 4 ºC. The samples were rinsed with 0.05 M cacodylate buffer three times for 5 min each and post fixed in 1% OsO_4 (osmium tetroxide, EMS) for 1 h at 4 ºC. The samples were rinsed again with 0.05 M cacodylate buffer three times for 5 min each. Serial dehydration was performed in

25%, 50%, 70%, 95%, 100% ethanol for 20 min each and 100% for 24–48 h at 4 ºC. Samples were critical point dried using a BAL-TEC CPD 030, mounted on stubs, and sputter coated with gold:palladium. Image analysis was performed using Tescan Mira3 FE-SEM microscope. At least 12 individual flies per genotype for eyes and thorax tissues each were analyzed, and four representative images per genotype are provided, one in **Figure 2.6** and three in **Figures S2.6–2.7**.

2.7 QUANTIFICATION AND STATISTICAL ANALYSIS

2.7.1 *Statistics and reproducibility*

All imaging figures show representative images from experiments performed in at least three biological replicates on different days. For all experiments involving quantification, significance was calculated using an unpaired two-tailed Student's t-test with unequal variance. Statistical significance of $p < 0.05$ or lower is reported. In figures containing bar graphs, the number of biological replicates analyzed has been stated in the legend, the height of the bar is the mean, the error bars represent standard deviation, and each overlaid dot represents an individual biological replicate. In the box plot shown in **Figure 2.7B**, the boxes represent the middle quartiles, with the line in the middle representing the median, and the whiskers denote the maximum and minimum values. Image analysis was performed in a blinded manner.

2.8 REFERENCES

(1) Clevers, H.; Nusse, R. Wnt/β-Catenin Signaling and Disease. *Cell* **2012**, *149* (6), 1192–1205. https://doi.org/10.1016/j.cell.2012.05.012.

(2) Janda, C. Y.; Waghray, D.; Levin, A. M.; Thomas, C.; Garcia, K. C. Structural Basis of Wnt. *Science (80-.).* **2012**, *337* (July), 59–64. https://doi.org/10.1126/science.1222879.Structural.

(3) Cadigan, K. M.; Peifer, M. Wnt Signaling from Development to Disease: Insights from Model Systems. *Cold Spring Harb. Perspect. Biol.* **2009**, *1* (2), 1–24. https://doi.org/10.1101/cshperspect.a002881.

(4) Gómez-Orte, E.; Sáenz-Narciso, B.; Moreno, S.; Cabello, J. Multiple Functions of the Noncanonical Wnt Pathway. *Trends Genet.* **2013**, *29* (9), 545–553. https://doi.org/10.1016/j.tig.2013.06.003.

(5) Devenport, D. The Cell Biology of Planar Cell Polarity. *J. Cell Biol.* **2014**, *207* (2), 171–179. https://doi.org/10.1083/jcb.201408039.

(6) Wallingford, J. B. Planar Cell Polarity and the Developmental Control of Cell Behavior in Vertebrate Embryos. *Annu. Rev. Cell Dev. Biol.* **2012**, *28*, 627–653. https://doi.org/10.1146/annurev-cellbio-092910-154208.

(7) MacDonald, B. T.; Tamai, K.; He, X. Wnt/β-Catenin Signaling: Components, Mechanisms, and Diseases. *Dev. Cell* **2009**, *17* (1), 9–26. https://doi.org/10.1016/j.devcel.2009.06.016.

(8) Mlodzik, M. *The Dishevelled Protein Family: Still Rather a Mystery After Over 20 Years of Molecular Studies*, 1st ed.; Elsevier Inc., 2016; Vol. 117. https://doi.org/10.1016/bs.ctdb.2015.11.027.

(9) Gao, C.; Chen, Y. G. Dishevelled: The Hub of Wnt Signaling. *Cell. Signal.* **2010**, *22* (5), 717–727. https://doi.org/10.1016/j.cellsig.2009.11.021.

(10) Wallingford, J. B.; Habas, R. The Developmental Biology of Dishevelled: An Enigmatic Protein Governing Cell Fate and Cell Polarity. *Development* **2005**, *132* (20), 4421–4436. https://doi.org/10.1242/dev.02068.

(11) Angers, S.; Thorpe, C. J.; Biechele, T. L.; Goldenberg, S. J.; Zheng, N.; MacCoss, M. J.; Moon, R. T. The KLHL12–Cullin-3 Ubiquitin Ligase Negatively Regulates the Wnt–β-Catenin Pathway by Targeting Dishevelled for Degradation. *Nat. Cell Biol.* **2006**, *8* (4), 348–357. https://doi.org/10.1038/ncb1381.

(12) Ganner, A.; Lienkamp, S.; Schafer, T.; Romaker, D.; Wegierski, T.; Park, T. J.; Spreitzer, S.; Simons, M.; Gloy, J.; Kim, E.; Wallingford, J. B.; Walz, G. Regulation of Ciliary Polarity by the APC/C. *Proc. Natl. Acad. Sci.* **2009**, *106* (42), 17799–17804. https://doi.org/10.1073/pnas.0909465106.

(13) Sharma, J.; Mulherkar, S.; Mukherjee, D.; Jana, N. R. Malin Regulates Wnt Signaling Pathway through Degradation of Dishevelled2. *J. Biol. Chem.* **2012**, *287* (9), 6830–6839. https://doi.org/10.1074/jbc.M111.315135.

(14) Miyazaki, K.; Fujita, T.; Ozaki, T.; Kato, C.; Kurose, Y.; Sakamoto, M.; Kato, S.; Goto, T.; Itoyama, Y.; Aoki, M.; Nakagawara, A. NEDL1, a Novel Ubiquitin-Protein Isopeptide Ligase for Dishevelled-1, Targets Mutant Superoxide Dismutase-1. *J. Biol. Chem.* **2004**, *279* (12), 11327–11335. https://doi.org/10.1074/jbc.M312389200.

(15) Gao, C.; Cao, W.; Bao, L.; Zuo, W.; Xie, G.; Cai, T.; Fu, W.; Zhang, J.; Wu, W.; Zhang, X.; Chen, Y. G. Autophagy Negatively Regulates Wnt Signalling by Promoting Dishevelled Degradation. *Nat. Cell Biol.* **2010**, *12* (8), 781–790. https://doi.org/10.1038/ncb2082.

(16) Wei, W.; Li, M.; Wang, J.; Nie, F.; Li, L. The E3 Ubiquitin Ligase ITCH Negatively Regulates Canonical Wnt Signaling by Targeting Dishevelled Protein. *Mol. Cell. Biol.* **2012**, *32* (19), 3903–3912. https://doi.org/10.1128/mcb.00251-12.

(17) Dubiel, W.; Dubiel, D.; Wolf, D. A.; Naumann, M. Cullin 3-Based Ubiquitin Ligases as Master Regulators of Mammalian Cell Differentiation. *Trends Biochem. Sci.* **2017**, 1–13. https://doi.org/10.1016/j.tibs.2017.11.010.

(18) Jin, L.; Pahuja, K. B.; Wickliffe, K. E.; Gorur, A.; Baumgärtel, C.; Schekman, R.; Rape, M. Ubiquitin-Dependent Regulation of COPII Coat Size and Function. *Nature* **2012**, *482* (7386), 495–500. https://doi.org/10.1038/nature10822.

(19) Rondou, P.; Haegeman, G.; Vanhoenacker, P.; Van Craenenbroeck, K. BTB Protein KLHL12 Targets the Dopamine D4 Receptor for Ubiquitination by a Cul3-Based E3 Ligase. *J. Biol. Chem.* **2008**, *283* (17), 11083–11096. https://doi.org/10.1074/jbc.M708473200.

(20) McGourty, C. A.; Akopian, D.; Walsh, C.; Gorur, A.; Werner, A.; Schekman, R.; Bautista, D.; Rape, M. Regulation of the CUL3 Ubiquitin Ligase by a Calcium-Dependent Co-Adaptor. *Cell* **2016**, *167* (2), 525-538.e14. https://doi.org/10.1016/j.cell.2016.09.026.

(21) Balla, T. Phosphoinositides: Tiny Lipids with Giant Impact on Cell Regulation. *Physiol. Rev.* **2013**, *93* (3), 1019–1137. https://doi.org/10.1152/physrev.00028.2012.

(22) Hammond, G. R. V; Fischer, M. J.; Anderson, K. E.; Holdich, J.; Koteci, A.; Balla, T.; Irvine, R. F. PI4P and PI(4,5)P2 Are Essential But Independent Lipid Determinants of Membrane Identity. *Science (80-.).* **2012**, *337* (August), 727–730.

(23) Lemmon, M. A. Membrane Recognition by Phospholipid-Binding Domains. *Nat. Rev. Mol. Cell Biol.* **2008**, *9* (2), 99–111. https://doi.org/10.1038/nrm2328.

(24) Hammond, G. R. V.; Balla, T. Polyphosphoinositide Binding Domains: Key to Inositol Lipid Biology. *Biochim. Biophys. Acta - Mol. Cell Biol. Lipids* **2015**, *1851* (6), 746–758. https://doi.org/10.1016/j.bbalip.2015.02.013.

(25) Lemmon, M. A. Pleckstrin Homology (PH) Domains and Phosphoinositides. *Biochem. Soc. Symp.* **2007**, *74* (74), 81–93. https://doi.org/10.1042/BSS0740081.

(26) Godi, A.; Di Campli, A.; Konstantakopoulos, A.; Di Tullio, G.; Alessi, D. R.; Kular, G. S.; Daniele, T.; Marra, P.; Lucocq, J. M.; De Matteis, M. A. FAPPS Control Golgi-to-Cell-Surface Membrane Traffic by Binding to ARF and PtdIns(4)P. *Nat. Cell Biol.* **2004**, *6* (5), 393–404. https://doi.org/10.1038/ncb1119.

(27) D'Angelo, G.; Polishchuk, E.; Tullio, G. Di; Santoro, M.; Campli, A. Di; Godi, A.; West, G.; Bielawski, J.; Chuang, C. C.; Van Der Spoel, A. C.; Platt, F. M.; Hannun, Y. A.; Polishchuk, R.; Mattjus, P.; De Matteis, M. A. Glycosphingolipid Synthesis Requires FAPP2 Transfer of Glucosylceramide. *Nature* **2007**, *449* (7158), 62–67. https://doi.org/10.1038/nature06097.

(28) Li, H.; Marshall, A. J. Phosphatidylinositol (3,4) Bisphosphate-Specific Phosphatases and Effector Proteins: A Distinct Branch of PI3K Signaling. *Cell. Signal.* **2015**, *27* (9), 1789–1798. https://doi.org/10.1016/j.cellsig.2015.05.013.

(29) Shah, J.; Guerrera, D.; Vasileva, E.; Sluysmans, S.; Bertels, E.; Citi, S. PLEKHA7: Cytoskeletal Adaptor Protein at Center Stage in Junctional Organization and Signaling. *Int. J. Biochem. Cell Biol.* **2016**, *75*, 112–116. https://doi.org/10.1016/j.biocel.2016.04.001.

(30) Dowler, S.; Currie, R. A.; Campbell, D. G.; Deak, M.; Kular, G.; Downes, P. C.; Alessi, D. R. Identification of Pleckstrin-Homology-Domain-Containing Proteins with Novel Phosphoinositide-Binding Specificities. *Biochem. J.* **2000**, *351* (1), 19–31. https://doi.org/10.1042/0264-6021:3510019.

(31) Jungmichel, S.; Sylvestersen, K. B.; Choudhary, C.; Nguyen, S.; Mann, M.; Nielsen, M. L. Specificity and Commonality of the Phosphoinositide-Binding Proteome Analyzed by Quantitative Mass Spectrometry. *Cell Rep.* **2014**, *6* (3), 578–591. https://doi.org/10.1016/j.celrep.2013.12.038.

(32) Schink, K. O.; Raiborg, C.; Stenmark, H. Phosphatidylinositol 3-Phosphate, a Lipid That Regulates Membrane Dynamics, Protein Sorting and Cell Signalling. *BioEssays* **2013**, *35* (10), 900–912. https://doi.org/10.1002/bies.201300064.

(33) Zhao, H.; Lappalainen, P. A Simple Guide to Biochemical Approaches for Analyzing Protein-Lipid Interactions. *Mol. Biol. Cell* **2012**, *23* (15), 2823–2830. https://doi.org/10.1091/mbc.E11-07-0645.

(34) Milburn, C.C., Komander, D., Deak, M., Alessi, D.R., Van Aalten, D. M. F. PDB ID: 1UPR. Crystal Structure of the PEPP1 Pleckstrin Homology Domain in Complex with Inositol 1,3,4,5-Tetrakisphosphate. **2004**.

(35) Falkenburger, B. H.; Jensen, J. B.; Hille, B. Kinetics of M1 Muscarinic Receptor and G Protein Signaling to Phospholipase C in Living Cells. *J. Gen. Physiol.* **2010**, *135* (2), 81–97. https://doi.org/10.1085/jgp.200910344.

(36) Falkenburger, B. H.; Jensen, J. B.; Hille, B. Kinetics of PIP2 Metabolism and KCNQ2/3 Channel Regulation Studied with a Voltage-Sensitive Phosphatase in Living Cells. *J. Gen. Physiol.* **2010**, *135* (2), 99–114. https://doi.org/10.1085/jgp.200910345.

(37) Li, P.; Banjade, S.; Cheng, H. C.; Kim, S.; Chen, B.; Guo, L.; Llaguno, M.; Hollingsworth, J. V.; King, D. S.; Banani, S. F.; Russo, P. S.; Jiang, Q. X.; Nixon, B. T.; Rosen, M. K. Phase Transitions in the Assembly of Multivalent Signalling Proteins. *Nature* **2012**, *483* (7389), 336–340. https://doi.org/10.1038/nature10879.

(38) Shin, Y.; Brangwynne, C. P. Liquid Phase Condensation in Cell Physiology and Disease. *Science (80-.).* **2017**, *357* (6357), eaaf4382. https://doi.org/10.1126/science.aaf4382.

(39) Hyman, A. A.; Weber, C. A.; Jülicher, F. Liquid-Liquid Phase Separation in Biology. *Annu. Rev. Cell Dev. Biol.* **2014**. https://doi.org/10.1146/annurev-cellbio-100913-013325.

(40) Mitrea, D. M.; Kriwacki, R. W. Phase Separation in Biology; Functional Organization of a Higher Order Short Linear Motifs - The Unexplored Frontier of the Eukaryotic Proteome. *Cell Commun. Signal.* **2016**, *14* (1), 1–20.

https://doi.org/10.1186/s12964-015-0125-7.

(41) Elbaum-Garfinkle, S.; Kim, Y.; Szczepaniak, K.; Chen, C. C. H.; Eckmann, C. R.; Myong, S.; Brangwynne, C. P. The Disordered P Granule Protein LAF-1 Drives Phase Separation into Droplets with Tunable Viscosity and Dynamics. *Proc. Natl. Acad. Sci. U. S. A.* **2015**, *112* (23), 7189–7194. https://doi.org/10.1073/pnas.1504822112.

(42) Nott, T. J.; Petsalaki, E.; Farber, P.; Jervis, D.; Fussner, E.; Plochowietz, A.; Craggs, T. D.; Bazett-Jones, D. P.; Pawson, T.; Forman-Kay, J. D.; Baldwin, A. J. Phase Transition of a Disordered Nuage Protein Generates Environmentally Responsive Membraneless Organelles. *Mol. Cell* **2015**, *57* (5), 936–947. https://doi.org/10.1016/j.molcel.2015.01.013.

(43) Lin, Y.; Protter, D. S. W.; Rosen, M. K.; Parker, R. Formation and Maturation of Phase-Separated Liquid Droplets by RNA-Binding Proteins. *Mol. Cell* **2015**, *60* (2), 208–219. https://doi.org/10.1016/j.molcel.2015.08.018.

(44) Shin, Y.; Berry, J.; Pannucci, N.; Haataja, M. P.; Toettcher, J. E.; Brangwynne, C. P. Spatiotemporal Control of Intracellular Phase Transitions Using Light-Activated OptoDroplets. *Cell* **2017**, *168* (1–2), 159-171.e14. https://doi.org/10.1016/j.cell.2016.11.054.

(45) Park, H.; Kim, N. Y.; Lee, S.; Kim, N.; Kim, J.; Heo, W. Do. Optogenetic Protein Clustering through Fluorescent Protein Tagging and Extension of CRY2. *Nat. Commun.* **2017**, *8* (1), 30. https://doi.org/10.1038/s41467-017-00060-2.

(46) Hoedt, E.; Zhang, G.; Neubert, T. A. Stable Isotope Labeling by Amino Acids in Cell Culture (SILAC) for Quantitative Proteomics. In *Advancements of Mass Spectrometry in Biomedical Research*; Springer International Publishing: Cham, 2014; pp 93–106. https://doi.org/10.1007/978-3-319-06068-2_5.

(47) Mai, A.; Jung, S. K.; Yonehara, S. HDKIR, a Human Homologue of the Drosophila Kelch Protein, Involved in a Ring-like Structure. *Exp. Cell Res.* **2004**, *300* (1), 72–83. https://doi.org/10.1016/j.yexcr.2004.06.023.

(48) Furukawa, M.; He, Y. J.; Borchers, C.; Xiong, Y. Targeting of Protein Ubiquitination by BTB-Cullin 3-Roc1 Ubiquitin Ligases. *Nat. Cell Biol.* **2003**, *5* (11), 1001–1007. https://doi.org/10.1038/ncb1056.

(49) Xu, L.; Wei, Y.; Reboul, J.; Vaglio, P.; Shin, T. H.; Vidal, M.; Elledge, S. J.; Harper, J. W. BTB Proteins Are Substrate-Specific Adaptors in an SCF-like Modular Ubiquitin Ligase Containing CUL-3. *Nature* **2003**, *425* (6955), 316–321. https://doi.org/10.1038/nature01985.

(50) Brown, A. M. C.; Wildin, R. S.; Prendergast, T. J.; Varmus, H. E. A Retrovirus Vector Expressing the Putative Mammary Oncogene Int-1 Causes Partial Transformation of a Mammary Epithelial Cell Line. *Cell* **1986**, *46* (7), 1001–1009. https://doi.org/10.1016/0092-8674(86)90699-9.

(51) Santiago, F.; Oguma, J.; Brown, A. M. C.; Laurence, J. Noncanonical Wnt Signaling Promotes Osteoclast Differentiation and Is Facilitated by the Human Immunodeficiency Virus Protease Inhibitor Ritonavir. *Biochem. Biophys. Res. Commun.* **2012**, *417* (1), 223–230. https://doi.org/10.1016/j.bbrc.2011.11.089.

(52) Boutros, M.; Paricio, N.; Strutt, D. I.; Mlodzik, M. Dishevelled Activates JNK and Discriminates between JNK Pathways in Planar Polarity and Wingless Signaling. *Cell* **1998**, *94* (1), 109–118. https://doi.org/10.1016/S0092-8674(00)81226-X.

(53) Wodarz, A.; Nusse, R. Mechanisms of Wnt Signaling in Development. *Annu. Rev. Cell Dev. Biol.* **1998**, *14*, 59–88. https://doi.org/10.1146/annurev.cellbio.14.1.59.

(54) Swarup, S.; Verheyen, E. M. Wnt/Wingless Signaling in Drosophila. *Cold Spring Harb. Perspect. Biol.* **2012**, *4* (6), a007930--a007930. https://doi.org/10.1101/cshperspect.a007930.

(55) Simons, M.; Mlodzik, M. Planar Cell Polarity Signaling: From Fly Development to Human Disease. *Annu. Rev. Genet.* **2008**, *42* (1), 517–540. https://doi.org/10.1146/annurev.genet.42.110807.091432.

(56) Axelrod, J. D. Progress and Challenges in Understanding Planar Cell Polarity Signaling. *Semin. Cell Dev. Biol.* **2009**, *20* (8), 964–971. https://doi.org/10.1016/j.semcdb.2009.08.001.

(57) Hale, R.; Strutt, D. Conservation of Planar Polarity Pathway Function Across the Animal Kingdom. *Annu. Rev. Genet.* **2015**, *49*, 529–551. https://doi.org/10.1146/annurev-genet-112414-055224.

(58) Axelrod, J. D. Unipolar Membrane Association of Dishevelled Mediates Frizzled Planar Cell Polarity Signaling. *Genes Dev.* **2001**, *15* (10), 1182–1187. https://doi.org/10.1101/gad.890501.

(59) Wu, J.; Klein, T. J.; Mlodzik, M. Subcellular Localization of Frizzled Receptors, Mediated by Their Cytoplasmic Tails, Regulates Signaling Pathway Specificity. *PLOS Biol.* **2004**, *2* (7), e158.

(60) Strutt, H.; Searle, E.; Thomas-MacArthur, V.; Brookfield, R.; Strutt, D. A Cul-3-BTB Ubiquitylation Pathway Regulates Junctional Levels and Asymmetry of

Core Planar Polarity Proteins. *Development* **2013**, *140* (8), 1693–1702. https://doi.org/10.1242/dev.089656.

(61) Schink, K. O.; Tan, K.-W.; Stenmark, H. Phosphoinositides in Control of Membrane Dynamics. *Annu. Rev. Cell Dev. Biol.* **2016**, *32* (1), 143–171. https://doi.org/10.1146/annurev-cellbio-111315-125349.

(62) Dickson, E. J.; Hille, B. Understanding Phosphoinositides: Rare, Dynamic, and Essential Membrane Phospholipids. *Biochem. J.* **2019**, *476* (1), 1–23. https://doi.org/10.1042/BCJ20180022.

(63) Banjade, S.; Rosen, M. K. Phase Transitions of Multivalent Proteins Can Promote Clustering of Membrane Receptors. *Elife* **2014**, *3*, 1–24. https://doi.org/10.7554/eLife.04123.

(64) Sear, R. P. Dishevelled: A Protein That Functions in Living Cells by Phase Separating. *Soft Matter* **2007**, *3* (6), 680–684. https://doi.org/10.1039/b618126k.

(65) Pan, W.; Choi, S.; Wang, H.; Qin, Y.; Volpicelli-daley, L.; Swan, L.; Lucast, L.; Khoo, C.; Zhang, X.; Li, L.; Abrams, C. S.; Sokol, S. Y.; Wu, D. Wnt3a-Mediated Formation of Phosphatidylinositol 4,5-Bisphosphate Regulates LRP6 Phosphorylation. *Science (80-.).* **2008**, *321* (September), 1350–1354.

(66) Qin, Y.; Li, L.; Pan, W.; Wu, D. Regulation of Phosphatidylinositol Kinases and Metabolism by Wnt3a and Dvl. *J. Biol. Chem.* **2009**, *284* (34), 22544–22548. https://doi.org/10.1074/jbc.M109.014399.

(67) Yin, H. L.; Janmey, P. A. Phosphoinositide Regulation of the Actin Cytoskeleton. *Annu. Rev. Physiol.* **2003**, *65* (1), 761–789. https://doi.org/10.1146/annurev.physiol.65.092101.142517.

(68) Shewan, A.; Eastburn, D. J.; Mostov, K. Phosphoinositides in Cell Architecture. *Cold Spring Harb. Perspect. Biol.* **2011**, *3* (8), 1–17. https://doi.org/10.1101/cshperspect.a004796.

(69) Hassan, B. A.; Prokopenko, S. N.; Breuer, S.; Zhang, B.; Paululat, A.; Bellen, H. J. Skittles, a Drosophila Phosphatidylinositol 4-Phosphate 5-Kinase, Is Required for Cell Viability, Germline Development and Bristle Morphology, but Not for Neurotransmitter Release. *Genetics* **1998**, *150* (4), 1527–1537.

(70) Gassama-Diagne, A.; Payrastre, B. *Chapter 8 Phosphoinositide Signaling Pathways. Promising Role as Builders of Epithelial Cell Polarity*, 1st ed.; Elsevier Inc., 2009; Vol. 273. https://doi.org/10.1016/S1937-6448(08)01808-X.

(71) Hu, J.; Yuan, Q.; Kang, X.; Qin, Y.; Li, L.; Ha, Y.; Wu, D. Resolution of Structure of PIP5K1A Reveals Molecular Mechanism for Its Regulation by Dimerization and Dishevelled. *Nat. Commun.* **2015**, *6*. https://doi.org/10.1038/ncomms9205.

(72) Yang, Y.; Mlodzik, M. Wnt-Frizzled/Planar Cell Polarity Signaling: Cellular Orientation by Facing the Wind (Wnt). *Annu. Rev. Cell Dev. Biol.* **2015**, *31*, 623–646. https://doi.org/10.1146/annurev-cellbio-100814-125315.

(73) Idevall-hagren, O.; Dickson, E. J.; Hille, B.; Toomre, D. K.; Camilli, P. De. Optogenetic Control of Phosphoinositide Metabolism. **2012**, *109* (35). https://doi.org/10.1073/pnas.1211305109/-/DCSupplemental.www.pnas.org/cgi/doi/10.1073/pnas.1211305109.

(74) Schindelin, J.; Arganda-Carreras, I.; Frise, E.; Kaynig, V.; Longair, M.; Pietzsch, T.; Preibisch, S.; Rueden, C.; Saalfeld, S.; Schmid, B.; Tinevez, J.-Y.; White, D. J.; Hartenstein, V.; Eliceiri, K.; Tomancak, P.; Cardona, A. Fiji: An Open-Source Platform for Biological-Image Analysis. *Nat. Methods* **2012**, *9*, 676.

(75) Bastos de Oliveira, F. M.; Kim, D.; Lanz, M.; Smolka, M. B. Quantitative Analysis of DNA Damage Signaling Responses to Chemical and Genetic Perturbations. *Methods Mol. Biol.* **2018**, *1672*, 645–660. https://doi.org/10.1007/978-1-4939-7306-4_42.

(76) Bastos de Oliveira, F. M.; Kim, D.; Cussiol, J. R.; Das, J.; Jeong, M. C.; Doerfler, L.; Schmidt, K. H.; Yu, H.; Smolka, M. B. Phosphoproteomics Reveals Distinct Modes of Mec1/ATR Signaling during DNA Replication. *Mol. Cell* **2015**, *57* (6), 1124–1132. https://doi.org/10.1016/j.molcel.2015.01.043.

(77) AU - Spratford, C. M.; AU - Kumar, J. P. Dissection and Immunostaining of Imaginal Discs from Drosophila Melanogaster. *JoVE* **2014**, No. 91, e51792. https://doi.org/doi:10.3791/51792.

(78) Bolatto, C.; Parada, C.; Colmenares, V. A Rapid and Efficient Method to Dissect Pupal Wings of Drosophila Suitable for Immunodetections or PCR Assays. *J. Vis. Exp.* **2017**, No. 130. https://doi.org/10.3791/55854.

2.9 APPENDIX

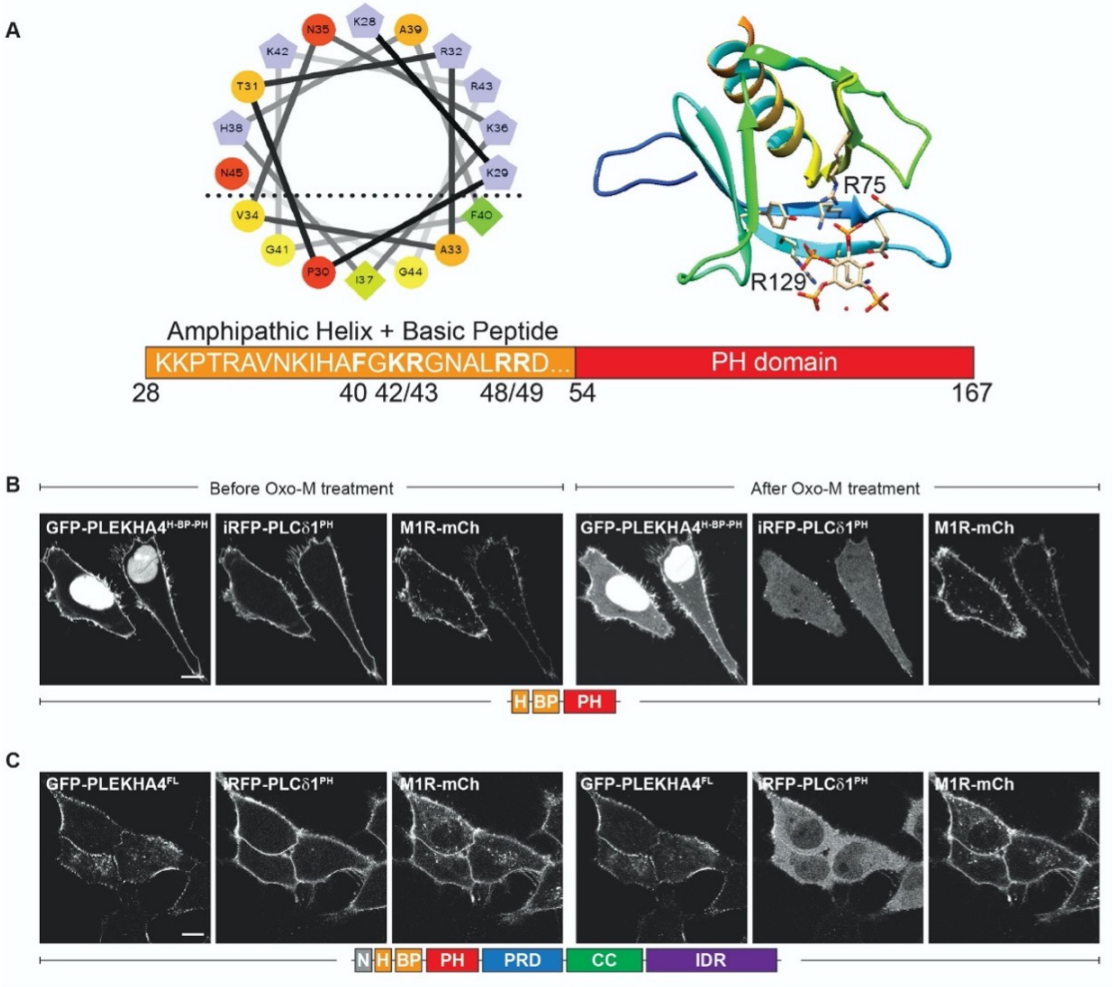

Figure S2.1, related to Figure 2.1. Minimal motif for PLEKHA4 plasma membrane localization via interaction with PI(4,5)P_2 comprises a putative amphipathic helix, basic peptide, and PH domain. (A) Shown at left is a helical wheel projection of residues 28–42 of human PLEKHA4, with dotted line separating hydrophobic (bottom) from hydrophilic (top) faces of the helix. The primary amino acid sequence of helix and adjacent basic peptide are provided below, with residues that were mutated for structure–function studies bolded. Shown at right is an x-ray crystal structure of the PLEKHA4 PH domain in complex with inositol-1,3,4,5-tetrakisphosphate (PDB ID: 1UPR), with the two key Arg residues indicated that form contacts with the PIP head group. (B) PLEKHA4$^{H\text{-}BP\text{-}PH}$ (28–167) interacts with PI(4,5)P_2 at the plasma membrane. HeLa cells co-transfected with a PI(4,5)P_2 marker (iRFP-PLCδ1^{PH}), an mCherry-tagged muscarinic M1 receptor (M1R-mCherry), and either GFP-PLEKHA4$^{H\text{-}BP\text{-}PH}$ or GFP-PLEKHA4^{FL} were imaged before and after PI(4,5)P_2 depletion induced by treatment with oxotremorine M (Oxo-M). Note that

Oxo-M treatment causes a decrease in plasma membrane localization and increase in cytosolic localization of PLEKHA4$^{H\text{-}BP\text{-}PH}$ but not of PLEKHA4^{FL}. Scale bar: 10 µm.

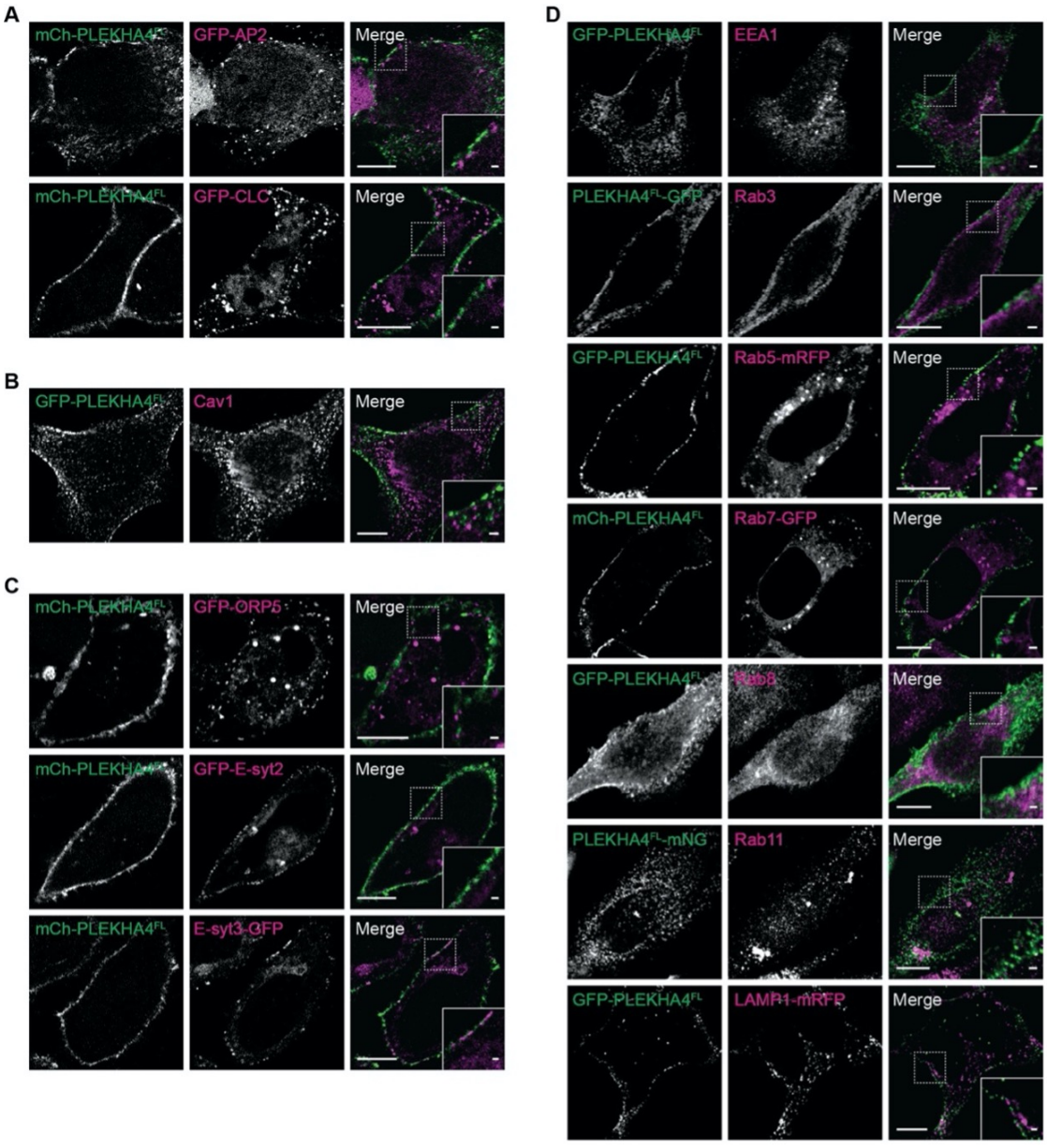

Figure S2.2, related to Figure 2.2. PLEKHA4 does not localize to known assemblies at the plasma membrane or endolysosomal compartments. Confocal microscopy images of HeLa cells showing that PLEKHA4 puncta do not colocalize or minimally colocalize with markers of established assemblies such as clathrin-coated pits (A), caveolae (B), endoplasmic reticulum–plasma membrane contact sites (C), or

endosomes and lysosomes (D). Cells were transfected with the indicated GFP, mCherry (mCh), or mRFP-tagged plasmids. For clarity, in the merged image, PLEKHA4 (PLEKHA4^{FL}, full-length) is shown in green and organelle markers are shown in magenta. For images where the organelle marker is a transfected plasmid (AP2, CLC (clathrin light chain), ORP5, E-syt2, E-syt3, Rab5, Rab7, and LAMP1), confocal microscopy imaging was performed on live cells. For images where the organelle marker is the endogenous protein (Cav1, EEA1, Rab3, Rab8, and Rab11), fixation and immunofluorescence labeling was performed, followed by confocal microscopy imaging. Scale bars: 10 μm; 1 μm (insets).

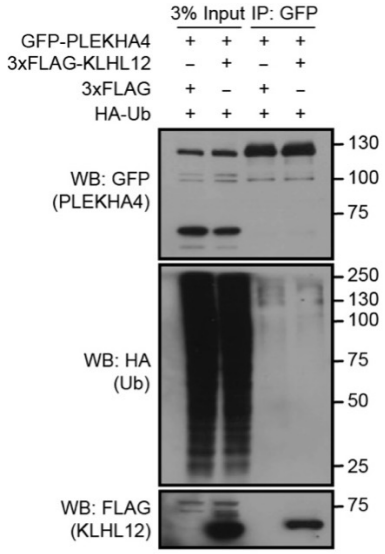

Figure S2.3, related to Figure 2.4. KLHL12 does not modulate ubiquitination of PLEKHA4. Western blot analysis of anti-GFP immunoprecipitates from HeLa cells transfected with plasmids for either 3xFLAG-KLHL12 or 3xFLAG only (empty vector) in combination with GFP-PLEKHA4 and HA-ubiquitin (HA-Ub).

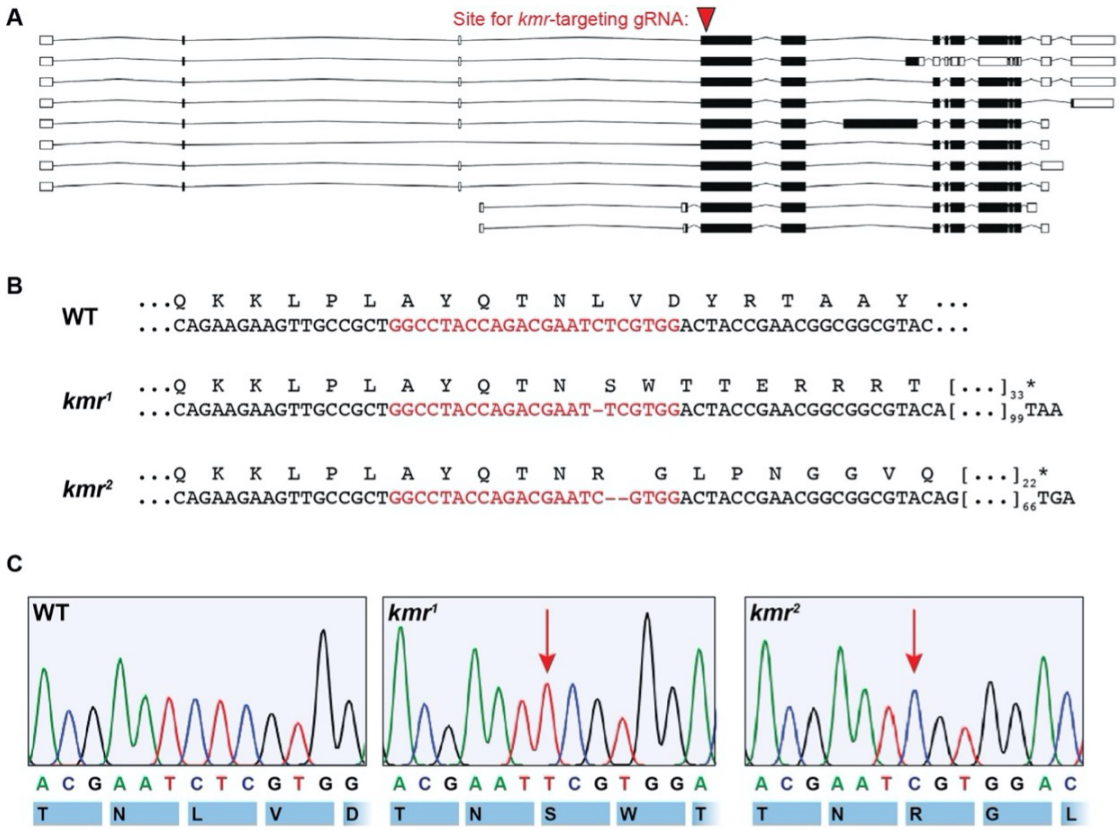

Figure S2.4, related to Figure 2.6. (A) Transcript alignment showing the guide RNA target site, early in the coding sequence, for generation of knockout strains of *kramer (kmr)*, the PLEKHA4 homolog in *Drosophila melanogaster*. Exons of *kmr* (*CG34383*) are shown in rectangles, with the open reading frame in black. (B) Alignment of partial genomic sequence after genotyping PCR reaction of the mutant alleles kmr^1 and kmr^2, compared to the wildtype, with predicted translation shown above. The guide RNA target sequences are colored in red. Note that for both the kmr^1 and kmr^2 alleles, the deletion of 1 and 2 bases, respectively, leads to a frameshift that causes an early stop codon in the Kramer protein. (C) Sanger sequencing traces verify the knockout in kmr^1 and kmr^2. Red arrows indicate the start of frameshift in the knockout clones.

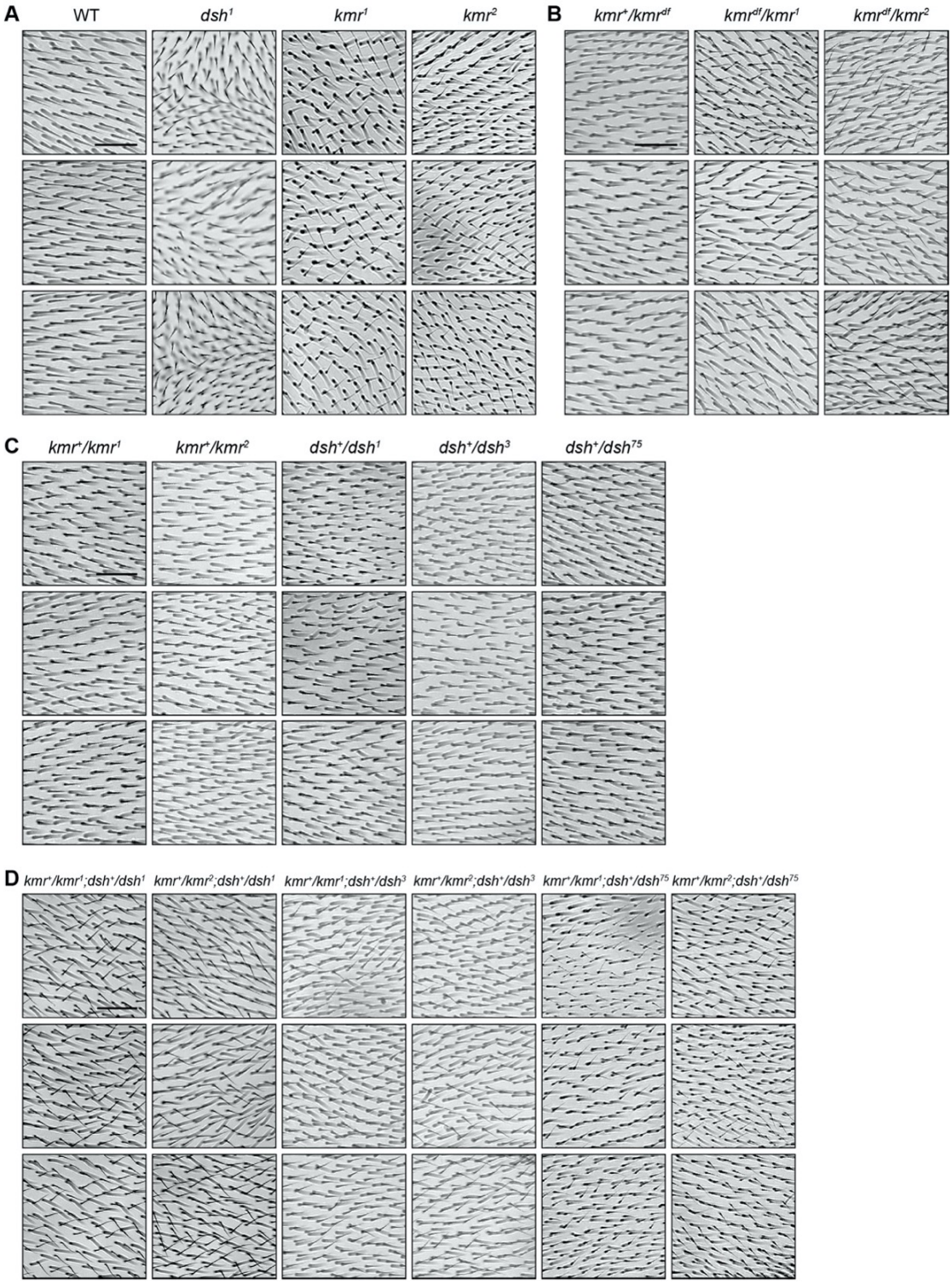

Figure S2.5, related to Figure 2.6. Knockout of the fly PLEKHA4 homolog, *kramer (kmr)*, results in defects in orientation of hair in the adult wing. Shown is brightfield imaging analysis of *Drosophila melanogaster* adult wings oriented proximal to distal (left to right) showing defects in PCP signaling. The panels here

provide three additional examples of the identical genotypes present in **Figure 2.6A–D**: wild-type and homozygotic *kmr* or *dsh* strains (A), complementation with a deletion fragment strain (B), simple heterozygotic *kmr* or *dsh* strains (C), and transheterozygotic strains for *kmr/dsh* (D). Scale bars: 50 μm.

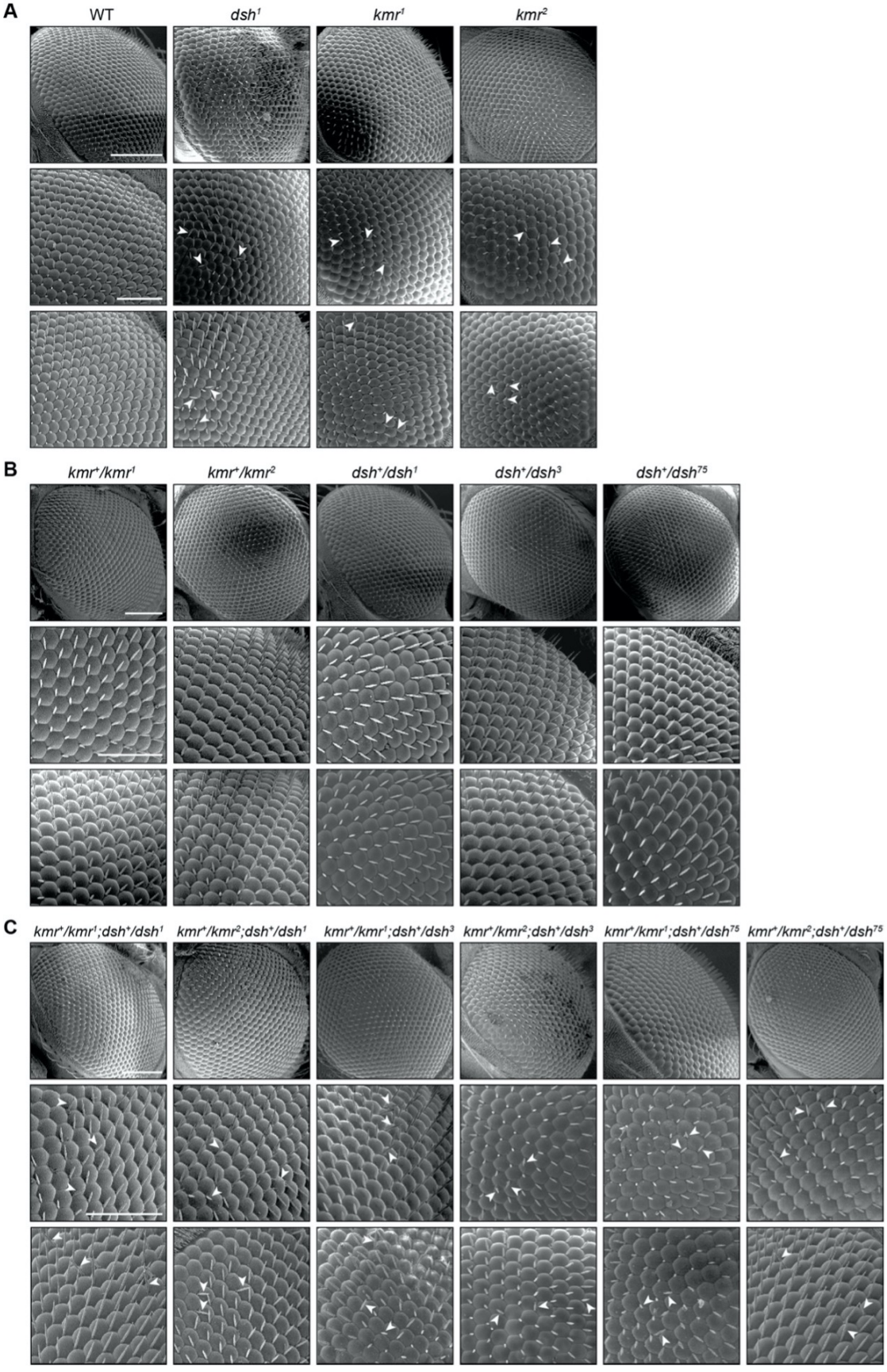
A
WT
dsh1
kmr1
kmr2
B
kmr+/kmr1
kmr+/kmr2
dsh+/dsh1
dsh+/dsh3
dsh+/dsh75
C
kmr+/kmr1;dsh+/dsh1
kmr+/kmr2;dsh+/dsh1
kmr+/kmr1;dsh+/dsh3
kmr+/kmr2;dsh+/dsh3
kmr+/kmr1;dsh+/dsh75
kmr+/kmr2;dsh+/dsh75

Figure S2.6, related to Figure 2.6. Knockout of the fly PLEKHA4 homolog, *kramer (kmr)*, results in defects in polarization of adult eye bristles. Shown are scanning electron microscopy (SEM) images of the eyes of adult flies. The top row of each part shows the complete eye, and the bottom two rows show additional zoomed in examples. The panels here correspond to and provide additional examples of the identical genotypes shown in **Figure 2.6E–G**: wild-type and homozygotic *kmr* or *dsh* strains (A), simple heterozygotic *kmr* or *dsh* strains (B), and transheterozygotic strains for *kmr/dsh* (C). Arrowheads indicate examples of hairs with altered orientations due to defective PCP signaling. Note loss of polarized eye bristle patterning in homozygotic strains and modest loss of patterning in transheterozygotes, compared to wild-type and simple heterozygote controls. Scale bars: 100 μm (top rows of each part; full eyes) and 50 μm (middle and bottom rows of each part; zoomed-in views).

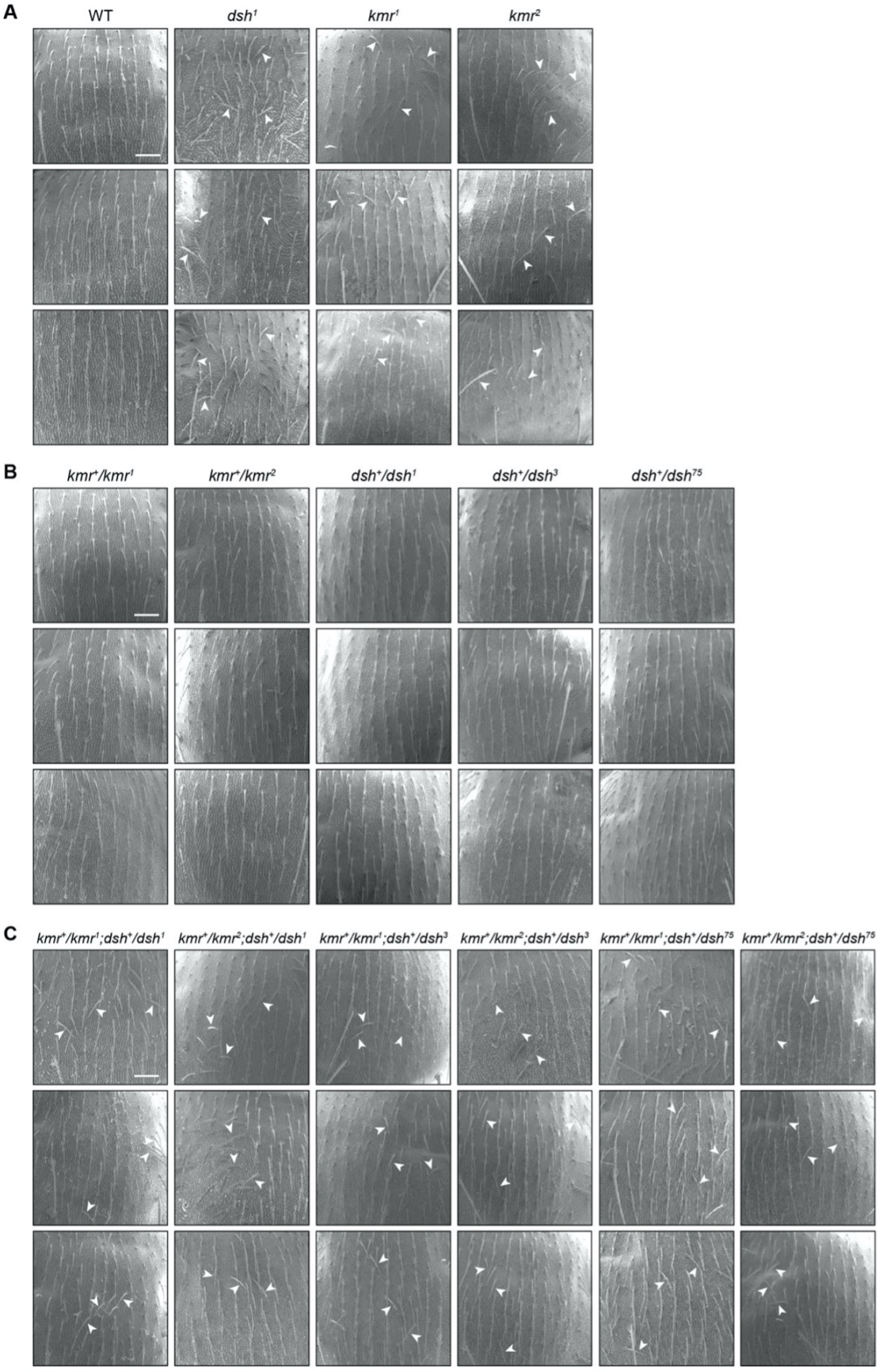
A
WT
dsh1
kmr1
kmr2
B
kmr+/kmr1
kmr+/kmr2
dsh+/dsh1
dsh+/dsh3
dsh+/dsh75
C
kmr+/kmr1;dsh+/dsh1
kmr+/kmr2;dsh+/dsh1
kmr+/kmr1;dsh+/dsh3
kmr+/kmr2;dsh+/dsh3
kmr+/kmr1;dsh+/dsh75
kmr+/kmr2;dsh+/dsh75

Figure S2.7, related to Figure 2.6. Knockout of the fly PLEKHA4 homolog, *kramer (kmr)*, results in defects in polarization of thoracic bristles. Shown are scanning electron microscopy (SEM) images of the thoraxes of adult flies. The panels here correspond to and provide additional examples of the identical genotypes shown in **Figure 2.6H–J**: wild-type and homozygotic *kmr* or *dsh* strains (A), simple heterozygotic *kmr* or *dsh* strains (B), and transheterozygotic strains for *kmr/dsh* (C). Arrowheads indicate examples of hairs with altered orientations due to defective PCP signaling. Note loss of polarized thoracic hair patterning in homozygotic strains and modest loss of patterning in transheterozygotes, compared to wild-type and simple heterozygote controls. Scale bars: 50 μm.

Table S2.1, related to **Figure 2.3.** Complete data set from SILAC proteomics to identify PLEKHA4 interaction partners. HEK 293 cells stably expressing PLEKHA4-GFP, GFP-PLEKHA4, or GFP were grown in the appropriate SILAC medium (heavy or light), and GFP immunoprecipitation was performed, followed by quantitative SILAC-enabled shotgun proteomics. Experiment #1: PLEKHA4-GFP (light), GFP (heavy); Experiment #2: GFP-PLEKHA4 (heavy), GFP (light). For a complete list of hits, please refer to Table S1 in **Shami Shah A. et al. *Cell Reports* (2019)**

Table S2.2 List of oligonucleotides used in this study.

Oligonucleotides		
REAGENT	SOURCE	IDENTIFIER
NC1 Negative Control dsiRNA Sense: rCrGrUrUrArArUrCrGrCrGrUrArUrArArUrArCrG rCrGrUAT	IDT	N/A
NC1 Negative Control dsiRNA Antisense: rArUrArCrGrCrGrUrArUrUrArUrArCrGrCrGrArU rUrArArCrGrArC	IDT	N/A
siRNA hPLEKHA4 Sense: rArGrCrUrArCrArArUrArUrUrArGrArCrCrArGrA rUrGrGGC	IDT	N/A

siRNA hPLEKHA4 Antisense: rGrCrCrCrArUrCrUrGrGrUrCrUrArArUrArUrUrG rUrArGrCrUrGrG	IDT	N/A
siRNA mPLEKHA4 Sense: rArGrCrUrUrGrGrArGrArCrArGrArUrArCrGrUrU rGrUrUGA	IDT	N/A
siRNA mPLEKHA4 Antisense: rUrCrArArCrArArCrGrUrArUrCrUrGrUrCrUrCrC rArArGrCrUrCrU	IDT	N/A
siRNA hKLHL12 Sense: rArArCrCrUrUrArUrGrUrUrGrArCrArUrCrCrArA rGrGrUTT	IDT	N/A
siRNA hKLHL12 Antisense: rArArArCrCrUrUrGrGrArUrGrUrCrArArCrArUrA rArGrGrUrUrUrC	IDT	N/A
siRNA mKLHL12 Sense: rArCrGrArGrArUrUrCrArGrGrUrGrGrArUrUrCrU rGrArAGA	IDT	N/A
siRNA mKLHL12 Antisense: rUrCrUrUrCrArGrArArUrCrCrArCrCrUrGrArArU rCrUrCrGrUrCrG	IDT	N/A

CG34383 gRNA: GTCGGCCTACCAGACGAATCTCG	IDT	N/A

Table S2.3 Key resource table for reagents used in this study.

REAGENT or RESOURCE	SOURCE	IDENTIFIER
Antibodies		
Rabbit polyclonal anti-PLEKHA4	Abcam	Cat#ab170537
Mouse monoclonal anti-KLHL12	ProMab Biotechnology	Cat#30058
Mouse monoclonal anti-DVL1	Santa Cruz Biotechnology	Cat#sc-8025 [3F12]
Rabbit polyclonal anti-DVL2	Cell Signaling Technology	Cat#3216
Mouse monoclonal anti-DVL3	Santa Cruz Biotechnology	Cat#sc-8027 [4D3]
Rabbit monoclonal anti-Axin2	Cell Signaling Technology	Cat#2151 [76G6]
Rabbit monoclonal anti-Axin2	Abcam	Cat#ab109307
Mouse monoclonal anti-p-JNK	Santa Cruz Biotechnology	Cat#sc-6254 [G7]
Mouse monoclonal anti-pan-JNK	Santa Cruz Biotechnology	Cat#sc-7345 [D2]
Mouse monoclonal anti-GFP	Takara Bio	Cat #632375 Living Colors
Mouse monoclonal anti-mCherry	Abcam	Cat#ab125096 [1C51]

Rabbit polyclonal anti-FLAG	Millipore Sigma	Cat#F7425
Rat monoclonal anti-HA	Roche	Cat#11867423001 [3F10]
Mouse monoclonal anti-Ubiquitin	Santa Cruz Biotechnology	Cat#sc-8017 [P4D1]
Mouse monoclonal anti-GAPDH	GeneTex	Cat#GTX78213 [1D4]
Rabbit polyclonal anti-Caveolin 1	BD Biosciences	Cat#610059
Rabbit polyclonal anti-EEA1	Thermo Fisher Scientific	PA1-063A
Mouse monoclonal anti-Rab3	Pietro De Camilli, Yale	CL42.1 ascites
Rabbit monoclonal anti-Rab8	Cell Signaling Technology	Cat#6975S [D22D8]
Rabbit monoclonal anti-Rab11	Thermo Fisher Scientific	Cat#700184 [3H18L5]
Chemicals, Peptides, and Recombinant Proteins		
Osmium Tetroxide (4% solution)	Electron Microscopy Sciences	Cat#RT 19140
Protein G–Sepharose resin	BioVision Inc.	Cat#6511-5

DPX	Millipore Sigma	Cat#06522
L-α-phosphatidylinositol (Liver, Bovine) (sodium salt) (PI)	Avanti Polar Lipids	Cat#840042
1,2-dioleoyl-*sn*-glycero-3-phospho-L-serine (sodium salt) (DOPS)	Avanti Polar Lipids	Cat#840035C
1,2-Dioleoyl-sn-glycero-3-phosphocholine (DOPC)	Echelon Biosciences	Cat#L-1182
DiR';DiIC$_{18}$(7) (1,1'-Dioctadecyl-3,3,3',3'-Tetramethylindotricarbocyanine Iodide)	Thermo Fisher Scientific	Cat#D12731
L-α-D-*myo*-Phosphatidylinositol 3-monophosphate, 3-O-phospho linked, D(+)-sn-1,2-di-O-hexadecanoylglyceryl (PI3P)	CellSignals Inc.	Cat#910
L-α-D-*myo*-Phosphatidylinositol 4-monophosphate, 3-O-phospho linked, D(+)-sn-1,2-di-O-hexadecanoylglyceryl (PI4P)	CellSignals Inc.	Cat#912

L-α-D-*myo*-Phosphatidylinositol 5-monophosphate, 3-O-phospho linked, D(+)-sn-1,2-di-O-hexadecanoylglyceryl (PI5P)	CellSignals Inc.	Cat#914
L-α-D-*myo*-Phosphatidylinositol 4,5-bisphosphate, 3-O-phospho linked, D(+)-sn-1,2-di-O-hexadecanoylglyceryl ($PI(4,5)P_2$)	CellSignals Inc.	Cat#902
L-α-D-*myo*-Phosphatidylinositol 3,4-bisphosphate, 3-O-phospho linked, D(+)-sn-1,2-di-O-hexadecanoylglyceryl ($PI(3,4)P_2$)	CellSignals Inc.	Cat#904
L-α-D-*myo*-Phosphatidylinositol 3,5-bisphosphate, 3-O-phospho linked, D(+)-sn-1,2-di-O-hexadecanoylglyceryl ($PI(3,5)P_2$)	CellSignals Inc.	Cat#906
L-α-D-*myo*-Phosphatidylinositol 3,4,5-trisphosphate, 3-O-phospho linked, D(+)-sn-1,2-di-O-hexadecanoylglyceryl ($PI(3,4,5)P_3$)	CellSignals Inc.	Cat#908
Experimental Models: Cell Lines		

Human: Flp-In T-REx HeLa	Pietro De Camilli, Yale	N/A
Human: Flp-In T-REx HeLa GFP	This work	N/A
Human: Flp-In T-REx HeLa GFP-PLEKHA4	This work	N/A
Human: Flp-In T-REx HeLa PLEKHA4-GFP	This work	N/A
Human: HEK 293TN	Tony Bretscher, Cornell	N/A
Human: Flp-In HEK293	Pietro De Camilli, Yale	N/A
Human: Flp-In HEK293–GFP (SILAC Heavy/Light)	This work	N/A
Human: Flp-In HEK293–GFP-PLEKHA4 (SILAC Heavy/Light)	This work	N/A
Human: Flp-In HEK293–PLEKHA4-GFP (SILAC Heavy/Light)	This work	N/A
Mouse: C57MG–WntRGreen	Anthony Brown, Weill Cornell Medicine[1]	N/A

Mouse: MV7 Rat2a (control) MV7 Rat2a–Wnt1	Gerlinde Van De Walle, Cornell	N/A
Mouse: L (control) L–Wnt3a	Anthony Brown, Weill Cornell Medicine	N/A
Mouse: L–Wnt5a	ATCC	CRL-2814
Experimental Models: Organisms/Strains		
D. melanogaster: *y[1] M{w[+mC]=Act5C-Cas9.P}ZH-2A w[*]*	Bloomington Drosophila Stock Center	Stock# 54590
D. melanogaster: y^1 v^1 $P\{y^{+t7.7}$ *nos-phiC31\int.NLS}; P{CaryP}attP40*	Bloomington Drosophila Stock Center	Stock# 25709
D. melanogaster: *y v; TM3, Sb / TM6B, Tb Hu*	This work	N/A
D. melanogaster: *sp/CyoW (II); TM2/TM6B, Tb (III)*	This work	N/A
D. melanogaster: *w[1] dsh[1]*	Bloomington Drosophila Stock Center	Stock# 5298

D. melanogaster: w[*] dsh[3] P{ry[+t7.2]=neoFRT}19A/FM7a	Bloomington Drosophila Stock Center	Stock# 6331
D. melanogaster: dsh[75] P{ry[+t7.2]=neoFRT}19A/FM7a	Bloomington Drosophila Stock Center	Stock# 68165
D. melanogaster: w[1118]; Df(3R)Exel6170, P{w[+mC]=XP-U}Exel6170/TM6B, Tb[1]	Bloomington Drosophila Stock Center	Stock# 7649
D. melanogaster: *pCasper4-Dsh-clover2*	Jeffrey Axelrod, Stanford	N/A
Recombinant DNA		
PLEKHA4 cDNA	DNASU	BC024157
pEGFP-C1	Clontech	Cat#6084-1
pEGFP-N1	Clontech	Cat#6085-1
mCherry-N1	Clontech	Cat#632523
mCherry-C1	Clontech	Cat#632524
GFP-PLEKHA4	This work	N/A
PLEKHA4-GFP	This work	N/A
mCherry-PLEKHA4	This work	N/A

PLEKHA4-mCherry	This work	N/A
GFP-PLEKHA4^{PH} (45–167)	This work	N/A
GFP-PLEKHA4^{PRD} (167–357)	This work	N/A
GFP-PLEKHA4^{PRD-CC} (167–495)	This work	N/A
GFP-PLEKHA4$^{PRD-CC-IDR}$ (167–779)	This work	N/A
GFP-PLEKHA4^{CC} (357–495)	This work	N/A
GFP-PLEKHA4^{CC-IDR} (357–779)	This work	N/A
GFP-PLEKHA4^{IDR} (495–779)	This work	N/A
GFP-PLEKHA4$^{H-BP-PH}$ (28–167)	This work	N/A
PLEKHA4$^{\Delta N+IDR}$ (28–495)-GFP	This work	N/A
GFP-PLEKHA4$^{\Delta CC+IDR}$ (1–357)	This work	N/A
GFP-PLEKHA4$^{\Delta N+H+BP}$ (54–779)	This work	N/A
GFP-PLEKHA4$^{\Delta PH}$ (1–45, 167–779)	This work	N/A
GFP-PLEKHA4$^{\Delta H+BP+PH}$ (1–27, 168–779)	This work	N/A
GFP-PLEKHA4$^{\Delta PRD}$ (1–167, 357–779)	This work	N/A
GFP-PLEKHA4$^{\Delta IDR}$ (1–495)	This work	N/A
pCDNA5-FRT	Thermo Fisher	Cat#K601002
pCDNA5-FRT-GFP-PLEKHA4	This work	N/A
pCDNA5-FRT-PLEKHA4-GFP	This work	N/A
pCDNA5-FRT-GFP	This work	N/A
pcDNA3.1+zeo-VSV-KLHL12	Addgene	Cat#16761
pCMV10-3xFLAG	Sigma	Cat#E7658

3xFLAG-KLHL12	This work	N/A
GFP-KLHL12	This work	N/A
mCherry-KLHL12	This work	N/A
pCMV-HA-N	Clontech	Cat#635690
CUL3 ORF	ORFeome8.1 library (Haiyuan Yu, Cornell University)	N/A
HA-CUL3	This work	N/A
HA-Ub	Pietro De Camilli, Yale	N/A
M1R-mCherry	Pietro De Camilli, Yale	N/A
iRFP-PLC□1-PH	Pietro De Camilli, Yale	N/A
mCherry-CRY2(PHR)	Pietro De Camilli, Yale[2]	N/A
mCherry-CRY2-PLEKHA4^{IDR}	This work	N/A
mCherry-CRY2-PLEKHA4$^{CC\text{-}IDR}$	This work	N/A
GFP-PLEKHA4^{PH} R75A	This work	N/A
GFP-PLEKHA4^{PH} R129A	This work	N/A

GST-PLEKHA4^{PH} R75A	This work	N/A
GST-PLEKHA4^{PH} R129A	This work	N/A
PLEKHA4$^{H\text{-}BP\text{-}PH}$-GFP	This work	N/A
PLEKHA4$^{H\text{-}BP\text{-}PH}$-GFP F40E	This work	N/A
PLEKHA4$^{H\text{-}BP\text{-}PH}$-GFP R75A	This work	N/A
PLEKHA4$^{H\text{-}BP\text{-}PH}$-GFP R129A	This work	N/A
PLEKHA4$^{H\text{-}BP\text{-}PH}$-GFP K42A/R43A/R48A/R49A (4A)	This work	N/A
GST-PLEKHA4$^{H\text{-}BP\text{-}PH}$	This work	N/A
GST-PLEKHA4$^{H\text{-}BP\text{-}PH}$ F40E	This work	N/A
GST-PLEKHA4$^{H\text{-}BP\text{-}PH}$ R75A	This work	N/A
GST-PLEKHA4$^{H\text{-}BP\text{-}PH}$ R129A	This work	N/A
GST-PLEKHA4$^{H\text{-}BP\text{-}PH}$ K42A/R43A/R48A/R49A (4A)	This work	N/A
pcDNA3.1+zeo-VSV-KLHL12: Q405X	This work	N/A
GFP-PLEKHA4 S103, I106, R107, D109, and G110 silent (siRNA resistant)	This work	N/A
PLEKHA4-GFP S103, I106, R107, D109, and G110 silent (siRNA resistant)	This work	N/A
Software and Algorithms		
Fiji (ImageJ)	Open source[3]	https://imagej.net/Fiji
Zen Blue 2.3	Zeiss	N/A

Zen Black	Zeiss	N/A
BD Accuri C6	BD Biosciences	N/A

REFERENCES

(1) Santiago, F.; Oguma, J.; Brown, A.M.C.; Laurence, J. Noncanonical Wnt Signaling Promotes Osteoclast Differentiation and Is Facilitated by the Human Immunodeficiency Virus Protease Inhibitor Ritonavir. *Biochem*. *Biophys*. *Res*. *Commun*. **2012**, *417* (1), 223–230. https://doi.org/10.1016/j.bbrc.2011.11.089.

(2) Idevall-hagren, O.; Dickson, E. J.; Hille, B.; Toomre, D. K.; Camilli, P. De. Optogenetic Control of Phosphoinositide Metabolism. **2012**, *109* (35). https://doi.org/10.1073/pnas.1211305109/-

(3) Schindelin, J.; Arganda-Carreras, I.; Frise, E.; Kaynig, V.; Longair, M.; Pietzsch, T.; Preibisch, S.; Rueden, C.; Saalfeld, S.; Schmid, B.; Tinevez, J.-Y.; White, D. J.; Hartenstein, V.; Eliceiri, K.; Tomancak, P.; Cardona, A. Fiji: An Open-Source Platform for Biological-Image Analysis. *Nat. Methods* **2012**, *9*, 676.

CHAPTER 3

PLEKHA4 PROMOTES WNT/β-CATENIN SIGNALING-MEDIATED G1/S TRANSITION AND PROLIFERATION IN MELANOMA

3.1 ABSTRACT

Despite recent promising advances in targeted therapies and immunotherapies, melanoma patients incur substantial mortality. In particular, inhibitors targeting BRAF-mutant melanoma can lead to resistance, and no targeted therapies exist for NRAS-mutant melanoma, motivating the search for additional therapeutic targets and vulnerable pathways. Here we identify a regulator of Wnt/β-catenin signaling, PLEKHA4, as a factor required for melanoma proliferation and survival. PLEKHA4 knockdown in vitro decreased Dishevelled levels, attenuated Wnt/β-catenin signaling, and blocked progression through the G1/S cell cycle transition. In mouse xenograft and allograft models, inducible PLEKHA4 knockdown attenuated tumor growth in BRAF- and NRAS-mutant melanomas and exhibited an additive effect with the clinically used inhibitor encorafenib in a BRAF-mutant model. As an E3 ubiquitin ligase regulator with both lipid and protein binding partners, PLEKHA4 presents several opportunities for targeting with small molecules. Our work identifies PLEKHA4 as a promising drug target for melanoma and clarifies a controversial role for Wnt/β-catenin signaling in the control of melanoma proliferation.

3.2 INTRODUCTION

Melanoma is the most aggressive and deadliest form of skin cancer. The root cause of most melanomas is somatic mutations in a relatively small number of genes[1]. Roughly 65% of melanoma cases feature a V600D/E mutation in the Ser/Thr kinase BRAF, and an additional 10% feature a Q61K/R mutation in the GTPase NRAS[2]. These genetic alterations cause phenotypic changes, including elevated signaling through MAP kinase, PI 3-kinase, and other related pathways, which lead to increased cell proliferation, differentiation, and ultimately tumorigenesis and malignancy[3].

Inhibitors of BRAF or the downstream kinase MEK heralded an era of targeted therapies for BRAF-mutant melanomas[4,5]. Nonetheless, resistance typically occurs in roughly one year, leading to relapse, and no targeted therapies exist for NRAS-mutant melanomas[6]. Further, immunotherapies, such as checkpoint inhibitors, have more long-lasting effects but are only successful in a subset of patients [7]. Combinations of BRAF targeted therapies and anti-PD1 immunotherapies are promising avenues but are still not universally effective[8]. Thus, new therapeutic strategies are needed to prevent melanomagenesis and progression.

Wnt/β-catenin signaling, which regulates proliferation, is aberrantly hyperactive in several cancers, including melanoma[9]. In the canonical, β-catenin-dependent form of this pathway, secreted Wnt ligands engage a receptor from the Frizzled family in the plasma membrane of the Wnt-receiving cell[10]. This binding event causes recruitment of Dishevelled (DVL), which mediates disassembly of a multicomponent β-catenin destruction complex, resulting in β-catenin stabilization, nuclear translocation, and altered gene expression at several loci, most notably those

associated with the TCF/LEF transcription factor family. In cancer, aberrant Wnt/β-catenin signaling leads to increased expression of Wnt/β-catenin target genes including Cyclin D1 and c-Myc, which regulate progression through the G1/S transition of the cell cycle, helping to promote proliferation, tumorigenesis, and malignancy[9].

Wnt signaling pathways have been linked to melanoma, but their exact roles remain controversial[9,11–13]. Wnt/β-catenin signaling has been shown to promote melanoma tumor initiation and growth in both BRAF and NRAS mutant backgrounds[14–17]. Further, a recent study using a new engineered mouse model implicated Wnt signaling in the transformation of healthy melanocyte stem cells to melanoma in a BRAF and PTEN mutant background[18]. As well, BRAF inhibition is more effective in settings with lower levels of β-catenin[19]. Yet, elevated levels of nuclear (active) β-catenin have correlated with diverging patient survival, depending on the study[12,20–23]. Beyond the controversial roles of Wnt/β-catenin signaling in melanoma, β-catenin-independent non-canonical Wnt signaling controls actin cytoskeletal dynamics and cell migration and has been implicated in melanoma metastasis[24,25]. In fact, melanoma progression has been proposed to involve a phenotype switching model wherein the canonical and non-canonical pathways alternate to allow cells to switch between proliferative and migratory phenotypes[9,26]. Thus, Wnt signaling pathways appear to be important players in melanoma progression in most contexts and are thus a potential point of therapeutic intervention.

Numerous efforts have been made to drug Wnt signaling in cancer[23,27]. These efforts have largely focused on inhibiting core Wnt components (e.g., PORCN, FZD,

β-catenin/CBP)[28]. Though efficacious in model systems, they have seen limited success in vivo due, in part, to undesirable side effects on homeostatic Wnt signaling in non-diseased tissues[29]. Fortunately, Wnt/β-catenin signaling is subject to many levels of regulation, and though core Wnt components are typically essential due to important roles in development and tissue homeostasis, many modulators, or tuners, of Wnt signaling strength may not be required for viability[10,27,30]. Thus, it is a high priority to identify modulators of Wnt signaling, whose inhibition downregulates but does not completely eliminate Wnt signaling, as potential therapeutic targets.

Among the many factors involved in Wnt signaling, DVL has emerged as a major point of regulation[31]. Several different E3 ubiquitin ligases act on DVL, modulating its levels and thus changing the strength of the Wnt signal in Wnt-receiving cells[32–35]. To this end, we recently discovered that the phosphoinositide-binding protein PLEKHA4 (pleckstrin homology containing family A, number 4) modulates the activity of the CUL3–KLHL12 E3 ligase that polyubiquitinates DVL[36,37]. PLEKHA4 acts to sequester the substrate-specific adaptor KLHL12 within plasma membrane-associated clusters, thus reducing DVL ubiquitination, increasing DVL levels, and enhancing Wnt/β-catenin signaling in mammalian cells. Thus, PLEKHA4 acts as a tuner for DVL levels and Wnt signaling strength, as near-complete elimination of PLEKHA4 resulted in only partial DVL depletion and attenuation of Wnt signaling.

Intriguingly, PLEKHA4 expression is high in melanoma but its levels are low in healthy melanocytes[2,38]. We were thus motivated to test whether PLEKHA4 is an important factor for promoting pathological Wnt signaling in melanoma, as a step

toward both validating Wnt/β-catenin signaling in general, and PLEKHA4 in particular, as therapeutic targets in melanoma. Here, we report that melanoma cells from both BRAF and NRAS mutant backgrounds require PLEKHA4 for survival and proliferation in vitro and in vivo in mouse xenograft and allograft models. Depletion of PLEKHA4 by siRNA and shRNA led to attenuated Wnt signaling in these models and phenocopied inhibitors or siRNA knockdown of core Wnt components. Further, inducible PLEKHA4 knockdown in the presence of the clinically used BRAF V600D/E inhibitor encorafenib[39] displayed an additive effect in a xenograft model of BRAF-mutant melanoma, suggesting the therapeutic potential of targeting PLEKHA4 in melanoma. This work highlights PLEKHA4 as a new modulator of Wnt/β-catenin signaling strength in melanoma that, by promoting the G1/S cell cycle transition, maintains cell proliferation in melanoma. Importantly, our study provides additional clarity on the pathological role of Wnt/β-catenin signaling in this disease and suggests that pharmacological inhibition of PLEKHA4 could represent a promising new avenue for targeted therapy in melanoma.

3.3 RESULTS

3.3.1 *PLEKHA4 knockdown blocks proliferation and increases apoptosis in melanoma cells*

In the course of earlier work in HeLa cells, we noticed that PLEKHA4 knockdown by siRNA had mild qualitative effects on cell proliferation and viability[36]. We reasoned that cancer cells expressing the highest levels of PLEKHA4 might be more sensitive to its loss. Analysis of patient gene expression data in the TCGA

database revealed widespread expression of PLEKHA4 in many types of cancers, but, relative to other cancers, PLEKHA4 levels were highest in melanoma (**Figure 3.1A**)[2]. This high expression of PLEKHA4 in melanoma was independent of genotype, across 121 different melanoma cell lines (**Figure S3.1A**), and of melanoma subtype (e.g., cutaneous vs. non-cutaneous) in 259 primary tumor samples (**Figure S3.1B**). In healthy melanocytes, however, PLEKHA4 levels were low, as analyzed in the Genevestigator database[38]. With a working hypothesis that PLEKHA4 might be an important factor in melanomagenesis and progression, we examined its requirement for proliferation and survival in two melanoma cell lines: WM266-4, a BRAF V600D mutant line, and SK-MEL-2, an NRAS Q61R mutant line.

We validated several PLEKHA4 siRNA duplexes (**Figure 3.1B** and **Table S3.1**) and examined effects of PLEKHA4 knockdown using automated, continual monitoring of cell number on IncuCyte system, wherein images were acquired every hour for 100–150 hours. We observed a strong reduction of cell proliferation upon PLEKHA4 knockdown in both cell lines, using multiple siRNA duplexes (**Figure 3.1B–C** and **Table S3.2**). Examination of the images suggested substantial cell death was occurring, and indeed, Western blot analysis of lysates from these cells revealed that PLEKHA4 knockdown caused increases in levels of cleaved PARP and activated caspase 3, two markers of apoptosis (**Figure 3.1D**). Interestingly, overexpression of PLEKHA4-GFP in WM266-4 cells resulted in a modest increase in proliferation relative to control (**Figure S3.1C**).

3.3.2 *PLEKHA4 promotes Wnt/β-catenin signaling in melanoma cells*

Given the role of PLEKHA4 as a positive regulator of Wnt/β-catenin signaling in other cells[36], we next investigated effects of PLEKHA4 knockdown on Wnt signaling in the context of melanoma. We found that siRNA-mediated PLEKHA4 knockdown led to reduced levels of DVL2 and DVL3, the two major DVL isoforms in both the BRAF and NRAS mutant melanoma cell lines (**Figure 3.1E–F**). To further reinforce the generality of this finding, we also determined that *Plekha4* knockdown reduces DVL2 and DVL3 levels in YUMM1.7 cells, a mouse melanoma cell line derived from a genetically engineered mouse model bearing several mutations commonly found within melanoma, including BRAF V600E, as well as inactivating mutations in PTEN and CDKN2A (**Figure S3.2A–C**)[40]. We then examined effects on Wnt/β-catenin signaling using two approaches. First, PLEKHA4 knockdown led to a >50% decrease in luminescence from the two human melanoma cell lines that were engineered to stably express a β-catenin-dependent luciferase transcriptional reporter (TOPFlash) and then stimulated with Wnt3a (**Figure 3.1G**). Second, we found that PLEKHA4 knockdown in cells stimulated with Wnt3a led to reduced levels of Axin2, whose expression is induced by canonical Wnt/β-catenin signaling, by Western blot (**Figure 3.1E–F**).

To complement these studies on PLEKHA4 knockdown, we examined whether perturbing Wnt signaling via two distinct mechanisms would similarly affect viability and proliferation of these melanoma cells. First, we used a pan Wnt inhibitor (IWP-4) that targets Porcupine, an O-acyltransferase that installs a posttranslational modification that is required for their secretion from Wnt-producing cells and thus for

Wnt signaling[41]. We found that IWP-4 treatment led to a drastic cell proliferation defect in both the cell lines (**Figure S3.3A–B**). Second, we performed siRNA-mediated knockdown of DVL2 or DVL3, the direct mechanistic targets of PLEKHA4 action[36], and found similar effects on cell proliferation in both human melanoma cell lines (**Figure S3.3C–D**). Further, Western blot analyses on DVL2 or DVL3 knockdown samples revealed increases in the levels of cleaved PARP and activated caspase 3, suggesting increases in apoptosis similar to PLEKHA4 knockdown (**Figure S3.3E**). Together, these data indicate that PLEKHA4 acts as a positive modulator of Wnt/β-catenin signaling in melanoma and suggests that it mediates cell survival and proliferation in melanoma.

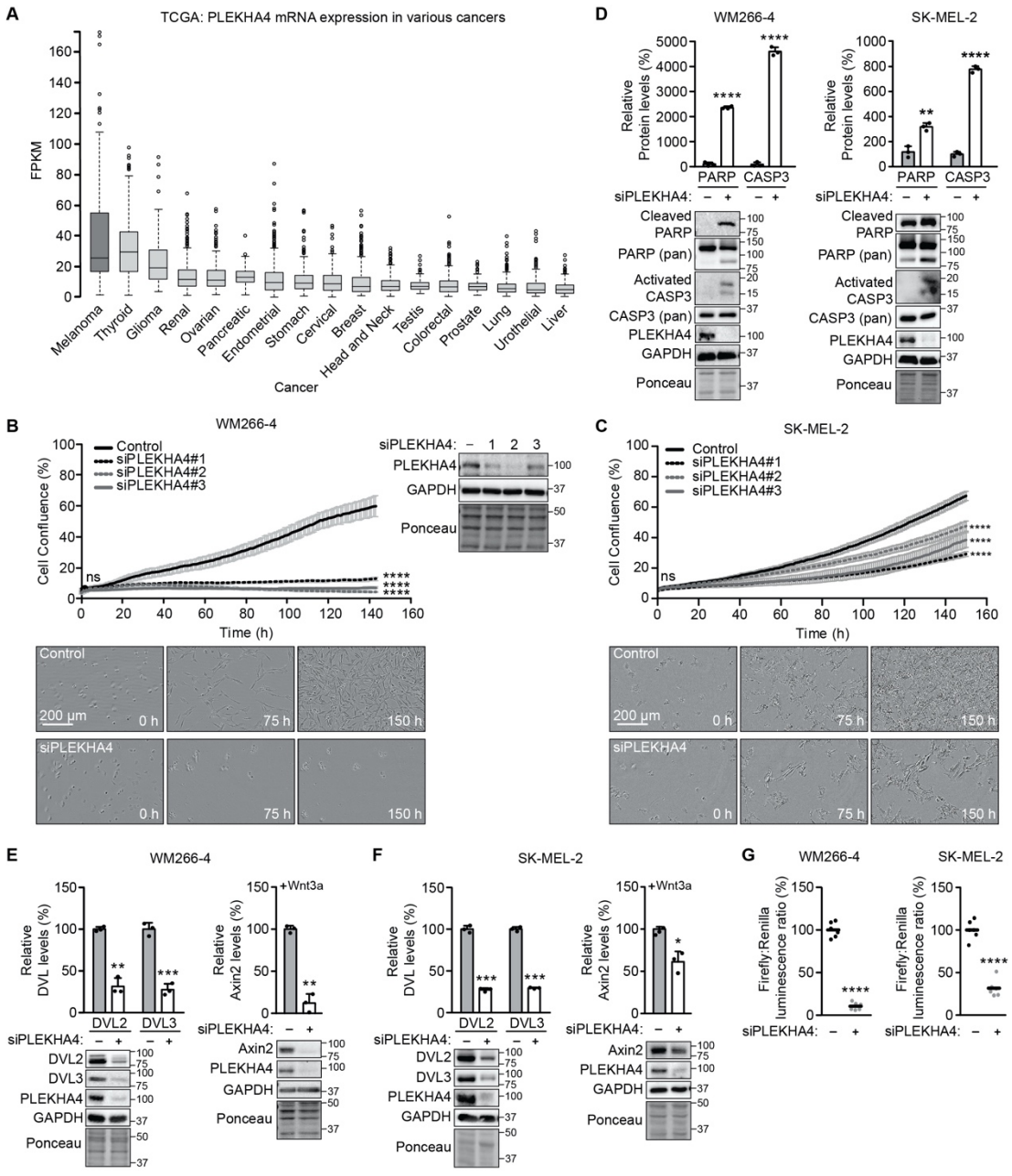

Figure 3.1 PLEKHA4 loss from melanoma cells reduces proliferation and increases apoptosis via attenuation of Wnt/β-catenin signaling.

(A) Analysis of PLEKHA4 mRNA levels in various cancers, based on data generated by the TCGA Research Network. FPKM, fragments per kilobase of transcript per million mapped reads. (B and C) PLEKHA4 knockdown by siRNA inhibits melanoma cell proliferation in vitro. Automated brightfield imaging of cell proliferation via IncuCyte of (B) WM266-4 and (C) SK-MEL-2 melanoma cells treated with siRNA duplexes targeting different regions of PLEKHA4 (siPLEKHA4 #1, #2 and #3) or a negative control siRNA (n=3). Western blot validation of siRNA duplexes is shown in

WM266-4 cells (B). (D–F) PLEKHA4 knockdown (using siPLEKHA4 #2) causes increased levels of apoptotic markers (cleaved PARP and activated Caspase 3 (CASP3)) and reduction in Wnt signaling (DVL2, DVL3, and Axin2) in mutant melanoma cells. Shown is Western blot analysis of WM266-4 and SK-MEL-2 cells subjected to siPLEKHA4 or a negative control siRNA (–) (n=3). For Axin2 analysis, cells were stimulated with Wnt3a-containing conditioned media concurrently with siRNA. (G) PLEKHA4 modulates Wnt/β-catenin signaling in WM266-4 and SK-MEL-2 cells. Shown is TOPFlash assay signal, i.e., ratio of β-catenin-dependent firefly luciferase activity to constitutive Renilla luciferase activity in WM266-4 or SK-MEL2 cells treated with siPLEKHA4 (#2) or negative control siRNA (–) and stimulated with Wnt3a-containing conditioned media (n=6). For Western blot analysis, GAPDH and Ponceau are shown as loading controls. * $p < 0.05$; ** $p < 0.01$; *** $p < 0.001$; **** $p < 0.0001$; ns, not significant. Scale bars: 200 μm.

3.3.3 *PLEKHA4 regulates the G1/S transition and melanoma cell proliferation*

A major role of Wnt/β-catenin signaling is to stimulate proliferation by promoting progression through the G1/S cell cycle transition. The effects of PLEKHA4 and Wnt perturbation on cell growth curves suggested an effect on proliferation, and we next examined whether the mechanism of action of PLEKHA4 occurred via perturbing the cell cycle. First, we analyzed the cell cycle phase of asynchronous WM266-4 cells treated with either control or two different PLEKHA4 siRNA duplexes and stained fixed cells with propidium iodide to measure DNA content. We found that PLEKHA4 knockdown led to an accumulation of cells in the G1 phase (**Figure 3.2A**). Importantly, this PLEKHA4 knockdown-induced G1/S transition defect could be rescued by introduction of an siRNA-resistant form of PLEKHA4 via lentiviral transduction (**Figure 3.2B**). Intriguingly, effects of PLEKHA4 knockdown could also be substantially, but not completely, rescued by overexpression of DVL2 or DVL3, the downstream targets of PLEKHA4 (**Figures 3.2B** and **S3.4**), suggesting that the established mechanism of action of PLEKHA4 on

DVL proteins, via effects on their ubiquitination by CUL3–KLHL12[36], accounts for a major portion of the effects of PLEKHA4 knockdown in these melanoma cells, though there are likely additional DVL-independent effects, discussed below.

To examine the G1/S phenotype in more detail, including its dynamics, we used the fluorescent ubiquitination-based cell cycle indicator (FUCCI) system, a live cell-compatible, dual color reporter that wherein cells in G1 phase express mRFP (red) and cells in S, G2, or M phase express GFP (green). We generated WM266-4 and SK-MEL-2 cell lines stably expressing the FUCCI reporters and synchronized either control or PLEKHA4 knockdown cells to G1 using serum starvation[42]. Upon release from this G1 arrest by addition of serum, we found that, for both cell lines, PLEKHA4 knockdown caused an increase in retention in G1 phase, i.e., a failure to progress to S phase (**Figures 3.2C–D** and **S3.4**).

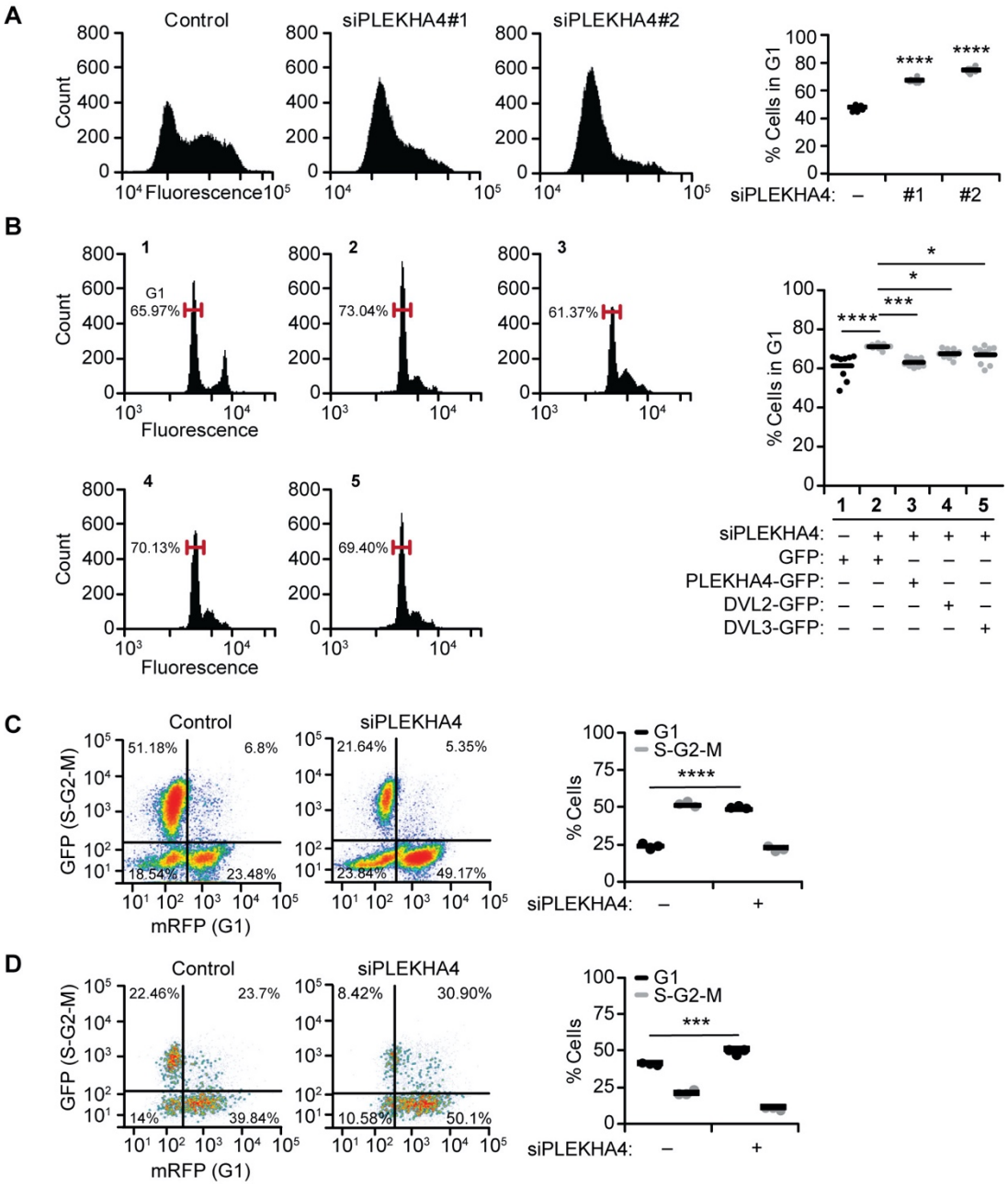

Figure 3.2 PLEKHA4 knockdown inhibits Wnt/β-catenin mediated G1/S cell cycle transition.

(A) PLEKHA4 knockdown leads to accumulation of WM266-4 cells in G1 phase. An asynchronous population of WM266-4 cells was treated with one of two different siRNA duplexes against PLEKHA4 (siPLEKHA4 #1 and #2) or a negative control siRNA (–), followed by fixation, propidium iodide staining, and flow cytometry analysis. (n=6) (B) PLEKHA4-GFP, DVL2-GFP, and DVL3-GFP can rescue the attenuation of the G1/S transition defect induced by PLEKHA4 knockdown (using siPLEKHA4 #2). WM266-4 cells were synchronized to G1 phase, subjected to

siPLEKHA4 or negative control siRNA (–), and stimulated with media containing FBS and simultaneously transduced with conditioned media containing lentivirus encoding GFP, siRNA-resistant PLEKHA4-GFP, DVL2-GFP, or DVL3-GFP, followed by fixation, propidium iodide staining, and flow cytometry analysis (n=9). (C–D) PLEKHA4 knockdown (using siPLEKHA4 #2) impairs G1/S transition in synchronized melanoma cells stably expressing the FUCCI cell cycle indicator. WM266-4-FUCCI (C) and SK-MEL-2-FUCCI (D) stable cells were synchronized to G1 phase via serum starvation and concurrent treatment with the indicated siRNA duplex for 48 h. Cells were then released into fresh medium containing FBS, followed by the quantification of mRFP (G1) and GFP (S-G2-M) fluorescence via flow cytometry (n=3). * $p < 0.05$; *** $p<0.001$; **** $p < 0.0001$.

To complement this phenotypic characterization of G1/S defects, we examined levels of Cyclin D1 and c-Myc, two well-studied transcriptional targets of Wnt/β-catenin signaling that affect the G1/S cell cycle transition[43,44]. In asynchronous populations of WM266-4 or SK-MEL-2 cells, we found that PLEKHA4 knockdown led to decreased levels of both Cyclin D1 and c-Myc in the two human melanoma cell lines (**Figure 3.3A–B**) and in YUMM1.7 cells (**Figure S3.2A**). Further, PLEKHA4 knockdown on G1-synchronized cells (via serum starvation) led to a similar decrease in the levels of Cyclin D1 and c-Myc, as well as DVL2 and DVL3 in WM266-4 or SK-MEL-2 cells (**Figures 3.3C–D**) and YUMM1.7 cells (Figure **S3.2B**). The decrease in the levels of these proteins induced by PLEKHA4 knockdown could be substantially rescued by lentiviral transduction with an siRNA-resistant form of PLEKHA4-GFP (**Figure 3.3E**). Interestingly, whereas the rescue of c-Myc levels was near-complete, the rescue of Cyclin D1 levels was only partial, suggesting other uncharacterized effects in this instance.

In the same experiment, we found that the decrease in levels of Cyclin D1 and c-Myc induced by PLEKHA4 knockdown could also be substantially, but not

completely, rescued — again, partially for Cyclin D1 and completely for c-Myc — by expression of DVL2-GFP, DVL3-GFP, or a combination of DVL2-GFP and DVL3-GFP (**Figure 3.3E**). Similar overexpression of DVL proteins could also partially rescue the induction of apoptosis markers, cleaved PARP and activated caspase 3, caused by PLEKHA4 knockdown (**Figure S3.5A–B**). Though the extent of reversal of these PLEKHA4 knockdown phenotypes by DVL overexpression in these experiments was substantial, further supporting the proposed mechanism of action, it was not complete, indicating additional DVL-independent effects of PLEKHA4 knockdown in melanoma cells, discussed below. Finally, to complement these findings, we found that DVL2 or DVL3 knockdown led to the same effects on Cyclin D1 and c-Myc levels in both human melanoma cell lines (**Figure 3.3F**) and in YUMM1.7 cells (**Figure S3.2C**). Overall, these data indicate that decreasing PLEKHA4 levels in melanoma leads to a Wnt/β-catenin-mediated G1/S cell cycle transition defect largely via effects on the key proliferation markers Cyclin D1 and c-Myc.

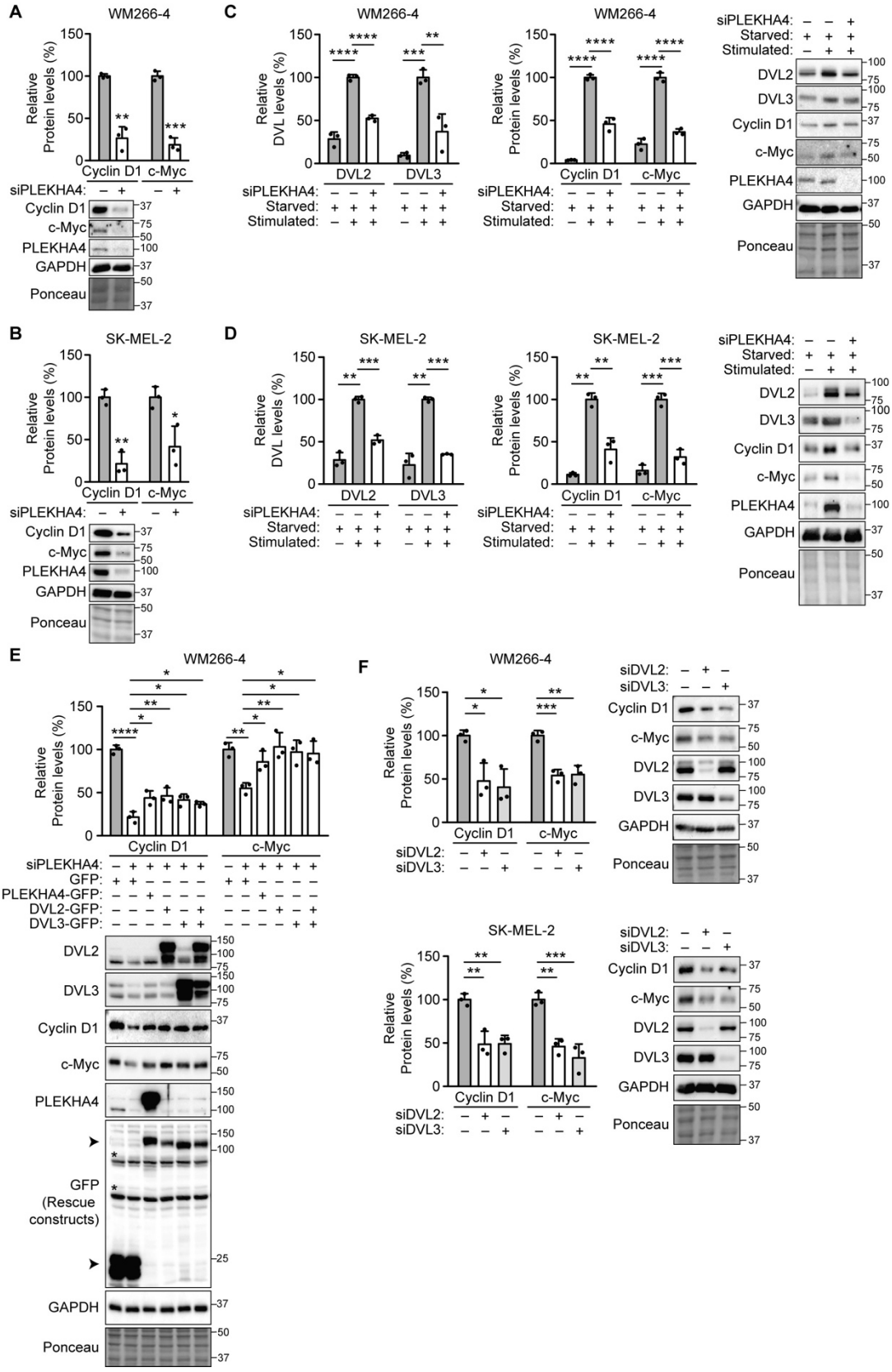
A
WM266-4
Relative Protein levels (%)
Cyclin D1
c-Myc
siPLEKHA4:
Cyclin D1
c-Myc
PLEKHA4
GAPDH
Ponceau
B
SK-MEL-2
C
WM266-4
Relative DVL levels (%)
DVL2
DVL3
Starved:
Stimulated:
D
SK-MEL-2
E
WM266-4
GFP:
PLEKHA4-GFP:
DVL2-GFP:
DVL3-GFP:
GFP (Rescue constructs)
F
WM266-4
SK-MEL-2
siDVL2:
siDVL3:

Figure 3.3 PLEKHA4 knockdown reduces levels of Wnt/β-catenin-controlled markers of proliferation.

(A and B) PLEKHA4 knockdown decreases Cyclin D1 and c-Myc levels in asynchronous WM266-4 (A) and SK-MEL-2 (B) cells. Shown is quantification and representative blot images of Western blot analysis of lysates from the indicated cells treated with an siRNA duplex against PLEKHA4 (siPLEKHA4, #2) or a negative control siRNA (–) (n=3). (C and D) PLEKHA4 modulates the levels of DVL2, DVL3, Cyclin D1, and c-Myc in G1-synchronized WM266-4 (C) and SK-MEL-2 (D) cells. Shown is Western blot analysis and quantification of lysates from melanoma cells synchronized to G1 phase via serum starvation that were treated with siPLEKHA4 (#2) or a negative control siRNA (–) and then stimulated with FBS-containing medium (n=3). (E) PLEKHA4-GFP, DVL2-GFP, and DVL3-GFP can partially rescue the changes in DVL2, DVL3, Cyclin D1, and c-Myc levels induced by PLEKHA4 knockdown in WM266-4 cells. Shown is quantification and representative blot images of Western blot analysis of lysates from WM266-4 cells subjected to siPLEKHA4 (#2) or negative control siRNA (–) and transduced with conditioned media containing lentivirus encoding GFP, siRNA-resistant PLEKHA4-GFP, DVL2-GFP, DVL3-GFP, or a combination of DVL2-GFP and DVL3-GFP (n=3). (F) Knockdown of DVL2 or DVL3 leads to a decrease in levels of Cyclin D1 and c-Myc. Shown is quantification and representative blot images of Western blot analysis of lysates from WM266-4 and SK-MEL-2 cells treated with the indicated siRNA duplex or negative control siRNA (n=3). GAPDH and Ponceau are shown as loading controls. * $p < 0.05$; ** $p < 0.01$; *** $p < 0.001$; **** $p < 0.0001$.

3.3.4 *PLEKHA4 is required for tumorigenic and malignant properties in melanoma in vitro*

The above molecular and phenotypic data implicate PLEKHA4 as a novel modulator of Wnt signaling in melanoma whose removal causes defects in cell cycle progression and proliferation. We therefore envisioned that loss of PLEKHA4 in melanoma cells might attenuate cancer-causing properties in vitro such as clonogenic capacity, or the ability of a single cell to proliferate into a colony.

We first examined effects of PLEKHA4 knockdown on the anchorage-dependent clonogenic capacity of melanoma cells, using crystal violet staining of colonies derived from single cells grown on traditional 2D cell culture surfaces.

PLEKHA4 knockdown in both WM266-4 and SK-MEL-2 cell lines led to substantial losses in clonogenic capacity (**Figure 3.4A**). Further, a similar effect was observed upon inhibition of Wnt signaling via other mechanisms, including knockdown of DVL2 or DVL3 (**Figure 3.4B**) and IWP-4 treatment (**Figure 3.4C**). In these assays, though the effects on anchorage-dependent clonogenic capacity were significant for all perturbations relative to control, we noticed a stronger effect for all siRNA experiments in the BRAF-mutant, WM266-4 cells compared to the NRAS mutant, SK-MEL-2 cells, similar to effects observed in proliferation assays (**Figure 3.1B–C**).

To evaluate tumorigenic potential of malignant cells grown in a soft substrate that better mimics the tumor environment, we employed an anchorage-independent colony formation assay[45]. Here, colony formation was measured after seeding cells in a 3D soft agar environment, followed by nitrotetrazolium blue staining. We found that PLEKHA4 knockdown in both melanoma cell lines strongly, and roughly equivalently, reduced anchorage-independent growth capacities (**Figure 3.4D**). Again, inhibition of Wnt signaling via DVL2 or DVL3 knockdown led to decreases in anchorage-independent growth (**Figure** 3.**4E**). The effect of DVL2 knockdown was stronger than DVL3 knockdown, suggesting a greater dependence on DVL2 in this setting. Collectively, these data indicate that loss of PLEKHA4 causes a drastic decrease in tumorigenic and malignant properties in BRAF and NRAS mutant melanoma in vitro.

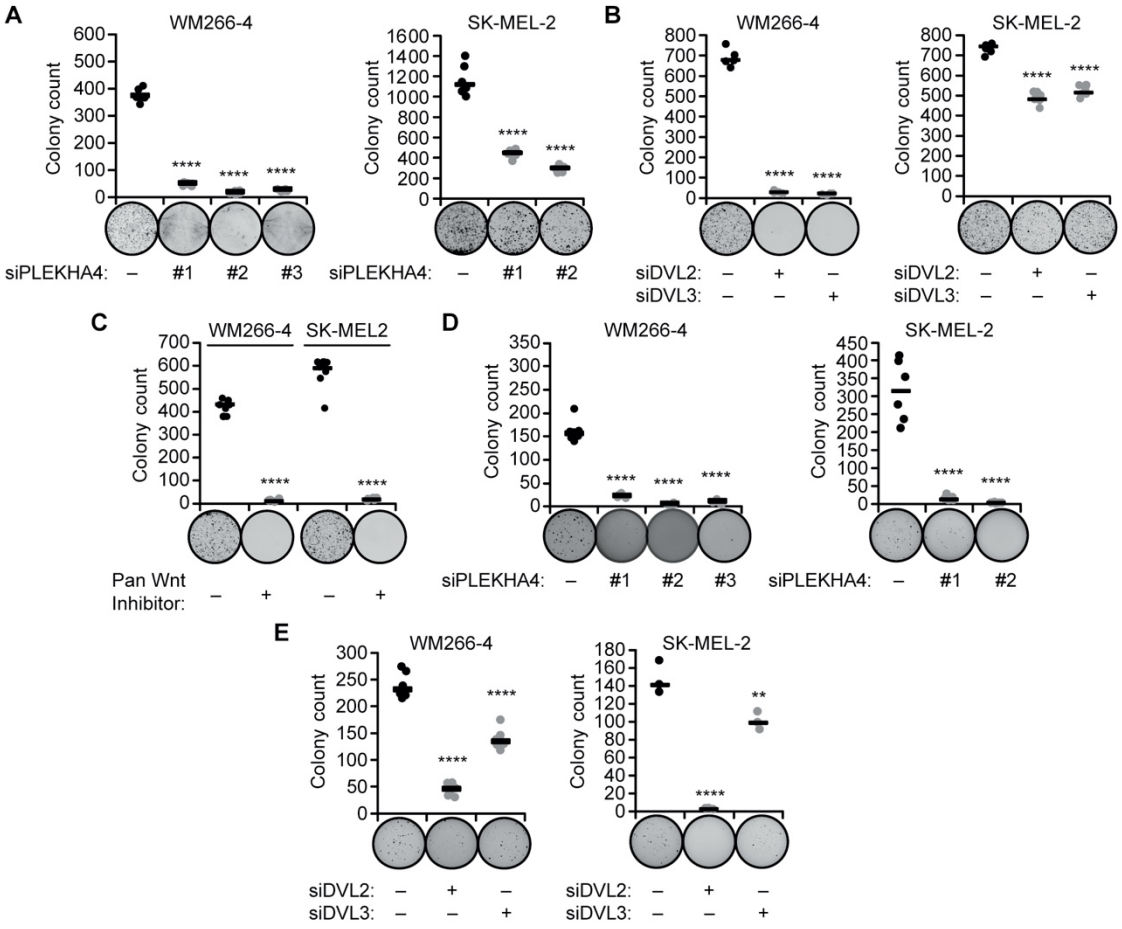

Figure 3.4 PLEKHA4 knockdown and Wnt inhibition causes loss of tumorigenic and malignant properties in melanoma cells in vitro.

Cells treated as described below were analyzed via anchorage-dependent colony formation assay with crystal violet staining (A–C) or anchorage-independent soft agar assay (D–E). Representative brightfield images are shown for each treatment, and graphs indicate colony count. (A and D) Cells were treated with the indicated siRNA duplex against PLEKHA4 or negative control siRNA (–) (n=6). (B and E) Cells were treated with siRNA duplexes against DVL2, DVL3, or negative control siRNA (n=6 for all, except for n=3 for SK-MEL-2 in (E)). (C) Cells were treated with the pan Wnt inhibitor IWP-4 or DMSO control (–) (n=6). ** $p < 0.01$; **** $p < 0.0001$.

3.3.5 *PLEKHA4 knockdown attenuates melanoma tumor growth in vivo*

Buoyed by the in vitro data implicating PLEKHA4 as a factor required for melanoma cell proliferation, we next tested whether PLEKHA4 played a similar role in vivo. Here, we used two different types of mouse models. First, we established xenografts in immunocompromised NOD *scid* gamma (NSG) mice using WM266-4 and SK-MEL-2 cells, the BRAF- and NRAS-mutant human melanoma cell lines that we had used for the in vitro studies above. Separately, to assess effects of PLEKHA4 knockdown within wild-type mice, we established allografts in C57BL6.J mice using the syngeneic, engineered YUMM1.7 mouse melanoma cell line[40].

For these in vivo experiments, we established PLEKHA4 knockdown by generating cell lines stably expressing a doxycycline-inducible shRNA against human PLEKHA4 and mouse *Plekha4*. To accomplish this, we generated stable cell lines expressing different shRNA constructs against human PLEKHA4 in WM266-4 cells (**Figure S3.6A–B**) and mouse *Plekha4* in YUMM1.7 cells (**Figure S3.7**). Cells were grown in vitro, PLEKHA4/*Plekha4* knockdown was induced by addition of doxycycline, and Western blot analysis was performed. We examined the levels of PLEKHA4, DVL2, DVL3, Cyclin D1, and c-Myc to determine the most effective shRNAs from each collection (**Figures S3.6A** and **S3.7**). We further validated the effectiveness of the human PLEKHA4 shRNAs at suppressing Wnt3a-stimulated Wnt/β-catenin signaling using the TOPFlash system within the PLEKHA4 stable knockdown lines (**Figure S3.6B**). The best-performing shRNAs against human PLEKHA4, as validated in WM266-4 cells, were subsequently stably expressed and validated in SK-MEL-2 cells (**Figure S3.8A–B**).

We then generated xenograft/allograft models by subcutaneous injection into the shoulder or hind leg flanks in the absence of doxycycline to allow tumors to form. For the WM266-4 xenograft and YUMM1.7 allografts, after 12 days in the absence of doxycycline to allow tumors to form, doxycycline was administered for 10–12 days to induce PLEKHA4/*Plekha4* knockdown (**Figure 3.5A**). As negative controls, stable cell lines expressing luciferase shRNA were employed. Importantly, in the absence of doxycycline, the rate of tumor formation was identical for all cells from the same parental cell line. We monitored tumor progression over this time span and, following the addition of doxycycline to induce shPLEKHA4 expression, observed a major attenuation of tumor growth for both BRAF-mutant models (**Figure 3.5B–C**). Further analysis of the tumors at the experimental endpoint revealed that shPLEKHA4-expressing tumors were approximately four-fold smaller in the WM266-4/NSG model (**Figure 3.5B**) and three-fold smaller in the YUMM1.7/C57BL6.J model (**Figure 3.5C**).

To test the effect of PLEKHA4 knockdown on NRAS-mutant melanoma in vivo, we established an SK-MEL-2 xenograft, and once visible tumors appeared at 1.5 months post-injection, doxycycline administration was carried out for 14 days (**Figure 3.5A**). Analysis of tumor progression and endpoint data revealed that tumor growth was attenuated two-fold in the PLEKHA4 knockdown samples compared to control (**Figure 3.5D**). These data demonstrate that PLEKHA4 knockdown in an in vivo, tumor xenograft or allograft setting results in a substantial decrease in tumor growth and implicate PLEKHA4 and, by extension, Wnt signaling, as a regulator of BRAF and NRAS-mutant melanoma progression in vivo.

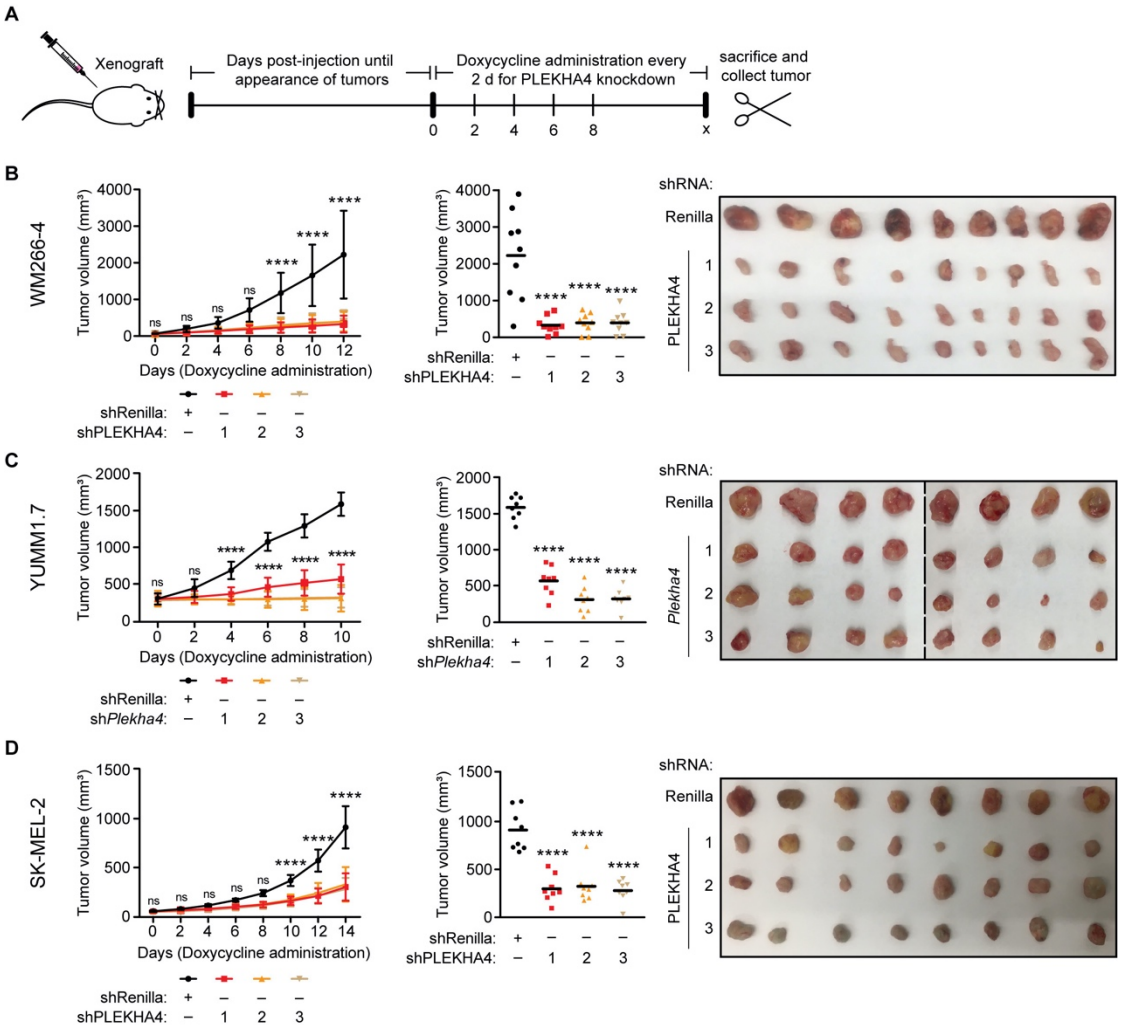

Figure 3.5 Inducible PLEKHA4 knockdown inhibits melanoma tumor xenograft/allograft growth in vivo.

(A) Schematic representation of experimental setup and timeline for xenograft/allograft analyses. Cell lines stably expressing doxycycline-inducible shRNA against human PLEKHA4 (shPLEKHA4; WM266-4 and SK-MEL-2) or mouse *Plekha4* (sh*Plekha4*; YUMM1.7) or a negative control shRNA (Renilla) were xenografted into NSG (for WM266-4 and SK-MEL-2) and C57BL/6J (for YUMM1.7) mice. Mice were monitored, and after small tumor bumps appeared (12 d for WM266-4 and YUMM1.7; 45 d for SK-MEL-2), doxycycline was administered through the drinking water for a total of 10–16 d to induce PLEKHA4 knockdown. Tumor progression over this time period was monitored by measurement of tumor dimensions using a digital caliper and calculation of tumor volume using the formula $v = 0.5233*l*w^2$. Mice were then sacrificed, and tumors were collected (n=12 for WM266-4-xenografted NSG mice, n=10 for YUMM1.7-allografted C57BL/6J mice,

and n=14 for SK-MEL-2-xenografted NSG mice). (B–D) Data from studies using WM266-4 xenografts (B), YUMM1.7 allografts (C), and SK-MEL-2 xenografts (D). The plots at left show changes in tumor volume over time, and the plot in the middle show final tumor volumes measured with a caliper post-harvesting, with images of tumors harvested at the endpoint shown at right. n=9 for WM266-4 and n=8 for YUMM1.7 and SK-MEL-2. **** $p < 0.0001$; ns, not significant.

To examine whether the mechanism underlying the effects of PLEKHA4 knockdown in vivo was similar to that determined in vitro, we performed Western blot analysis on tumor samples (**Figure 3.6**). We found that, for xeno-/allografts from all three cell lines — WM266-4, **(Figure 3.6A)**, YUMM1.7 (**Figure 3.6B**), and SK-MEL-2 (**Figure 3.6C**) — the PLEKHA4 shRNAs were highly effective at reducing PLEKHA4 protein levels, relative to the control tumors expressing control shRNA. Further, this analysis revealed substantial decreases in DVL2, DVL3, Cyclin D1, and c-Myc in PLEKHA4 shRNA-expressing tumors compared to controls expressing control shRNA (**Figure 3.6**). This analysis is consistent with the effects of PLEKHA4 siRNA and shRNA observed in vitro and supports the conclusion that PLEKHA4 knockdown attenuates proliferation via effects on Wnt/β-catenin signaling.

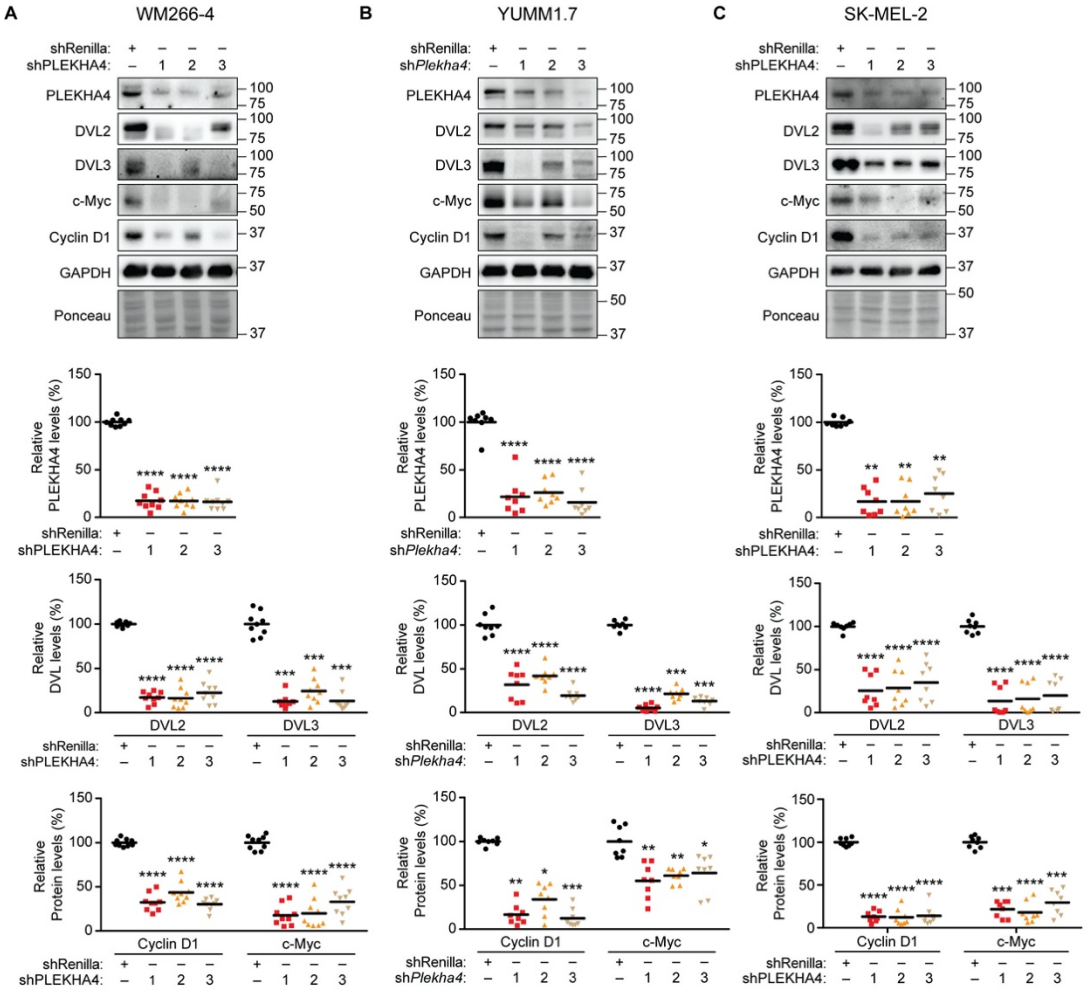

Figure 3.6 Inducible PLEKHA4 knockdown in tumor xenograft/allografts reduces levels of Wnt/β-catenin signaling and proliferation markers.

Tumor samples were harvested at the endpoints of the xenograft experiments described in Figure 6. Lysates were generated and analyzed by Western blot for PLEKHA4, to verify shRNA efficacy, and for DVL2, DVL3, Cyclin D1, and c-Myc, to assess effects on Wnt/β-catenin signaling and proliferation. GAPDH and Ponceau are shown as loading controls. Representative Western blots are shown at top, with quantification in scatter plots below. Results are shown for all xenograft studies, from WM266-4 (A), YUMM1.7 (B), and SK-MEL-2 (C). n=9 for WM266-4 and n=8 for YUMM1.7 and SK-MEL-2. * $p < 0.05$; ** $p < 0.01$; *** $p < 0.001$; **** $p < 0.0001$.

3.3.6 *PLEKHA4 knockdown has an additive effect with a BRAF inhibitor on preventing tumor proliferation in vivo*

Finally, we wanted to establish the feasibility of targeting PLEKHA4 in a model of a therapeutic setting. Targeted BRAF therapy, i.e., BRAF and/or MEK inhibitors, represents a frontline treatment for melanoma[46,47]. Though effective, this treatment has its limitations, including resistance, leading to relapse[6,48]. PLEKHA4 and its effect on Wnt signaling could represent a second, parallel druggable pathway to block melanoma progression. Thus, we examined whether the anti-proliferative effects of encorafenib (BRAFi), an FDA-approved BRAF inhibitor used routinely to treat BRAF-mutant melanoma, would be enhanced by simultaneous knockdown of PLEKHA4 in vivo[39]. We generated WM266-4 xenografts bearing doxycycline-inducible PLEKHA4 or control shRNA as before. On day 12 post-injection, following the formation of tumors, mice were administered both doxycycline to induce shRNA expression and encorafenib, via daily oral gavage, to inhibit BRAF and downstream MAP kinase signaling (**Figure 3.7A**).

This study was divided into two phases. In the first phase, we examined effects of PLEKHA4 knockdown and encorafenib treatment separately or in combination. We found that encorafenib treatment prevented tumor growth compared to control, similar to effects of PLEKHA4 knockdown alone (**Figure 3.7B**). Encouragingly, encorafenib treatment in the context of PLEKHA4 knockdown resulted in significantly reduced tumor growth compared to either PLEKHA4 knockdown or encorafenib treatment alone (**Figure 3.7B**). These data indicate an additive effect of PLEKHA4 knockdown and BRAF inhibition. Further analysis of tumor size and endpoint data confirmed that

encorafenib treatment and PLEKHA4 knockdown exhibited similar effects on tumor size compared to control samples (**Figure 3.7C–D**).

Clinically, melanoma tumors can relapse upon development of resistance to BRAF inhibitors such as encorafenib, as well as withdrawal of the inhibitor[6,48]. This relapse is problematic, leading to further disease progression and poor patient outcomes. As a model for resistance, we examined the effects of continued PLEKHA4 inhibition on tumor regrowth of residual melanoma cells after removal of encorafenib. In the second phase of the study, we extended the study on both control and PLEKHA4 knockdown groups that had been treated with encorafenib during the first phase of the study. Here, we removed encorafenib but continued doxycycline treatment for an additional 14 days to sustain PLEKHA4 knockdown. We observed that, upon encorafenib withdrawal, both the control and PLEKHA4 knockdown samples started to grow, but to different extents (**Figure 3.7B**). Further analysis of the tumor xenografts during the 14-day timecourse and at the endpoint confirmed that upon encorafenib withdrawal, both the encorafenib + PLEKHA4 knockdown and encorafenib alone samples had grown, but to different extents (**Figure 3.7C–D**). Notably, the encorafenib + PLEKHA4 knockdown sample exhibited a slower growth during the regrowth phase compared to encorafenib only.

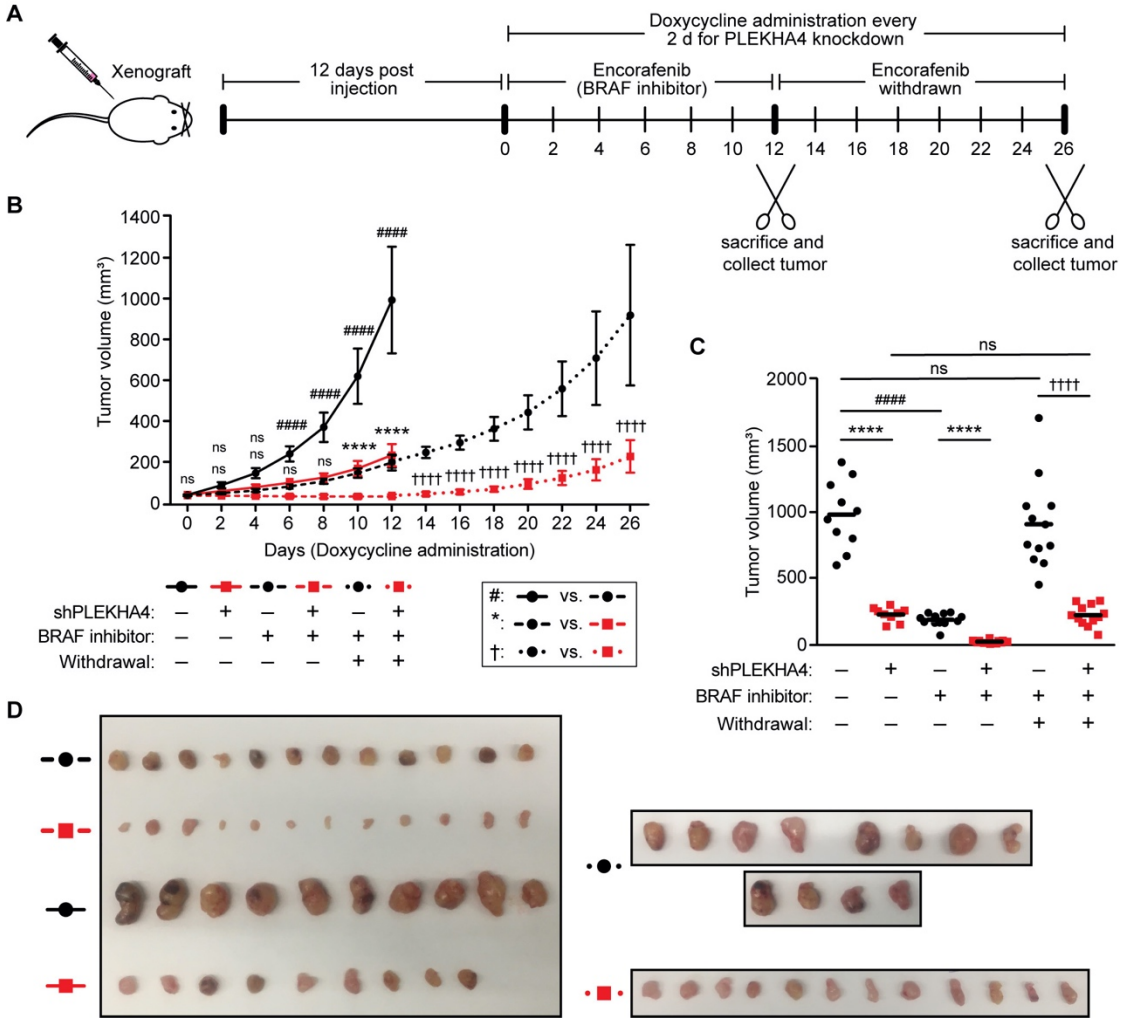

Figure 3.7 PLEKHA4 knockdown exhibits an additive effect with the BRAF inhibitor encorafenib to attenuate melanoma tumor xenograft growth in vivo.

(A) Schematic representation of experimental setup and timeline. WM266-4 cells stably expressing a doxycycline-inducible shRNA hairpin against PLEKHA4 (shPLEKHA4 #1) or a control shRNA (–) were xenografted into NSG mice. Mice were monitored, and after tumors became visible 12 d post-injection (labeled as day 0), doxycycline was administered through the drinking water and the BRAF inhibitor encorafenib or vehicle control was administered via oral gavage every day for 12 d. On day 12, all vehicle-treated mice and half of the encorafenib-treated mice bearing control and PLEKHA4 knockdown tumors were sacrificed for tumor collection. For the remaining mice, doxycycline treatment was continued but encorafenib was withdrawn to assess effect of PLEKHA4 knockdown on relapse for another 14 d. On day 26, mice were sacrificed for tumor collection. (B–D) Data from these studies. (B) Plot showing changes in tumor volume over time, with dimensions determined as

described in the Figure 6 legend. (C) Final tumor volumes measured with a caliper post-harvesting. (D) Images of tumors harvested at endpoints: day 12 (left) and day 26 (right) (n=10-12 for each group). ****, ####, and ††††: $p < 0.0001$; ns, not significant.

From these data, we conclude that PLEKHA4 knockdown, in combination with BRAF inhibition, prevents melanoma growth in a xenograft model more efficaciously than BRAF inhibition alone. Further, sustained PLEKHA4 knockdown following encorafenib removal, which in this setting serves as a model for melanoma relapse from minimal persister cells[49] that had survived the encorafenib treatment, had a partial but substantial effect on proliferation, suggesting that inactivation of PLEKHA4 might be therapeutically beneficial in combination with existing targeted therapies.

3.4 DISCUSSION

Wnt/β-catenin signaling is a central pathway in embryonic development. In adults, it controls many aspects of cell and tissue homeostasis, including cell proliferation, differentiation, migration[10]. Alterations that perturb Wnt signaling beyond the normal homeostatic range occur in many diseases; in particular, elevated Wnt signaling occurs in many cancers. In certain instances, mutations to core Wnt components are clearly understood to be drivers of oncogenesis, e.g., in colorectal cancer, where more than 80% of cases feature mutations in adenomatous polyposis coli (APC) that lead to hyperactive Wnt signaling and associated pathogenesis[27]. In other cancers with elevated levels of Wnt signaling, the causal nature of this pathway in oncogenesis is not as clear.

Several studies have implicated increased Wnt signaling in melanoma, and yet the functional consequences of this dysregulation in melanoma are not entirely understood[11–13]. In particular, elevated levels of nuclear β-catenin have been implicated in both increased proliferation but also, unexpectedly, better prognosis, and they are not a marker of the initial transformation event[13,50]. Nuclear β-catenin alone may not necessarily correlate with cellular phenotype, suggesting an interplay of additional factors in the regulation of Wnt/β-catenin signaling in melanoma[51]. Though the role of Wnt signaling as a sole driver of melanoma progression is controversial, its role in supporting proliferation in certain mutant backgrounds is clearer[14–18]. In this context, our study provides important additional evidence implicating Wnt/β-catenin in melanoma proliferation in both BRAF and NRAS mutant backgrounds.

Inhibition of Wnt signaling is a promising route to new anti-cancer therapies, if achievable in a selective or targeted manner that minimizes damage to non-cancerous tissues[12,27,28,52]. Because of challenges associated with targeting core Wnt pathway components, efforts have shifted in recent years toward gaining a deeper understanding of proteins that regulate the strength of Wnt signaling. Among this growing list of modulators, or tuners, PLEKHA4 stands out as a protein with a unique mechanism of action and potential relevance to melanoma.

Previously, we established that PLEKHA4 enhances Wnt signaling by sequestering and inactivating the Cullin-3 (CUL3) substrate-specific adaptor KLHL12 and preventing DVL polyubiquitination by the CUL3–KLHL12 E3 ubiquitin ligase[36,53]. Here, we establish that this fundamental mechanism of tuning Wnt signaling strength could be highly beneficial in the context of melanoma. Melanoma

cells express higher levels of PLEKHA4 than more than other 20 cancers, and even partial removal of PLEKHA4 by siRNA or shRNA dramatically lowers proliferation and increases apoptosis in vitro and in vivo.

PLEKHA4 knockdown exhibited similar effects in melanoma cells, i.e., on DVL levels and Wnt signaling strength, as well as strong effects on clonogenic capacity in vitro. These results point to Wnt/β-catenin signaling, and its regulator PLEKHA4, as important players controlling proliferation in both BRAF- and NRAS-mutant melanomas. PLEKHA4 knockdown in melanoma cells strongly affected levels of the canonical Wnt/β-catenin targets Cyclin D1 and c-Myc, which ensure progression through the G1/S cell cycle transition. Disruption of Wnt signaling via other means (DVL knockdown or global pharmacological inhibition of Wnt production) resulted in similar phenotypes to PLEKHA4 knockdown.

The ability of DVL overexpression to partially rescue the effects of PLEKHA4 knockdown both supports this mechanism and also highlights potential undetermined, DVL-independent mechanisms underlying the effect of PLEKHA4 knockdown on melanoma cell proliferation and apoptosis. In particular, effects on other CUL3–KLHL12 ubiquitination substrates, including the COPII coat component SEC31, may be responsible[54]. Notably, CUL3 loss of function attenuates proliferation in various settings, including mouse embryonic stem cells and the *Drosophila* pupal wing epithelium, and CUL3–KLHL12 has further been proposed to control proliferation in other contexts[54,55].

In tumor xenograft and allograft models using both BRAF- and NRAS-mutant melanomas, removal of PLEKHA4 by shRNA prevented tumor growth. Further, in a

BRAF-mutant melanoma, PLEKHA4 shRNA exhibited an additive effect with a clinically used BRAF inhibitor, leading to much stronger anti-proliferative effects, and its effects help to keep growth slow even after removal of the inhibitor. These results from the combination treatment studies reinforce that, whereas MAP kinase signaling is a predominant player in melanoma, Wnt/β-catenin plays important roles in supporting proliferation. Other modulators of Wnt signaling affect melanoma proliferation. For example, Dkk-1, a negative regulator of Wnt signaling, exhibits reduced expression in melanoma, and its activation inhibits tumorigenicity and induces apoptosis in melanoma[56,57]. Another negative regulator of Wnt signaling, WIF-1 (Wnt inhibitory factor-1), is downregulated in melanoma progression[58]. Both MAP kinase and Wnt/β-catenin signaling regulate the activity of MITF, a master regulator of melanoma progression in both BRAF and NRAS mutant backgrounds[59,60].

Yet, the interactions between Wnt/β-catenin and MAP kinase signaling in melanoma are complex. Elevated levels of the former, rather than its inhibition, enhanced the efficacy of BRAF inhibition at inducing apoptosis[61]. However, chronic BRAF inhibition-induced resistance caused elevated levels of Wnt5a, which were associated with increased cell growth, suggesting that Wnt5a inhibition might counteract these effects[25]. In light of this work, our study, performed using different melanoma cell lines and showing that a combination of PLEKHA4 shRNA and BRAF inhibition has stronger anti-proliferative effects compared to BRAF inhibition alone, further highlights the context-dependent effects of Wnt signaling and its relationship to BRAF and MAP kinase signaling in melanoma[11–13].

Our results suggest that PLEKHA4 inhibition might be therapeutically beneficial in both NRAS-mutant melanomas, for which there are no targeted therapies, and for BRAF-mutant melanomas, where PLEKHA4 inhibition could be investigated in combination with existing BRAF and/or MEK inhibitors. In principle, PLEKHA4 inhibition in combination with immunotherapies could also represent an interesting future direction.

PLEKHA4 is not a canonical drug target. It is a multidomain adaptor protein, not a receptor, ion channel, or enzyme. Yet, our previous work sheds light on several protein-lipid and protein-protein interactions that could be targeted[36]. Its tripartite N-terminal region, which includes a pleckstrin homology (PH) domain, binds to anionic phosphoinositides to localize the protein to the plasma membrane. C-terminal coiled-coil and intrinsically disordered regions mediate oligomerization into membrane-associated clusters that are potentially phase-separated. A central proline-rich domain binds to KLHL12, and all three of these molecular elements (lipid binding, oligomerization, and KLHL12 binding) are featured in its mechanism of action to prevent DVL ubiquitination and enhance Wnt signaling.

In principle, small-molecule ligands could be developed to target the phosphoinositide binding site of the PH domain[62] or disrupt interactions between the proline-rich domain and KLHL12 or homotypic interactions involved in oligomerization and cluster formation. Further, ligands that bind to PLEKHA4 but do not disrupt function could still serve as starting points for development of PROTACs/degraders[63]. Finally, a global knockout of the *Drosophila* ortholog of PLEKHA4, *kramer*, is viable[36], raising the possibility that mammalian PLEKHA4

may be dispensable for development and less critical for maintaining homeostatic Wnt signaling. This study, however, implicates it as a vulnerability for melanoma cells. Thus, we believe that PLEKHA4 defines a new type of drug target for melanoma.

Interestingly, our previous work on PLEKHA4 and *kramer* established that these proteins can also mediate non-canonical, β-catenin-independent Wnt signaling[36]. In particular, in *Drosophila*, *kramer* knockout resulted in defects in planar cell polarity through effects on *dishevelled*, a pathway that shares key aspects with mammalian non-canonical Wnt signaling, including profound effects on the actin cytoskeleton[64]. In melanoma, non-canonical Wnt signaling is implicated in a migratory phenotype, whereas canonical Wnt/β-catenin signaling controls proliferation. Melanoma progression has been described to involve a phenotype switching scenario, wherein alternating cycles of proliferation and migration lead to disease spread and eventually to metastasis[51].

Crucially, DVL is a central signaling molecule in both the canonical and non-canonical pathways[31], and thus it is not surprising that PLEKHA4, which regulates DVL levels, has the potential to affect multiple types of Wnt signaling, depending on the context[36]. In the in vitro and xenograft models here, which are geared toward evaluation of the proliferative stages of melanoma, we found a strong effect on removal of PLEKHA4. Examination of effects of PLEKHA4 removal on non-canonical Wnt signaling in the context of a migratory phenotype represents an interesting future direction and could reveal that a single protein, PLEKHA4, might be relevant in suppressing later stages of melanoma, including metastasis, where the cancer cells exhibit an invasive phenotype. Notably, chronic inhibition of mutant

BRAF in melanoma causes an elevation in levels of Wnt5a[25]. Whereas that study examined effects on Wnt5a-induced cell growth, Wnt5a can also mediate non-canonical Wnt signaling, which is implicated in migration and metastasis, suggesting potential interplay in melanoma between BRAF and Wnt signaling pathways in multiple contexts.

In summary, we have identified PLEKHA4 as an important mediator of a proliferative phenotype in BRAF- and NRAS-mutant melanoma. We demonstrate that PLEKHA4 knockdown negatively regulates Wnt/β-catenin signaling in this context, helping to clarify the role of Wnt/β-catenin signaling in melanoma and revealing another layer of regulation in the Wnt/β-catenin signaling axis that controls the G1/S cell cycle transition to maintain melanoma proliferation.

3.5 EXPERIMENTAL MODEL AND SUBJECT DETAILS

3.5.1 *Cell culture*

WM266-4 cells (RRID:CVCL_2765, NCI PSOC Bioresource Core) and SK-MEL-2 cells (RRID:CVCL_0069, NCI PSOC Bioresource Core) were cultured in minimum essential medium (MEM, Corning), L Wnt-3a cells (RRID:CVCL_0635, ATCC) were cultured in Dulbecco's modified Eagle medium (DMEM, Corning) and YUMM1.7 cells (RRID:CVCL_JK16, ATCC) were cultured in Dulbecco's modified Eagle medium/Ham's F-12 medium (DMEM/F-12, Corning) supplemented with 10% fetal bovine serum (FBS, Corning) and 1% penicillin/streptomycin (P/S, Corning) at 37 ºC in a 5% CO_2 atmosphere. Because all cells were obtained from commercial or

government repositories, no cell line authentication was performed. Mycoplasma testing (MycoSensor PCR assay, Agilent) was performed at regular yearly intervals.

All cells were grown for at least 2–3 passages (approximately one week) prior to use in experiments. Stable expression of doxycycline-inducible shRenilla control, shPLEKHA4 hairpins or mouse shPLEKHA4 hairpins in WM266-4 or SK-MEL-2 (human) and YUMM1.7 (mouse) cells was achieved by transducing above-mentioned hairpin plasmids cloned in LT3GEPIR vector (a gift from Lewis Cantley) as previously described[65]. Stable expression of cell cycle indicator plasmid pLenti6.2-FUCCI (Fluorescence Ubiquitination Cell Cycle Indicator, a gift from Jan Lammerding) was achieved by transducing FUCCI plasmid into WM266-4 and SK-MEL-2 cells. After transduction (48 h), hairpin transduced cells were selected with 2.5 μg/mL puromycin (Sigma-Aldrich) and FUCCI plasmid-transduced cells were selected with 2 μg/mL blasticidin (Alfa Aesar). Upon completion of drug selection, FUCCI transduced WM266-4 and SK-MEL-2 cells were sorted using FACS to ensure 99.9% of fluorescent cell population before use. Conditioned media (CM) from L Wnt-3a cells was harvested as previously described[36]. Cell lines were obtained and used without further authentication.

3.5.2 *Animal husbandry*

All mice used for experiments were approved by Center for Animal Resources and Education (CARE) facility at Cornell University. The C57BL/6J mice were purchased from Jackson laboratory and NSG (NOD scid gamma) mice were purchased from the PATh PDX facility at Cornell University. The animals were housed and bred

on a 12 h light and dark cycle. C57BL/6J mice were used for xenografting/allografting the YUMM1.7 syngeneic mouse cell line, and NSG mice were used for xenografting WM266-4 or SK-MEL-2 (human melanoma) cell lines. Mice were euthanized when tumors reached the maximum size allowed by the approved animal protocol accounting for the animal's health and mobility.

3.6 METHOD DETAILS

3.6.1 *Plasmids and cloning*

The cloning for GFP and siRNA-resistant PLEKHA4-GFP plasmids for rescue experiments have been described previously[36]. Viral transduction vector pCDH-mCherry-Blasticidin was obtained as a gift from Jan Lammerding's lab at Cornell University. The vector was digested using standard cloning procedure with EcoRI and NotI to remove mCherry. The full length GFP or siRNA resistant PLEKHA4-GFP PCR fragments were subcloned into the digested pCDH vector. For cloning pCDH-DVL2-GFP and pCDH-DVL3-GFP, full length DVL2 and DVL3 PCR-fragments were amplified from 3X-FLAG-DVL2 (Addgene #24802) and XE251-pcDNA3.1 (zeo) FLAG-hDsh3 (Addgene #16758) respectively. pCDH-PLEKHA4-GFP was digested with EcoRI and AgeI to remove PLEKHA4 fragment and the remaining vector was used to subclone the DVL2 or DVL3 fragments.

For generation of doxycycline-inducible stable shPLEKHA4 lines, 12 shRNA constructs each again human PLEKHA4 or mouse *Plekha4* were cloned into LT3GEPIR vector as described previously[65]. All constructs were verified by Sanger sequencing (Cornell University Biotechnology Resource Center Genomics Facility).

3.6.2 *Transfection of siRNA*

DsiRNA duplexes were obtained from Integrated DNA Technologies. Transfections with siRNA were performed using Lipofectamine RNAiMAX with the appropriate duplexes (see **Table S3.1**) as described previously[36], and 48 h post transfection, cells were analyzed via Western blot, flow cytometry or other readouts.

3.6.3 *Lentivirus production*

Exogenous protein expression was achieved in WM266-4 and SK-MEL-2 cells via lentiviral transduction. Lentivirus was produced in HEK 293TN cells, which were seeded to achieve a 90% confluency on the day of transfection with the viral plasmids. Packaging plasmids VSVg and PAX2, along with the lentiviral plasmid, were transfected overnight in the ratio of 1:3.1:4.2 in the HEK 293TN cells (RRID:CVCL_UL49, obtained from The Bretscher Lab, Cornell University) using Lipofectamine 2000. Fresh media was changed the next morning and the transfection media was discarded. Thirty-six h post transfection, the lentivirus-containing media was collected, and cells were replenished with new fresh media. The media collection was performed every 8 h for a total of four times. The lentivirus-containing media was filtered through 0.45 μm syringe filters and stored in 4 ºC until use. The lentivirus media was used within two weeks after production. For production of shRNA-containing lentivirus, the same protocol was used, except that packaging plasmids VSVg and PAX2, along with shRNA plasmids, were mixed and transfected overnight in the ratio of 1:1.8:3.7.

3.6.4 *Lentivirus transduction*

Depending on the experiment, cells were seeded 1–2 d prior to viral transduction. On the day of transduction, media was aspirated, and one part of fresh media was added with 8 μg/mL of Polybrene (Millipore) and spread evenly. Three parts of filtered lentivirus media was added and gently mixed. For the highest transduction efficiency, the process was repeated four times every 10-12 h. For stable cell line generation, cells were selected with the appropriate selection drug as described above. For all other experiments, cells were used without selection. Transduction efficiency was determined using fluorescence microscopy for every lentivirus transduction experiment using Hoechst 33342 (Thermo Fisher) as the counterstain. The transduction efficiency for these experiments were determined to be 80–90%. Images were acquired on a Zeiss LSM 800 confocal laser scanning microscope equipped with Plan Apochromat objectives (20x 0.8 NA or 40x 1.4 NA), and two GaAsP PMT detectors. Solid-state lasers (405, 488, 561, and 640 nm) were used to excite blue, green, red and far-red fluorescence respectively. Images were acquired using Zeiss Zen Blue 2.3 (confocal) and analyzed using ImageJ.

3.6.5 *Cell proliferation assays*

SiRNA (50 nM) against PLEKHA4, DVL2, and DVL3 was performed overnight on WM266-4 or SK-MEL-2 cells on a 6-well plate. After 16 h, cells were lifted, and 4000 cells were seeded in each well of a low-evaporation 96-well plate. For Wnt inhibition experiments, cells were seeded in media containing either DMSO

vehicle or 2.5 μM IWP-4 (Inhibitor of Wnt Production-4). Images were acquired every hour for at least 4 d in an IncuCyte incubator (20X objective).

3.6.6 *Anchorage-dependent colony formation assays*

SiRNA (50 nM) against PLEKHA4, DVL2, and DVL3 was performed overnight on WM266-4 or SK-MEL-2 cells in a 6-well plate. After 16 h, cells were lifted, and 4000 cells were plated evenly in each well of a 6-well plate. Fresh media was changed every 3 d. For Wnt inhibition experiments, 4000 untreated cells were plated in media containing either DMSO or IWP-4 (2.5 μM). The cells were grown for two weeks until colonies were observed. Cells were washed with PBS, fixed with methanol for 1 h at room temperature, and stained overnight with 0.1% crystal violet in 95% ethanol. The lids were propped open slightly to allow the stain solution to evaporate overnight. Plates were then rinsed gently with cold water to remove excess stain and allowed to dry for 3 h. Images were acquired with a Bio-Rad ChemiDoc, and colonies were counted using ImageJ.

3.6.7 *Anchorage-independent colony formation assays*

SiRNA (50 nM) against PLEKHA4, DVL2, and DVL3 was performed overnight on WM266-4 or SK-MEL-2 cells in a 6-well plate. After 16 h, cells were lifted, and 5000 cells were plated evenly in each well of a 6-well plate. The soft agar assay was set up as described previously[45]. Three weeks after the seeding, colonies were observed and stained overnight at 37 ºC with nitrotetrazolium blue (1 mg/mL in

PBS). Images were acquired with a Bio-Rad Chemidoc, and colonies were counted using ImageJ.

3.6.8 *Cell cycle analysis*

Unsynchronized: For cell cycle analysis in unsynchronized WM266-4 cells, siRNA (50 nM) against PLEKHA4 was performed in a 12-well plate. After 48 h, cells were lifted, fixed overnight with prechilled ethanol, and stained using propidium iodide as described previously[66], and analyzed by flow cytometry.

Synchronized: Stable cells expressing FUCCI were seeded on a 15-cm dish, grown to 90% confluence, and starved with FBS-free media for 48 h. SiRNA (50 nM) against PLEKHA4 was added for the final 16 h of serum starvation. Cells were then stimulated by addition of fresh FBS-containing media for 36 h, and then lifted and fixed overnight with pre-chilled ethanol at 4 ºC. Cells were washed three times with FACS buffer (0.1% FBS in PBS) and analyzed via flow cytometry.

Rescue: Media containing lentivirus encoding rescue constructs (GFP, PLEKHA4-GFP, DVL2-GFP, DVL3-GFP, or a combination of DVL2-GFP and DVL3-GFP) was generated. RNAi against PLEKHA4 was performed as above on a 60-mm plate, and 16 h post RNAi, cells were stimulated with rescue media (a mix of 1.5 mL of fresh media and 2.5 mL of virus-containing rescue media). After 32 h, cells were harvested and fixed overnight with prechilled ethanol at 4 ºC. Cell cycle analysis

by flow cytometry was performed either by propidium iodide on wild-type cells or FUCCI-expressing stable lines, quantifying fraction of cells in G1.

3.6.9 *Tumor xenograft and allograft studies of PLEKHA4 shRNA*

Stable cell lines with doxycycline inducible PLEKHA4 or control shRNA were generated. One day before the cell injections, the dorsal sides of mice (4-6 week-old) were shaved to enable four injections per animal, two each near the upper and lower flanks. On injection day, cells were lifted, and resuspended in media containing 1% penicillin/streptomycin. A 1:1 mixture of cells:Matrigel was made, and $1x10^6$ of shRNA-expressing WM266-4 or SK-MEL-2 cells were injected subcutaneously into NSG mice using a 28-gauge needle. The same procedure was used for shRNA-expressing YUMM1.7 cells except that $1x10^5$ cells were injected subcutaneously into C57BL/6J mice. Injections were performed within 30 min of preparing the cells/Matrigel mixture. Mice were monitored every 2 d. For WM266-4 and YUMM1.7 xenografts, tumor formation appeared at day 12, whereas for SK-MEL-2, the tumor formation appeared at 1.5 months post injection. To induce shRNA expression, doxycycline (1 mg/mL in sterile water) was added to the drinking water in amber bottles and changed every 2 d (WM266-4: 12 d; YUMM1.7: 10 d; SK-MEL-2: 16 d). Tumor progression was measured every 2 d with a digital caliper, with volume calculated using $v = 0.5233*l*w^2$. All mouse studies were approved by the Cornell Institutional Animal Care and Use Committee.

3.6.10 *Tumor xenograft studies of PLEKHA4 shRNA combined with BRAFi treatment*

PLEKHA4 or control shRNA-expressing WM266-4 cells ($1x10^6$) were injected subcutaneously as described above. Mice were monitored every 2 d. Tumors appeared at day 12. Doxycycline (1 mg/mL in sterile water) was then added to the drinking water to induce shRNA as described above, and, concurrently, encorafenib or vehicle was administered daily via oral gavage (30 mg/kg in 0.5% carboxymethylcellulose and 0.05% Tween-80 in PBS, freshly prepared) for 12 d. Tumor progression was monitored as described above. At the end of 12 d of encorafenib treatment, the encorafenib treatment was terminated but doxycycline was continued for another 14 d. Tumor progression was monitored every 2 days, and volumes were calculated as described above.

3.6.11 *Western blot analysis of DVL, c-Myc, and Cyclin D1 levels*

SiRNA duplexes (50 nM) against PLEKHA4, DVL2, or DVL3 were used to perform knockdown on either WM266-4 or SK-MEL-2 cells on a 6-well plate. Forty-eight h post-RNAi, cells were harvested and analyzed by Western blot as described previously[36]. The levels of DVL2, DVL3, c-Myc, and Cyclin D1 were quantified. Reported quantifications are from at least three biological replicates. For analysis of endogenous Axin2 levels, siRNA duplexes (50 nM) against PLEKHA4 were transfected into WM266-4 or SK-MEL-2 cells on a 6-well plate. Cells were stimulated with Wnt3a-conditioned media, harvested, analyzed by Western blot, and Axin2 levels were quantified as described previously[36]. For rescue experiments, samples were

generated as described above for cell cycle rescue analysis. Forty-eight h post-RNAi, cells were harvested, normalized and analyzed via Western blot for DVL2, DVL3, c-Myc, and Cyclin D1 levels. Reported quantifications are from at least three biological replicates. Sources of antibodies are provided in **Table S3.2**.

3.6.12 *Luciferase Wnt reporter assays*

Generation of cells stably expressing Wnt reporters: WM266-4 or SK-MEL-2 cells were co-transduced with lentiviruses expressing Firefly luciferase-7TFP (Addgene #24308) and Renilla luciferase pLenti.PGK.blast-Renilla_Luciferase (Addgene #74444). After 48 h, puromycin dihydrochloride (2.5 μg/mL) and blasticidin S hydrochloride (2 μg/mL) selection was performed until resistant colonies appeared. These reporter cell lines were used in siRNA-based Wnt reporter luciferase assays below.

Transient knockdown: SiRNA-mediated knockdown against PLEKHA4 was performed in Wnt/β-catenin luciferase reporter-expressing WM266-4 and SK-MEL-2 cells on 6-well plates. After 30 h of cell growth post-transfection, cells were treated with sterile-filtered, Wnt3a-containing conditioned media in a 1:1 ratio with fresh media for 30 h. Cells were then lysed, and 150 μL of lysates were transferred to an opaque 96-well flat-bottom plate (Greiner) for measuring chemiluminescence. Firefly luciferin substrate (50 μL of a 470 μM stock solution) was added to each well, and the firefly luciferase signal was measured by a Tecan plate reader. Subsequently, Renilla luciferase substrate (50 μL of a 5.5 μM stock solution also containing 25 μM of the

firefly luciferase inhibitor 4-(6-methyl-1,3-benzothiazol-2-yl)-aniline (Enamine.net)) was added to each well, and the Renilla luciferase signal was measured.

Stable knockdown: ShRNA expression against PLEKHA4 in WM266-4 and SK-MEL-2 cells was induced by addition of 2.5 μg/mL doxycycline for 10 d in 6-well plates. As a negative control, stable cells bearing inducible Renilla shRNA were treated in the absence of doxycycline. Doxycycline-containing media was exchanged for fresh media every 2 d. On day 8, cells were treated with a 1:1:1 mixture of 7TFP lentivirus-containing conditioned media:PGK-Renilla lentivirus-containing conditioned media:fresh media, and 8 μg/mL polybrene and 2.5 μg/mL doxycycline for 24 h. Spent media was exchanged for fresh 1:1:1 media mixture as described above every 12 h. On day 9, Wnt signaling was induced by adding Wnt3a-containing conditioned media in a 1:1 ratio with fresh media containing doxycycline for 30 h. Firefly and Renilla luciferase signals were then measured as described above.

3.7 QUANTIFICATION AND STATISTICAL ANALYSIS

3.7.1 *Statistics and reproducibility*

All experiments were performed in at least three biological replicates. Imaging figures show representative images from each experiment. For experiments involving quantification of comparisons between two groups, statistical significance was calculated using unpaired two-tailed Student's t-test with unequal variance in Excel or GraphPad Prism. For experiments involving quantification of comparisons between more than two experimental groups, statistical significance was calculated using a

one-way ANOVA with post-hoc Tukey test in R. The number of biological replicates analyzed is stated in the legend, and statistical significance of $p < 0.05$ or lower is reported. All raw data were plotted using either Excel or GraphPad Prism. In figures containing bar graphs, the height of the bar is the mean, the error bars represent standard deviation, and each overlaid dot represents an individual biological replicate. In figures containing scatter plots, the black line is the mean, and each dot represents an individual biological replicate. In figures containing IncuCyte proliferation data and tumor xenograft progression data, the means at various time points were plotted, and error bars represent standard deviation. Tumor xenograft progression measurements were performed in a blinded manner. In Figure 1A, the boxes represent the middle quartiles, with the line in the middle denoting the median.

3.8 REFERENCES

(1) Miller, A. J.; Mihm, M. C. Melanoma. *N. Engl. J. Med.* **2006**, *355* (1), 51–65. https://doi.org/10.1056/NEJMra052166.

(2) Akbani, R.; Akdemir, K. C.; Aksoy, B. A.; Albert, M.; Ally, A.; Amin, S. B.; Arachchi, H.; Arora, A.; Auman, J. T.; Ayala, B.; Baboud, J.; Balasundaram, M.; Balu, S.; Barnabas, N.; Bartlett, J.; Bartlett, P.; Bastian, B. C.; Baylin, S. B.; Behera, M.; Belyaev, D.; Benz, C.; Bernard, B.; Beroukhim, R.; Bir, N.; Black, A. D.; Bodenheimer, T.; Boice, L.; Boland, G. M.; Bono, R.; Bootwalla, M. S.; Bosenberg, M.; Bowen, J.; Bowlby, R.; Bristow, C. A.; Brockway-Lunardi, L.; Brooks, D.; Brzezinski, J.; Bshara, W.; Buda, E.; Burns, W. R.; Butterfield, Y. S. N.; Button, M.; Calderone, T.; Cappellini, G. A.; Carter, C.; Carter, S. L.; Cherney, L.; Cherniack, A. D.; Chevalier, A.; Chin, L.; Cho, J.; Cho, R. J.; Choi, Y. La; Chu, A.; Chudamani, S.; Cibulskis, K.; Ciriello, G.; Clarke, A.; Coons, S.; Cope, L.; Crain, D.; Curley, E.; Danilova, L.; D'Atri, S.; Davidsen, T.; Davies, M. A.; Delman, K. A.; Demchok, J. A.; Deng, Q. A.; Deribe, Y. L.; Dhalla, N.; Dhir, R.; Dicara, D.; Dinikin, M.; Dubina, M.; Ebrom, J. S.; Egea, S.; Eley, G.; Engel, J.; Eschbacher, J. M.; Fedosenko, K. V.; Felau, I.; Fennell, T.; Ferguson, M. L.; Fisher, S.; Flaherty, K. T.; Frazer, S.; Frick, J.; Fulidou, V.; Gabriel, S. B.; Gao, J.; Gardner, J.; Garraway, L. A.; Gastier-Foster, J. M.; Gaudioso, C.; Gehlenborg, N.; Genovese, G.; Gerken, M.; Gershenwald, J. E.; Getz, G.; Gomez-Fernandez, C.; Gribbin, T.; Grimsby, J.; Gross, B.; Guin, R.; Gutschner, T.; Hadjipanayis, A.; Halaban, R.; Hanf, B.; Haussler, D.; Haydu, L. E.; Hayes, D. N.; Hayward, N. K.; Heiman, D. I.; Herbert, L.; Herman, J. G.; Hersey, P.; Hoadley, K. A.; Hodis, E.; Holt, R. A.; Hoon, D. S.; Hoppough, S.; Hoyle, A. P.; Huang, F. W.; Huang, M.; Huang, S.; Hutter, C. M.; Ibbs, M.; Iype, L.; Jacobsen, A.; Jakrot, V.; Janning, A.; Jeck, W. R.; Jefferys, S. R.; Jensen, M. A.; Jones, C. D.; Jones, S. J. M.; Ju, Z.; Kakavand, H.; Kang, H.; Kefford, R. F.; Khuri, F. R.; Kim, J.; Kirkwood, J. M.; Klode, J.; Korkut, A.; Korski, K.; Krauthammer, M.; Kucherlapati, R.; Kwong, L. N.; Kycler, W.; Ladanyi, M.; Lai, P. H.; Laird, P. W.; Lander, E.; Lawrence, M. S.; Lazar, A. J.; Łaźniak, R.; Lee, D.; Lee, J. E.; Lee, J.; Lee, K.; Lee, S.; Lee, W.; Leporowska, E.; Leraas, K. M.; Li, H. I.; Lichtenberg, T. M.; Lichtenstein, L.; Lin, P.; Ling, S.; Liu, J.; Liu, O.; Liu, W.; Long, G. V.; Lu, Y.; Ma, S.; Ma, Y.; Mackiewicz, A.; Mahadeshwar, H. S.; Malke, J.; Mallery, D.; Manikhas, G. M.; Mann, G. J.; Marra, M. A.; Matejka, B.; Mayo, M.; Mehrabi, S.; Meng, S.; Meyerson, M.; Mieczkowski, P. A.; Miller, J. P.; Miller, M. L.; Mills, G. B.; Moiseenko, F.; Moore, R. A.; Morris, S.; Morrison, C.; Morton, D.; Moschos, S.; Mose, L. E.; Muller, F. L.; Mungall, A. J.; Murawa, D.; Murawa, P.; Murray, B. A.; Nezi, L.; Ng, S.; Nicholson, D.; Noble, M. S.; Osunkoya, A.; Owonikoko, T. K.; Ozenberger, B. A.; Pagani, E.; Paklina, O. V.; Pantazi, A.; Parfenov, M.; Parfitt, J.; Park, P. J.; Park, W. Y.; Parker, J. S.; Passarelli, F.; Penny, R.; Perou, C. M.; Pihl, T. D.; Potapova, O.; Prieto, V. G.;

Protopopov, A.; Quinn, M. J.; Radenbaugh, A.; Rai, K.; Ramalingam, S. S.; Raman, A. T.; Ramirez, N. C.; Ramirez, R.; Rao, U.; Rathmell, W. K.; Ren, X.; Reynolds, S. M.; Roach, J.; Robertson, A. G.; Ross, M. I.; Roszik, J.; Russo, G.; Saksena, G.; Saller, C.; Samuels, Y.; Sander, C.; Sander, C.; Sandusky, G.; Santoso, N.; Saul, M.; Saw, R. P.; Schadendorf, D.; Schein, J. E.; Schultz, N.; Schumacher, S. E.; Schwallier, C.; Scolyer, R. A.; Seidman, J.; Sekhar, P. C.; Sekhon, H. S.; Senbabaoglu, Y.; Seth, S.; Shannon, K. F.; Sharpe, S.; Sharpless, N. E.; Shaw, K. R. M.; Shelton, C.; Shelton, T.; Shen, R.; Sheth, M.; Shi, Y.; Shiau, C. J.; Shmulevich, I.; Sica, G. L.; Simons, J. V.; Sinha, R.; Sipahimalani, P.; Sofia, H. J.; Soloway, M. G.; Song, X.; Sougnez, C.; Spillane, A. J.; Spychała, A.; Stretch, J. R.; Stuart, J.; Suchorska, W. M.; Sucker, A.; Sumer, S. O.; Sun, Y.; Synott, M.; Tabak, B.; Tabler, T. R.; Tam, A.; Tan, D.; Tang, J.; Tarnuzzer, R.; Tarvin, K.; Tatka, H.; Taylor, B. S.; Teresiak, M.; Thiessen, N.; Thompson, J. F.; Thorne, L.; Thorsson, V.; Trent, J. M.; Triche, T. J.; Tsai, K. Y.; Tsou, P.; Van Den Berg, D. J.; Van Allen, E. M.; Veluvolu, U.; Verhaak, R. G.; Voet, D.; Voronina, O.; Walter, V.; Walton, J. S.; Wan, Y.; Wang, Y.; Wang, Z.; Waring, S.; Watson, I. R.; Weinhold, N.; Weinstein, J. N.; Weisenberger, D. J.; White, P.; Wilkerson, M. D.; Wilmott, J. S.; Wise, L.; Wiznerowicz, M.; Woodman, S. E.; Wu, C. J.; Wu, C. C.; Wu, J.; Wu, Y.; Xi, R.; Xu, A. W.; Yang, D.; Yang, L.; Yang, L.; Zack, T. I.; Zenklusen, J. C.; Zhang, H.; Zhang, J.; Zhang, W.; Zhao, X.; Zhu, J.; Zhu, K.; Zimmer, L.; Zmuda, E.; Zou, L. Genomic Classification of Cutaneous Melanoma. *Cell* **2015**, *161* (7), 1681–1696. https://doi.org/10.1016/j.cell.2015.05.044.

(3) Hayward, N. K.; Wilmott, J. S.; Waddell, N.; Johansson, P. A.; Field, M. A.; Nones, K.; Patch, A.-M.; Kakavand, H.; Alexandrov, L. B.; Burke, H.; Jakrot, V.; Kazakoff, S.; Holmes, O.; Leonard, C.; Sabarinathan, R.; Mularoni, L.; Wood, S.; Xu, Q.; Waddell, N.; Tembe, V.; Pupo, G. M.; De Paoli-Iseppi, R.; Vilain, R. E.; Shang, P.; Lau, L. M. S.; Dagg, R. A.; Schramm, S.-J.; Pritchard, A.; Dutton-Regester, K.; Newell, F.; Fitzgerald, A.; Shang, C. A.; Grimmond, S. M.; Pickett, H. A.; Yang, J. Y.; Stretch, J. R.; Behren, A.; Kefford, R. F.; Hersey, P.; Long, G. V; Cebon, J.; Shackleton, M.; Spillane, A. J.; Saw, R. P. M.; López-Bigas, N.; Pearson, J. V; Thompson, J. F.; Scolyer, R. A.; Mann, G. J. Whole-Genome Landscapes of Major Melanoma Subtypes. *Nature* **2017**, *545* (7653), 175–180. https://doi.org/10.1038/nature22071.

(4) Long, G. V; Stroyakovskiy, D.; Gogas, H.; Levchenko, E.; de Braud, F.; Larkin, J.; Garbe, C.; Jouary, T.; Hauschild, A.; Grob, J. J.; Chiarion Sileni, V.; Lebbe, C.; Mandalà, M.; Millward, M.; Arance, A.; Bondarenko, I.; Haanen, J. B. A. G.; Hansson, J.; Utikal, J.; Ferraresi, V.; Kovalenko, N.; Mohr, P.; Probachai, V.; Schadendorf, D.; Nathan, P.; Robert, C.; Ribas, A.; DeMarini, D. J.; Irani, J. G.; Casey, M.; Ouellet, D.; Martin, A.-M.; Le, N.; Patel, K.; Flaherty, K. Combined BRAF and MEK Inhibition versus BRAF Inhibition Alone in Melanoma. *N. Engl. J. Med.* **2014**, *371* (20), 1877–1888. https://doi.org/10.1056/NEJMoa1406037.

(5) Larkin, J.; Ascierto, P. A.; Dréno, B.; Atkinson, V.; Liszkay, G.; Maio, M.; Mandalà, M.; Demidov, L.; Stroyakovskiy, D.; Thomas, L.; de la Cruz-Merino, L.; Dutriaux, C.; Garbe, C.; Sovak, M. A.; Chang, I.; Choong, N.; Hack, S. P.; McArthur, G. A.; Ribas, A. Combined Vemurafenib and Cobimetinib in BRAF-Mutated Melanoma. *N. Engl. J. Med.* **2014**, *371* (20), 1867–1876. https://doi.org/10.1056/NEJMoa1408868.

(6) Lito, P.; Rosen, N.; Solit, D. B. Tumor Adaptation and Resistance to RAF Inhibitors. *Nat. Med.* **2013**, *19* (11), 1401–1409. https://doi.org/10.1038/nm.3392.

(7) Hamid, O.; Robert, C.; Daud, A.; Hodi, F. S.; Hwu, W.-J.; Kefford, R.; Wolchok, J. D.; Hersey, P.; Joseph, R. W.; Weber, J. S.; Dronca, R.; Gangadhar, T. C.; Patnaik, A.; Zarour, H.; Joshua, A. M.; Gergich, K.; Elassaiss-Schaap, J.; Algazi, A.; Mateus, C.; Boasberg, P.; Tumeh, P. C.; Chmielowski, B.; Ebbinghaus, S. W.; Li, X. N.; Kang, S. P.; Ribas, A. Safety and Tumor Responses with Lambrolizumab (Anti–PD-1) in Melanoma. *N. Engl. J. Med.* **2013**, *369* (2), 134–144. https://doi.org/10.1056/NEJMoa1305133.

(8) Hu-Lieskovan, S.; Mok, S.; Homet Moreno, B.; Tsoi, J.; Robert, L.; Goedert, L.; Pinheiro, E. M.; Koya, R. C.; Graeber, T. G.; Comin-Anduix, B.; Ribas, A. Improved Antitumor Activity of Immunotherapy with BRAF and MEK Inhibitors in BRAF–V600E Melanoma. *Sci. Transl. Med.* **2015**, *7* (279), 279ra41. https://doi.org/10.1126/scitranslmed.aaa4691.

(9) Zhan, T.; Rindtorff, N.; Boutros, M. Wnt Signaling in Cancer. *Oncogene* **2017**, *36* (11), 1461–1473. https://doi.org/10.1038/onc.2016.304.

(10) MacDonald, B. T.; Tamai, K.; He, X. Wnt/β-Catenin Signaling: Components, Mechanisms, and Diseases. *Dev. Cell* **2009**, *17* (1), 9–26. https://doi.org/10.1016/j.devcel.2009.06.016.

(11) Webster, M. R.; Weeraratna, A. T. A Wnt-Er Migration: The Confusing Role of β-Catenin in Melanoma Metastasis. *Sci. Signal.* **2013**, *6* (268), pe11. https://doi.org/10.1126/scisignal.2004114.

(12) Jackstadt, R.; Hodder, M. C.; Sansom, O. J. WNT and β-Catenin in Cancer: Genes and Therapy. *Annu. Rev. Cancer Biol.* **2020**, *4* (1), 177–196. https://doi.org/10.1146/annurev-cancerbio-030419-033628.

(13) Gajos-Michniewicz, A.; Czyz, M. Wnt Signaling in Melanoma. *Int J Mol Sci* **2020**, *21*, 4852.

(14) Delmas, V.; Beermann, F.; Martinozzi, S.; Carreira, S.; Ackermann, J.; Kumasaka, M.; Denat, L.; Goodall, J.; Luciani, F.; Viros, A.; Demirkan, N.; Bastian, B. C.; Goding, C. R.; Larue, L. β-Catenin Induces Immortalization of Melanocytes by Suppressing P16INK4a Expression and Cooperates with N-Ras in Melanoma Development. *Genes Dev.* **2007**, *21* (22), 2923–2935. https://doi.org/10.1101/gad.450107.

(15) Pawlikowski, J. S.; McBryan, T.; van Tuyn, J.; Drotar, M. E.; Hewitt, R. N.; Maier, A. B.; King, A.; Blyth, K.; Wu, H.; Adams, P. D. Wnt Signaling Potentiates Nevogenesis. *Proc. Natl. Acad. Sci.* **2013**, *110* (40), 16009–16014. https://doi.org/10.1073/pnas.1303491110.

(16) Juan, J.; Muraguchi, T.; Iezza, G.; Sears, R. C.; McMahon, M. Diminished WNT -> β-Catenin -> c-MYC Signaling Is a Barrier for Malignant Progression of BRAFV600E-Induced Lung Tumors. *Genes Dev.* **2014**, *28* (6), 561–575. https://doi.org/10.1101/gad.233627.113.

(17) Damsky, W. E.; Curley, D. P.; Santhanakrishnan, M.; Rosenbaum, L. E.; Platt, J. T.; Gould Rothberg, B. E.; Taketo, M. M.; Dankort, D.; Rimm, D. L.; McMahon, M.; Bosenberg, M. β-Catenin Signaling Controls Metastasis in Braf-Activated Pten-Deficient Melanomas. *Cancer Cell* **2011**, *20* (6), 741–754. https://doi.org/https://doi.org/10.1016/j.ccr.2011.10.030.

(18) Sun, Q.; Lee, W.; Mohri, Y.; Takeo, M.; Lim, C. H.; Xu, X.; Myung, P.; Atit, R. P.; Taketo, M. M.; Moubarak, R. S.; Schober, M.; Osman, I.; Gay, D. L.; Saur, D.; Nishimura, E. K.; Ito, M. A Novel Mouse Model Demonstrates That Oncogenic Melanocyte Stem Cells Engender Melanoma Resembling Human Disease. *Nat. Commun.* **2019**, *10* (1), 1–16. https://doi.org/10.1038/s41467-019-12733-1.

(19) Chien, A. J.; Haydu, L. E.; Biechele, T. L.; Kulikauskas, R. M.; Rizos, H.; Kefford, R. F.; Scolyer, R. A.; Moon, R. T.; Long, G. V. Targeted BRAF Inhibition Impacts Survival in Melanoma Patients with High Levels of Wnt/β-Catenin Signaling. *PLoS One* **2014**, *9* (4), e94748.

(20) Kageshita, T.; Hamby, C. V; Ishihara, T.; Matsumoto, K.; Saida, T.; Ono, T. Loss of β-Catenin Expression Associated with Disease Progression in Malignant Melanoma. *Br. J. Dermatol.* **2001**, *145* (2), 210–216. https://doi.org/10.1046/j.1365-2133.2001.04336.x.

(21) Bachmann, I. M.; Straume, O.; Puntervoll, H. E.; Kalvenes, M. B.; Akslen, L. A. Importance of P-Cadherin, β-Catenin, and Wnt5a/Frizzled for Progression of Melanocytic Tumors and Prognosis in Cutaneous Melanoma. *Clin. Cancer Res.* **2005**, *11* (24), 8606 LP – 8614. https://doi.org/10.1158/1078-0432.CCR-05-0011.

(22) Chien, A. J.; Moore, E. C.; Lonsdorf, A. S.; Kulikauskas, R. M.; Rothberg, B. G.; Berger, A. J.; Major, M. B.; Hwang, S. T.; Rimm, D. L.; Moon, R. T. Activated Wnt/ß-Catenin Signaling in Melanoma Is Associated with Decreased Proliferation in Patient Tumors and a Murine Melanoma Model. *Proc. Natl. Acad. Sci.* **2009**, *106* (4), 1193–1198. https://doi.org/10.1073/pnas.0811902106.

(23) Xue, G.; Romano, E.; Massi, D.; Mandalà, M. Wnt/β-Catenin Signaling in Melanoma: Preclinical Rationale and Novel Therapeutic Insights. *Cancer Treat. Rev.* **2016**, *49*, 1–12. https://doi.org/10.1016/j.ctrv.2016.06.009.

(24) Webster, M. R.; Xu, M.; Kinzler, K. A.; Kaur, A.; Appleton, J.; O'Connell, M. P.; Marchbank, K.; Valiga, A.; Dang, V. M.; Perego, M.; Zhang, G.; Slipicevic, A.; Keeney, F.; Lehrmann, E.; Wood III, W.; Becker, K. G.; Kossenkov, A. V; Frederick, D. T.; Flaherty, K. T.; Xu, X.; Herlyn, M.; Murphy, M. E.; Weeraratna, A. T. Wnt5A Promotes an Adaptive, Senescent-like Stress Response, While Continuing to Drive Invasion in Melanoma Cells. *Pigment Cell Melanoma Res.* **2015**, *28* (2), 184–195. https://doi.org/10.1111/pcmr.12330.

(25) Anastas, J. N.; Kulikauskas, R. M.; Tamir, T.; Rizos, H.; Long, G. V; von Euw, E. M.; Yang, P.-T.; Chen, H.-W.; Haydu, L.; Toroni, R. A.; Lucero, O. M.; Chien, A. J.; Moon, R. T. WNT5A Enhances Resistance of Melanoma Cells to Targeted BRAF Inhibitors. *J. Clin. Invest.* **2014**, *124* (7), 2877–2890. https://doi.org/10.1172/JCI70156.

(26) Hoek, K. S.; Eichhoff, O. M.; Schlegel, N. C.; Döbbeling, U.; Kobert, N.; Schaerer, L.; Hemmi, S.; Dummer, R. In Vivo Switching of Human Melanoma Cells between Proliferative and Invasive States. *Cancer Res.* **2008**, *68* (3), 650 LP – 656. https://doi.org/10.1158/0008-5472.CAN-07-2491.

(27) Nusse, R.; Clevers, H. Wnt/β-Catenin Signaling, Disease, and Emerging Therapeutic Modalities. *Cell* **2017**, *169* (6), 985–999. https://doi.org/10.1016/j.cell.2017.05.016.

(28) Tran, F. H.; Zheng, J. J. Modulating the Wnt Signaling Pathway with Small Molecules. *Protein Sci.* **2017**, *26* (4), 650–661. https://doi.org/10.1002/pro.3122.

(29) Kahn, M. Can We Safely Target the WNT Pathway? *Nat. Rev. Drug Discov.* **2014**, *13* (7), 513–532. https://doi.org/10.1038/nrd4233.

(30) Clevers, H.; Nusse, R. Wnt/β-Catenin Signaling and Disease. *Cell* **2012**, *149* (6), 1192–1205. https://doi.org/10.1016/j.cell.2012.05.012.

(31) Mlodzik, M. *The Dishevelled Protein Family: Still Rather a Mystery After Over 20 Years of Molecular Studies*, 1st ed.; Elsevier Inc., 2016; Vol. 117. https://doi.org/10.1016/bs.ctdb.2015.11.027.

(32) Nielsen, C. P.; Jernigan, K. K.; Diggins, N. L.; Webb, D. J.; MacGurn, J. A. USP9X Deubiquitylates DVL2 to Regulate WNT Pathway Specification. *Cell Rep.* **2019**, *28* (4), 1074-1089.e5. https://doi.org/10.1016/j.celrep.2019.06.083.

(33) Tauriello, D. V. F.; Haegebarth, A.; Kuper, I.; Edelmann, M. J.; Henraat, M.; Canninga-van Dijk, M. R.; Kessler, B. M.; Clevers, H.; Maurice, M. M. Loss of the Tumor Suppressor CYLD Enhances Wnt/β-Catenin Signaling through K63-Linked Ubiquitination of Dvl. *Mol. Cell* **2010**, *37* (5), 607–619. https://doi.org/https://doi.org/10.1016/j.molcel.2010.01.035.

(34) Ding, Y.; Zhang, Y.; Xu, C.; Tao, Q. H.; Chen, Y. G. HECT Domain-Containing E3 Ubiquitin Ligase NEDD4L Negatively Regulates Wnt Signaling by Targeting Dishevelled for Proteasomal Degradation. *J. Biol. Chem.* **2013**, *288* (12), 8289–8298. https://doi.org/10.1074/jbc.M112.433185.

(35) Wei, W.; Li, M.; Wang, J.; Nie, F.; Li, L. The E3 Ubiquitin Ligase ITCH Negatively Regulates Canonical Wnt Signaling by Targeting Dishevelled Protein. *Mol. Cell. Biol.* **2012**, *32* (19), 3903–3912. https://doi.org/10.1128/MCB.00251-12.

(36) Shami Shah, A.; Batrouni, A. G.; Kim, D.; Punyala, A.; Cao, W.; Han, C.; Goldberg, M. L.; Smolka, M. B.; Baskin, J. M. PLEKHA4/Kramer Attenuates Dishevelled Ubiquitination to Modulate Wnt and Planar Cell Polarity Signaling. *Cell Rep.* **2019**, *27* (7), 2157-2170.e8. https://doi.org/10.1016/j.celrep.2019.04.060.

(37) Angers, S.; Thorpe, C. J.; Biechele, T. L.; Goldenberg, S. J.; Zheng, N.; MacCoss, M. J.; Moon, R. T. The KLHL12–Cullin-3 Ubiquitin Ligase Negatively Regulates the Wnt–β-Catenin Pathway by Targeting Dishevelled for Degradation. *Nat. Cell Biol.* **2006**, *8* (4), 348–357. https://doi.org/10.1038/ncb1381.

(38) Hruz, T.; Laule, O.; Szabo, G.; Wessendorp, F.; Bleuler, S.; Oertle, L.; Widmayer, P.; Gruissem, W.; Zimmermann, P. Genevestigator V3: A Reference Expression Database for the Meta-Analysis of Transcriptomes. *Adv. Bioinformatics* **2008**, *2008*, 1–5. https://doi.org/10.1155/2008/420747.

(39) Koelblinger, P.; Thuerigen, O.; Dummer, R. Development of Encorafenib for BRAF-Mutated Advanced Melanoma. *Curr. Opin. Oncol.* **2018**, *30* (2), 125–133. https://doi.org/10.1097/CCO.0000000000000426.

(40) Meeth, K.; Wang, J. X.; Micevic, G.; Damsky, W.; Bosenberg, M. W. The YUMM Lines: A Series of Congenic Mouse Melanoma Cell Lines with Defined Genetic Alterations. *Pigment Cell Melanoma Res.* **2016**, *29* (5), 590–597. https://doi.org/10.1111/pcmr.12498.

(41) Chen, B.; Dodge, M. E.; Tang, W.; Lu, J.; Ma, Z.; Fan, C.-W.; Wei, S.; Hao, W.; Kilgore, J.; Williams, N. S.; Roth, M. G.; Amatruda, J. F.; Chen, C.; Lum, L. Small Molecule-Mediated Disruption of Wnt-Dependent Signaling in Tissue Regeneration and Cancer. *Nat Chem Biol* **2009**, *5* (2), 100–107. https://doi.org/10.1038/nchembio.137.Small.

(42) Sakaue-Sawano, A.; Kurokawa, H.; Morimura, T.; Hanyu, A.; Hama, H.; Osawa, H.; Kashiwagi, S.; Fukami, K.; Miyata, T.; Miyoshi, H.; Imamura, T.; Ogawa, M. Visualizing Spatiotemporal Dynamics of Multicellular Cell-Cycle Progression. *Cell* **2008**, *132*, 487–498. https://doi.org/10.1016/j.cell.2007.12.033.

(43) Shtutman, M.; Zhurinsky, J.; Simcha, I.; Albanese, C.; D'Amico, M.; Pestell, R.; Ben-Ze'ev, A. The Cyclin D1 Gene Is a Target of the β-Catenin/LEF-1 Pathway. *Proc. Natl. Acad. Sci.* **1999**, *96* (10), 5522–5527. https://doi.org/10.1073/pnas.96.10.5522.

(44) He, T.-C.; Sparks, A. B.; Rago, C.; Hermeking, H.; Zawel, L.; da Costa, L. T.; Morin, P. J.; Vogelstein, B.; Kinzler, K. W. Identification of C-MYC as a Target of the APC Pathway. *Science (80-.).* **1998**, *281* (5382), 1509–1512. https://doi.org/10.1126/science.281.5382.1509.

(45) Rafehi, H.; Orlowski, C.; Georgiadis, G. T.; Ververis, K.; El-Osta, A.; Karagiannis, T. C. Clonogenic Assay: Adherent Cells. *J. Vis. Exp.* **2011**, No. 49, 15–17. https://doi.org/10.3791/2573.

(46) Flaherty, K. T.; Puzanov, I.; Kim, K. B.; Ribas, A.; McArthur, G. A.; Sosman, J. A.; O'Dwyer, P. J.; Lee, R. J.; Grippo, J. F.; Nolop, K.; Chapman, P. B. Inhibition of Mutated, Activated BRAF in Metastatic Melanoma. *N. Engl. J. Med.* **2010**, *363* (9), 809–819. https://doi.org/10.1056/NEJMoa1002011.

(47) Bollag, G.; Hirth, P.; Tsai, J.; Zhang, J.; Ibrahim, P. N.; Cho, H.; Spevak, W.; Zhang, C.; Zhang, Y.; Habets, G.; Burton, E. A.; Wong, B.; Tsang, G.; West, B. L.; Powell, B.; Shellooe, R.; Marimuthu, A.; Nguyen, H.; Zhang, K. Y. J.; Artis, D. R.; Schlessinger, J.; Su, F.; Higgins, B.; Iyer, R.; D'Andrea, K.; Koehler, A.; Stumm, M.; Lin, P. S.; Lee, R. J.; Grippo, J.; Puzanov, I.; Kim, K. B.; Ribas, A.; McArthur, G. A.; Sosman, J. A.; Chapman, P. B.; Flaherty, K. T.; Xu, X.; Nathanson, K. L.; Nolop, K. Clinical Efficacy of a RAF Inhibitor Needs Broad Target Blockade in BRAF-Mutant Melanoma. *Nature* **2010**, *467* (7315), 596–599. https://doi.org/10.1038/nature09454.

(48) Rizos, H.; Menzies, A. M.; Pupo, G. M.; Carlino, M. S.; Fung, C.; Hyman, J.; Haydu, L. E.; Mijatov, B.; Becker, T. M.; Boyd, S. C.; Howle, J.; Saw, R.; Thompson, J. F.; Kefford, R. F.; Scolyer, R. A.; Long, G. V. BRAF Inhibitor Resistance Mechanisms in Metastatic Melanoma: Spectrum and Clinical Impact. *Clin. Cancer Res.* **2014**, *20* (7), 1965–1977. https://doi.org/10.1158/1078-0432.CCR-13-3122.

(49) Shen, S.; Vagner, S.; Robert, C. Persistent Cancer Cells: The Deadly Survivors. *Cell* **2020**, *183* (4), 860–874. https://doi.org/10.1016/j.cell.2020.10.027.

(50) Lucero, O. M.; Dawson, D. W.; Moon, R. T.; Chien, A. J. A Re-Evaluation of the "Oncogenic" Nature of Wnt/β-Catenin Signaling in Melanoma and Other Cancers. *Curr. Oncol. Rep.* **2010**, *12* (5), 314–318. https://doi.org/10.1007/s11912-010-0114-3.

(51) Webster, M. R.; Kugel, C. H.; Weeraratna, A. T. The Wnts of Change: How Wnts Regulate Phenotype Switching in Melanoma. *Biochim. Biophys. Acta - Rev. Cancer* **2015**, *1856* (2), 244–251. https://doi.org/10.1016/j.bbcan.2015.10.002.

(52) Krishnamurthy, N.; Kurzrock, R. Targeting the Wnt/Beta-Catenin Pathway in Cancer: Update on Effectors and Inhibitors. *Cancer Treat. Rev.* **2018**, *62*, 50–60. https://doi.org/10.1016/j.ctrv.2017.11.002.

(53) Angers, S.; Thorpe, C. J.; Biechele, T. L.; Goldenberg, S. J.; Zheng, N.; MacCoss, M. J.; Moon, R. T. The KLHL12–Cullin-3 Ubiquitin Ligase Negatively Regulates the Wnt–β-Catenin Pathway by Targeting Dishevelled for Degradation. *Nat. Cell Biol.* **2006**, *8* (4), 348–357. https://doi.org/10.1038/ncb1381.

(54) Jin, L.; Pahuja, K. B.; Wickliffe, K. E.; Gorur, A.; Baumgärtel, C.; Schekman, R.; Rape, M. Ubiquitin-Dependent Regulation of COPII Coat Size and Function. *Nature* **2012**, *482* (7386), 495–500. https://doi.org/10.1038/nature10822.

(55) Strutt, H.; Searle, E.; Thomas-MacArthur, V.; Brookfield, R.; Strutt, D. A Cul-3-BTB Ubiquitylation Pathway Regulates Junctional Levels and Asymmetry of Core Planar Polarity Proteins. *Development* **2013**, *140* (8), 1693–1702. https://doi.org/10.1242/dev.089656.

(56) Kuphal, S.; Lodermeyer, S.; Bataille, F.; Schuierer, M.; Hoang, B. H.; Bosserhoff, A. K. Expression of Dickkopf Genes Is Strongly Reduced in Malignant Melanoma. *Oncogene* **2006**, *25* (36), 5027–5036. https://doi.org/10.1038/sj.onc.1209508.

(57) Mikheev, A. M.; Mikheeva, S. A.; Rostomily, R.; Zarbl, H. Dickkopf-1 Activates Cell Death in MDA-MB435 Melanoma Cells. *Biochem. Biophys. Res. Commun.* **2007**, *352* (3), 675–680. https://doi.org/10.1016/j.bbrc.2006.11.079.

(58) Haqq, C.; Nosrati, M.; Sudilovsky, D.; Crothers, J.; Khodabakhsh, D.; Pulliam, B. L.; Federman, S.; Miller, J. R.; Allen, R. E.; Singer, M. I.; Leong, S. P. L.; Ljung, B. M.; Sagebiel, R. W.; Kashani-Sabet, M. The Gene Expression Signatures of Melanoma Progression. *Proc. Natl. Acad. Sci. U. S. A.* **2005**, *102* (17), 6092–6097. https://doi.org/10.1073/pnas.0501564102.

(59) Widlund, H. R.; Horstmann, M. A.; Roydon Price, E.; Cui, J.; Lessnick, S. L.; Wu, M.; He, X.; Fisher, D. E. β-Catenin-Induced Melanoma Growth Requires the Downstream Target Microphthalmia-Associated Transcription Factor. *J. Cell Biol.* **2002**, *158* (6), 1079–1087. https://doi.org/10.1083/jcb.200202049.

(60) Hartman, M. L.; Czyz, M. MITF in Melanoma: Mechanisms behind Its Expression and Activity. *Cell. Mol. Life Sci.* **2015**, *72* (7), 1249–1260. https://doi.org/10.1007/s00018-014-1791-0.

(61) Biechele, T. L.; Kulikauskas, R. M.; Toroni, R. A.; Lucero, O. M.; Swift, R. D.; James, R. G.; Robin, N. C.; Dawson, D. W.; Moon, R. T.; Chien, A. J. Wnt/β-Catenin Signaling and AXIN1 Regulate Apoptosis Triggered by Inhibition of the Mutant Kinase BRAF V600E in Human Melanoma. *Sci. Signal.* **2012**, *5* (206). https://doi.org/10.1126/scisignal.2002274.

(62) Sierecki, E.; Sinko, W.; McCammon, J. A.; Newton, A. C. Discovery of Small Molecule Inhibitors of the PH Domain Leucine-Rich Repeat Protein Phosphatase (PHLPP) by Chemical and Virtual Screening. *J. Med. Chem.* **2010**, *53* (19), 6899–6911. https://doi.org/10.1021/jm100331d.

(63) Lai, A. C.; Crews, C. M. Induced Protein Degradation: An Emerging Drug Discovery Paradigm. *Nat. Rev. Drug Discov.* **2017**, *16* (2), 101–114. https://doi.org/10.1038/nrd.2016.211.

(64) Simons, M.; Mlodzik, M. Planar Cell Polarity Signaling: From Fly Development to Human Disease. *Annu. Rev. Genet.* **2008**, *42* (1), 517–540. https://doi.org/10.1146/annurev.genet.42.110807.091432.

(65) Fellmann, C.; Hoffmann, T.; Sridhar, V.; Hopfgartner, B.; Muhar, M.; Roth, M.; Lai, D. Y.; Barbosa, I. A. M.; Kwon, J. S.; Guan, Y.; Sinha, N.; Zuber, J. An Optimized MicroRNA Backbone for Effective Single-Copy RNAi. *Cell Rep.* **2013**, *5* (6), 1704–1713. https://doi.org/10.1016/j.celrep.2013.11.020.

(66) Rodgers, L. Measurement of DNA Content Using Propidium Iodide (PI)

Staining of Fixed Whole Cells. *Cold Spring Harb. Protoc.* **2006**, *2006* (1), pdb.prot4436. https://doi.org/10.1101/pdb.prot4436.

3.9 APPENDIX

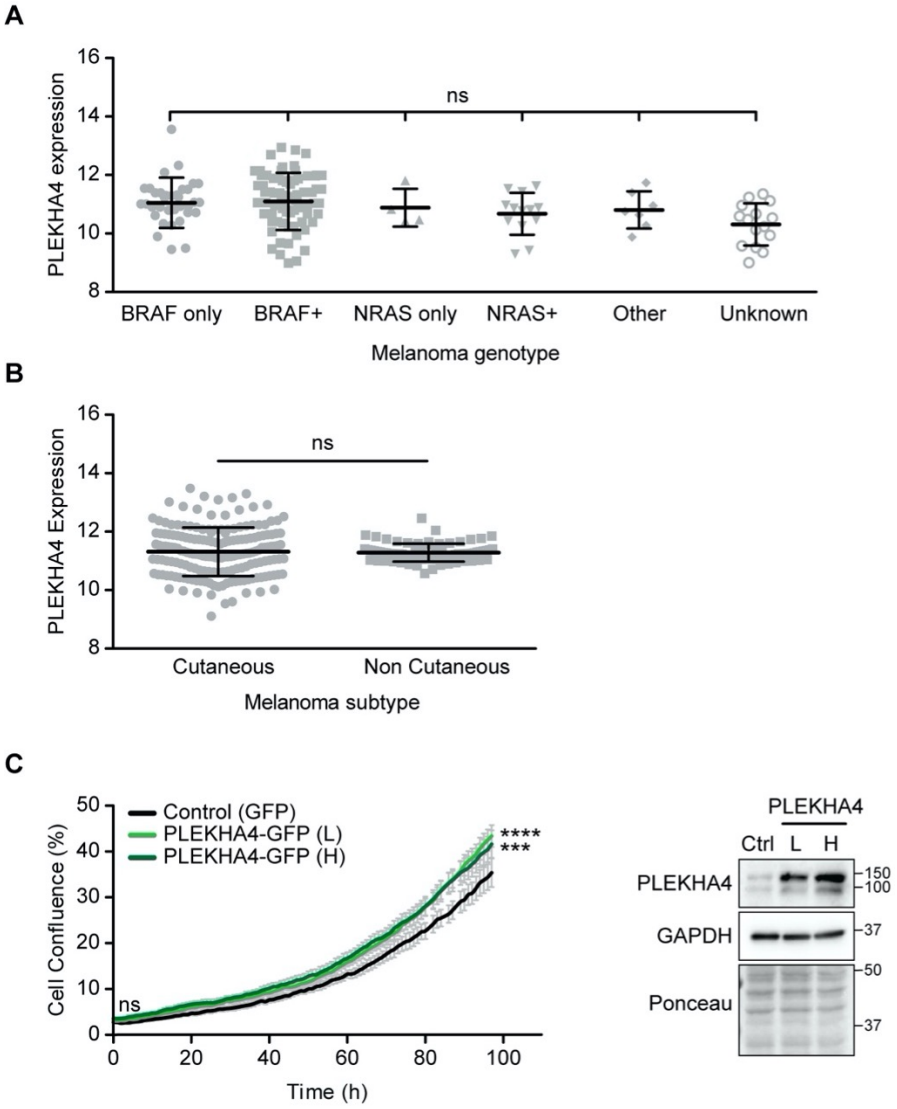

Figure S3.1. PLEKHA4 expression levels in melanoma subtypes and ability of PLEKHA4 overexpression to increase melanoma proliferation. (A) Analysis of relative PLEKHA4 mRNA levels from Genevestigator in melanoma cell lines, grouped by genotype. BRAF only: mutations only in BRAF (n=26); BRAF+: mutations in BRAF and other genes (n=56); NRAS only: mutations only in NRAS (n=4); NRAS+: mutations in NRAS and other genes (n=13); Other: mutations in genes other than BRAF or NRAS (n=7); Unknown: genotype unknown (n=15). (B) Analysis of relative PLEKHA4 mRNA levels from Genevestigator in human melanoma patient samples, grouped according to cutaneous (n=178) and non-cutaneous (n=81). (C) WM266-4 cells stably overexpressing GFP (Control/Ctrl) or PLEKHA4-GFP to

different extents (L: lower relative levels of overexpression; H: higher relative levels of overexpression) were generated, and their proliferation rate was measured relative to control cells using automated brightfield imaging of cell proliferation via IncuCyte (n=3). Shown at left is proliferation curve; shown at right are representative Western blots to indicate PLEKHA4 levels. GAPDH and Ponceau are shown as loading controls. *** $p < 0.001$; **** $p < 0.0001$; ns, not significant.

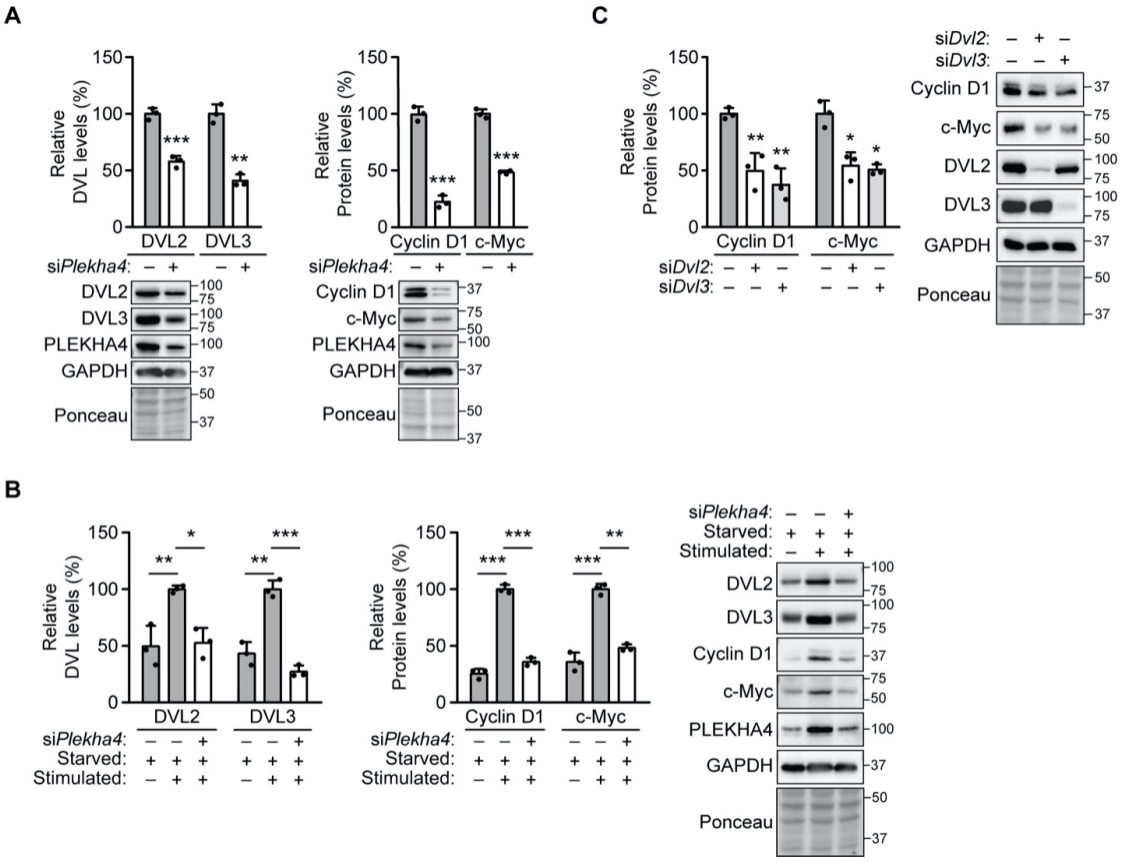

Figure S3.2. Knockdown of Plekha4, Dvl2, or Dvl3 causes defects in proliferation in YUMM1.7 cells. Shown is Western blot analysis of YUMM1.7 cells treated with the indicated siRNA duplexes against mouse *Plekha4* (A and B) and either *Dvl2* or *Dvl3* (C). In (B), cells were synchronized to G1 phase via serum starvation for 48 h (starved), with concurrent treatment with the indicated siRNA duplex. A portion of cells were then released into fresh medium containing FBS (stimulated, +) or control media containing no FBS (stimulated, –) for 36 h, followed by generation of lysates and Western blot analysis. GAPDH and Ponceau are shown as loading controls. Shown are representative Western blots and quantification in plots (n=3). * $p < 0.05$; ** $p < 0.01$; *** $p < 0.001$.

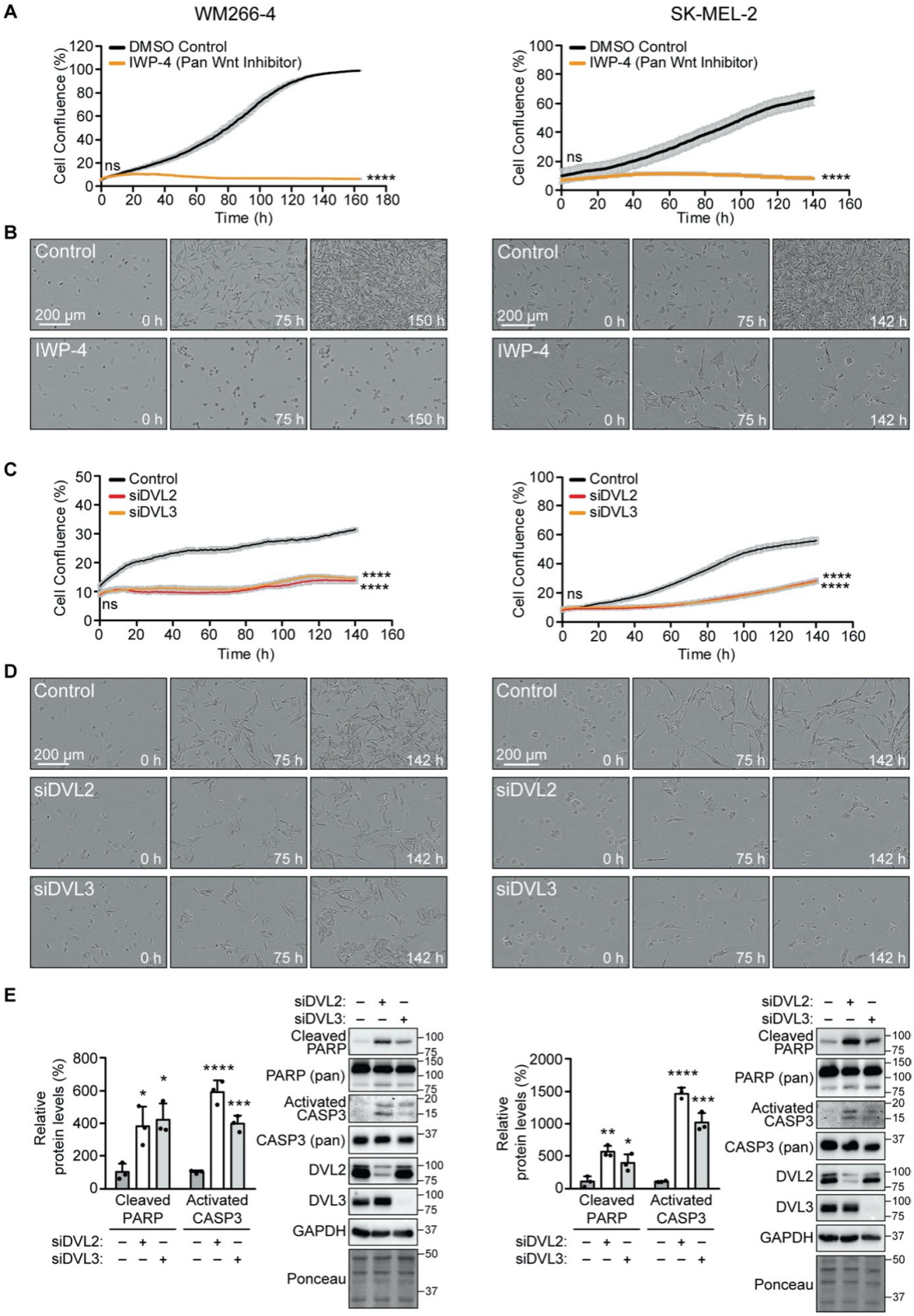
A
WM266-4
SK-MEL-2
DMSO Control
IWP-4 (Pan Wnt Inhibitor)
Cell Confluence (%)
Time (h)
ns
****
B
Control
IWP-4
200 µm
0 h
75 h
150 h
142 h
C
Control
siDVL2
siDVL3
****
ns
D
E
Relative protein levels (%)
Cleaved PARP
Activated CASP3
siDVL2:
siDVL3:
PARP (pan)
CASP3 (pan)
DVL2
DVL3
GAPDH
Ponceau

Figure S3.3. Inhibition of Wnt signaling decreases proliferation and induces apoptosis in melanoma cells. (A–D) Pan Wnt inhibition via treatment with the inhibitor IWP-4, compared to DMSO control (A–B), and knockdown of DVL2 (siDVL2) or DVL3 (siDVL3), compared to negative control siRNA (C–D), both attenuate proliferation of WM266-4 (left) and SK-MEL-2 (right) cells, as assessed by automated brightfield imaging of cell proliferation using an IncuCyte system (n=3). Growth curves are shown in (A) and (C) and representative brightfield images at the indicated timepoints are shown in (B) and (D). (E) Knockdown of DVL2 or DVL3 causes apoptosis in WM266-4 and SK-MEL-2 cells. Shown is Western blot analysis of WM266-4 (left) and SK-MEL-2 (right) cells subjected to siDVL2, siDVL3, or a negative control siRNA (–) (n=3). GAPDH and Ponceau are shown as loading controls. * $p < 0.05$; ** $p < 0.01$; *** $p < 0.001$; **** $p < 0.0001$; ns, not significant.

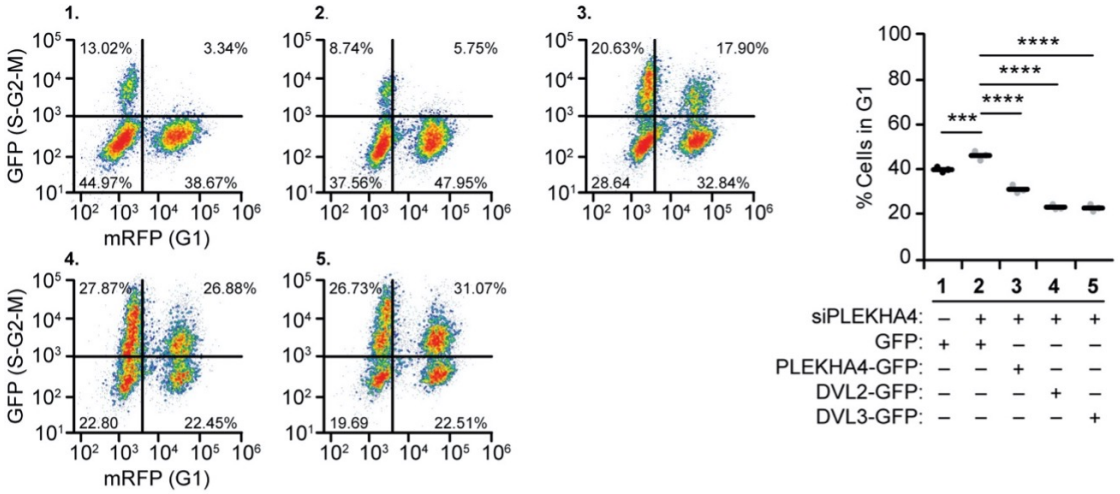

Figure S3.4. PLEKHA4-GFP, DVL2-GFP and DVL3-GFP can rescue the attenuation of G1/S transition defect induced by PLEKHA4 knockdown. WM266-4 cells stably expressing the dual color FUCCI reporters were synchronized to G1 phase, subjected to siPLEKHA4 or negative control siRNA (–), and stimulated with media containing FBS and simultaneously transduced with conditioned media containing lentivirus encoding GFP, siRNA-resistant PLEKHA4-GFP, DVL2-GFP, or DVL3-GFP, followed by flow cytometry analysis. The plots at left show populations of cells expressing mRFP (G1) and GFP (S-G2-M), and the fraction of mRFP+ cells is plotted at right (n=3). *** $p < 0.001$, **** $p < 0.0001$.

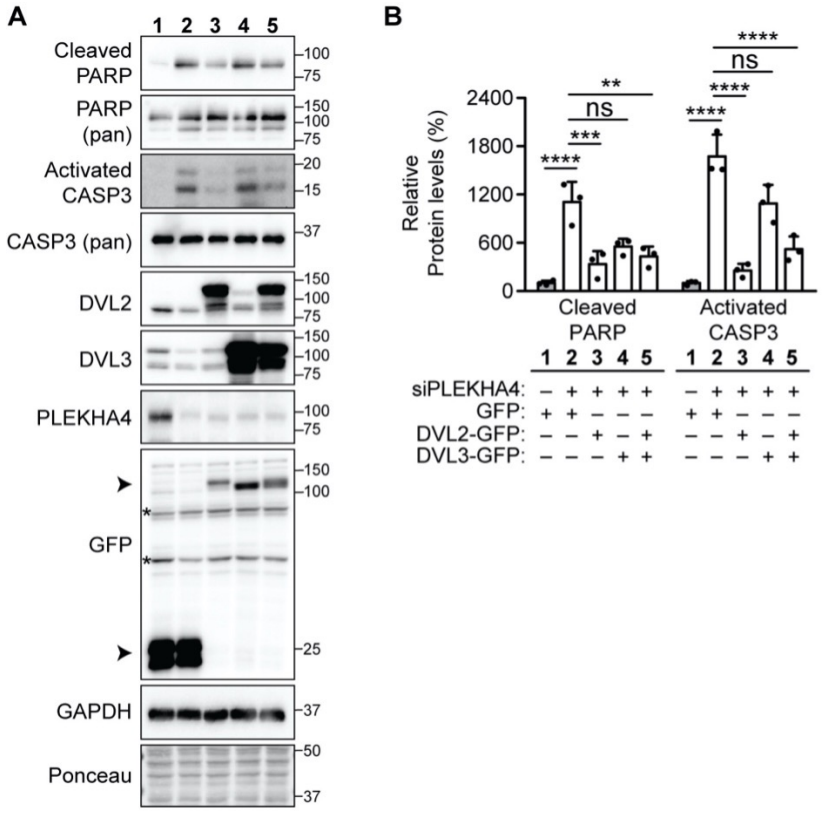

Figure S3.5. DVL overexpression can partially reverse the increase in apoptosis markers caused by PLEKHA4 knockdown. Shown is quantification and representative blot images of Western blot analysis of lysates from WM266-4 cells subjected to siPLEKHA4 (#2) or negative control siRNA (–) and transduced with conditioned media containing lentivirus encoding GFP, DVL2-GFP, DVL3-GFP, or a combination of DVL2-GFP and DVL3-GFP. (A) Representative Western blots. GAPDH and Ponceau are shown as loading controls. (B) Quantification of cleaved PARP (normalized ratio of cleaved PARP to PARP (pan)) and activated CASP3 (normalized ratio of activated CASP3 to CASP3 (pan)) (n=3). In the GFP blot, arrowheads indicate the expected migration of GFP (lanes 1–2) and DVL2-GFP or DVL3-GFP (lanes 3–5), and asterisks denote major antibody background bands. * $p < 0.05$; ** $p < 0.01$; *** $p < 0.001$; **** $p < 0.0001$; ns, not significant.

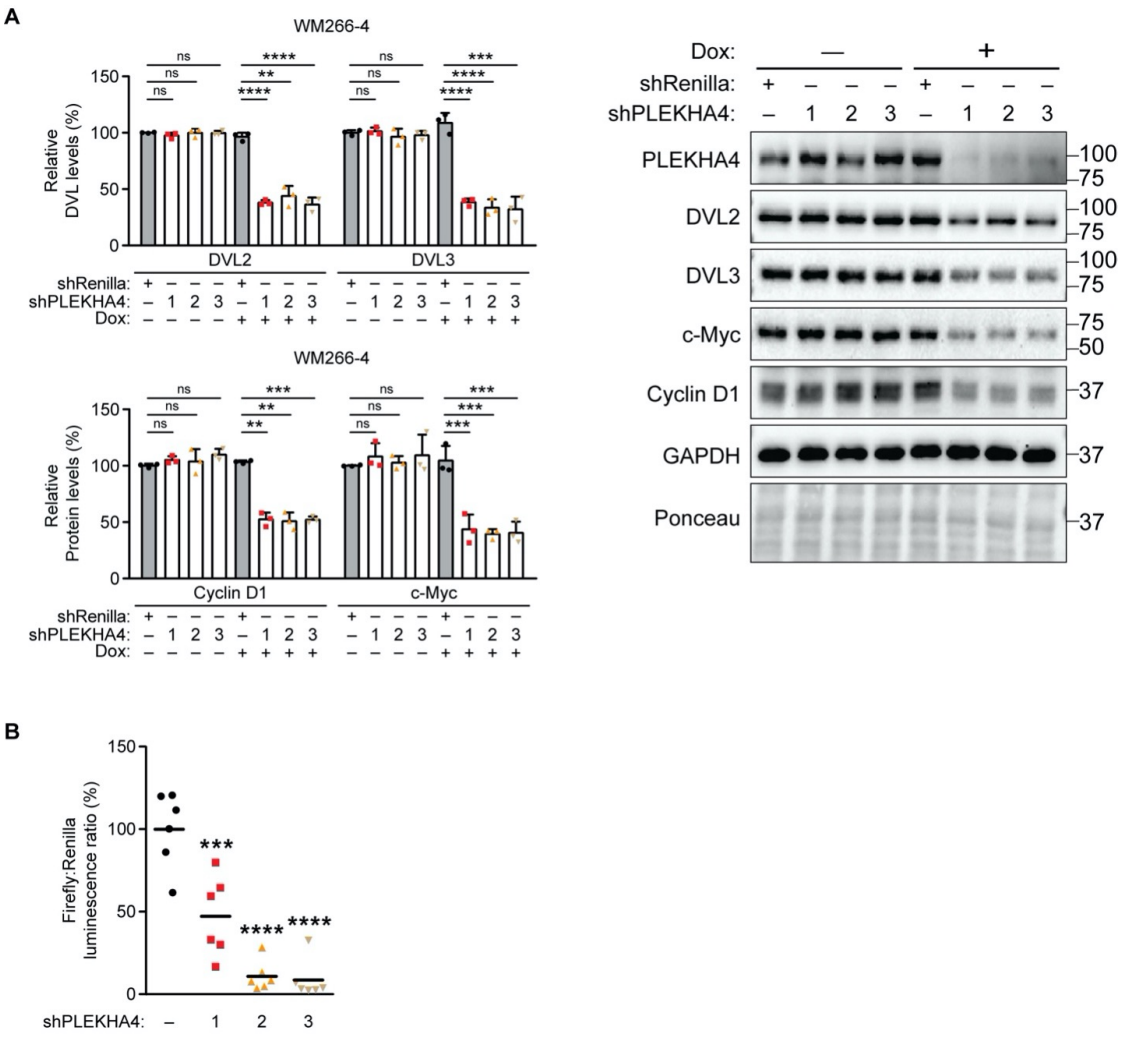

Figure S3.6. Characterization of WM266-4 cell lines stably expressing inducible human PLEKHA4 shRNA. WM266-4 cell lines were generated that stably expressed the indicated doxycycline (dox)-inducible shRNA constructs targeting human PLEKHA4 (#1, 2, or 3) or, as a control, Renilla luciferase. (A) Shown are quantification (left, n=3) and representative Western blots (right) of these shPLEKHA4 cell lines, evaluating levels of PLEKHA4 as well as Wnt signaling-related genes DVL2, DVL3, Cyclin D1, and c-Myc. Note the dox-dependent decreases in levels of PLEKHA4 as well as DVL2, DVL3, Cyclin D1, and c-Myc in the three shPLEKHA4 cell lines, but not in the shRenilla line. GAPDH and Ponceau are shown as loading controls. (B) Wnt3a-stimulated β-catenin-dependent TOPFlash assay of these cell lines (n=6). ** $p < 0.01$; *** $p < 0.001$; **** $p < 0.0001$; ns, not significant.

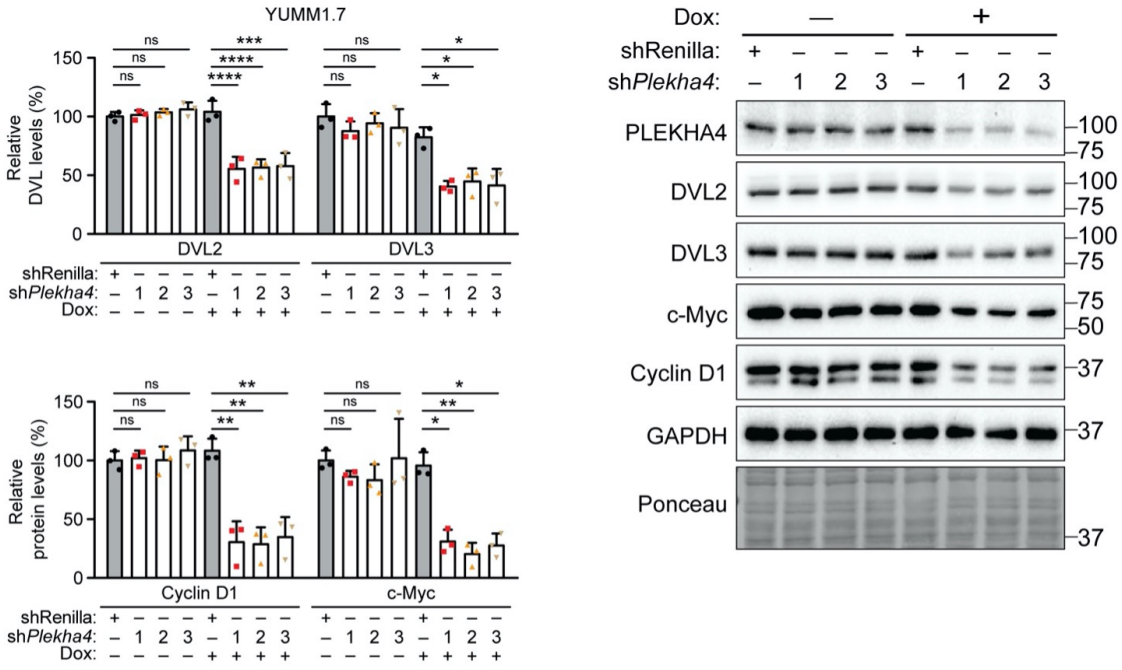

Figure S3.7. Characterization of YUMM1.7 cell lines stably expressing inducible mouse Plekha4 shRNA. YUMM1.7 cell lines were generated that stably expressed the indicated doxycycline (dox)-inducible shRNA constructs targeting mouse *Plekha4* (#1, 2, or 3) or, as a control, Renilla luciferase. Shown are quantification (left, n=3) and representative Western blots (right) of these sh*Plekha4* cell lines, evaluating levels of PLEKHA4 as well as Wnt signaling-related genes DVL2, DVL3, Cyclin D1, and c-Myc. Note the dox-dependent decreases in levels of PLEKHA4 as well as DVL2, DVL3, Cyclin D1, and c-Myc in the three sh*Plekha4* cell lines, but not in the shRenilla line. GAPDH and Ponceau are shown as loading controls. *, $p < 0.05$; ** $p < 0.01$; *** $p < 0.001$; **** $p < 0.0001$; ns, not significant.

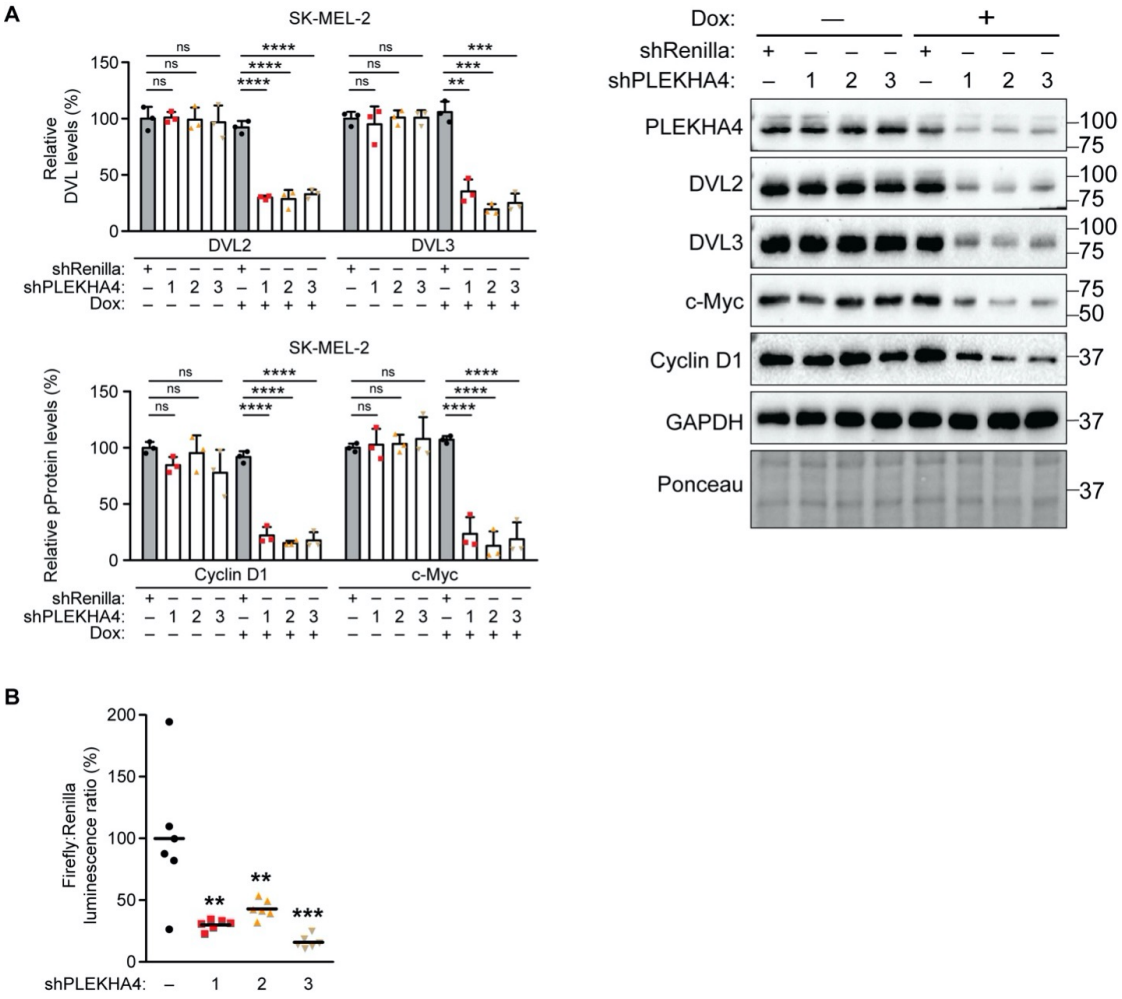

Figure S3.8. Characterization of SK-MEL-2 cell lines stably expressing inducible human PLEKHA4 shRNA. SK-MEL-2 cell lines were generated that stably expressed the indicated doxycycline (dox)-inducible shRNA constructs targeting human PLEKHA4 (#1, 2, or 3) or, as a control, Renilla luciferase. (A) Shown are quantification (left, n=3) and representative Western blots (right) of these shPLEKHA4 cell lines, evaluating levels of PLEKHA4 as well as Wnt signaling-related genes DVL2, DVL3, Cyclin D1, and c-Myc. Note the dox-dependent decreases in levels of PLEKHA4 as well as DVL2, DVL3, Cyclin D1, and c-Myc in the three shPLEKHA4 cell lines, but not in the shRenilla line. GAPDH and Ponceau are shown as loading controls. (B) Wnt3a-stimulated β-catenin-dependent TOPFlash assay of these cell lines (n=6). ** $p < 0.01$; *** $p < 0.001$; **** $p < 0.0001$; ns, not significant.

Table S3.1 Sequences for siRNA[i] and shRNA[ii].

Name	Sequence
Negative control siRNA	Sense: rCrGrUrUrArArUrCrGrCrGrUrArUrArArUrArCrGrCrGrUAT
	Antisense: rArUrArCrGrCrGrUrArUrUrArUrArCrGrCrGrArUrUrArArCrGrArC
siPLEKHA4 #1 (human)	Sense: rGrArArUrGrArGrArCrArGrArGrArCrUrUrArArGrGrArAGA
	Antisense: rUrCrUrUrCrCrUrUrArArGrUrCrUrCrUrGrUrCrUrCrArUrUrCrUrC
siPLEKHA4 #2 (human)	Sense: rArGrCrUrArCrArArUrArUrUrArGrArCrCrArGrArUrGrGGC
	Antisense: rGrCrCrCrArUrCrUrGrGrUrCrUrArArUrArUrUrGrUrArGrCrUrGrG
siPLEKHA4 #3 (human)	Sense: rUrCrUrCrArArCrArCrUrGrUrCrUrArArArUrUrUrGrGrATT
	Antisense: rArArUrCrCrArArArUrUrUrArGrArCrArGrUrGrUrUrGrArGrArArA

si*Plekha4* (mouse)	Sense: rArGrCrUrUrGrGrArGrArCrArGrArUrArCrGrUrUrGrUrUGA
	Antisense: rUrCrArArCrArArCrGrUrArUrCrUrGrUrCrUrCrCrArArGrCrUrCrU
siDVL2 (human)	Sense: rGrUrCrArCrGrCrUrArArArCrArUrGrGrArGrArArGrUrACA
	Antisense: rUrGrUrArCrUrUrCrUrCrCrArUrGrUrUrUrArGrCrGrUrGrArCrUrG
si*Dvl2* (mouse)	Sense: rGrGrUrGrArUrUrUrArCrCrArUrCrUrGrGrArUrGrArArGAA
	Antisense: rUrUrCrUrUrCrArUrCrCrArGrArUrGrGrUrArArArUrCrArCrCrUrU
siDVL3 (human)	Sense: rGrArUrArUrGrUrUrGrUrUrArCrArGrGrUrArArArCrGrAGA
	Antisense: rUrCrUrCrGrUrUrUrArCrCrUrGrUrArArCrArArCrArUrArUrCrUrC
si*Dvl3* (mouse)	Sense: rGrArUrArUrGrCrUrArCrUrGrCrArGrGrUrArArArUrGrAGA

	Antisense: rUrCrUrCrArUrUrUrArCrCrUrGrCrArGrUrArGrCrArUrArUrCrUrC
Negative control Renilla shRNA	TGCTGTTGACAGTGAGCGCAGGAATTATAATGCTTATCTATAGTGAAGCCACAGATGTATAGATAAGCATTATAATTCCTATGCCTACTGCCTCGGA
shPLEKHA4 #1 (human)	TGCTGTTGACAGTGAGCGCAGAGTCAACTTTCCACCAAAATAGTGAAGCCACAGATGTATTTTGGTGGAAAGTTGACTCTATGCCTACTGCCTCGGA
shPLEKHA4 #2 (human)	TGCTGTTGACAGTGAGCGCAGCTACAATATTAGACCAGAATAGTGAAGCCACAGATGTATTCTGGTCTAATATTGTAGCTATGCCTACTGCCTCGGA
shPLEKHA4 #3 (human)	TGCTGTTGACAGTGAGCGCAGGTTCTCAGCCTCTCCCAAATAGTGAAGCCACAGATGTATTTGGGAGAGGCTGAGAACCTATGCCTACTGCCTCGGA
sh*Plekha4* #1 (mouse)	TGCTGTTGACAGTGAGCGCAGCGCATGCGTAGAAACCAAATAGTGAAGCCACAGATGTATTTGGTTTCTACGCATGCGCTATGCCTACTGCCTCGGA
sh*Plekha4* #2 (mouse)	TGCTGTTGACAGTGAGCGCACAGTGGATCTGCAGACTGAATAGTGAAGCCACAGATGTATTCAGTCTGCAGATCCACTGTATGCCTACTGCCTCGGA
sh*Plekha4* #3	TGCTGTTGACAGTGAGCGAACAGATACGTTGTTGACTA

(mouse)	AGTAGTGAAGCCACAGATGTACTTAGTCAACAACGTAT CTGTCTGCCTACTGCCTCGGA

[i] The siRNA sequences were obtained as DsiRNA duplexes from IDT.

[ii] For shRNA, the indicated 97-mers were designed and cloned into LT3GEPIR as described previously[1].

Table S3.2 Antibodies used in this study.

Antibody	Source	RRID
Rabbit monoclonal anti-Axin2	Cell Signaling Technology (Cat# 2151 [76G6])	AB_2062432
Rabbit polyclonal anti-activated CASP3	Cell Signaling Technology (Cat# 9661S)	AB_2341188
Rabbit polyclonal anti-CASP3 (pan)	Cell Signaling Technology (Cat# 9662S)	AB_331439
Mouse monoclonal anti-c-Myc	Enzo Life Sciences (Cat# BML-SA294-0500)	AB_2051150
Mouse monoclonal anti-Cyclin D1	Santa Cruz Biotechnology (Cat# sc-8396 [A12])	AB_627344
Rabbit polyclonal anti-DVL2	Cell Signaling Technology (Cat# 3216)	AB_2093338
Mouse monoclonal anti-DVL3	Santa Cruz Biotechnology (Cat# sc-8027 [4D3])	AB_627434
Mouse monoclonal anti-GAPDH	GeneTex (Cat# GTX78213 [1D4])	AB_625368
Mouse monoclonal anti-GFP	Takara Bio (Cat# 632375 Living Colors)	AB_2756343
Rabbit polyclonal anti-cleaved PARP	Cell Signaling Technology (Cat# 9541S)	AB_331426

Rabbit polyclonal anti-PARP (pan)	Cell Signaling Technology (Cat# 9542S)	AB_2160739
Rabbit polyclonal anti-PLEKHA4	Abcam (Cat# ab170537)	N/A

REFERENCES

(1) Fellmann C, Hoffmann T, Sridhar V, Hopfgartner B, Muhar M, Roth M, et al. An optimized microRNA backbone for effective single-copy RNAi. Cell Rep. 2013;5:1704–13.

CHAPTER 4

SUMMARY AND OUTLOOK

Phosphoinositides are phospholipids that have emerged as platforms for intra and intercellular signaling processes. Although very low in cellular abundance, these molecules are known for their profound contributions in governing an array of physiological and phenotypic outcomes[1,2]. As lipid-based code of the cellular membrane identity, phosphoinositides provide a platform by presenting their headgroups as ligands to recruit and mediate interactions with phosphoinositides "reader" proteins at correct membrane locales[2,3]. PH (pleckstrin homology) domain-containing proteins represent a major class of such reader proteins[3,4,5]. Even though PH-domain containing proteins represent the largest such reader protein family, the majority of them still remain poorly understood.

This dissertation has described a novel PH-domain containing protein, PLEKHA4 and established its key roles in connecting the phosphoinositide signaling at the plasma membrane with ubiquitination and Wnt signaling machineries. Utilizing various microscopy and biochemical techniques, we discovered that PLEKHA4 localizes at the plasma membrane of the cells in a clustered fashion. Further analysis of the plasma membrane puncta revealed that the clusters may represent liquid-liquid phase-separated oligomers of multiple PLEKHA4 units at $PI(4,5)P_2$-rich regions. While functionally, these clusters act as signaling hubs where PLEKHA4 sequesters KLHL12, a CUL3 E3 ubiquitin ligase adaptor and inhibits the polyubiquitination and degradation of DVL proteins, much is yet to be known about the dynamic nature of

these clusters. Deconvoluting these plasma membrane oligomers can present additional mechanistic insights of Wnt pathways regulation via PLEKHA4. One way to understand the composition of these structures is via proximity labeling approaches[6,7]. This strategy could further aid in identifying novel partners of PLEKHA4 that are short-lived and interact only in a context-dependent manner in cells. Such discoveries could help to identify the biophysical nature of these phase-separated clusters in space and time, eliciting other unidentified roles of PLEKHA4 in signaling cascades initiating at the plasma membrane.

Our in vitro characterization supports a model wherein PLEKHA4 is a positive modulator of both canonical, β-catenin-dependent, and non-canonical, β-catenin-independent, Wnt signaling pathways. We further validated the in vitro findings with in vivo studies. Genetic knockout of the PLEKHA4 homolog in *Drosophila melanogaster*, *kramer (kmr)*, corroborated our in vitro model and revealed a Dishevelled-dependent attenuation of PCP signaling, equivalent to non-canonical Wnt signaling in *Drosophila.* To further elucidate the roles of PLEKHA4/*kmr* in the Wingless pathway, equivalent to canonical Wnt β-catenin-dependent signaling in *Drosophila*, one could exploit novel genetic approaches to probe specific tissues where Wingless signaling is more prominent[8,9]. Examining these tissues at various developmental stages could shed light on the modulatory role of PLEKHA4/*kmr* in Wingless signaling in this organism. Overall, **Chapter 2** establishes the novel role of PLEKHA4/*kmr* as a tuner to attenuate polyubiquitination of DVL proteins by sequestration of their E3 ligase, CUL3–KLHL12, further modulating the canonical and non-canonical Wnt signaling strength in vitro and in vivo.

Wnt signaling pathways are tightly regulated throughout development, and their dysregulation is associated with many diseases. Wnt pathways dictate key phenotypic outcomes of cell and tissue homeostasis, including cell proliferation, differentiation, polarity formation, and migration[10]. Mutations in the core components of the canonical Wnt/β-catenin signaling have been implicated as drivers of oncogenesis, in many cases. For instance, in colorectal cancer more than 80% of cases feature mutations in adenomatous polyposis coli (APC) that lead to hyperactive Wnt signaling and associated pathogenesis[11]. Many cancers that exhibit aberrant Wnt pathway activation leading to pathogenesis still remain poorly characterized. Melanoma, the most aggressive form of skin cancer, shows dysregulation in Wnt signaling homeostasis, and yet the functional consequence of this dysregulation is poorly understood[12,13,14]. The role of Wnt signaling as a sole driver of melanoma progression is controversial; yet, its role in supporting melanoma proliferation and progression in certain mutational background is clearer[15,16,17,18,19].

This dissertation provides additional evidence supporting the role of Wnt/β-catenin signaling in melanoma proliferation in both BRAF and NRAS mutant backgrounds. **Chapter 3** establishes the fundamental mechanism of tuning Wnt signaling strength through the role of PLEKHA4 could be highly beneficial in the context of melanoma. Through TCGA analysis, we revealed that PLEKHA4 levels are highest in melanoma compared to more than 20 other cancers. Capitalizing on the mechanistic insights of PLEKHA4 as a modulator of Wnt pathways from **Chapter 2**, we showed that even partial removal of PLEKHA4 by siRNA or shRNA dramatically lowers proliferation and increases apoptosis in vitro and in vivo via Wnt signaling

attenuation. Disruption of Wnt signaling in melanoma cells through the knockdown of either core Wnt pathway components such as DVL or modulatory components such as PLEKHA4 strongly affected levels of the canonical Wnt/β-catenin targets Cyclin D1 and c-Myc, which ensure progression through the G1/S cell cycle transition. The effects of PLEKHA4 knockdown could be partially rescued by DVL overexpression highlighting potential undetermined, DVL-independent mechanisms underlying the effect of PLEKHA4 knockdown on melanoma cell proliferation and apoptosis. Characterizing the effects of PLEKHA4 on other CUL3–KLHL12 ubiquitination substrates, including the COPII coat component SEC31, could further provide additional mechanistic evidence[20].

Inhibition of Wnt signaling is a promising route to new anti-cancer therapies in many cancers including melanoma. Selectively targeting the core components of Wnt signaling while minimizing damage to non-cancerous tissues has been challenging[11,13,21]. In recent years, efforts have shifted toward gaining a deeper understanding of and targeting the proteins that regulate the strength of Wnt signaling. As a modulator of Wnt signaling with a multi-domain architecture, PLEKHA4 stands out as a protein with a unique mechanism of action and potential relevance to melanoma. In **Chapter 3** of this thesis, we showed that removal of PLEKHA4 by shRNA prevented tumor growth in both BRAF- and NRAS-mutant tumor xenograft and allograft melanoma mouse models. Additionally, PLEKHA4 shRNA exhibited an additive effect with an FDA-approved BRAF inhibitor, leading to much stronger anti-proliferative effects, and its effects helped to keep growth slow even after removal of the inhibitor. These results reinforce that targeting MAP kinase signaling together with

modulators of Wnt pathways such as PLEKHA4 could be critical to extending the length of time that targeted therapies are effective in combating melanoma. Further mechanistic studies delineating the complex crosstalk between Wnt/β-catenin and MAP kinase signaling in melanoma is vital for the success of such therapy regimen[22].

Although PLEKHA4 is not a conventional drug target, its multidomain architecture provides a unique platform to target this molecule in different context. The N-terminus motif of PLEKHA4 that includes the amphipathic helix, basic peptide and the PH-domain partly mediates the plasma membrane localization via interaction with phosphoinositides. From **Chapter 2**, it is evident that the plasma membrane location is vital for the cellular function of PLEKHA4. Therefore, in principle a small molecule inhibitor targeting the N-terminus motif could be developed to interrupt the lipid-protein interaction, disrupting the function of PLEKHA4[23]. Such an inhibitor could further be exploited for future mechanistic studies and therapeutic applications for diseases such as melanoma. Additionally, small-molecule inhibitors and PROTACs/degraders[24] could also be developed to disrupt the homo and heterotypic protein-protein interactions of PLEKHA4. This dissertation provides evidence that targeting modulatory rather than the core components of cell signaling can be a new promising approach for targeted therapy.

In summary, this dissertation identifies a novel lipid-binding protein, PLEKHA4, as a critical modulator of both canonical and non-canonical Wnt signaling in vitro and in vivo. PLEKHA4 tunes the strength of Wnt/β-catenin signaling in melanoma progression and provides further clarity on the pathological role of Wnt/β-

catenin signaling in this disease, suggesting that pharmacological inhibition of PLEKHA4 could represent a promising new avenue for targeted therapy in melanoma.

4.1 REFERENCES

(1) Balla, T. Phosphoinositides: Tiny Lipids with Giant Impact on Cell Regulation. *Physiol. Rev.* **2013**, *93* (3), 1019–1137. https://doi.org/10.1152/physrev.00028.2012.

(2) Dickson, E. J.; Hille, B. Understanding Phosphoinositides: Rare, Dynamic, and Essential Membrane Phospholipids. *Biochem J* **2019**, *476* (1), 1–23. https://doi.org/10.1042/BCJ20180022.

(3) Lemmon, M. A. Membrane Recognition by Phospholipid-Binding Domains. *Nat. Rev. Mol. Cell Biol.* **2008**, *9* (2), 99–111. https://doi.org/10.1038/nrm2328.

(4) Kutateladze, T. G. Translation of the Phosphoinositide Code by PI Effectors. *Nat. Chem. Biol.* **2010**, *6* (7), 507–513. https://doi.org/10.1038/nchembio.390.

(5) Lemmon, M. A. Pleckstrin Homology (PH) Domains and Phosphoinositides. *Biochem. Soc. Symp.* **2007**, *74* (74), 81–93. https://doi.org/10.1042/BSS0740081.

(6) Branon, T. C.; Bosch, J. A.; Sanchez, A. D.; Udeshi, N. D.; Svinkina, T.; Carr, S. A.; Feldman, J. L.; Perrimon, N.; Ting, A. Y. Efficient Proximity Labeling in Living Cells and Organisms with TurboID. *Nat. Biotechnol.* **2018**, *36* (9), 880–898. https://doi.org/10.1038/nbt.4201.

(7) Cho, K. F.; Branon, T. C.; Udeshi, N. D.; Myers, S. A.; Carr, S. A.; Ting, A. Y. Proximity Labeling in Mammalian Cells with TurboID and Split-TurboID. *Nat. Protoc.* **2020**, *15* (12), 3971–3999. https://doi.org/10.1038/s41596-020-0399-0.

(8) Chien, A. J.; Conrad, W. H.; Moon, R. T. A Wnt Survival Guide: From Flies to Human Disease. *J. Invest. Dermatol.* **2009**, *129* (7), 1614–1627. https://doi.org/10.1038/jid.2008.445.

(9) Ammeux, N.; Housden, B. E.; Georgiadis, A.; Hu, Y.; Perrimon, N. Mapping Signaling Pathway Cross-Talk in Drosophila Cells. *Proc. Natl. Acad. Sci. U. S. A.* **2016**, *113* (35), 9940–9945. https://doi.org/10.1073/pnas.1610432113.

(10) MacDonald, B. T.; Tamai, K.; He, X. Wnt/β-Catenin Signaling: Components, Mechanisms, and Diseases. *Dev. Cell* **2009**, *17* (1), 9–26. https://doi.org/10.1016/j.devcel.2009.06.016.

(11) Nusse, R.; Clevers, H. Wnt/β-Catenin Signaling, Disease, and Emerging Therapeutic Modalities. *Cell* **2017**, *169* (6), 985–999. https://doi.org/10.1016/j.cell.2017.05.016.

(12) Webster, M. R.; Weeraratna, A. T. A Wnt-Er Migration: The Confusing Role of β-Catenin in Melanoma Metastasis. *Sci. Signal.* **2013**, *6* (268), pe11. https://doi.org/10.1126/scisignal.2004114.

(13) Jackstadt, R.; Hodder, M. C.; Sansom, O. J. WNT and β-Catenin in Cancer: Genes and Therapy. *Annu. Rev. Cancer Biol.* **2020**, *4* (1), 177–196. https://doi.org/10.1146/annurev-cancerbio-030419-033628.

(14) Gajos-Michniewicz, A.; Czyz, M. Wnt Signaling in Melanoma. *Int J Mol Sci* **2020**, *21*, 4852.

(15) Delmas, V.; Beermann, F.; Martinozzi, S.; Carreira, S.; Ackermann, J.; Kumasaka, M.; Denat, L.; Goodall, J.; Luciani, F.; Viros, A.; Demirkan, N.; Bastian, B. C.; Goding, C. R.; Larue, L. β-Catenin Induces Immortalization of Melanocytes by Suppressing P16INK4a Expression and Cooperates with N-Ras in Melanoma Development. *Genes Dev.* **2007**, *21* (22), 2923–2935. https://doi.org/10.1101/gad.450107.

(16) Pawlikowski, J. S.; McBryan, T.; van Tuyn, J.; Drotar, M. E.; Hewitt, R. N.; Maier, A. B.; King, A.; Blyth, K.; Wu, H.; Adams, P. D. Wnt Signaling Potentiates Nevogenesis. *Proc. Natl. Acad. Sci.* **2013**, *110* (40), 16009–16014. https://doi.org/10.1073/pnas.1303491110.

(17) Juan, J.; Muraguchi, T.; Iezza, G.; Sears, R. C.; McMahon, M. Diminished WNT -> β-Catenin -> c-MYC Signaling Is a Barrier for Malignant Progression of BRAFV600E-Induced Lung Tumors. *Genes Dev.* **2014**, *28* (6), 561–575. https://doi.org/10.1101/gad.233627.113.

(18) Damsky, W. E.; Curley, D. P.; Santhanakrishnan, M.; Rosenbaum, L. E.; Platt, J. T.; Gould Rothberg, B. E.; Taketo, M. M.; Dankort, D.; Rimm, D. L.; McMahon, M.; Bosenberg, M. β-Catenin Signaling Controls Metastasis in Braf-Activated Pten-Deficient Melanomas. *Cancer Cell* **2011**, *20* (6), 741–754. https://doi.org/https://doi.org/10.1016/j.ccr.2011.10.030.

(19) Sun, Q.; Lee, W.; Mohri, Y.; Takeo, M.; Lim, C. H.; Xu, X.; Myung, P.; Atit, R. P.; Taketo, M. M.; Moubarak, R. S.; Schober, M.; Osman, I.; Gay, D. L.; Saur, D.; Nishimura, E. K.; Ito, M. A Novel Mouse Model Demonstrates That Oncogenic Melanocyte Stem Cells Engender Melanoma Resembling Human Disease. *Nat. Commun.* **2019**, *10* (1), 1–16. https://doi.org/10.1038/s41467-019-12733-1.

(20) Jin, L.; Pahuja, K. B.; Wickliffe, K. E.; Gorur, A.; Baumgärtel, C.; Schekman, R.; Rape, M. Ubiquitin-Dependent Regulation of COPII Coat Size and Function. *Nature* **2012**, *482* (7386), 495–500.

https://doi.org/10.1038/nature10822.

(21) Tran, F. H.; Zheng, J. J. Modulating the Wnt Signaling Pathway with Small Molecules. *Protein Sci.* **2017**, *26* (4), 650–661. https://doi.org/10.1002/pro.3122.

(22) Guardavaccaro, D.; Clevers, H. Wnt/β-Catenin and MAPK Signaling: Allies and Enemies in Different Battlefields. *Sci. Signal.* **2012**, *5* (219), 1–3. https://doi.org/10.1126/scisignal.2002921.

(23) Sierecki, E.; Sinko, W.; McCammon, J. A.; Newton, A. C. Discovery of Small Molecule Inhibitors of the PH Domain Leucine-Rich Repeat Protein Phosphatase (PHLPP) by Chemical and Virtual Screening. *J. Med. Chem.* **2010**, *53* (19), 6899–6911. https://doi.org/10.1021/jm100331d.

(24) Lai, A. C.; Crews, C. M. Induced Protein Degradation: An Emerging Drug Discovery Paradigm. *Nat. Rev. Drug Discov.* **2017**, *16* (2), 101–114. https://doi.org/10.1038/nrd.2016.211.